Titre: Title:	Keggin-Type Catalysts Partially Oxidize 2-Methyl-1,3- Propanediol to Methacrylic Acid in a Micro-Fluidized Bed Reactor
Auteur: Author:	Mohammad Jaber Darabi Mahboub
Date:	2018
Type:	Mémoire ou thèse / Dissertation or Thesis
Référence: Citation:	Darabi Mahboub, M. J. (2018). Keggin-Type Catalysts Partially Oxidize 2-Methyl-1,3- Propanediol to Methacrylic Acid in a Micro-Fluidized Bed Reactor [Thèse de doctorat, École Polytechnique de Montréal]. PolyPublie. https://publications.polymtl.ca/3088/

UNIVERSITÉ DE MONTRÉAL

KEGGIN–TYPE CATALYSTS PARTIALLY OXIDIZE 2–METHYL–1,3–PROPANEDIOL TO METHACRYLIC ACID IN A MICRO–FLUIDIZED BED REACTOR

MOHAMMAD JABER DARABI MAHBOUB
DÉPARTEMENT DE GÉNIE CHIMIQUE
ÉCOLE POLYTECHNIQUE DE MONTRÉAL

THÈSE PRÉSENTÉE EN VUE DE L'OBTENTION
DU DIPLÔME DE PHILOSOPHIÆ DOCTOR
(GÉNIE CHIMIQUE)
MAI 2018

UNIVERSITÉ DE MONTRÉAL

ÉCOLE POLYTECHNIQUE DE MONTRÉAL

Cette thèse intitulée :

KEGGIN–TYPE CATALYSTS PARTIALLY OXIDIZE 2–METHYL–1,3–PROPANEDIOL TO METHACRYLIC ACID IN A MICRO–FLUIDIZED BED REACTOR

présentée par : DARABI MAHBOUB Mohammad Jaber
en vue de l'obtention du diplôme de : Philosophiæ Doctor
a été dûment acceptée par le jury d'examen constitué de :

M. FRADETTE Louis, Ph. D., président
M. PATIENCE Gregory S., Ph. D., membre et directeur de recherche
M. PERRIER Michel, Ph. D., membre
M. CHIN Ya–Huei(Cathy), Ph. D., membre

DEDICATION

Dedicated to
My beloved parents, my lovely siblings,
My guardian angel nephew and niece forever, Nihad and Lia
Thank you for your endless love,
sacrifices, and support . . .

ACKNOWLEDGMENTS

I would like to acknowledge all who in one way or another contributed to the completion of this thesis. First and foremost, I wish to express my deep and sincere gratitude to my supervisor Prof. Gregory S. Patience for his solid support, motivation, caring and patience, as well as for providing me with an excellent atmosphere in which to conduct my research. His vast knowledge and logical way of thinking helped me throughout this process. It was a pleasure to work with him ; the lessons he taught me go beyond what is written in this thesis and will help me in all aspects of my life.

I would like to acknowledge the members of my committee, Prof. Cathy Chin, Prof. Michele Perrier and Prof. Louis Fradette for taking interest in my work, examining my thesis and providing insightful comments.

I also wish to gratefully acknowledge the financial support from Arkema, Mitacs and CRIBIQ which made this research work possible.

I thank the unforgettable kindness of Dr. Jean–Luc Dubois (Scientific Advisor, Catalysis, Processes and Renewables at Arkema). His knowledgeable and warmth made the collaboration highly beneficial for me. I made a number of friends all around Canada and my best memories are the times I have spent with them.

I would like to acknowledge the other professors and technical staff at the Chemical Engineering department at École polytechnique de Montréal, especially the CM^2 laboratory for providing the best possible assistance with my project.

I would also like to extend my thanks to all my colleagues in Prof. Patience's group for sharing their knowledge and ideas, and to all my colleagues who helped me at various points during the Ph.D. thesis process.

My deepest appreciation goes to the technicians in the Department of Chemical Engineering, particularly Sylvain Fleury–simard, Martine Lamarche and Gino Robin, for their excellent technical assistance. I am also thankful to Mr. Charles Bruel for translating abstract to French.

And last but not least, from the bottom of my heart, I would like to express my endless gratitude to my parent, lovely siblings, my brother–in–law and sister–in–law, and also my lovely nephew and lovely niece for the absolute support they have provided me throughout my entire life, and without whose love, spiritual encouragement and altruism I would not be where I am now. Words are powerless to express what I feel in my heart for them.

RÉSUMÉ

Le méthacrylate de méthyle est le monomère du polyméthacrylate de méthyle. Ce dernier, commercialisé sous les noms de marques Acrylite®, Plexiglas®, Lucite®, Optix®, Perspex®, Oroglas®, Cyrolite®, Sumipex® et Altuglas®, a diverses applications industrielles dans les peintures et revêtements ou l'électronique, comme modificateur pour le PVC, ou pour les implants osseux Nagai (2001); Godfrey (1963); Kung (1994); W.Dormer *et al.* (1998); Smith *et al.* (1999). La demande en MMA dépassera les 4.8 millions de tonnes d'ici à 2020 Global Market Analysts (2016). La région Asie–Pacifique est son principal marché, elle inclut notamment la Chine, son premier producteur et consommateur mondial. L'Amérique du Nord et l'Europe se classent deuxième et troisième, respectivement, tandis que le Moyen–Orient, l'Afrique, et l'Amérique Latine représentent les marchés en plus forte croissance Global Market Analysts (2016). Le PMMA (produit à partir de MMA) dépassera lui les 2.8 millions de tonne en demande annuelle. Mitsubishi Rayon a ainsi rapporté une croissance de la demande de plus de 0.2 millions de tonnes en rythme annuel (5 % to 6 %) Nagai et Ui (2004); Program (2006); Schunk et Brem (2011). Cette hausse de la demande en PMMA se traduit en moyenne par une augmentation annuelle de l'ordre de 10 % du prix au gros du MMA Jing (2012). En 2015, la demande globale égalait la capacité de production à l'échelon mondial Markit (2016); Global Market Analysts (2016).

La production de méthacrylate de méthyle (MMA) par le procédé acétone cyanohydrine (ACH) dépend de matières premières couteuses et toxiques et souffre de faibles conversions. L'estérification de l'acide méthacrylique (MAA) en MMA est une alternative au ACH. Cependant, les procédés de synthèse de MAA requièrent plusieurs étapes et leurs catalyseurs ont une faible durée de vie. L'oxydation d'oléfines légères en acide méthacrylique (MAA)– en tant que matières premières alternative pour le MMA— réduit les lacunes du précédé actuel Montag et Mckenna (1991); Drent et Budzelaar (1996); Zhou *et al.* (2015). Toutefois, les voies proposées depuis ces matières premières souffrent également de faibles conversions, de multiples étapes et de la faible durée de vie des catalyseurs. Nous avons employé un micro-lit fluidisé gaz-solide pour oxyder partiellement, et pour la première fois, du 2–méthyl–1,3–propanediol (2MPDO) sur un catalyseur hétérogène.

Au travers du choix du catalyseur, du design du micro-lit fluidisé, de la réaction des composés thermosensibles en produits à valeur ajouté, et du modèle cinétique, nous avons cherché à optimiser l'ensemble du procédé catalytique pour développer une nouvelle approche pour l'oxydation partielle du 2MDPO en produits chimiques de spécialité.

Avant de s'attaquer au corps de ce projet de recherche, nous avons réalisé dans le second chapitre une étude compréhensive de l'ensemble des procédés actuels, commerciaux et potentiels permettant la "Synthèse catalytique d'acide méthacrylique et de méthacrylate de méthyle" (Chapitre 2 : "Catalysis for the synthesis of methacrylic acid and methyl methacrylate") afin de comprendre les points suivants :

1. Les avantages et inconvénients des procédés actuels ;
2. Le choix, potentiel ou commercial, du catalyseur pour chaque approche ;
3. Les conditions opératoires optimales et les mécanismes réactionnels possibles.

Pour le premier objectif spécifique, nous proposons un nouveau procédé hétérogène gaz-solide-liquide dans lequel nous atomisons le réactif, liquide, sur le catalyseur pour réaliser l'oxydation partielle du 2MPDO en MAA et en méthacroléine (MAC). À cet égard, nous avons assigné les chapitres 3 et 4 de cette thèse– ainsi que deux articles publiés– à cet objectif spécifique. Le chapitre 3 est intitulé : "Oxydation en phase gaz du 2–méthyl–1,3–propanediol en acide méthacrylique sur des catalyseurs hétéropolyacidiques" ("Gas phase oxidation of 2–methyl–1,3–propanediol to methacrylic acid over heteropolyacid catalysts"). Le quatrième chapitre, portant sur le même thème, est intitulé : "Oxydation partielle du 2–méthyl–1,3–propanediol en acide méthacrylique : modélisation expérimentale et du réseau neural" ("Partial oxidation of methyl–1,3–propanediol to methacrylic acid : experimental and neural network modeling").

Le 2MPDO liquide est atomisé par de l'argon sur la surface du catalyseur à une température de 250 °C. La première difficulté expérimentale est l'agglomération du catalyseur au cours du temps qui conduit à l'obstruction du distributeur après quelques expériences. Afin de surmonter ce problème, nous avons optimisé le ratio Ar/2MPDO (gaz/réactif liquide), la configuration de la buse, et la perte de charge. Parmi tous les catalyseurs hétérogènes synthétisés, les hétéropolycomposés de type Keggin sont ceux qui se sont montrés les plus actifs pour réaliser le clivage de la liaison C−H et oxyder sélectivement le 2MPDO en MAA+MAC. La température et le ratio 2 MPDO :O_2 affectent de façon prépondérante le rendement en produits désirés. Les autres éléments à considérer pour ce procédé sont la formation de coke, le haut taux de conversion, et la formation de sous-produits.

Bien que nous ayons testé différent types de catalyseurs avec différentes conditions opératoires, nous n'avons toujours aucune idée de la nature de la relation entre structure du catalyseur et sélectivité en produits. Il nous faut également réfléchir à la nature des sites actifs pour ce type de catalyseur et pour cette réaction sachant que la température de calcination est le paramètre de synthèse ayant le plus d'impact sur les performances du catalyseur. Notre second objectif spécifique a ainsi consisté à calciner le catalyseur optimal (déterminé au premier objectif) à différentes températures. Nous avons caractérisé le catalyseur avec différentes

techniques pour distinguer les différences induites par la calcination en termes de structures. Nous proposons ainsi un nouveau mécanisme qui lie la structure du catalyseur, les réactifs, et les produits. Les résultats du second objectif ont été publiés dans un article reproduits dans le chapitre 5. Le chapitre 5 est intitulé “Des catalyseurs de type Keggin à base de Cs, V et Cu oxydent partiellement le 2–méthyl–1,3–propanediol en acide méthacrylique” (“Cs, V, Cu Keggin–type catalysts partially oxidize 2–methyl–1,3–propanediol to methacrylic acid”).

La dernière étape a consisté à modéliser les données expérimentales des différents mécanismes. Le modèle de Mars et Van Krevelen caractérise nos données mieux que ceux de Langmuir–Hinshelwood ou de Eley–Rideal : la séquence réactionnelle implique à la fois des réactions en série et en parallèle dans lesquelles le 2MDPO forme du MAC et du MAA directement et où le MAC formé réagit ensuite pour donner du MAA. Le taux de réaction en série du MAC en MAA est 50 fois plus rapide que celui de la réaction en parallèle (formation du MAC et du MAA). La réaction de 2MPDO sur les sites oxydés pour former des produits est la étape limitante. Le chapitre 6 intitulé “Cinétique d’oxydation du 2-méthyle-1,3-propanediol en acide méthacrylique”.

À l’aide de la compréhension glanée dans ce projet, nous pouvons conclure que l’oxydation partielle du 2MDPO dans un réacteur à lit fluidisé gaz-solide est une approche novatrice pour valoriser le 2MDPO en produits chimiques de spécialité et en acides carboxyliques en particulier. Dans le système gaz-solide-liquide, le 2MDPO est introduit lentement dans le lit avec lequel il est en contact direct. Il s’évapore, et s’oxyde soit à la surface du catalyseur, soit dans le lit. Il est converti en acides carboxyliques. Les catalyseurs acides à base de vanadium et de molybdène font preuve de performances prometteuses pour la conversion du 2MDPO en produits à valeur ajoutée. Si l’activité catalytique affecte le rendement et la sélectivité en produits, les conditions opératoires telles que la température et la concentration en O_2 ont elles-aussi un impact majeur. Le modèle cinétique proposé prédit de façon précise, tout en restant simple, la conversion en 2MDPO, la sélectivité en produits, et l’effet des différents paramètres. Le co-produit de la méthode ici-présentée est du syngaz, un mélange de $CO+H_2$ pouvant être transformé en carburants et autres produits chimiques.

ABSTRACT

Methyl methacrylate (MMA) is a specialty monomer for poly–methyl–methacrylate (PMMA), which is marketed under trademarks Acrylite®, Plexiglas®, Lucite®, Optix®, Perspex®, Oroglas®, Cyrolite®, Sumipex® and Altuglas® and applied in diverse industries including paints and coatings, electronics, as a modifier for PVC, and as bone inserts Nagai (2001); Godfrey (1963); Kung (1994); W.Dormer *et al.* (1998); Smith *et al.* (1999). Demand of MMA will surpass 4.8 million metric tonne by 2020 Global Market Analysts (2016), where Asia–Pacific is the main market in which China ranks first for production and consumption. North America and Europe are ranked second and third, respectively, while the Middle East, Africa, and Latin America are the areas growing the fastest Global Market Analysts (2016). PMMA (produced from MMA) surpassed 2.8 million tonne annually. Mitsubishi Rayon reported annual growth in demand of more than 0.2 million tonnes (5 % to 6 %) Nagai et Ui (2004); Program (2006); Schunk et Brem (2011). Due to the increasing demand for PMMA, the price of bulk MMA increased by 10 % annually Jing (2012).In 2015, the worldwide demand equalled the global supply capacity Markit (2016); Global Market Analysts (2016).

The acetone cyanohydrin process (ACH) to produce methyl methacrylate (MMA) relies on expensive and toxic feedstock and suffers from low yield. Methacrylic acid (MAA) esterification to MMA is an alternative to ACH. However, current processes to produce MAA require multi steps and catalysts lifetime are short. Oxidizing light olefins to methacrylic acid (MAA)– as an alternative feedstock for MMA– reduces the deficiencies of the current process Montag et Mckenna (1991); Drent et Budzelaar (1996); Zhou *et al.* (2015). However, the proposed routes from these feedstocks also suffer from low yield, multiple steps, and short catalyst lifetime. We employed a gas–solid micro fluidized bed reactor to partially oxidize 2–methyl–1,3–propanediol (2MPDO) over the heterogeneous catalysts for the first time.

We targeted developing a catalytic process, the catalyst used, temperature sensitive materials to value added chemicals, a micro fluidized-bed reactor, and kinetic modeling to pave a new road in the partial oxidation of 2MPDO into specialty chemicals.

Before starting the main body of the research, we did a comprehensive study as the second chapter entitled “Catalysis for the synthesis of methacrylic acid and methyl methacrylate” on all current commercialized/potential processes to understand the following aspects:

1. The advantages or disadvantages of the current approaches;
2. The potential commercial or developed catalysts for each route;
3. The optimum operating conditions and possible mechanisms.

As the fist specific objective, we propose a new gas-solid-liquid heterogeneous process in which we atomize the liquid reactant over the catalyst to partially oxidize 2MPDO into MAA and methacrolein (MAC). In this regard, we assigned chapters 3 and 4 of this thesis–as two published papers– to this specific objective. The third chapter is "Gas phase oxidation of 2–methyl–1,3–propanediol to methacrylic acid over heteropolyacid catalysts". The fourth chapter is also assigned to "Partial oxidation of methyl–1,3–propanediol to methacrylic acid: experimental and neural network modeling". Argon atomized the liquid 2MPDO over the catalyst surface operating at 250 °C. However, the first encountered issue was catalyst agglomeration with time which blocked injector after some experiments. To overcome this problem, we optimized the Ar/2MPDO ratio, the nozzle configuration and pressure drop. Among the synthesized heterogeneous catalysts, Keggin–type heteropolycompounds were active to cleavage C−H bond of hydrocarbon and selectively oxidize 2MPDO to MAA+MAC. Temperature and the 2 MPDO:O_2 ratio affect the yield of desired products. Coke formation, high conversion and forming byproducts are the other issues of this process.

Although we tested several kind of catalysts over different operating conditions, we still have no idea what the correlation between catalyst structure and products selectivity. On the other hand what the active sites in this catalyst type for this reaction? Moreover, calcination temperature is the most effective parameters on charge transfer among metal ions of catalyst that affects its performance. Therefore as the second objective, we calcined the optimum catalyst structure (obtained from the first objective) at different temperatures. We characterized the catalyst with several techniques to distinguish the differences in their structures. We propose a new mechanism that correlates the catalyst structure, reactant, and products. The results of second objective published as a paper in chapter 5. Chapter 5 entitled "Cs, V, Cu Keggin–type catalysts partially oxidize 2–methyl–1,3–propanediol to methacrylic acid".

As the last step, we modeled experimental data by different mechanisms. The Mars and Van Krevelen model characterizes the experimental data better than the either the Langmuir–Hinshelwood or Eley–Rideal models: The reaction sequence involves both parallel and series reactions in which 2MPDO for MAC and MAA directly and MAC reacts to form MAA but the series reaction rate to MAA is 50 times faster than the parallel reaction rate. Reacting of 2MPDO over the oxidized sites to form products is the rate–limiting step. Chapter 6 entitled "Oxidation kinetics of 2–methyl–1,3–propanediol to methacrylic acid".

With the help of the insight gained in this study we can say that the partial oxidation of 2MPDO in the gas–solid fluidized–bed reactor is a novel approach for upgrading 2MPDO to value–added chemicals and in particularly carboxylic acids as an open chain product from

2MPDO. In the gas-solid-liquid system, 2MPDO was introduced to the bed slowly, directly contacted with the catalyst, evaporates, and oxidized on the surface of the catalyst or in the bed and converted to carboxylic acids. Acidic catalyst based on vanadium and molybdenum demonstrated promising performance in the conversion of 2MPDO to fine chemicals. However, catalyst activity and selectivity changes the liquid product yield and selectivity but reaction condition such as temperature and O_2 concentration have a considerable effect, as well. The proposed kinetic model, however, was simple but accurately predicts 2MPDO conversion, product selectivity and the effect of various parameters. The by-product of the introduced method was syngas, which can be converted into fuel and chemicals.

TABLE OF CONTENTS

LIST OF TABLES

LIST OF FIGURES

LIST OF SCHEMES

LIST OF SYMBOLS AND ABBREVIATIONS

D = axial dispersion, m^2s^{-1}

n = number of tanks in the n–CSTR in series model

Pe = Peclet number of axial dispersion

r_i = reaction rate, $mol\,s^{-1}m^{-3}$

E_{aj} = activation energy, $kcalmol^{-1}$

k_i = reaction rate constant, various units

$R^2_{X,2MPDO}$ = coefficient of determination for 2MPDO conversion

$R^2_{S,MAA}$ = coefficient of determination for MAA selectivity

$R^2_{S,MAC}$ = coefficient of determination for MAC selectivity

R^2_{S,CO_x} = coefficient of determination for CO_x selectivity

S_i = selectivity to compound i

T = reaction temperature, K

t_m = mean residence time, s

U_{mf} = minimum fluidization velocity, $m\,s^{-1}$

U_g = gas linear velocity, $m\,s^{-1}$

X = butane conversion, %

P_i = partial pressure of reactants

P_j = partial pressure of products

F_i = gas flow rate of reactants, $mL\,min^{-1}$

X= active (oxidized) sites over different mechanisms (eqs 4–11)

V = reduced sites over different mechanisms (eqs 9–10)

C_X= concentration of oxidized sites for Mar and Van Krevelen mechanism

C_V= concentration of reduced sites for Mar and Van Krevelen mechanism

C_{2MPDO}= concentration of sites occupied by 2MPDO for Mar and Van Krevelen mechanism

C_V^{C4}= concentration of sites occupied by coke for Mar and Van Krevelen mechanism

K_r= reaction rate constant for reduction step of Mar and Van Krevelen mechanism

K_o= reaction rate constant for oxidation step of Mar and Van Krevelen mechanism

GreekLetters

ϕ = objective function for modeling

β= a portion of active sites occupied by oxygen that reacts with adsorbed 2MPDO

τ= contact time

CHAPTER 1 INTRODUCTION

Oxidation of waste bio–based or low value added materials to specialty chemicals is an attractive chemistry due to fossil reserve depletion and climate pollution. Methyl methacrylate (MMA) is a specialty monomer for poly methyl methacrylate (PMMA) that the demand of MMA will surpass 4.8 million metric tonne by 2020 Global Market Analysts (2016). PMMA (produced from MMA) surpassed 2.8 million tonne annually. Mitsubishi Rayon reported annual growth in demand of more than 0.2 million tonnes (5 % to 6 %) Nagai et Ui (2004); Program (2006); Schunk et Brem (2011). Due to the increasing demand for PMMA, the price of bulk MMA increased by 10 % annually Jing (2012). and its increasing demand motivates industry to develop clean technologies based on renewable resources.

The dominant commercial process reacts acetone and hydrogen cyanide to MMA (ACH route) but the intermediates (hydrogen cyanide, and acetone cyanohydrin) are toxic and represent an environmental hazard. Esterification of methacrylic acid (MAA) to MMA is a compelling alternative together with ethylene, propyne and isobutene/t–butanol as feedstock. However, processes starting from these feedstock suffer from some drawbacks such as short catalyst life time, multi step reactions, extra separation units to separate unreacted raw materials from products, and high amount of byproduct. Partially oxidizing isobutane in a single–step is nascent technology to replace current processes ; however, because the feedstock is isobutane, it must operate at upper flammability area. Then the conversion has to keep low (less than 10 %) and to improve the yield we need to separate and recycle the unreacted isobutane.

Recently, Pyo et al. proposed a bio–process in which 2–methyl–1,3–propanediol (2MPDO) oxidizes to 3–hydroxy–2–methylpropionic acid via 3–hydroxy–2–methylpropanal in micro–organisms and then this intermediate dehydrates to MAA and MAC over titanium dioxide at 210 °C Pyo *et al.* (2012). However, the productivity of this bioroute remains low and expensive due to the enzymes. 2MPDO is a co–product of 1,4–butanediol in the hydroformylation process of allyl alcohol and can be an attractive feedstock to produce MAA Dubois (2014); Mahboub *et al.* (2016a). Therefore, oxidation of 2MPDO to MAA would be an interesting alternative to overcome or diminish the problems of current processes. As such a catalyst that selectively oxidizes 2MPDO to MAA is the main and first step of this new process.

The main objective of this project, then, is to introduce the production of methacrylic acid and methacrolein from 2MPDO as a new route for the polymer-based industry to produce highly valued chemicals while reducing the number of process steps through gas-solids heterogeneous catalysis. Target chemicals are MAA and MAC. Up until now, this processing

route has not been explored.

The synthesizing of highly selective catalyst for deriving these specialty chemicals in one–step reaction has as of late shown to improve the both economics and performance of this process. High conversion and low undesired products (as byproducts) is highly important which affect the economic and environmental impact of the whole process. Also, catalyst deactivation rate is important to improve its performance and product yield.

Gas–liquid reaction over solid heterogeneous catalysts are used widely in the industry (Lioyd, 2011). Reducing the corrosion, separation and deposal problems associated with homogeneous catalysis is the main advantages of heterogeneous catalysis. Porous solid catalysts provide higher surface area that active sites were dispersed uniformly over the surface and thermally stabilize the catalyst structure Fechete *et al.* (2012). A heterogeneous catalyst decreases catalyst expenses and supports in heterogeneous catalysts permit greater efficiency in the use of an expensive metal by increasing the active surface. Normally, a higher surface area offers higher selectivity and activity Bagheri *et al.* (2014).

We conducted all experiments in a micro–scale reactor because of its advantageous such as :

1. Less catalyst consumption
2. Iso–thermal situation
3. On-line monitoring of effluent gas Yu *et al.* (2011b); Munirathinam *et al.* (2015)

Fluidized–bed reactors favor for thermal sensitive materials than fixed-beds that deactivation (carbon deposition) is significant for systems with liquid injection (for gas–solid systems). Homogeneity and well solid mixing are the most other significant advantages of fluidized bed reactors, compared to other types Godefroy *et al.* (2010); Lorences *et al.* (2006). Micro fluidized–bed reactors are suitable to model the system and for kinetics and investigating reaction characteristics Liu *et al.* (2008).

Based on the main objective, oxidation of 2MPDO to MAA and MAC in the presence of heterogeneous catalyst in the micro–fluidized, one of the main issue is to synthesize the selective catalyst to oxidize 2MPDO to these products. Another major challenge is developing a process in accordance with the benefits of gas–solid heterogeneous catalyst's ability to minimize or even eliminate agglomeration and improve performance. A kinetic model helps us to optimize the process and consequently scale up. Therefore, the research is divided into three main parts corresponding to the targeted specific objectives :

– Objective # 1

  1. Synthesize the heterogeneous catalysts that are active, and selectively oxidize 2MPDO to MAA and MAC. The sub–objectives of this imperative include : 1.1- Designing a process

in accordance with the benefits of gas–solid heterogeneous catalysts.

1.2- Synthesize different kinds of catalysts by inserting different metal ions.

1.3- Catalyst characterization to find the correlation among catalysts structure, their properties, products, and reactants.

1.4- Identify the most active and selective catalyst.

– Objective # 2

2. Propose a gas–solid process to partially oxidize 2MPDO in gas phase.

2.1- Identify and optimize an effective process for partial oxidation of 2MPDO.

2.2- Evaluate and test the catalyst performance in oxidation of 2MPDO.

– Objective # 3

3. Derive a kinetic expression that adequately characterizes the reaction kinetics

The last series of experiments consist of data aimed to kinetic modelling. Optimum reaction condition will be predicted and the targets include :

3.1- To study the significantly of each variable : 2MPDO/O_2 concentration ratio, steam flow rate, temperature, and residence time on yield of acids.

3.2- To develop a suitable model for 2MPDO conversion.

3.3- To define a kinetic model for MAA and MAC production.

CHAPTER 2 COHERENCE OF THE ARTICLES

A brief description of the chapters and the link in between is as follows :

Chapter 3 represent a review article about all commercialized or potential approaches to produce methacrylic acid (MAA) and methyl methacrylate (MMA) (as specialty chemicals) from both industrial and scientific sides. Light hydrocarbons (C_2–C_4) are affordable feedstock to produce these compounds ; however, catalytic oxidation of these raw materials suffer from short catalyst life time, multiple reaction step, toxic byproducts and low desired product selectivity. Partially oxidizing isobutane or 2–methyl–1,3–propanediol (2MPDO) over heteropolycompounds to MAA in a single–step is nascent technology to replace current processes. Renewable sources for the MMA or MAA route include acetone, isobutanol, ethanol, lactic, itaconic, and citric acids. End–of–life polymers (PMMA) are expected to grow as a future source of MMA and MAA. This chapter reviewed in details all processes and mechanisms for different feedstock and investigated the effect of each metals, cations, and supports to produce MMA and MAA. The other operating conditions such as feed composition, reaction temperature and catalyst synthesis have been also studied. This field of research has been the focus of many valuable publications and a thorough review of them has been attempted. At the end, this review gives a comprehensive view to the readers to understand the role of active sites on producing MAA. This article is under review by **Chemical Society Review**.

Chapter 4 : The first objective of this study was to evaluate and test different catalysts to oxidize 2MPDO to MAA in a gas–solid fluidized bed reactor. As there is not data available to oxidize 2MPDO to MAA, firstly, it was important to introduce a catalyst able to breakage the C−H bond. We had tested several catalysts containing different active sites dispersed over supports. We found that the Keggin–type heteropolycompounds are the potential alternative in which we inserted metal cations with different ratio (V, Cs, and Cu) to maximize MAA and MAC selectivity. Inserting vanadium into the HPA reduced the Mo^{6+} to Mo^{5+}, and promoting it with copper increased selectivity to MAA but decreased conversion.

More than just studying the catalyst, process performance is important. Feed composition (oxidizing or reducing condition). To maximize acids yield, we evaluated the effect of temperature and 2MPDO :O_2 ratio on 2MPDO conversion and selectivity. We finally proposed a general mechanism for this process in which MAC is the main intermediate. In the first step, oxygen reacts with 2MPDO to form 3–hydroxy–2–methylpropanal. This intermediate dehydrates to MAC in the second step, and finally in the third step oxygen reacts with MAC to form MAA.

Based on our achievements to the initial specific objectives, the first paper is “Gas phase oxidation of 2–methyl–1,3–propanediol to methacrylic acid over heteropolyacid catalysts” which **Catalysis Science and Technology** has published it in 2016.

Chapter 5 is a simulation via artificial neural network based on experimental data published in a first article. A paper entitled “Partial oxidation of 2–methyl–1,3–propanediol to methacrylic acid : Experimental and neural network modeling” has been published by **RSC Advances** (2016). We considered metal ions (V, Cs, and Cu) inserted in catalyst structure and feed composition levels as input layers and counted MAA selectivity as an output layer. We tested different learning algorithm to find an optimum catalyst structure and feed composition. At the end, we evaluated the interaction between metal ions and also 2MPDO/O_2 ratio.

Chapter 6 : This chapter covers two main aspects : the first of is solid understanding of the correlation between catalyst structure and products as an inevitable topic. The second one is studying the effect of calcination temperature on catalyst performance and products selectivities that the results have published in **Applied Catalysis A : General** (2018).

In this paper, we establish the relationship between heteropoly acid performance and calcination temperature at 300 °C and 350 °C. The molybdenum oxidation state was higher after the high temperature treatment but it reduced to a greater extent during reaction (from Mo^{6+} to Mo^{5+}). The higher extent of reduction confirms the higher $O^{2-} \rightarrow Mo^{6+}$ charge–transfer in the Keggin anion. Though, the route of direct dehydration of 2MPDO (C−OH bond cleavage) followed by oxidation to MAC is the most direct path to the products detected, we proposed a mechanism that passes through the homolitic dissociation of the tertiary C−H bond, in reason of the very similar bonding energies.

Chapter 7 : The effects of 2MPDO and O_2 concentrations, wider temperature range, and residence time (τ) on products selectivities and reactant conversion in "Oxidation kinetics of 2–methyl–1,3–propanediol to methacrylic acid" were tested. We performed a full factorial design on operating conditions to develop kinetic modelling. We evaluated different mechanisms and assumed different steps as a rate– limiting step to propose the best model that fits with experimental data. Baed on the model, we predicted the mechanism, activation energy and reaction rate constant of each step that led to a better understanding of the underlying processes. The results of this chapter has been submitted to **Chemical Engineering Journal** (2018).

Chapter 8 is a general discussion and summary of the results.

Chapter 9 summarized the key conclusions and provides recommendations for future studies.

CHAPTER 3 LITERATURE REVIEW - ARTICLE 1 - CATALYSIS FOR THE SYNTHESIS OF METHACRYLIC ACID AND METHYL METHACRYLATE

Mohammad Jaber Darabi Mahboub, Fabrizi Cavani, Jean–Luc Dubois, Mohammad Rostamizadeh, Gregory S Pateince

Submitted to : Chemical Society Reviews (2018)

3.1 Abstract

Methyl methacrylate (MMA) is a specialty monomer for poly methyl methacrylate (PMMA) and its increasing demand motivates industry to develop clean technologies based on renewable resources. The dominant commercial process reacts acetone and hydrogen cyanide to MMA (ACH route) but the intermediates (hydrogen cyanide, and acetone cyanohydrin) are toxic and represent an environmental hazard. Esterification of methacrylic acid (MAA) to MMA is a compelling alternative together with ethylene and isobutene/t-butanol as feedstock. Partially oxidizing isobutane or 2–methyl–1,3–propanediol (2MPDO) over heteropoly-compounds to MAA in a single–step is nascent technology to replace current processes. Here, we describe the role of metals, cations, and supports to produce MMA and MAA. Keggin type–heteropoly compounds with cesium and vanadium are promising catalysts to convert isobutane and 2MPDO to MAA. Renewable sources for the MMA or MAA route include acetone, isobutanol, ethanol, lactic, itaconic, and citric acids. End–of–life polymers (PMMA) are expected to grow as a future source of MMA.

3.2 Introduction and scope

Methyl methacrylate (MMA) is a specialty monomer for poly–methylmethacrylate (PMMA), which is marketed under trademarks Acrylite®, Plexiglas®, Lucite®, Optix®, Perspex®, Oroglas®, Cyrolite®, Sumipex® and Altuglas® and applied in diverse industries including paints and coatings, electronics, as a modifier for PVC, and as bone inserts Nagai (2001); Godfrey (1963); Kung (1994); W.Dormer *et al.* (1998); Smith *et al.* (1999). Demand of MMA will surpass 4.8 million metric tonne by 2020 Global Market Analysts (2016), where Asia–Pacific is the main market in which China ranks first for production and consumption. North America and Europe are ranked second and third, respectively, while the Middle East, Africa, and Latin America are the areas growing the fastest Global Market Analysts (2016). PMMA

(produced from MMA) surpassed 2.8 million tonne annually. Mitsubishi Rayon reported annual growth in demand of more than 0.2 million tonnes (5 % to 6 %) Nagai et Ui (2004); Program (2006); Schunk et Brem (2011). Due to the increasing demand for PMMA, the price of bulk MMA increased by 10 % annually Jing (2012).In 2015, the worldwide demand equalled the global supply capacity Markit (2016); Global Market Analysts (2016).

Academia and industry continue to develop technologies and modify current processes with novel materials, catalysts, and optimizing operating conditions. Web of Science (WoS), indexed over 12 000 scientific manuscripts since 1989 related to MAA/MMA and their applications in polymers, catalyst synthesis and characterization, reaction engineering, kinetics and process and physical chemical properties. China published the most articles and patents followed by USA, Japan, India, and Germany. Bibliometric maps group work streams together in related clusters and demonstrate how major research axes are related between clusters (Fig. 3.1) Eck et Waltman (2010). The four major research clusters for MAA/MMA relate to chemistry/material sciences (red) ; polymers and kinetics (green) ; physical–chemical properties (lime green), and formulation (blue). The size of the circle is proportional to research intensity and in the red cluster, methacrylic acid dominates. Polymerization science—green cluster—is equally important as methacrylic acid. Blending dominates the blue cluster related to formulation and processing while research intensity in the property characterization cluster (lime green) is more equally distributed. The "Journal of Applied Polymer Science" and "Macromolecules" have published the most research in the field.

A dozen technologies are practiced commercially or are under development to produce MAA and MMA with diverse feedstocks ranging from acetone–cyanohydrin (ACH) to light hydrocarbons (Table 3.1) Ballarini *et al.* (2007b); Nagai et Ui (2004).

3.3 ACH process

The ACH process dominates the market, especially in Europe and North America Ballarini *et al.* (2007b); Schunk et Brem (2011). Acetone and hydrogen cyanide (HCN) react to form acetone cyanohydrin ; this intermediate then reacts with excess concentrated sulfuric acid to methacrylamide sulfate. Methacrylamide is then treated with excess aqueous methanol ; the amide is hydrolyzed and esterified forming a mixture of MMA and NH_4HSO_4 Ballarini *et al.* (2007b); Jing (2012). Although this process is economically attractive (especially in Europe), it still suffers from some drawbacks such as the toxic reactant HCN and a large volume of co–product–ammonium bisulphate ($\sim$ 1.2 kg for each kg of MMA) which companies sell as a fertilizer or reprocess to produce H_2SO_4. Producing H_2SO_4 requires additional processing units and investment Cavani (2010); Mizuno *et al.* (1996b); Knapp *et al.* (2001); Deng *et al.*

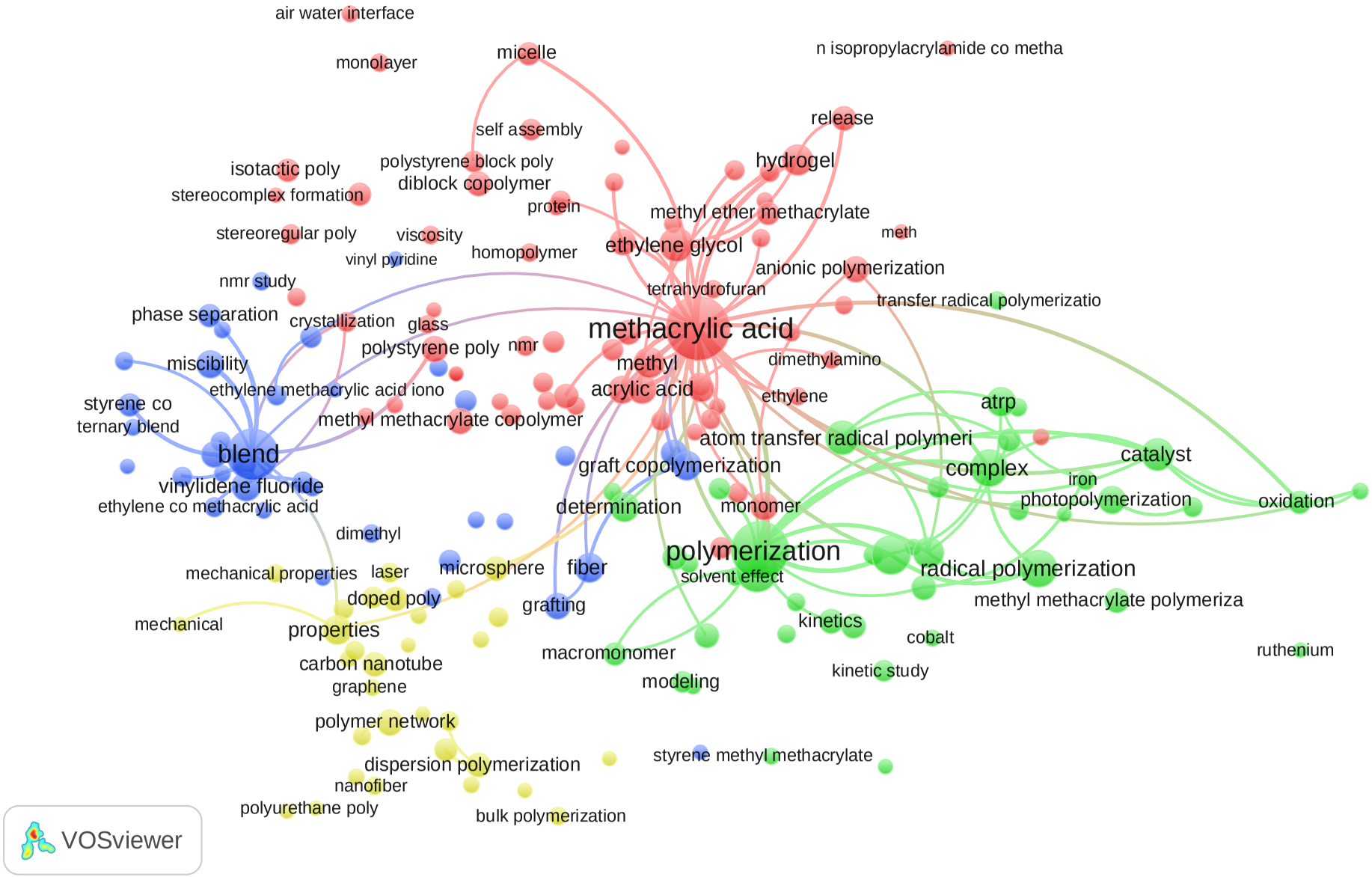

Figure 3.1 VOSViewer journal map for MAA/MMA research since 1954

Table 3.1 Technologies to produce MMA. MAA is the intermediate of some processes after which CH_3OH esterifies it to MMABallarini *et al.* (2007b)

Process	Raw materials (with/without esterification)	Feature, Issue	Catalytic reaction	Producer (Industrialized)
ACH	C_3H_6O, HCN, H_2SO_4	Toxic materials High amount of co–product	———————-	Several companies (1937)
New ACH	C_3H_6O, $C_2H_4O_2$,	Three step reaction No co–products HCN recycle H_2SO_4 process obsolete	Amidation :MnO_2 Esterification : NaOMe Dehydration : Zeolite	Mitsubishi Gas (1997) Chemical
C_2 approach	C_2H_4, CO, H_2, H_2CO,	Carbonylation of ethylene via propionaldehyde, and catalytic condensation with formaldehyde	Condensation : Amine Oxidation : Mo−P	BASF (1989)
Alpha route	C_2H_4, CO, H_2CO,	Uses two C_1 compounds via methylpropionate	Carbonylation : Pd Condensation : Cs/SiO_2	Lucite (2008)
Propyne	C_3H_4, CO,	Lack of feedstock	Catalytic carbonylation : Pd One–step reaction High yield	Shell (Not yet)
Propylene	C_3H_6, CO,	Multi–step reactions	Catalytic carbonylation to isobutyraldehyde + oxidation to isobutyric	Ashland & Atochem (Not yet)
Isobutene (t–butanol) oxidation (with esterification)	C_4H_8, O_2	2 step oxidation reaction and esterification	1^{st} oxidation : Mo−Bi 2^{st} oxidation : Mo−P, Pd−Pb or Au−NiO_x	Mitsubishi Rayon/Asahi Kasei, Sumitomo/Nippon Mitsui/Kuraray (1982)
Isobutene ammoxidation	C_4H_8, O_2, NH_3, H_2SO_4	Via methacrylonitrile Co–product disposal	Ammoxidation : Mo−Bi	Asahi Kasei (1984-1999)
Isobutane process	C_4H_{10}, O_2	One–step process	Oxidation : Mo−P	Several companies (Not yet)
2–methyl–1,3–propanediol	O_2	One-step process	Oxidation : Mo−V−P	Arkema (Not yet)

(2005); Program (2006) (Scheme 3.1).

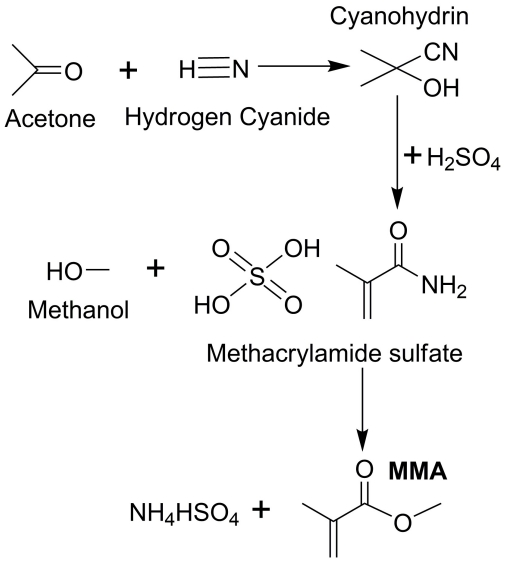

Schème 3.1 – Common ACH approach to produce MMA Nagai et Ui (2004); Cavani (2010)

Mitsubishi Gas Chemical hydrates acetone–cyanohydrin to 2–hydroxyisobutylamide over an MnO_2 catalyst ; the amide reacts with methylformiate forming the methyl ester of 2–hydroxyisobutyric acid over CaO as formamide is a main co–product. Na–Y zeolite dehydrates the ester to MMA. The recycled formamide forms hydrogen cyanide, which reacts with acetone Shuji *et al.* (1994); Kiochi (1999). This improved reaction sequence eliminates byproduct–ammonium bisulphate and generates HCN in situ, which eliminates it as a feedstock (Scheme 3.2). However, catalyst lifetime is the main drawback of this process.

Evonik commercialized the AVENEER process (2015) to produce 120 kt MMA (at an overall yield of 93 %) in which ammonia, methane, acetone and methanol are the feedstocks. AVENEER eliminates sulfuric acid thereby decreasing capital investment and reducing the energy load. It eleminates aluminum bisulphate and thereby cuts CO_2 emissions by nearly 50 %.

Light hydrocarbons—C_2–C_4—are promising feedstocks for MAA and esterification of MAA to MMA, which we detail in the following sections.

3.4 C−2 routes

Crude oil is a source of ethylene by steam cracking or fluidized catalytic cracking (FCC) Rostamizadeh et Taeb (2015, 2016). Ethylene forms MAA and MMA via intermediates including propanal (propionaldehyde), propionic acid or methyl propionate (Scheme. 3.3) Gogate *et al.*

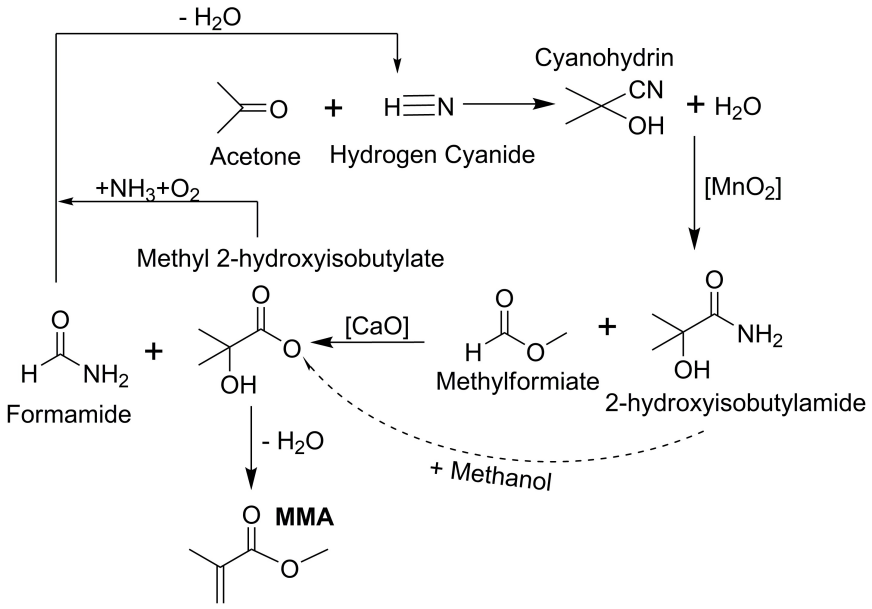

Schème 3.2 – Improved ACH method to produce MMA proposed by Mitsubishi Gas Shuji *et al.* (1994); Kiochi (1999)

(1997).

Hydroformylation of ethylene over cobalt or rhodium catalyst produces propionaldehyde. In the liquid phase with a secondary amine, propanal reacts with formaldehyde. Cracking of the Mannich base intermediate of the reaction produces methacrolein (MAC), which then oxidizes to MAA Considine (2006). Alternatively, the crossed aldol condensation with formaldehyde in the gas phase and over a molecular sieve forms MAC that oxidizes to MAA Considine (2006). “BASF” and “Alpha” are the two main processes to produce MMA and MAA from C_2 hydrocarbons.

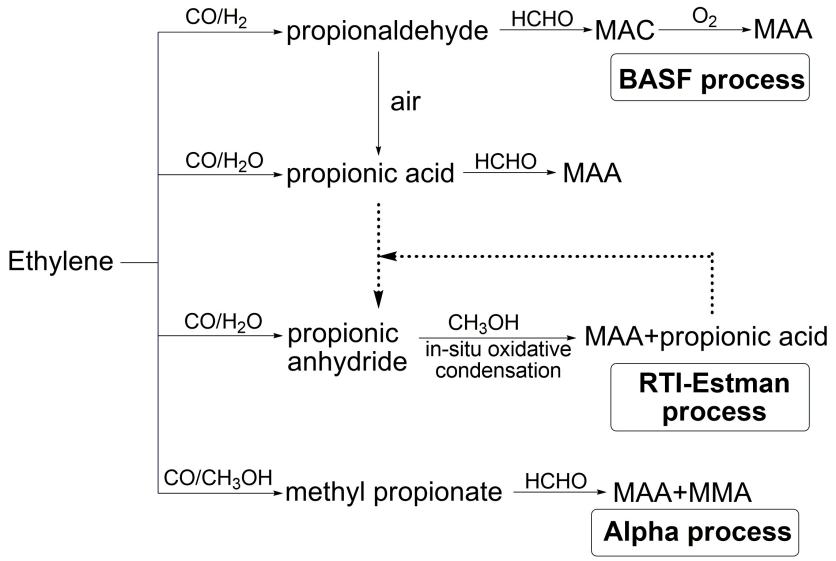

Schème 3.3 – Possible Processes to produce MAA and MMA from ethylene Considine (2006). Reprinted with permission from Considine (2006) Copyright 1997 Elsevier B.V.

3.4.1 BASF process

BASF produced MAA and MMA from ethylene in the presence of carbon monoxide and hydrogen (Scheme. 3.4) Nagai (2001) :

1. Hydroformylation of ethylene to propionaldehyde
2. Condensation with formaldehyde to MAC
3. Oxidizing MAC to MAA
4. Esterification of MAA to MMA

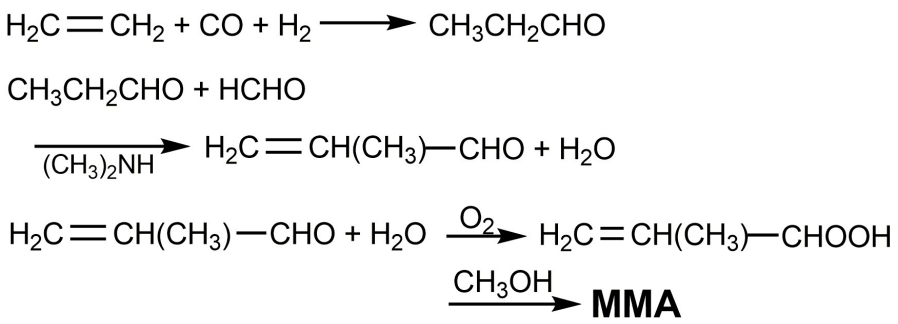

Schème 3.4 – MAA and MMA production from ethylene–BASF process Nagai (2001)

They claimed high MAC selectivity (99 %) but the main disadvantages were the high cost of the oxidation step, low yield, and low single pass conversion Merger et Foerster (1983); Duembgen *et al.* (1985); Sugiyama *et al.* (2009). Amoco Co. developed a gas phase process

including molecular sieve catalysts in which 57 % of the propionaldeyde reacted at 98 % MAC selectivity Hagen (1984). They commercialized the technology in Germany (1989) and produced 40 kt MMA/year and 5 kt MAA/year.Nagai (2001)

3.4.2 Alpha process

Lucite (formerly ICI, then INEOS, and now Mitsubishi) developed the ethylene-based "Alpha process" that converts ethylene to methyl propionate through methoxycarbonylation coupled carbonylation and esterification (Scheme 3.5) Nagai et Ui (2004).

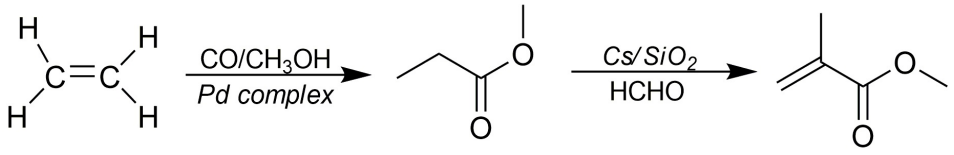

Schème 3.5 – Alpha process reaction schemeNagai et Ui (2004)

The raw materials are ethylene, carbon monoxide, methanol and formaldehyde. Methyl propionate reacts with formaldehyde over a Pd homogeneous catalyst in close to anhydrous conditions to form MMA Cavinato et Toniolo (2014). Bin et al. Bin *et al.* (2014) developed a SBA–15 metal–doped cesium ion catalyst that converts methyl propionate with formaldehyde to MMA in the gas phase. The optimum catalyst composition consists of a mass fraction of 15 % Cs–loading (15 % Zr–Fe–Cs/SBA–15) as a promoter and achieved 24 % MMA yield at 94 % conversion after 3.5 h time–on–stream Bin *et al.* (2014). Gogate et al. Gogate *et al.* (1997) reported a high yield of MAA (56 %) over a V–Si–P catalyst for the aldol condensation of methyl propionate with formaldehyde at 300 °C and 2 bar. The catalyst atomic ratio of V :Si :P was 1 :10 :2.8.

Methyl propionate reacts with formaldehyde over Cs/SiO_2 to MMA at 14 % conversion and 86 % selectivity.Ai (2005) Solid base catalysts promote vapor–phase aldol condensation of methyl propionate with formaldehyde (Table 3.2) .

A cesium hydroxide catalyst produced the most MMA+MAA (85 % selectivity at 19 % methyl propionate conversion) at a Cs/Si atomic ratio of 0.02 (Fig. 3.2). Although, increasing the Cs content favored MP conversion, it decreased selectivity Ai (2005).

Table 3.2 Effect of promoters on silica supported catalyst performance in the vapor–phase aldol condensation of methyl propionate with formaldehyde.Ai (2005)

Promoter	Based on methyl propionate feed, %	
	Conversion	MMA+MAA Selectivity
Mg	11	28
Ca	6	34
Ba	7	36
Na	10	17
K	15	54
Rb	15	68
Cs	14	86

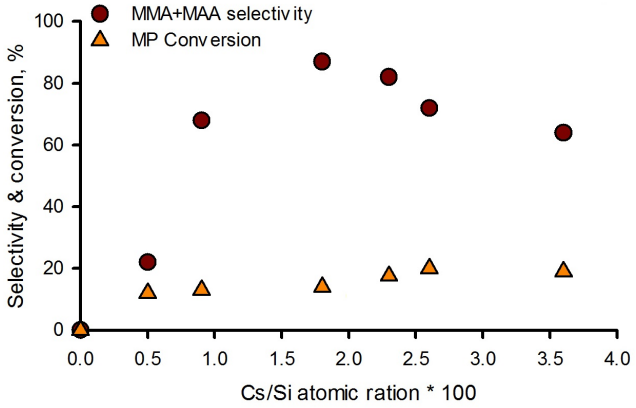

Figure 3.2 Effect of Cs/Si ratio over silica–supported cesium hydroxide catalyst on MMA+MAA selectivity and methyl propionate (MP) conversion with molar ratio of MP/HCHO/methanol/water= 1/0.2/1.5/0.5 at 360 °C Ai (2005)

Silica minimizes side reactions and produces more MMA+MAA compared to other supports (Table 3.3). Silica–alumina and zeolite 13X supports promote methanol dehydration to dimethyl ether over acid sites but overall selectivity and yield are lower versus silica.Ai (2005) $Ca(OH)_2$ support is very active and hydrolyzes the methyl propionate completelyAi (2005).

Co–feeding water (10 vol %) decreases both the reaction rate and MMA+MAA selectivity (Fig. 3.3). MMA hydrolyzes in water to MAA and methanol Ai (2005). Both MMA and MAA yields increased with temperature from 320 °C to 380 °C with and without water (Fig. 3.3).

Table 3.3 Performance of different catalyst supports Ai (2005)

Support	Based on methyl propionate feed, %	
	Conv.	MMA+MAA Sel.
SiO_2	14	85
SiO_2–Al_2O_3	16	30
Al_2O_3	6	27
Zeolite 13X	15	0
SiC	2	0.0
Active carbon	11	6
$Ca(OH)_2$	99	0

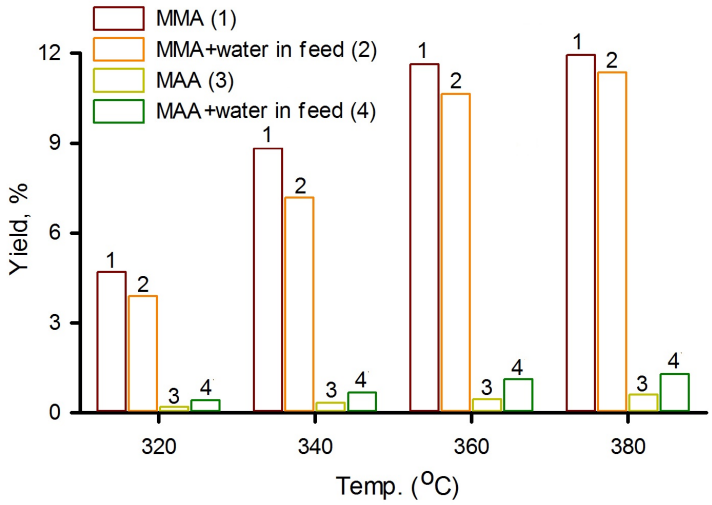

Figure 3.3 Effect of water addition in the reactor feed on MMA and MAA yield over silica–supported cesium hydroxide catalyst at 360 °C Ai (2005)

Ai Ai (2006) studied the reaction of methyl propionate and methanol in the vapour phase over Ag–Zr–Cs/SiO_2 catalyst at an atomic ratio of 4/10/22/1000 which converts MeOH to HCHO in the presence of oxygen at 360 °C . Ag–Zr–Cs/SiO_2 catalyst deactivated after 20 h on stream operating at 360 °C and feed rates of 50/75/250 mmol/h (methyl propionate/methanol/N_2) (Scheme 3.6–Fig. 3.4). High contact time favors MMA because the oxidative dehydrogenation of methanol is faster than the aldol–condensation reaction Ai (2005).

From an industrial point of view, the key problems of the C_2 routes are the low conversion and short catalyst lifetime; however, MAA selectivity is good Nagai (2001). An advantage of the process is that it produces no MACEastham *et al.* (2013). Alpha technology was commercialized in 2008 with a 100 kt y^{-1} MAA plant in Singapore and a joint venture

between Lucite International and SABIC is building a 250 kt y^{-1} MAA plant Nagai et Ui (2004).

$$CH_3CH_2COOCH_3 + CH_3OH \longrightarrow H_2C{=}C(CH_3)COOCH_3 + H_2O + H_2$$

$$CH_3CH_2COOCH_3 + CH_3OH + 0.5O_2 \longrightarrow H_2C{=}C(CH_3)COOCH_3 + 2H_2O$$

Schème 3.6 – Direct conversion of methyl propionate and methanol to MMA Ai (2006)

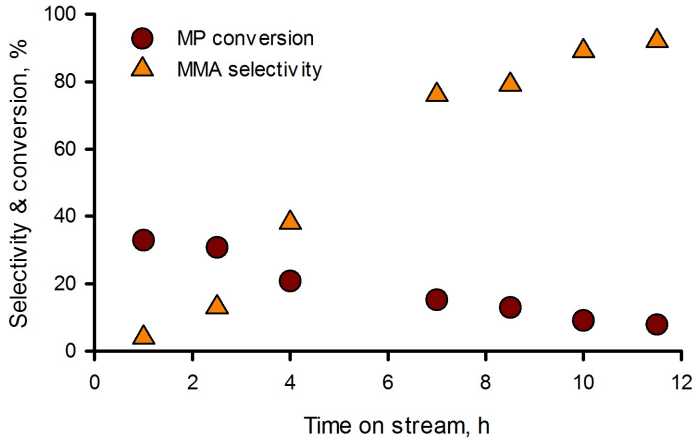

Figure 3.4 MMA selectivity and MP conversion with time on stream over Ag–Zr–Cs/SiO_2 catalyst (with an atomic ratio of 4/10/22/1000) and a feed rate of methyl propionate/methanol/N_2= 50/75/250 mmol/h at 360 °C Ai (2006)

3.4.3 Research Triangle Institute (RTI)–Eastman–Bechtel route

Metal carbonyl catalyst converts ethylene to propionic acid in Reppe's hydroxycarbonylation reaction. Propionic acid and formaldehyde react to form MAA (Scheme 3.7) Nagai (2001). This process has only three reaction steps, which is a considerable advantage over other processes and commercialization is likely Spivey *et al.* (1997) :

1. Hydroxycarbonylation of ethylene to propionic acid
2. Condensation with formaldehyde to MAA
3. Esterification of MAA to MMA

MAA selectivity is higher in the Alpha process but capital costs are lower in the Eastman–Bechtal route (Scheme 3.7). Furthermore, catalyst lifetime is short Spivey *et al.* (1997).

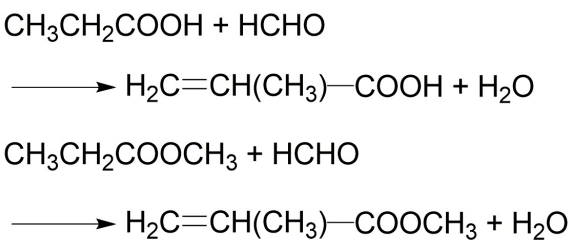

Schème 3.7 – Reaction steps of the RTI–Eastman–Bechtel route Nagai (2001)

It operates in the gas phase between 300 °C to 400 °C over acid or base heterogeneous catalysts Tai et Davis (2007); Ai *et al.* (2003). Amoco reported 91 % MAA selectivity at 39 % propionic acid conversion over a Cs/SiO_2–SnO_2 catalyst Montag et Mckenna (1991). Mitsubishi Rayon Co. Ltd developed a Si–Cs–W–Ag–O catalyst for which MAA selectivity was 98.8 % at 41 % propionic acid conversion Nagai (2001). Toagosei Co. Ltd. synthesized a V–P–O/Zr–Al–O catalyst for which the MAA selectivity was 66 % with a formaldehyde conversion of 68 % Hiroshi *et al.* (1987). Nb/SiO_2 and Ta/SiO_2 catalysts have been developed for condensation reactions in the gas phase Spivey *et al.* (1997). Daicel Co. reported propionic acid conversion over an acid catalyst in the liquid phase at 180 °C for 1 h Nagai (2001). The catalyst was a mixture of aluminum propionate and formaldehyde, and 5MAA yield reached 24 %.

Acid catalysts for condensation reactions include metal oxides like vanadium–phosphorous oxides–$V_2O_2(P_2O_7)$, Nb_2O_5 and Ta_2O_5 Gogate *et al.* (1997); Wierzchowski et Zatorski (1991). Base catalysts include alkali metal oxides or alkaline metal oxides supported on silica or zeolite Ai *et al.* (2003); Junhui *et al.* (2006).

3.4.4 LiMA process

Evonik developed the so called LiMA process (Leading in Methacrylates) based on C_2 hydrocarbons. MMA yields are as high as 90 % under mild conditions (liquid phase) and low CO_2 emissions (2.6 t per MMA tone). The main feedstocks for the LiMA process are ethylene and methanol. The process includes the following steps :

1. Reacting ethylene and synthesis gas to produce propionaldehyde (Hydroformylation step) ;
2. Oxidizing methanol to formaldehyde ;
3. Converting propionaldehyde and formaline to form MAC (Mannich condensation step) ; and,
4. Esterification of MAC with methanol to produce MMA.

Evonik piloted the process in Darmstadt (Germany) and now produces 160 000 kt per year.

3.5 C−3 routes

3.5.1 Propane

Carbonylation of propane to isobutryaldehyde remains an option to produce MMA but so far propane as a feedstock has had little success.Luzgin *et al.* (2000) Sulfated zirconia catalyst carbonylates propane with CO to isobutyraldehyde and isobutyric acid between 100 °C and 150 °C Luzgin *et al.* (2004). Low temperature favors isobutyraldehyde and selectivities reach 76 % at 100 °C Luzgin *et al.* (2004). An alternative is to produce acetone from propane via methane–oxidizing methylomonas biocatalyst (sp. DH–1), for example Hur *et al.* (2017). Average and specific acetone productivity of 0.678 mmol h^{-1} and 0.141 mmol h^{-1} g^{-1} cell have been demonstrated. Photo–oxidation of propane over molybdenum oxides supported on mesoporous alumina also produces acetone and propene Ichikuni *et al.* (2013). Mononuclear TiO_x with an Au promoter partially oxidizes propane to acetone at 30 % selectivity Mashayekhi *et al.* (2014).

3.5.2 Propylene

Propylene–as a raw material– requires adding a carbon atom to form a four–carbon methacrylate back–bone and include Mizuno *et al.* (2008); Millet et Védrine (2001) :

1. Hydroxy carbonylation of propylene to isobutyric acid
2. Oxidative dehydrogenation of isobutyric acid to MAA
3. Esterification of MAA to MMA

Research to carbonylate olefins over heterogeneous catalysts began in the early 1930s. Catalysts comprise : Carpenter (1933a,b).

1. Metal complexes including polymers, amorphous oxides or zeolites and support ;
2. The analogues of liquid strong–acid catalysts.

Propylene carbonylation produces both n–butyric and isobutyric acid. To minimize the costs and the complication of separating propylene, isobutryic acid, and MAA require high isobutyric acid selectivity in the first step and full conversion in the third step. Lower temperature favors higher isobutyric acid selectivity (54 %) over 5 % Pd on activated carbon (Table 3.4) Stepanov (2002).

Impregnating Pd (active phase) on zeolite carbonylates propylene in the liquid phase : 1 %Pd/0.8CaNaY and 1 %Pd/HMOR catalysts reached 97 % and 99 % conversion and isobutyric acid selectivity was 48 % and 51 %, respectively (Table 3.5) Stepanov (2002).

Table 3.4 Propylene carbonylation over 5 % Pd/C catalyst Stepanov (2002)

Temp., °C	C_3H_6 conversion, %	i$-C_4H_{802}$ selectivity, %
100	98	54
120	99	51
150	100	50
200	100	45

Table 3.5 Propylene carbonylation over different zeolite supports Stepanov (2002)

Catalyst	Propylene conversion, %	Isobutyric acid selectivity, %
1 %Pd / 0.8 CaNaY	97.0	47.7
1 %Pd / HMOR	99.0	51.0

Propylene conversion and isobutyric acid selectivity were 55 % and 29 %, respectively over palladium sulfonate catalyst ($\frac{P}{Pd} = 4$) Waller (1983). Chem System Inc. developed a BF_3 catalyst complex ($BF_3 \cdot H_2O$) to carbonylate propylene for which the isobutyric acid selectivity was 98 % at 50 °C and 60 bar Jung et Peress (1981). Röhm Gmbh reached maximum isobutyric acid yield (94 %) over hydrogen fluoride at 120 °C Besecke *et al.* (1984).

Atochem and Rohm and Haas proposed a mechanism to produce MAA from propylene via isobutyric acid (Scheme 3.8) Nagai (2001). The first step is the Koch reaction that operates at low temperature. Low isobutyric acid yield and catalyst lifetime hinders its commercialization Nagai (2001). Mixed oxides (Fe–P–O) and heteropoly acids (Mo–P–O, Mo–P–V–O) perform well for the second reaction (isobutyric acid to MAA). Aboukais *et al.* (1994); Watzenberger *et al.* (1990); Bayer *et al.* (1996); Lee *et al.* (1997); Roch-Marchal *et al.* (2000a); Laronze *et al.* (2003); Roch-Marchal *et al.* (2000b); Marchal-Roch *et al.* (2000); Toshiaki *et al.* (2013)

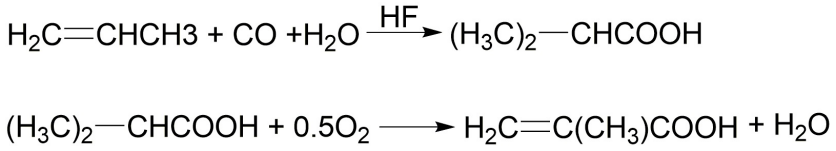

Schème 3.8 – Reactions for propylene-based production of MAA

Sugiyama et al. calculated the Net Present Value (NPV) and Cumulative Energy Demand (CED) to produce MAA from ethylene and propylene (Tables 3.6–3.7) Sugiyama *et al.* (2009). They also considered global warming, acid rain and particle emissions in their analysis. The process produces steam, which is a benefit with respect to CED but overall costs may still

be too high to be commercially viable. Raw material costs with ethylene are lower and it produces more steam compared to propylene. However, other costs and investment are higher so the economics of the C−3 process are better with a production cost of 0.9 $/kg MMA.

3.5.3 Propyne

Shell developed propyne-based technology with MMA yield of 99 % in a single step reaction (Scheme 3.9) Drent (1988). This technology now belongs to INEOS.

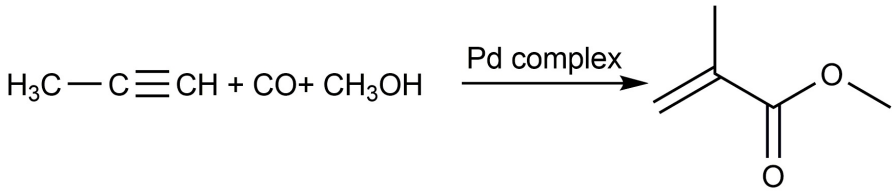

Schème 3.9 – Reactions for propyne–based production of MAA Mizuno *et al.* (2009); Drent (1988)

The methoxy carbonylation reaction includes propyne, carbon monoxide and methanol and group VII metal catalyst systems like palladium acetate, organic phosphine and a protonic acid Mizuno *et al.* (2009); Drent *et al.* (1994). Sumitomo Chemical Co. proposed a hybrid process that coupled producing and converting propyne Mizuno *et al.* (2009). The process includes thermal decomposition of hydrocarbons with three or more carbon atoms at 400 °C to 1100 °C and 0.05 MPa to 0.3 MPa that forms at least a mass fraction of 2 % propyne and propadiene in the effluent. Several distillation and isomerization steps separate and purify the propyne Mizuno *et al.* (2009). Catalyst for the carbonylation step contains 0.01 % or less palladium and a ligand like diaryl (alkyl–substituted 2–pyridyl) phosphine Mizuno *et al.* (2009). The maximum reaction temperature is 100 °C to limit MMA polymerization. The conversion of propyne and yield of MMA were 66 % and 73 %, respectively Mizuno *et al.* (2009). The key limitation of the propyne approach is the limited supply of propyne. Thermal decomposition of naphta and ethane produce only 23–33 kt and 1 kt propyne per 1000 kt ethylene, respectively Mizuno *et al.* (2009).

Table 3.6 Operating costs of C−2 and C−3 routes to MAA (2009) Sugiyama *et al.* (2009)

Route	Raw material cost*	Catalyst cost*	Steam cost*	Others cost*	Income by produced steam*	Total*
Propylene	ca. -0.9	ca. -0.05	ca. -0.01	ca. -0.06	ca. +0.06	ca. 0.9
Ethylene	ca. -0.7	ca. -0.2	ca. -0.1	ca. -0.18	ca. +0.18	ca. 1

*units are ($/kg MMA)

Table 3.7 Investment and overall costs of C−2 and C−3 routes to MAA : 100 kt annual production Sugiyama *et al.* (2009)

Route	Ethylene	Propylene
Cradle–to–gate CED (MJ–eq/kg MMA)	98	ca. 90
NPV (million $)	120	115
Investment cost (million $)	205	290

Environmental issues, process yield, costs related to raw materials, operation, waste removal, and capital are limiting factors to commercializing these processes Considine (2006). Like the ethylene process, catalyst lifetime is short and process yields are low Considine (2006).

3.6 C−4

3.6.1 Isobutene/t-butanol routes

Nippon Shokubai Kagaku Kogyo Co. Wilczynski et Juliette (2011); Kurimoto *et al.* (1989); Nagai et Ui (2004) proposed oxidizing isobutylene to MAA and MMA in 1982, and Mitsubishi Rayon Co. quickly followed with an alternative in 1983 (Scheme 3.10) Oh-Kita et Taniguchi (1992); Nagai et Ui (2004). Japan Methacrylic Monomer Co. (a joint venture of Nippon Shokubai and Sumitomo Chemical Co.) established a plant to produce MAA and MMA from isobutylene in 1984. Asahi (in 1998) and Thai MMA (in 1999) built several plants to oxidize isobutene to MAA and MMA Wilczynski et Juliette (2011); Nagai et Ui (2004) : in the first step of the two step process, MAC forms from either isobutene or tert-butyl alcohol. In the second step MAC oxyesterifies to MMA. Recently, Evonik filed a patent to produce MMA by esterification during oxidation Balduf (2008).

Matar et al. also studied this three step process in which bismuth molybdate partially oxidizes isobutene to MAC at between 350 °C to 400 °C and atmospheric pressure. Heteropoly compounds catalysts MAC to MAA between 250 °C to 350 °C followed by esterification of MAA to MMA (Scheme 3.10) Matar et Hatch (2001).

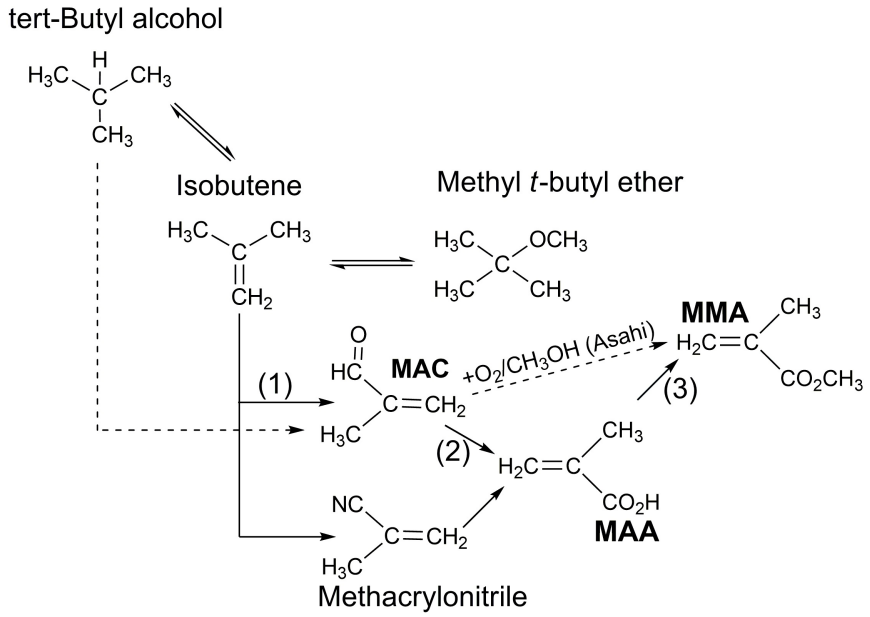

Schème 3.10 – Process of oxidation of isobutene to MMA/MAA Wilczynski et Juliette (2011); Matar et Hatch (2001)

At 380 °C, vanadium pyrophosphate (VPP) converts 33 % isobutene at a MAC selectivity of 24 % and MAA selectivity 16 % Guan *et al.* (2008c). The V^{5+} ions on the surface promote the formation of MAC but high V^{5+} on the surface can also oxidize MAC further.

Corberan et al. tested the MoO_3-UO_3/SiO_2 catalyst in an isothermal reactor in the range of 320–380 °C. Selectivity to MAA was less than 1 %. They proposed the following mechanism (Scheme. 3.11) Corberán *et al.* (1984).

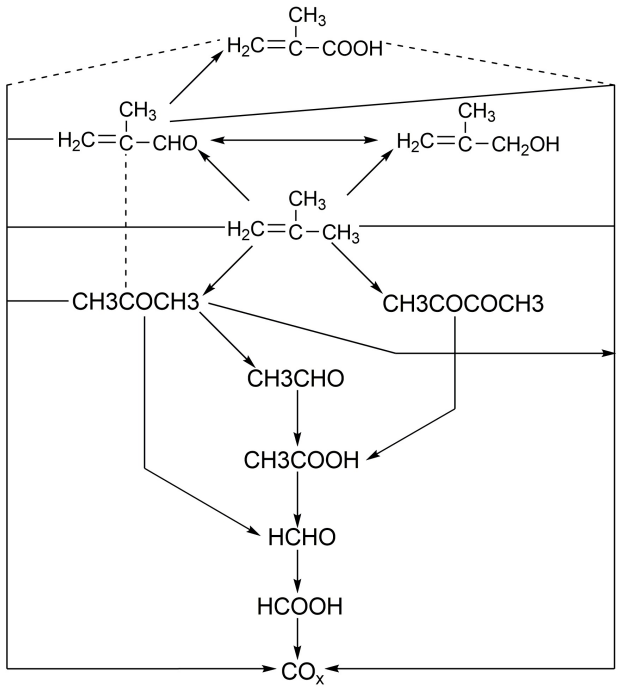

SCHÈME 3.11 – Reaction network of isobutene to MAA over $MoO_3{-}UO_3/SiO_2$ Corberán *et al.* (1984). Reprinted with permission from ref. 75 Copyright 1984 American Chemical Society.

An iron cobalt potassium molybdate catalyst (Co−Fe−K−Mo) reached a MAA+MAC yield of 10 % Breiter et Lintz (1995). Adding bismuth tungstate (a mass fraction of 27 % BiW_2O_x) increased the yield to 67 % with an isobutene conversion of 92 % at 420 °C (Fig. 3.5) Breiter et Lintz (1995).

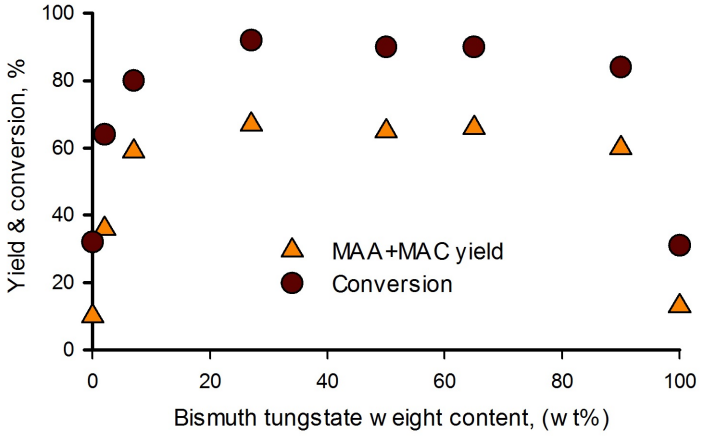

Figure 3.5 Effect of BiW_2O_x content in $Fe_{0.35}Co_6K_{0.5}Mo_{12}O_x$ on isobutene conversion and MAA+MAC yield over isobutene/O_2/inert= 5 %/10 %/85 % Breiter et Lintz (1995)

Peng et al., tested $CsFeCoBiMnMoO_x$ catalysts at around 350 °C. In the first step of their process, Mo−Bi catalyst oxidizes isobutene to MAC and in the second step, P−Mo heteropolyacid structured catalysts oxidize MAC to MAAPeng *et al.* (2004). The isobutene conversion increased with temperature from 34 % to 98 % Peng *et al.* (2004). However, the selectivity to MAC was invariant (∼ 80 %) ; so, MAC yield increased from 28 % to 80 %. The maximum yield to MAC and MAA was 80 % and 8 %, respectively over $Cs_{0.1}Fe_2Co_6BiMnMo_{12}O_x$. They proposed a mechanism in which isobutene chemically adsorbs to the surface. The catalyst extracts α–hydrogen atoms then inserts oxygen Peng *et al.* (2004). They suggested that Bi^{3+} cations accelerate these steps. Both iron and molybdenum promote oxygen exchange between the gas phase and surface following a redox couple– Fe^{3+}/Fe^{2+} and Mo^{4+}/Mo^{2+} (Scheme 3.12) Peng *et al.* (2004).

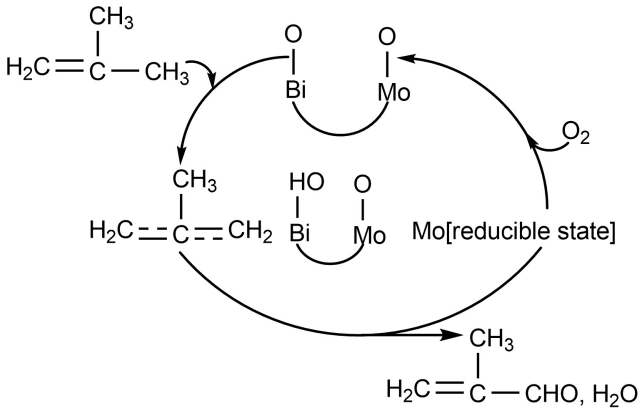

Schème 3.12 – Reaction schematic for the proposed redox recycle Peng *et al.* (2004)

MoO_3 was a poor catalyst and the maximum MAA and MAC selectivity were 1.3 % and 38 %, respectively Guan *et al.* (2008a). Adding vanadium increased selectivity of MAA and MAC to 2.6 % and 49 %, respectively Guan *et al.* (2008a,d). Increasing the vanadium content beyond $MoV_{0.3}$ decreased conversion and selectivity. Other studies confirmed this trend and achieved MAA and MAC selectivity of 1.9 % and 27 %, respectively, at 52 % conversion Guan *et al.* (2009a, 2008b). Adding tellurium–$MoV_{0.3}Te_{0.25}$– increased conversion to 69 % at 420 °C and improved MAA and MAC selectivity to 3 % and 65 %, respectively (Table 3.8) Guan *et al.* (2009a). Data confirmed the positive effect of Te^{4+}–containing phases on the oxidation of isobutene to MAA and MAC.

Guan et al. studied the effect of cerium–$MoTe_{0.23}Ce_{0.2}$, $MoV_{0.23}Ce_{0.2}$ and $MoV_{0.3}Te_{0.23}Ce_{0.2}$– and found that the MAC was the primary product for all catalysts and its selectivity increased gradually with decreasing isobutylene conversion Guan *et al.* (2007c). Adding cerium to $MoV_{0.3}Te_{0.23}$ improved catalytic performance because of the higher Mo^{6+}/Mo^{5+} surface ato-

Table 3.8 Effect of tellurium content in $MoV_{0.3}Te_x$ catalysts on isobutene conversion and product selectivity Guan *et al.* (2009a)

x	Conversion, %	Selectivity, %			Sum of yield, %
		MAA	MAC	CO_x	MAA+MAC
0	52	1.9	27	46	15
0.15	71	2.2	40	41	30
0.17	77	2.3	43	37	35
0.2	75	2.4	52	32	41
0.23	70	2.6	58	27	43
0.25	69	2.9	65	23	46
0.3	48	1.4	57	30	28
0.35	46	1.3	56	31	26
0.4	46	1.2	55	32	26

mic ratio at high reactant conversion. They proposed that Mo^{6+} is involved in the selective oxygen insertion of olefinic intermediates Guan *et al.* (2007c).

The MAA and MAC selectivity varied with cations in the $PVMo_{11}(O_{40})^{4-}$ anion structure. The cations were ranked in terms of selectivity as follows : $K^+ > NH_4^+ > Cs^+ > Ti^+$ Dayun *et al.* (2000). Adding arsenic to $H_3PMo_{12}O_{40}$ increased MAA yield and decreased byproducts. Adding potassium and vanadium to the $PMo_{12}As_{0.6}Cu_{0.1}O_x$ structure affects catalyst performance. $K_{0.33}V_{0.11}PMo_{12}As_{0.6}Cu_{0.1}O_x$ was the best for which MAA and MAC yields were 20 % and 48 %, respectively under optimal reaction conditions (Table 3.9) Dayun *et al.* (2000).

Precipitation of $K(NH_4)_2PMo_{12}O_{40}$ over $FeO_{1.5}$ (as a support) increased MAA and MAC selectivities that reached 21 % and 14 %, respectively at 11.5 % isobutene conversion and 350 °C Busca *et al.* (1996).

From the process point of view, oxidizing isobutylene to MAA suffers from short catalyst

Table 3.9 MAA and MAC yields over $K_yV_zPMo_{12}As_{0.6}Cu_{0.1}O_x$ Dayun *et al.* (2000)

Catalyst	Yield, %		
K_yV_z	MAA	MAC	CO_x
$K_{2.41}V_{0.96}$	17	30	36
$K_{0.54}V_{0.17}$	12	35	46
$K_{0.33}V_{0.11}$	19	48	20
$K_{0.21}V_{0.07}$	13	43	32
$K_{0.16}V_{0.11}$	12	46	34

lifetime, higher separation costs, and power for compression ; but the exothermic reaction allows for heat recovery Nagai et Ui (2004).

In a two step process with isobutene/t-butanol feedstocks, MAC reaches high selectivity (first step) while minimizing MAA because full conversion of the C_4 substrate eliminates a separation step. The main difficulty remains to convert all the MAC produced in the first step to MAA in the second step. This process produces less than the other C_4 processes because the second step runs at low temperature to achieve high selectivity.

3.6.2 Oxidation/Oxidative estrification of MAC to MAA/MMA

MAC is the main intermediate to produce MAA ; however, the yield of MAC → MAA is low ; therefore synthesizing a proper catalyst to maximize selectivity and conversion is necessary Naitou *et al.* (2010). Keggin–type heteropolycompounds catalysts are promising for this reaction where partially inserting cesium changes the structure and catalytic performance Xiaojun *et al.* (2008); Aoki (1998); Kozhevnikov (1998). Increasing Cs increased the surface area and decreased the acidity and reducibility of $H_{3.2-x}Cs_xCu_{0.25}As_{0.1}PMo_{11}VO_{40}$ (x=0–2.5) in the oxidative-esterification reaction (Table 3.10).

Table 3.10 Catalytic activity in the conversion of MAC to MMA and MAA over $H_{3.2-x}Cs_xCu_{0.25}As_{0.1}PMo_{11}VO_{40}$ catalysts Xiaojun *et al.* (2008)

x	MAC Conversion, %	MMA Selectivity, %	MAA Selectivity, %
0	60	39	28
0.5	85	45	38
1.5	93	45	46
2.5	89	31	56

Illies et al. studied the effect of operating conditions over $Cs_1Mo_{12}P_{1.5}V_{0.6}Cu_{0.5}Sb$ on MAC conversion and MAA selectivity. High temperature (<320 °C) favors MAC conversion and MAA selectivity (Fig. 3.6) Illies et Kraushaar-Czarnetzki (2016).

Co–feeding acetic acid at 300 °C had no effect on MAC conversion or MAA selectivity Illies et Kraushaar-Czarnetzki (2016) but water vapor in the feed decreased MAA degradation on active sites Kim *et al.* (1985); Jaroslav *et al.* (1993); Misono (2001). The stoichiometric feed ratio (MAC :O_2= 1 :0.5) is insufficient to achieve 100 % MAA selectivity. High oxygen concentrations favor MAA selectivity and MAC conversion. MAC conversion dropped from 81 % to 63 % after 192 days.

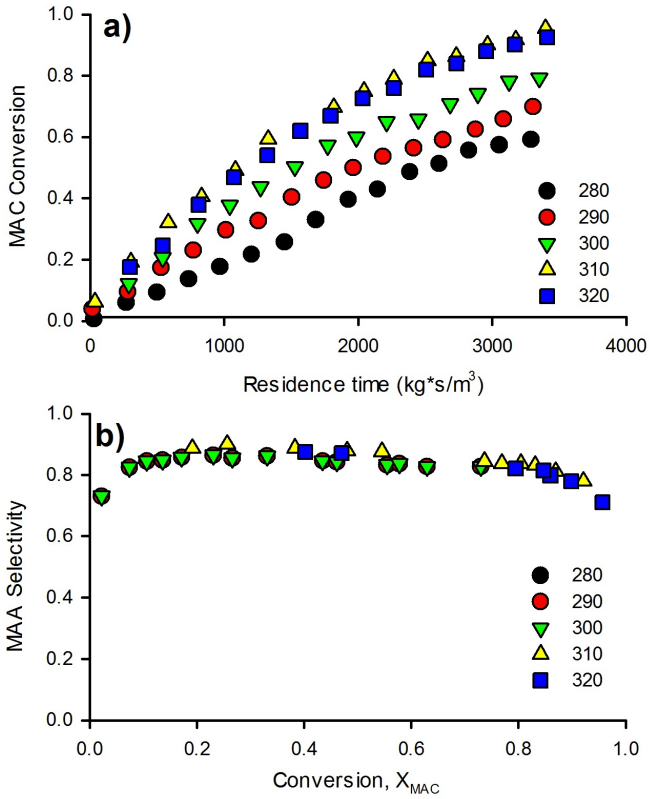

Figure 3.6 MAC conversion versus MAA selectivity at temperatures, 3.4 % V/V MAC and MAC :O_2=1 :2 Illies et Kraushaar-Czarnetzki (2016)

NH_4^+ ions in the catalyst structure ($Cs(NH_4)_xH_{3-x}PMo_{11}VO_{40}$) influence the surface area, acidity and active species (V^{4+}/VO_4) Cao *et al.* (2017). At an intermediate concentration of ammonium (x=1.5), MAA selectivity and MAC conversion were highest at 93 % and 83 %, respectively. Both conversion and selectivity were stable during 100 h of reaction (Fig. 3.7) Cao *et al.* (2017).

Cu– and Fe–doped acidic cesium salts of molybdovanadophosphoric acids ($CsH_3PMo_{11}VO_{40}$) were calcined at 360 °C for 12 h in air or N_2 Zhang *et al.* (2013). Cu and Fe doping favored the redox properties and selective oxidation of MAC to MAA (Table 3.11) Zhang *et al.* (2013).

Table 3.11 Catalytic activity of catalysts in selective oxidation of MAC to MAA Zhang *et al.* (2013)

Catalyst	Ammonium source	Calcination atmosphere	MAC Conversion, %	MMA Selectivity, %
CsCuFePMoV	—-	air	60	46
		N_2	73	58
CsCuFePMoV–NV	NH_4VO_3	air	86	87
		N_2	91	83
CsCuFePMoV–NN	NH_4NO_3	air	73	68
		N_2	88	75
CsCuFePMoV–NH	NH_3(25 wt%)	air	77	85
		N_2	82	90
CsCuFePMoV–NV	NH_4VO_3	air	60	77

Calcining in N_2 reduced the MoO_3 phase concentration of the CsCuFePMoV–NN but it disappeared entirely in the CsCuFePMoV–NH catalyst, which improved activityZhang *et al.* (2013). Zheng et al., studied transition metal (M=Fe, Co, Ni, Cu, Zn) insertion into heteropoly compounds– $Cs_1M_{0.5}{}^{x+}H_{3-0.5x}P_{1.2}Mo_{11}VO_{40}$ and $Cs_1Cu_yH_{3-2y}P_{1.2}Mo_{11}VO_{40}$ (y= 0.1, 0.3, 0.7) Yanxia *et al.* (2016). The metal–doped catalysts represented the Keggin structure and the catalysts with Fe and Cu promoters included cubic secondary structures while Co, Ni or Zn promoters produced both triclinic and cubic phases Yanxia *et al.* (2016). Metal doping changed the acidity of heteropoly compounds in the following order Yanxia *et al.* (2016) : $Cs_1H_3P_{1.2}Mo_{11}VO_{40}$ < CsPMoVO–Zn < CsPMoVO–Cu < CsPMoVO–Fe < CsPMoVO–Ni < CsPMoVO–Co and MAC conversion and MAA selectivity varied with metal doping (Fig. 3.8) Yanxia *et al.* (2016). Iron improved the redox properties and increased the electron transfer in Fe^{3+}–O–Mo^{5+} by Fe–doping, respectively Huynh et Millet (2005). Co, Ni, and Zn metals decreased the catalytic activity because MoO_3 formed. Increasing the content of copper in the catalyst structure reduced the activity and the strength of the acid sites for the $Cs_1Cu_yH_{3-2y}P_{1.2}Mo_{11}VO_{40}$ catalysts as follows Yanxia *et al.* (2016) : y=0.7<y=0.3<y=0.5<y=0.1.

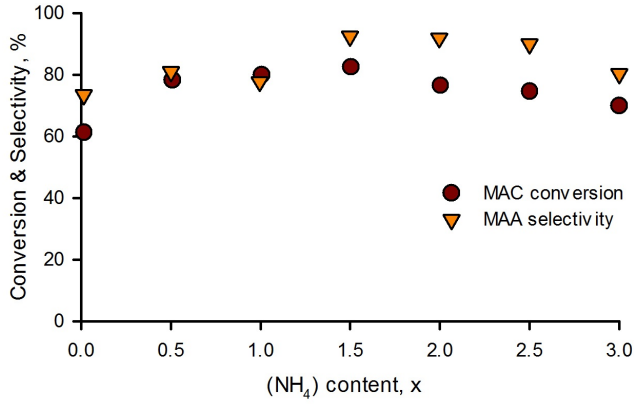

Figure 3.7 MAC conversion and MAA selectivity over the catalysts with different value of x Cao *et al.* (2017)

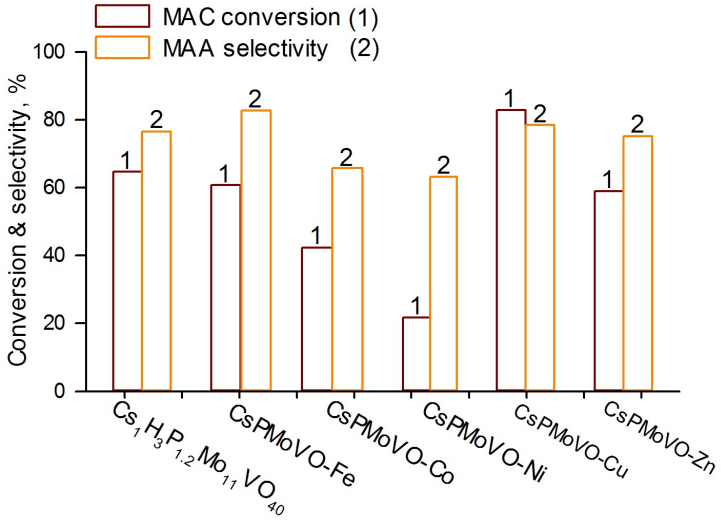

Figure 3.8 The selective oxidation of MAC to MAA over mixed oxide catalysts Yanxia *et al.* (2016)

A moderate concentration of copper (y= 0.3) favored the selective oxidation of MAC to MAA and MAC conversion reached (89 %) and MAA selectivity (74 %) (Table 3.12) Yanxia *et al.* (2016) ; MoO_3 formed when y>0.5 and consequently MAA selectivity decreased.

Increasing the calcination temperature accelerated vanadium migration from inside the Keggin structure to the secondary structure and thereby surface vanadyl species formed. Consequently, the vanadyl species in the secondary structure of the catalysts oxidized MAC to MAA.

Producing MMA via the direct oxidative esterification process is attractive because of it energy efficiency and low environmental footprint. The main research focus is to improve catalyst activity to react MeOH with MAC Diao *et al.* (2013). Several studies have synthesized supported and bimetallic catalysts to partially oxidize MAC Diao *et al.* (2013); Miyake et Asakawa (2005); Wei *et al.* (2006); Haifeng *et al.* (2006). Catalyst activity varies with morphology (pore size distribution, surface area, etc.), support, synthesis procedure and the nature of the precursor Nikolay *et al.* (2013); Dung *et al.* (2011); Prasad *et al.* (2011); Chuanjing *et al.* (2007); Yu *et al.* (2011a). MMA selectivity exceeds 80 % at 86 % MAC conversion over Pd–Pb catalysts supported on Mg–Al_2O_3 (Table 3.13) Yanyan *et al.* (2015).

Table 3.12 Catalytic activity of $Cs_1Cu_yH_{3-2y}P_{1.2}Mo_{11}VO_{40}$ in the selective oxidation of MAC to MAA Yanxia *et al.* (2016)

y	MAC Conversion, %	MMA Selectivity, %
0.1	93	65
0.3	89	74
0.5	83	79
0.7	91	51

Table 3.13 The direct oxidative esterification of MAC with MeOH in air to MMA. Reaction conditions : 2.5 g catalyst, 15.5 ml MAC, and 60 ml MeOH at 80 °C under 0.3 MPa for 2.0 h Yanyan *et al.* (2015)

Catalyst	Precursor	MAC Conversion, %	MAA Selectivity, %
5%Pd/Al_2O_3	Na_2PdCl_4	34	42
5%Pd–5% Pb/Al_2O_3	Na_2PdCl_4	65	68
5%Pd–5% Bi/Al_2O_3	Na_2PdCl_4	37	49
5%Pd–5% Pb/MgO–Al_2O_3	Na_2PdCl_4	94	81
5%Pd–5% Pb/ZnO–Al_2O_3	Na_2PdCl_4	85	76
5%Pd–5% Pb/K_2O–Al_2O_3	Na_2PdCl_4	84	75
5%Pd–5% Pb/ZSM-5	Na_2PdCl_4	41	65
5%Pd–5% Pb/MgO–Al_2O_3–SiO_2	Na_2PdCl_4	67	75
5%Pd–5% Pb/MgO–Al_2O_3	H_2PdCl_4	86	81
5%Pd–5% Pb/MgO–Al_2O_3	$Pd(NH_3)_4Cl_2$	26	30

Supported noble metal catalysts are highly active, which makes them likely candidates for commercial application Garetto *et al.* (2009); Simson *et al.* (2011); Lee *et al.* (2012); Doronkin *et al.* (2012); Fan *et al.* (2012). The major deactivation mechanisms include : metal crystallite growth, metal leaching from the catalyst structure, oligomerization of MAC and MMA on the surface, and irreversible adsorption of other intermediates. Conversion decreased and the selectivity increased as the Pd–Pb/γ–Al_2O_3 deactivates during repeat runs for the direct oxidative esterification of MAC with methanol in air (Fig. 3.9) Diao *et al.* (2013) : MAC conversion dropped from 94 % to 81 %. MMA selectivity increased as MeOH chemically adsorbs to the catalyst forming Pd–H bonds Diao *et al.* (2013). Catalysts regenerate in MeOH and hydrazine solutions and calcination in air at 500 °C. Catalyst activity and selectivity are highest after the MeOH soak, likely due to Pd–H bonds forming. As PdO_x and PbO_x reduce to bimetallic Pd_3Pb crystallite formation Diao *et al.* (2013).

Asahi Chemical developed a catalyst including Pd-Pb as the active phase that achieved 93 % MMA yield Tamura *et al.* (1979). Among all of the catalysts available in their laboratory, a Lindlar hydrogenation catalyst (a Pd-Pb type for acetylenic compounds) performed best. Based on their initial screening program they optimized the composition to Pd_3Pb. They developed other catalysts, like Au/NiO_x, with better selectivity, activity, stability, yield, and feedstock utilization. The performance of the Au/NiO_xat the industrial scale was verified in a 100 kt/y MMA plant in 2008.

Li et al. loaded MgO, $(NH_4)_2SO_4$, and MoO_3 promoters onto Au/$Ce_{1-x}Zr_xO_2$ and studied

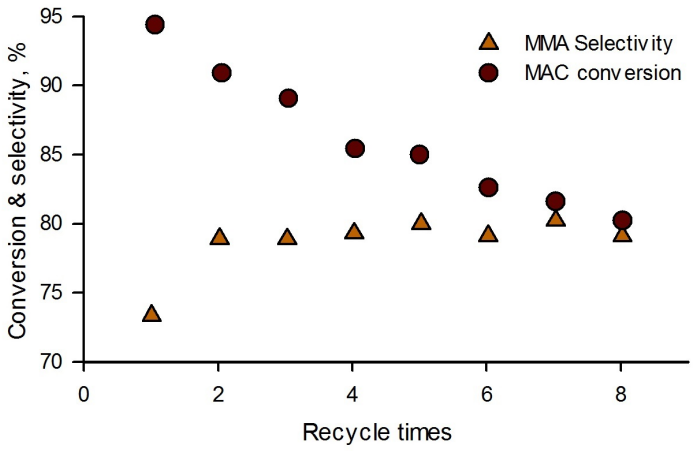

Figure 3.9 Pd–Pb/γ–Al_2O_3 catalyst deactivation in the batch process of direct oxidative esterification of MAC with methanol in air Diao *et al.* (2013)

the oxidative esterification of MAC with methanol to MMA Yuchao *et al.* (2016). The Mg promoter provided the highest catalytic activity including both high MAC conversion (98 %) and high MMA selectivity (90 %) as well as the best low temperature redox activity that generate oxygen species on Au nanoparticles. (Table 3.14)Yuchao *et al.* (2016).

Al_2O_3 Diao *et al.* (2009), ZnO Yanyan *et al.* (2015), MgO R. et Endalkachew (2004) and SiO_2 Atsutaka *et al.* (1990) as hydrophilic catalyst supports and a porous styrene-divinyl benzene copolymer (SDB) as a hydrophobic support have also been studied Huang *et al.* (2000); Xie *et al.* (2001); Lin *et al.* (1999). The advantage of a hydrophobic catalyst support relates to by–product water that diffuses inside and decreases the accessibility of active sites to the products. Asahi Chemical developed a supported composite particle material (NiOAu/SiO_2–Al_2O_3–MgO) including 1.05 wt % nickel and 0.91 wt % gold to convert MAC to MMA Suzuki et Yamaguchi (2013). It produced 9.5 mol h^{-1} kg^{-1} after 2000 h on stream at 75 % conversion Suzuki et Yamaguchi (2013).

Table 3.14 Oxidative esterification of MAC with methanol to MMA over different catalysts Yuchao *et al.* (2016)

Catalyst	Conversion, %	MMA selectivity, %	Acetal selectivity, %
Au/CZ	78.5	66.9	18.5
Au/MgCZ	98.1	89.9	3.1
Au/SCZ	79.9	82.6	5.1
Au/MoCZ	79.2	78.6	13.2

Several patents claim Pb and Bi promote catalytic activity of Pd-based supported catalysts for selective oxidation reactions Baer *et al.* (1985); Broecker *et al.* (1987); Yoshida *et al.* (2002); Mikami *et al.* (1999); Aoshima *et al.* (1985). Wang et al. reported MMA production in the direct oxidative esterification of MAC with methanol and oxygen over Pb and Bi–doped hydrophobic styrene–divinyl benzene copolymer (SDB) under mild conditions Wang *et al.* (2013). They prepared catalysts with Pb, Pd and Bi promoters over SDB (hydrophobic) or Al_2O_3 and SiO_2 (hydrophilic) by incipient impregnation Wang *et al.* (2013) (Table 3.15).

Table 3.15 Catalytic performance of different supported catalysts Wang *et al.* (2013)

Catalyst	MAC Conversion, %	MMA Selectivity, %
SDB(X–5)	87	91
SDB(NKA)	88	91
SDB(D3520)	76	89
SDB(D4006)	72	88
γ–Al_2O_3	5	79
SiO_2	3	59

The excellent performance of SDB supports confirms the utility of hydrophobicity. Promoters improve catalytic activity when compared with mono–metallic and bi–metallic catalysts, which we attribute to the adsorption and transfer of electrons on the multi–metallic catalysts (Table 3.16)Wang *et al.* (2013).

Table 3.16 Effect of promoters on catalytic activity Wang *et al.* (2013)

Catalyst	MAC Conversion, %	MMA Selectivity, %
Bi/SDB(X–5)	0	0
Pb/SDB(X–5)	0	0
Pd_3/SDB(X–5)	43	54
$Pd_3Pb_{0.6}$/SDB(X–5)	79	86
$Pd_3Bi_{1.5}$/SDB(X–5)	53	71
$Pd_3Pb_{0.6}Bi_{1.5}$/SDB(X–5)	87	91

Reaction conditions : T=323 K, pH=10.5, O_2 flow rate=6 mLmin^{-1} and molar ratio methanol/MAC of 40.

Increasing reduction temperature from 120 °C to 200 °C improved MAC conversion and MMA selectivity as the precursor reduced to the optimal metal valence. Higher temperatures

(>240 °C) sintered the Pd promoter and depolymerized the catalyst support (Fig. 3.10a) Wang *et al.* (2013). Longer time favored the complete reduction of metals (Fig. 3.10b) Wang *et al.* (2013).

Jiang et al. Li *et al.* (2014) prepared Pd–Pb/MgO–SBA–15 supported catalysts varying Mg loading, Mg precursors and molar concentration of hydrochloric acid (MgO–SBA–15(X–P)–Y). *X* and *Y* are Mg^{2+} and HCl molar ratio, respectively based on TEOS in the synthesis mixture Li *et al.* (2014). Pd and Pb loading were 5 wt % of MgO–SBA–15 supports. Table 3.17 represents the catalytic performance of catalysts in the oxidative esterification of MAC to MMA with methanol and oxygen at 80 °C and 0.3 MPa for 2 h Li *et al.* (2014).

Magnesium acetate created the highest surface area ($402\,m^2\,g^{-1}$) and total pore volume ($0.72\,cm^3g^{-1}$) compared with other Mg sources. Consequently, MAC conversion was highest at 68 % and MMA selectivity was 72 %. The highest MAC conversion (79 %) and MMA selectivity (72 %) have been reported over catalyst which was prepared using hydrochloric acid molar concentration of $0.8\,molL^{-1}$ Li *et al.* (2014). Low HCl molar concentration ($<0.8\,mol\,L^{-1}$) led to non–uniform dispersion and large particle size of Pd_3Pb.

Table 3.17 Catalytic activity of catalysts in the oxidative esterification of MAC to MMA with methanol and oxygen Li *et al.* (2014)

Catalyst	MAC Conversion, %	MMA Selectivity, %
Pd–Pb/MgO–SBA-15(0.150-N)	68	67
Pd–Pb/MgO–SBA-15(0.150-Cl)	76	67
Pd–Pb/MgO–SBA-15(0.150-A)	68	72
Pd–Pb/MgO–SBA-15(0-A)	0	49
Pd–Pb/MgO–SBA-15(0.015-A)	36	63
Pd–Pb/MgO–SBA-15(0.075-A)	55	63
Pd–Pb/MgO–SBA-15(0.300-A)	72	67
Pd–Pb/MgO–SBA-15(0.450-A)	83	52
Pd–Pb/MgO–SBA-15(0.150-A)-1.6M	68	72
Pd–Pb/MgO–SBA-15(0.150-A)-0.8M	78	72
Pd–Pb/MgO–SBA-15(0.150-A)-0.4M	77	58

3.6.3 Isobutane Partial Oxidation

Partial oxidation of isobutane to MAA and MAC is a compelling alternative chemistry due to the improved atom–economy. Moreover, it is inexpensive and it would have a lower environmental impact than other fossil feedstocks and optimally converts to MAA in a single

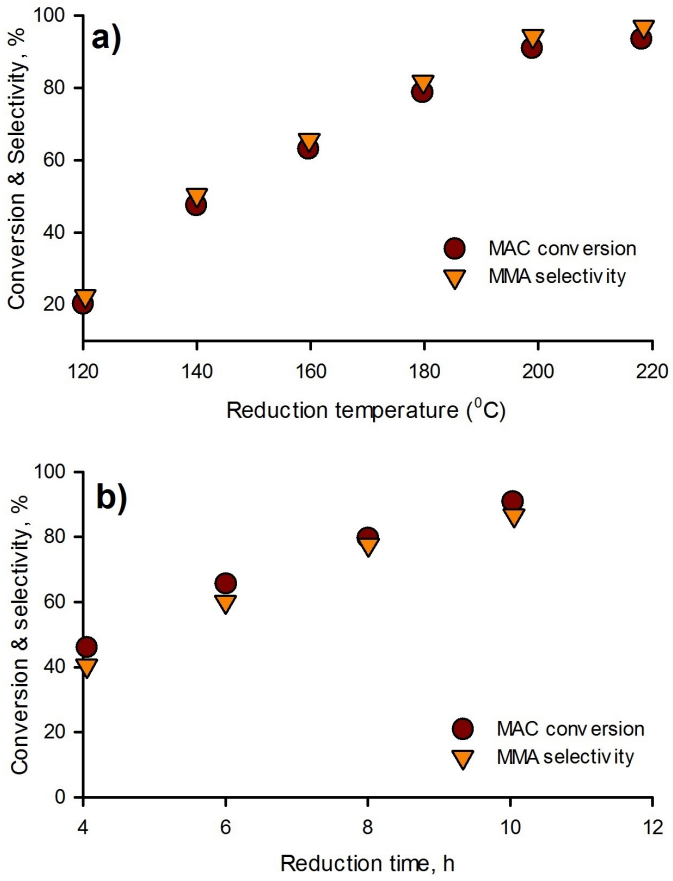

Figure 3.10 Catalytic performance of $Pd_3Pb_{0.6}Bi_{1.5}$/SDB(X–5) as a function of reduction temperature (a) and time (b) Wang *et al.* (2013)

step Sultan *et al.* (2004); Cavani *et al.* (2001f); Vedrine et Fechete (2016); Kendel et Brown (2011); Yamamatsu et Yamaguchi (1990, 1993). In the first step, catalyst extracts hydrogen from the compound to form a double bond. In the following steps the adjacent methyl group partially oxidizes to a carboxyl group (allylic oxidation). Acidic and bi–functional catalysts are necessary to activate the C−H bond Mizuno et Mison (1998); Misono (2001); Vanhove (1996). Redox properties also have an inevitable effect on the oxygen insertion reactions which generate the oxidized products Mizuno et Mison (1998); Mizuno *et al.* (1998); Jing *et al.* (2014a); Wang *et al.* (2016); He *et al.* (2015).

Keggin–type heteropolyacids, mixed metal oxides and VPP are the most common catalysts to oxidize isobutane to MAA and MAC Okuhara *et al.* (1996); Saadatkhah *et al.* (2017). Operating conditions (reaction temperature, feed composition, time–on–stream and residence time) also affect the MAA and MAC selectivity and reactant conversion. Mixed metal oxides and vanadium pyrophosphate (VPP) favor oxidizing isobutane to MAC but not to MAA. Heteropoly compounds are the most effective catalyst to oxidize isobutane to MAA Schindler *et al.* (2003); Guan *et al.* (2007a, 2008d, 2009d).

Heteropolycompound catalysts for oxidizing isobutane to MAA and MAC

Phosphomolybdic acid ($H_3PMo_{12}O_{40}$), as a basic Keggin structure, performed well when oxidizing MAC to MAA Kanno *et al.* (2010) but not for isobutane oxidation as the catalyst stability was poor but more importantly the maximum yield of MAA and MAC were only 6.2 % and 1.2 %, respectively Kozhevnikov *et al.* (1996); Kendell *et al.* (2008); Sun *et al.* (2002); Mizuno *et al.* (1996b); Ding *et al.* (2016); Krieger et Kirch (1979). Studies correlated the catalyst performance with their physico–chemical features Inumaru *et al.* (1998); Bielmeier *et al.* (1995); Sultan *et al.* (1999); Langpape *et al.* (1999).

Reduced $H_3PMo_{12}O_{40}$ formed by the heat–treatment of pyridinium or quinolinium salts was active in which the selectivity of MAA was 58 % at 12 % conversion of isobutane at 300 °C (Table 7.1) Li et Ueda (1997); Li *et al.* (1999). Higher activity and selectivity were due to the stable reduced state and structure of the activated heteropoly molybdophosphate catalyst.

Table 3.18 Selectivity of MAA and MAC over pyridinium 12–molybdophosphates as a function of temperature and feed concentration Li et Ueda (1997)

Feed comp. (mol %)	Temp. °C	Conversion, %	Selectivity, %		
$C_4/O_2/H_2O$/inert			MAA	MAC	CO_x
2.2/7/33.5/57.3	280	8	56	7	25
2.2/7/33.5/57.3	300	17	53	13	19
2.2/7/33.5/57.3	340	47	18	3	36
2.2/13.7/33.5/50.6	300	22	51	0	23
2.2/20.7/33.5/43.6	300	28	34	0	28
2.2/13.7/33.5/50.6	300	12	58	0.4	21
2.2/13.7/33.5/50.6	300	11	51	14	19

Inserting metal ions such as cesium, vanadium, and iron into the $H_3PMo_{12}O_{40}$ catalyst improved the catalyst's performance Huynh *et al.* (2009a,b); Mizuno *et al.* (1996b); Etienne *et al.* (2003); Li et Ueda (1997); Langpape et Millet (2000); Paul *et al.* (1997); Punniyamurthy *et al.* (2005). Below we identify the effect of each metal ion in Keggin–type catalyst and the reaction conditions on product selectivity and conversion of reactant. Li et Ueda (1997).

Effect of cesium and ammonium on catalyst performance Inserting cesium (Cs^+) and ammonium ($NH_4{}^+$) with H^+ in $H_3PMo_{12}O_{40}$ improved both activity and carboxylic acid selectivity Okuhara *et al.* (2000); Sultan *et al.* (2004). Several catalysts have been prepared and tested to maximize the selectivity of the desired products (Table 3.19). Mizuno et al. tested $Cs_xH_{3-x}PMo_{12}O_{40}$ catalysts and the optimum was $Cs_{2.5}H_{0.5}PMo_{12}O_{40}$ for which the conversion and selectivity reached 16 % and 24 % after 4 h, respectively Mizuno *et al.* (1996b). The $Cs_{2.5}H_{0.5}PMo_{12}O_{40}$ performance changes with feed composition which, under isobutane–lean conditions, the maximum yield of MAA+MAC was 1.3 % and the conversion was 6 %, whereas, under the isobutane–rich conditions the conversion of isobutane and MAA+MAC yield were 6.5 % and 3.9 %, respectively Min et Mizuno (2001a).

Ammonium in the catalyst structure ($(NH_4)_3PMo_{12}O_{40}$) required a time–on–stream of 80–100 h in both isobutane–rich and lean conditions in order to reach steady state Cavani *et al.* (2000, 2001f). In isobutane–rich conditions, conversion and MAA selectivity increased slightly and reached 6.5 % and 43 %, respectively, at 380 °C (Fig. 3.11a) Cavani *et al.* (2000). Otherwise, in isobutane–lean conditions, catalyst conversion was invariant (7 %), while the selectivity of MAA decreased from 24 % and dropped to 5 % at steady state (Fig. 3.11b) Cavani *et al.* (2000). They suggested that under isobutane–rich conditions, ammonium reduced the active phase that improved catalyst performance Cavani *et al.* (2000, 2001f).

Table 3.19 Selectivity of MAA and MAC with substituting of Cs^+ and NH_4^+ in $H_3PMo_{12}O_{40}$ catalyst

Catalyst	Temp., °C	Conversion, %	Selectivity, %			Sum of yields, %	Ref.
			MAA	MAC	CO_x	MAA+MAC	
$H_3PMo_{12}O_{40}$	340	7	4	18	70	1.5	Mizuno *et al.* (1996b); Mizuno et Yahiro (1998); Min et Mizuno (2001a); Mizuno et Mison (1998)
$H_3PMo_{12}O_{40}$	340	4.1	4	12	NA	0.6	Sultan *et al.* (2004)
$H_3PMo_{12}O_{40}$	310	1.3	11	16	61	0.4	Huynh *et al.* (2009a)
$H_3PMo_{12}O_{40}$	345	3.5	9	9	67	0.6	Huynh *et al.* (2009a)
$H_3PMo_{12}O_{40}$	355	4.4	6	10	66	0.7	Huynh *et al.* (2009a)
$H_3PMo_{12}O_{40}$	310	5.1	12	10	66	1.1	Ding *et al.* (2016)
$H_3PMo_{12}O_{40}$	340	5	3	7	82	0.5	Langpape et Millet (2000)
$(NH_4)_3PMo_{12}O_{40}$	340	3.8	33	21	NA	2	Sultan *et al.* (2004)
$CsH_2PMo_{12}O_{40}$	340	6	23	17	50	2.4	Mizuno *et al.* (1996b); Min et Mizuno (2001a); Mizuno et Mison (1998)
$Cs_2HPMo_{12}O_{40}$	340	11	34	10	50	4.8	Mizuno *et al.* (1996b); Min et Mizuno (2001a); Mizuno et Mison (1998)
$Cs_2HPMo_{12}O_{40}$	340	7	12	14	61	1.8	Langpape et Millet (2000)
$Cs_{2.5}H_{0.5}PMo_{12}O_{40}$	340	16	24	7	62	5.1	Mizuno *et al.* (1996b); Min et Mizuno (2001a); Mizuno et Mison (1998)
$Cs_{2.5}H_{0.5}PMo_{12}O_{40}$	340	10	0	15	42	1.5	Min et Mizuno (2001a,b)
$Cs_{2.5}H_{0.5}PMo_{12}O_{40}$	340	10.3	12	10	68	2.3	Langpape *et al.* (1999)
$Cs_{2.85}H_{0.15}PMo_{12}O_{40}$	340	17	5	10	81	2.4	Mizuno *et al.* (1996b); Min et Mizuno (2001a); Mizuno et Mison (1998)
$Cs_3PMo_{12}O_{40}$	340	8	0	10	67	0.8	Mizuno *et al.* (1996b); Min et Mizuno (2001a); Mizuno et Mison (1998)

All studies agree that Cs^+ forms an alkaline salt in the catalyst structure ($Cs_3PMo_{12}O_{40}$) which acts as a support and thermally stabilizes the catalyst over which the active phase disperses ($(NH_4)_3PMo_{12}O_{40}$ or $H_3PMo_{12}O_{40}$) Mizuno et Yahiro (1998); Misono (2001); Mizuno et Mison (1998); Paul *et al.* (2010); Okuhara (2002). Cesium increased catalytic activity for which the surface oxidizing ability and protonic acidity are controlling factors Paul *et al.* (2010); Okuhara *et al.* (2000); Okuhara (2002); Alsalme *et al.* (2010). However, a high content of Cs is unfavorable Mizuno *et al.* (1996b); Min et Mizuno (2001a,b). NH_4^+ ions enhance MAA selectivity by increasing the surface area Jing *et al.* (2014b, 2013); Cavani *et al.* (2001f).

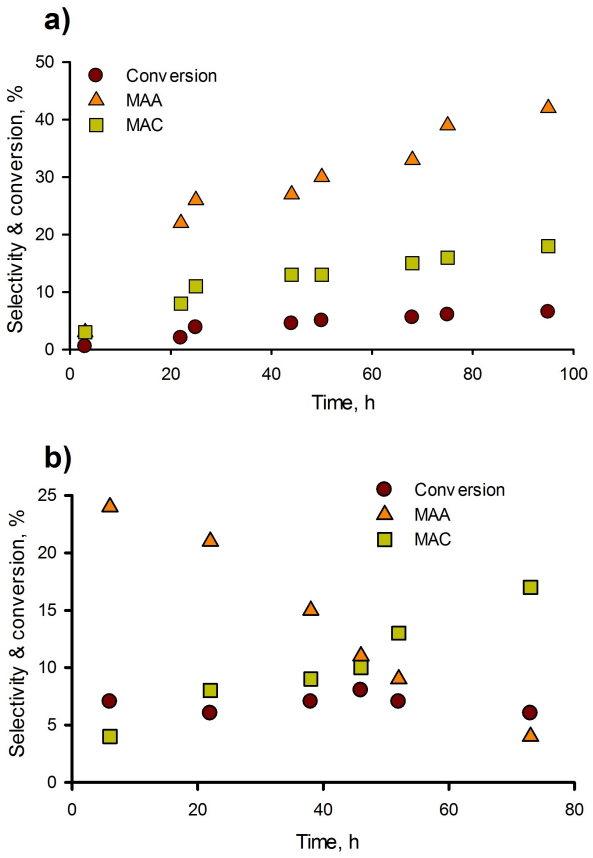

Figure 3.11 Conversion and product selectivity over $(NH_4)_3PMo_{12}O_{40}$ at 380 °C under a) isobutane–rich (isobutane/O_2/H_2O= 26 %/13 %/12 % and b) isobutane–lean (isobutane/O_2/H_2O= 1 %/13 %/12 %) conditions Cavani *et al.* (2000, 2001f).

Low pH reduces the number of active sites since the Keggin–structure partially decomposes as molybdenum migrates from the Keggin anion into the cationic position of the structure and forms crystalline MoO_3 Cavani *et al.* (2001f,a). During the first several hours, conversion and selectivity are higher for catalyst prepared under mildly acid conditions. After 20 h, the heteropolyacid catalyst prepared at a pH<1 achieved the same catalytic activity as the catalyst prepared under mild conditions (Fig. 3.12). Catalytic activity of the two catalysts were the same after 80 h time-on-stream : isobutane conversion reached 7 % and the MAA and MAC approached 40 % and 10 %, respectively over isobutane–rich condition at a mild pH Cavani *et al.* (2001f).

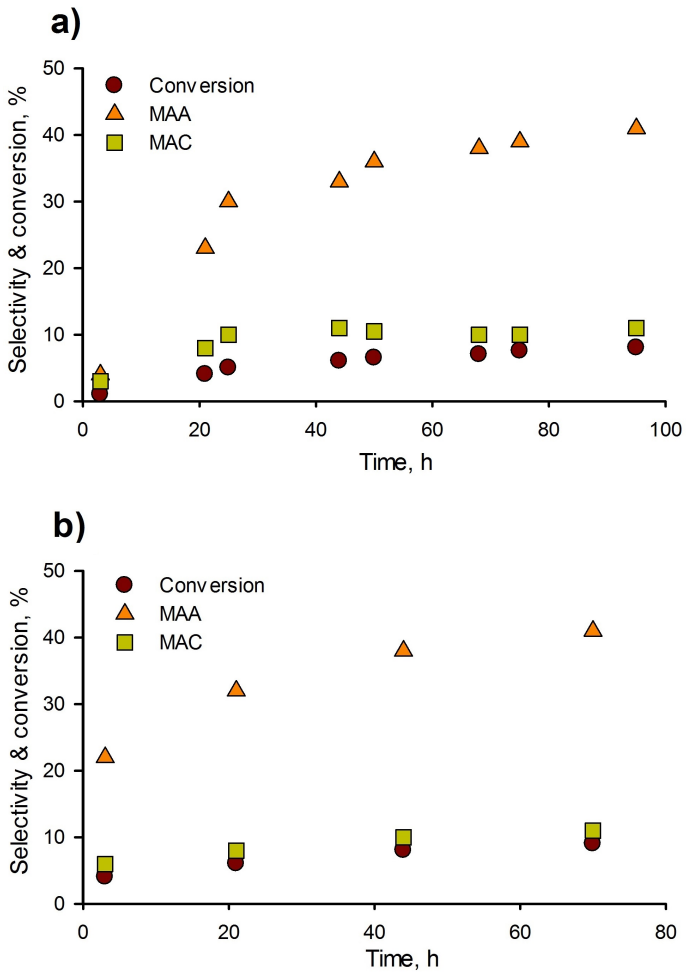

Figure 3.12 Conversion and product selectivity over $(NH_4)_3PMo_{12}O_{40}$ at 380 °C over a) catalyst prepared at strongly acid pH, and b) catalyst prepared at mildly acid pH (isobutane/O_2/H_2O= 26 %/13 %/12 %) Cavani *et al.* (2001f).

Effect of cesium on Keggin–type catalyst containing vanadium Partial insertion of vanadium ions (V^{5+}) with Mo accelerates the oxidation of MAC to MAA and suppresses the consecutive oxidation of MAC and MAA to CO_x Mizuno *et al.* (1996b). Vanadium reduces molybdenum from Mo^{6+} to Mo^{5+}, which improves their redox properties during calcination Cavani (1998); Chieregato *et al.* (2015). Inserting V^{5+} into $H_3PMo_{12}O_{40}$ formed $H_4PVMo_{11}O_{40}$. Vanadium occupies the cationic position and acts as an active site after high temperature expels it from the primary structure. Substituting Cs^+ for H^+ in $H_4PMo_{11}VO_{40}$ improved performance compared to the V–free sample in terms of MAA and MAC selectivities Mizuno *et al.* (1996b); Mizuno et Yahiro (1998). Several studies have investigated the effect of vanadium (in the presence of other ions such as Cs and NH_4) on performance over

a range of feed compositions and reaction temperatures (Table 3.20).

Cs^+ as a counter–ion in the presence of V in $Cs_xH_{1-x}VO[PMo_{12}O_{40}]$ achieved the highest MAA and MAC selectivity : selectivity decreased as x increased from 0 to 0.5. It then increased and reached a maximum of 76 % (MAA+MAC) for $Cs_{0.75}H_{0.25}VO[PMo_{12}O_{40}]$. It dropped again for x= 1, where all the H^+ are replaced by Cs^+ Liu-Cai *et al.* (2002). The oxidative activity was invariant with Cs^+ concentration Liu-Cai *et al.* (2002). Inserting cesium (x<0.75) makes the particles more hydrophobic so they have a greater tendency to expel MAA and MAC, which are polar. These compounds desorb more readily from the catalyst surface and thus selectivity is higher Liu-Cai *et al.* (2002). For x>0.75, the catalyst has no Brønsted acid sites in its initial structure, confirming a key role of acidity in both catalytic activity and selectivity Liu-Cai *et al.* (2002). Acidity activates the C−H bond, meanwhile, the redox properties play an important role to add a carboxylic acid functional group to the hydrocarbon Jing *et al.* (2013).

Cesium in $Cs_x(NH_4)_{3-x}HPMo_{11}VO_{40}$ (0<x<3) catalysts not only stabilize the catalyst structure but also maintain V atoms in the primary structure Jing *et al.* (2013, 2014b). Cs increases isobutane and oxygen conversion in V based catalysts, while oxygen conversion is about 10 % for Cs–free catalysts and isobutane conversion is only 2 % Jing *et al.* (2014b); Sultan *et al.* (2004). The maximum selectivity for MAA+MAC was 57 % (maximum yield was 5.9 %) over $Cs_{1.7}(NH_4)_{1.3}HPMo_{11}VO_{40}$ with isobutane and oxygen conversions of 9.6 % and 53 %, respectively Jing *et al.* (2014a).

Several studies demonstrated that the isobutane oxidation mechanism involves an oxidative dehydrogenation step to produce isobutene, which subsequently oxidizes to MAC and MAA, 500 times faster than it's formation Jing *et al.* (2014a); Wu *et al.* (2012); Shishido *et al.* (2000). Surface acidic sites activate C−H bond as the rate–limiting step Liu *et al.* (2016). Jalowiechi–Duhamel et al. proposed that the rate determining step was the initial dehydrogenation of isobutane to isobutene : isobutane → isobutene → MAC → MAA Jalowiecki-Duhamel *et al.* (1996).

The effect of vanadium in catalysts containing nickel ($Cs_{2.5}Ni_{0.08}H_{0.34+x}PV_xMo_{12-x}O_{40}$ which x=0–3) showed that the conversion and MAA selectivity increased for 0<x<1 and then decreased for x= 1 (Table 3.21). Conversely, the selectivity to MAC decreased for x<1 and was almost constant for x>1 Mizuno *et al.* (1996b); Mizuno et Yahiro (1998); Mizuno *et al.* (1998). The maximum selectivity was 36 % with the substitution of one mole of vanadium ($Cs_{2.5}Ni_{0.08}H_{1.34}PVMo_{11}O_{40}$). They suggested that the complete oxidation of MAC and MAA is suppressed and that V^{5+} substitution accelerates the MAC → MAA step.

Table 3.20 Selectivity of MAA and MAC with partial substituting of vanadium with molybdenum in presence of cesium and ammonium

Catalyst	Temp., °C	Conversion, %	Selectivity, %			Sum of yields, %	Ref.
			MAA	MAC	CO_x	MAA+MAC	
$H_4PMo_{11}VO_{40}$	340	5	30	36	34	3.3	Mizuno et Yahiro (1998)
$H_4PMo_{11}VO_{40}$	350	10.9	29	6	56	3.9	Wu *et al.* (2012)
$H_4PMo_{11}VO_{40}$	340	2.5	25	39	NA	1.6	Sultan *et al.* (2004)
$H_5PMo_{10}V_2O_{40}$	340	5	34	28	36	3.1	Mizuno et Yahiro (1998)
$H_6PMo_9V_3O_{40}$	340	10	14	14	60	2.8	Mizuno et Yahiro (1998)
$H_6PMo_9V_3O_{40}$	390	9.6	14	10	56	2.4	Ding *et al.* (2016)
$(NH_4)_3HPMo_{11}VO_{40}$	340	2.3	49	32	NA	1.9	Sultan *et al.* (2004)
$(NH_4)_3HPMo_{11}VO_{40}$	340	2.5	34	20	36	1.4	Sultan *et al.* (2004)
$(NH_4)_3HPMo_{11}VO_{40}$	340	2	33	11	37	0.9	Jing *et al.* (2014a)
$Cs_{0.5}(NH_4)_{2.5}HPMo_{11}VO_{40}$	340	4.1	41	29	17	2.9	Jing *et al.* (2014a)
$Cs_{1.15}(NH_4)_{1.85}HPMo_{11}VO_{40}$	340	6	45	15	NA	3.6	Sultan *et al.* (2004)
$Cs_{1.5}(NH_4)_{1.5}HPMo_{11}VO_{40}$	340	5.8	45	22	19	3.9	Jing *et al.* (2014a)
$Cs_{1.7}(NH_4)_{1.3}HPMo_{11}VO_{40}$	340	9.6	43	14	26	5.5	Jing *et al.* (2014a)
$Cs_{1.75}(NH_4)_{1.25}HPMo_{11}VO_{40}$	340	10.3	32	8	NA	4.1	Sultan *et al.* (2004)
$Cs_{1.78}(NH_4)_{2.22}HPMo_{11}VO_{40}$ (supported)	340	11.4	24	7	NA	3.5	Sultan *et al.* (2004)
$Cs_{2.4}(NH_4)_{0.6}HPMo_{11}VO_{40}$	340	2.1	10	16	NA	0.65	Sultan *et al.* (2004)
$Cs_{2.5}(NH_4)_{0.5}HPMo_{11}VO_{40}$	340	9.9	19	10	53	2.9	Jing *et al.* (2014a)
$Cs_3HPMo_{11}VO_{40}$	340	1.2	32	16	23	0.6	Jing *et al.* (2014a)
$Cs_{1.6}H_{2.4}P_{1.7}Mo_{11}V_{1.1}O_{40}{}^{\star}$	349	10.6	37	8	NA	4.8	Jalowiecki-Duhamel *et al.* (1996)

Table 3.21 Oxidation of isobutane catalyzed by $Cs_{2.5}Ni_{0.08}H_{0.34+x}PV_xMo_{12-x}O_{40}$ Mizuno et Yahiro (1998)

x	Conversion, %	Selectivity, %			Sum of yields, %
		MAA	MAC	CO_x	MAA+MAC
1	15	36	9	49	6.75
2	13	28	8	58	4.7
3	12	10	8	73	2.2

Based on the catalyst modification with the substitution of vanadium and the widespread influence of acidity and surface area on activity and selectivity, Jing et al. proposed a reaction route for isobutane oxidation over V–substituted bifunctional heteropolycompound catalysts (Scheme 3.13) Jing *et al.* (2014b).

Effect of Iron on catalyst performance Iron has two effects on catalyst performance that depend on inserting it in the Keggin–anion ($[PMo_{12}O_{40}]^{3-}$) or in the bulk (H^+) Langpape et Millet (2000). Substituting iron (Fe^{3+}) with hydrogen in the bulk of $H_3PMo_{12}O_{40}$ formed $Fe_xH_{3-3x}PMo_{12}O_{40}$, which increased the selectivity of MAA and MAC Langpape et Millet (2000). Over this catalyst, the acidity decreased up to the composition corresponding to x= 0.2 Deng *et al.* (2005); Mizuno *et al.* (1996b). At a higher cation content, the acidity was constant ; iron could partially be present as $[Fe(OH)_{3-x}]^+$ species that would act as active

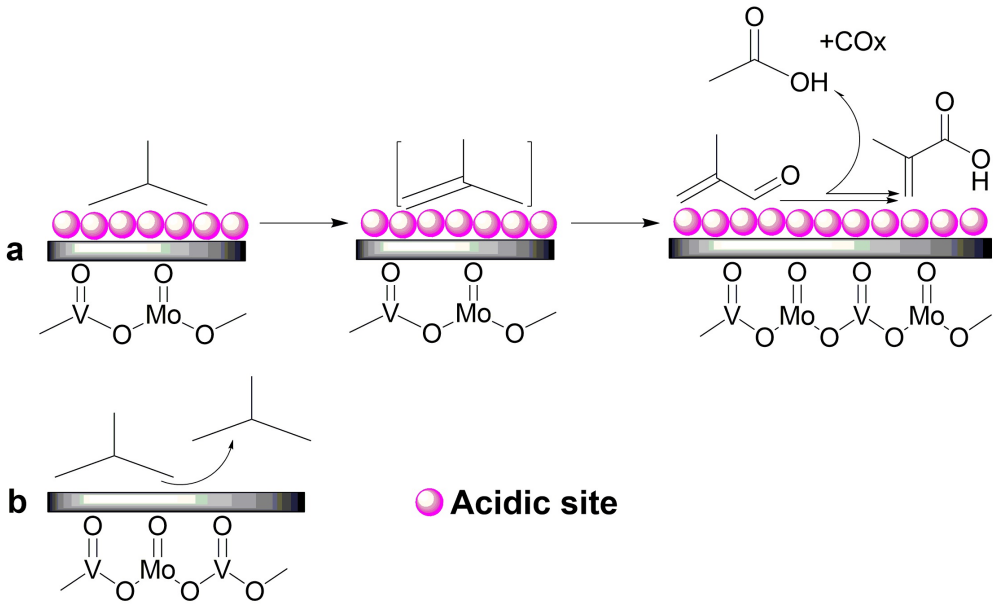

Schème 3.13 – The effect of acidity over heteropolycompounds containing vanadium for oxidation of isobutane to MAA+MAC Jing *et al.* (2014b). Reprinted with permission from ref. 171 Copyright 2014 Elsevier B.V.

sites and compensate for the loss of activity due to the decrease in the number of protons Deng *et al.* (2005); Mizuno *et al.* (1996b).

Inserting iron into the cesium salted catalysts ($Cs_xFe_yH_{3-x-3y}PMo_{12}O_{40}$) increased only the selectivity and had no effect on conversion Min et Mizuno (2001b); Mizuno *et al.* (1996b). For example, over $Cs_2Fe_x{}^{y+}H_{1-xy}PMo_{12}O_{40}$, the activity was invariant with iron and selectivity to MAA increased for $x<0.43$ and at higher iron content ($x>0.43$), this trend was reversed (Table 3.22) Langpape et Millet (2000); Langpape *et al.* (1999).

Several studies tested the effect of iron with higher cesium content ($Cs_{2.5}Fe_xH_{0.5-3x}PMo_{12}O_{40}$) under both isobutane–rich and lean conditions (Table 3.22) Mizuno *et al.* (1996b,a). Under isobutane–lean conditions, the yield of MAA and MAC increased up to $x= 0.08$, for which the yield of MAA+MAC peaked at 6.3 % and decreased above 0.08 ; however, conversion decreased (Fig. 3.13) Min et Mizuno (2001a); Mestl *et al.* (2001). Under isobutane–rich conditions, iron had the same effect on both selectivity and activity Min et Mizuno (2001a). Fe mainly suppresses the complete oxidation of MAA (and MAC) produced and accelerates the reaction MAC $\rightarrow$ MAA.

Table 3.22 Selectivity of MAA and MAC with substituting of iron into Keggin–structure

Catalyst	Temp., °C	Conversion, %	Selectivity, %			Sum of yields, %	Ref.
			MAA	MAC	CO_x	MAA+MAC	
$Fe_{0.85}H_{0.45}PMo_{12}O_{40}$	340	4	9	27	53	1.4	Langpape et Millet (2000)
$Cs_2Fe_{0.05}H_{0.85}PMo_{12}O_{40}$	340	6.7	21	15	53	2.4	Langpape *et al.* (1999)
$Cs_2Fe_{0.1}H_{0.7}PMo_{12}O_{40}$	340	6.8	21	16	51	2.5	Langpape *et al.* (1999)
$Cs_2Fe_{0.2}H_{0.4}PMo_{12}O_{40}$	340	6.8	24	17	50	2.8	Langpape et Millet (2000)
$Cs_2Fe_{0.25}H_{0.25}PMo_{12}O_{40}$	340	6	17	18	52	2.1	Langpape *et al.* (1999)
$Cs_2Fe_{0.3}H_{0.1}PMo_{12}O_{40}$	340	6.3	18	17	52	2.2	Langpape *et al.* (1999)
$Cs_{2.5}Fe_{0.04}H_{0.38}PMo_{12}O_{40}$	340	15	26	10	58	5.4	Mizuno *et al.* (1996b)
$Cs_{2.5}Fe_{0.05}H_{0.35}PMo_{12}O_{40}$	340	10.4	15	10	63	2.6	Langpape *et al.* (1999)
$Cs_{2.5}Fe_{0.08}H_{0.26}PMo_{12}O_{40}$	340	15	0	30	40	4.5	Min et Mizuno (2001a)
$Cs_{2.5}Fe_{0.08}H_{0.26}PMo_{12}O_{40}$	300	14	35	11	53	6.3	Mizuno *et al.* (1996b)
$Cs_{2.5}Fe_{0.08}H_{0.26}PMo_{12}O_{40}$	340	15	0	30	48	4.5	Min et Mizuno (2001b)
$Cs_{2.5}Fe_{0.08}H_{0.26}PMo_{12}O_{40}$	340	15	0	15	60	1.5	Mizuno *et al.* (1996b)
$Cs_{2.5}Fe_{0.1}H_{0.2}PMo_{12}O_{40}$	340	10.3	19	10	58	3	Langpape *et al.* (1999)
$Cs_{2.5}Fe_{0.16}H_{0.02}PMo_{12}O_{40}$	340	13	0	7	74	0.9	Min et Mizuno (2001a)
$Cs_{2.5}Fe_{0.16}H_{0.02}PMo_{12}O_{40}$	340	11	22	13	62	3.9	Mizuno *et al.* (1996b)
$Cs_{2.5}Fe_{0.16}H_{0.02}PMo_{12}O_{40}$	340	13	0	7	74	1.2	Min et Mizuno (2001b)

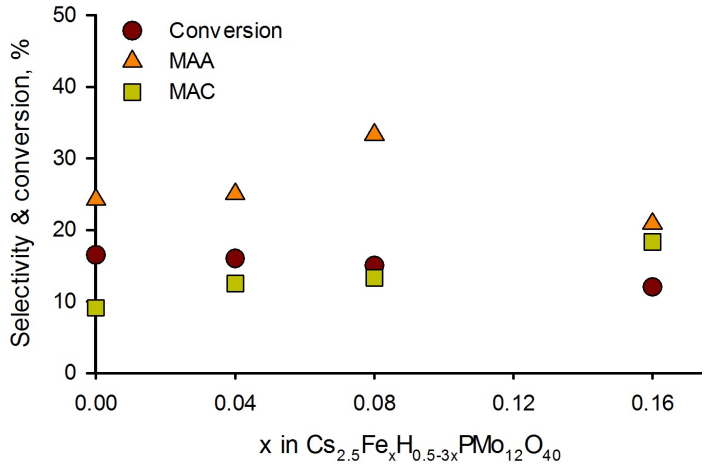

Figure 3.13 The effect of various amount of iron in catalyst structure for conversion and products selectivity in isobutane–lean (isobutane/O_2/N_2= 17 %/33 %/50 %) Min et Mizuno (2001a)

Transition metal cations affect the protonic acidity, which increases MAA and MAC selectivity more than the activity Mizuno *et al.* (1994a, 1995); Langpape *et al.* (1999). Reducibility was the main factor which controlled the activity of Fe–catalysts for which the hydration–oxidation mechanism promoted the reducibility of the solid and its catalytic activity thereafter Min et Mizuno (2001b); Langpape et Millet (2000). This hydration–oxidation mechanism is due to the existence of an electron transfer between iron and molybdenum

occurring only in the bulk acid Langpape et Millet (2000). Knapp et al. compared the effect of iron on catalyst structure as a counter–cation ($Cs_{1.5}Fe_{0.5}(NH_4)_2PMo_{12}O_{40}$) or inserting inside the Keggin anion ($Cs_{1.5}(NH_4)_2PMo_{11.5}Fe_{0.5}O_{39.5}$). As a counter–cation, selectivity to MAA was 21 % against 15 % for Fe inserted into the Keggin–anion at 6 % and 8 % conversion, respectively, at 390 °C (Fig.3.14a) Knapp *et al.* (2001). Increasing Fe content in the Keggin–structure decreased the selectivity to MAA which dropped from 15 % to 0 %, additionally the conversion also decreased from 16 % to 10 % (Fig.3.14b) Knapp *et al.* (2001).

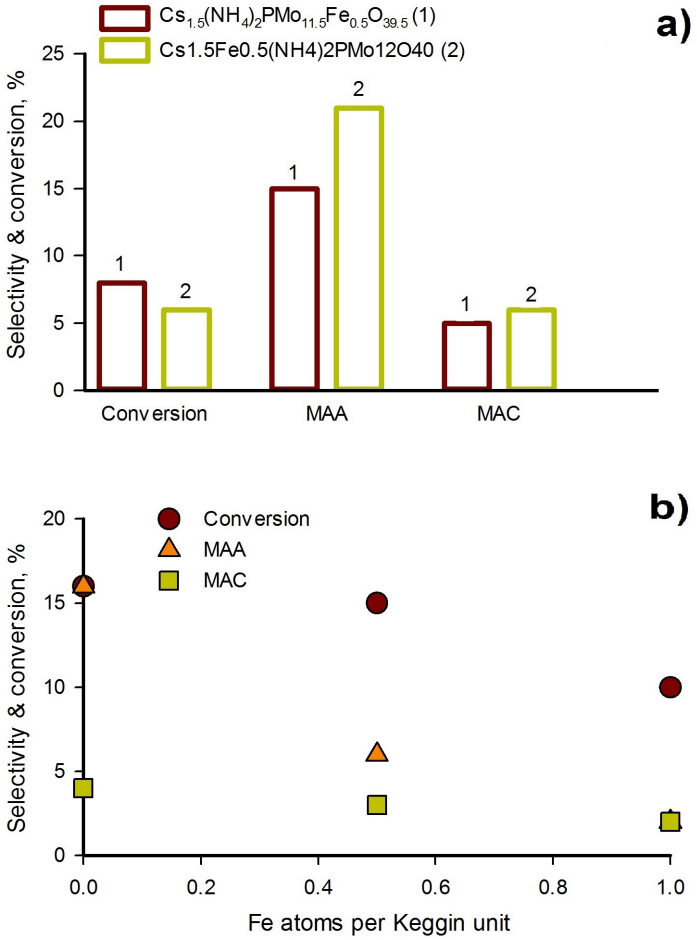

Figure 3.14 Selectivity and conversion a) as a function of Fe insertion in the Keggin–structure and b) number of Fe atoms per Keggin unit (isobutane/O_2/H_2O= 25 %/25 %/15 %) Knapp *et al.* (2001)

Substituting NH_4^+ with Fe in ammonium/potassium salts of 12–molybdophosphoric acid ($K_1(NH_4)_2PMo_{12}O_{40}$) increased the catalytic activity ; whereas, it decreased the selectivity to MAA Busca *et al.* (1996). Increasing iron content from 8 % to 12 % in the presence of arsenic

increased isobutane conversion from 21 % to 24 % and MAA selectivity went up from 42 % to 70 % (Table 3.23) Deng *et al.* (2005). Increasing iron content further to 16 % dropped both yield and selectivity. Presumably, the Fe^{3+}/Fe^{2+} redox couple in the bulk affects performance.

Table 3.23 $H_xFe_bMo_{11}VPAs_{0.3}O_y$ performance at 370 °C Deng *et al.* (2005)

Catalyst	Conversion, %	Yield, %			Sum of yields, %
		MAA	MAC	CO_x	MAA+MAC
$H_xFe_{0.08}Mo_{11}VPAs_{0.3}O_y$	21	9	1	8	10.2
$H_xFe_{0.12}Mo_{11}VPAs_{0.3}O_y$	24	17	1	2	17.7
$H_xFe_{0.16}Mo_{11}VPAs_{0.3}O_y$	19	9	1	7	10
$H_xKFe_{0.12}Mo_{11}VPAs_{0.3}O_y$	28	3	0.2	22	3.7
$H_xCsFe_{0.12}Mo_{11}VPAs_{0.3}O_y$	22	8	1	10	8.8

Effect of Nickel on catalyst performance Just like iron, a small amount of nickel in the cesium salted Keggin catalyst had a positive effect on both selectivity and conversion, whereas, over $Cs_{2.5}Ni_xH_{0.5-2x}PMo_{12}O_{40}$, both selectivity and conversion increased with x up to 0.08 and then decreased with more nickel. The maximum selectivity and conversion was 27 % and 24 %, respectively when x= 0.08 (Fig. 3.15) Mizuno *et al.* (1996b); Mizuno et Yahiro (1998). The partial and full oxidation of reactants–as the first step–is the rate–determining step and is mainly catalyzed by the molybdenum ion Mizuno *et al.* (1996b); Shinachi *et al.* (2005). Conversion increased more than the MAA selectivity. This difference may be due to the acceleration of the rate–determining step, isobutane → MAA (and MAC), or by the decrease in Brønsted acidity with nickel Mizuno *et al.* (1996b); Moro-oka *et al.* (1993).

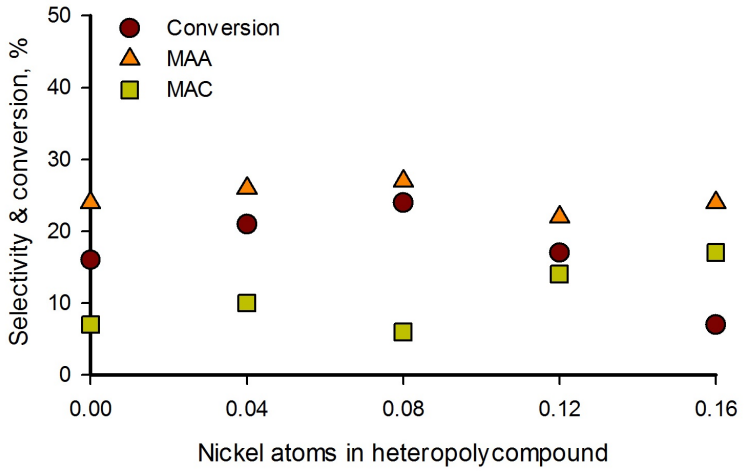

Figure 3.15 The effect of nickel content in $Cs_{2.5}Ni_xH_{0.5-2x}PMo_{12}O_{40}$ on conversion, MAA and MAC selectivity over isobutane/O_2/inert= 17 %/33 %/50 % Mizuno *et al.* (1996b)

The conversion of isobutane increased with temperature and reached 47 % at 360 °C on $Cs_{2.5}Ni_{0.08}H_{0.34}PMo_{12}O_{40}$ under isobutane–lean conditions. However, MAC selectivity decreased with increasing temperature Mizuno *et al.* (1996b). The maximum selectivity of MAA was achieved between 320 °C to 340 °C and the maximum MAA yield was only (8.5 %) at 360 °C (Fig. 3.16).

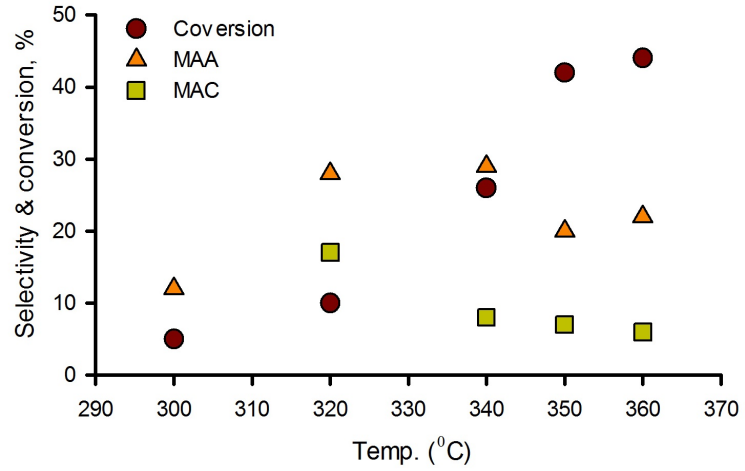

Figure 3.16 The effect of temperature on product selectivity and conversion over $Cs_{2.5}Ni_{0.08}H_{0.34}PMo_{12}O_{40}$ over isobutane/O_2/inert= 17 %/33 %/50 % Mizuno *et al.* (1996b)

Mizuno et al. proposed that isobutane first oxidatively dehydrogenates to isobutene, and then isobutene oxidizes to form MAC followed by oxidation to MAA (Scheme 3.14). However, they

also suggested a direct oxidative path from isobutane to MAC–shown by the dotted line in Scheme 3.14 Mizuno *et al.* (1996b); Mizuno et Yahiro (1998).

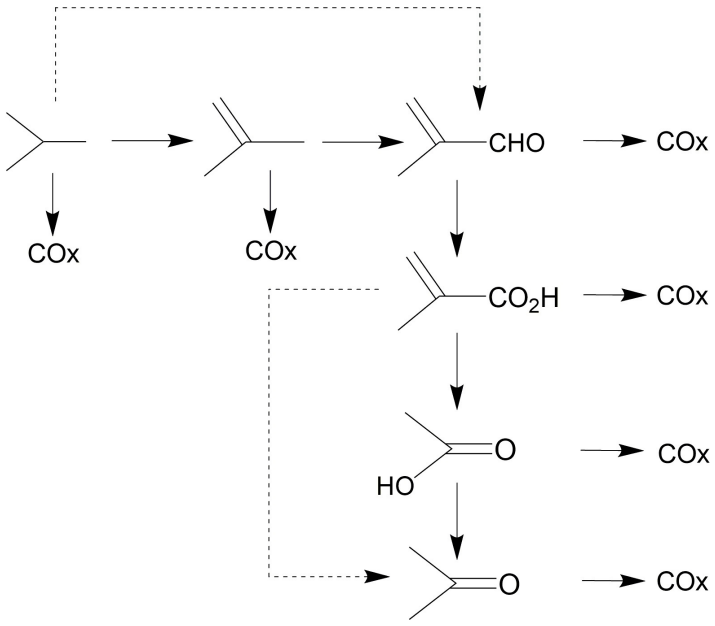

Schème 3.14 – Mechanism for the oxidation of isobutane to Methacrylic acid and methacrolein over $Cs_{2.5}Ni_{0.08}H_{0.34}PMo_{12}O_{40}$. Mizuno et Yahiro (1998); Mizuno *et al.* (1996b)

Nickel appears to improve catalyst performance but cesium confounds the data such that the change may not be solely attributable to Ni. Mizuno substituted Cs with Li, Na and K in $M_{2.5}Ni_{0.08}H_{0.34}PMo_{12}O_{40}$. The catalytic activity increased in the order of H<Li<Na<K<Cs and the MAA selectivity followed the same trend Mizuno *et al.* (1996b).

Effect of tellurium on catalyst performance Adding tellurium (Te^{4+}) in heteropoly compounds (cesium salted or its acid parent) had a positive effect on selectivity to MAA and MAC (Table 3.24). Inserting tellurium into a pure acid decreased activity, whereas, it increased activity for the cesium salted catalyst Huynh *et al.* (2009a,b). The maximum isobutane conversion and yield for MAA+MAC were 17.5 % and 12 %, respectively at 360 °C over a $Cs_2Te_{0.3}(VO)_{0.1}H_xPMo_{12}O_{40}$ catalyst Huynh *et al.* (2009a).

In the absence of Cs, the tellurium type catalysts—$Te_{(1.5+0.5x)}PMo_{12-x}V_xO_n$ (x=1–3)—were less active and selective but they were more selective to MAC (Table 3.24) Wu *et al.* (2012); Ding *et al.* (2016). Others confirmed that isobutane conversion and MAA selectivity improved substituting Mo with V in Te–molybdophosphoric catalysts, while the rate of isobutane conversion decreased in the sequence $H_4PMo_{11}VO_{40}$>$Te_{1.5}PMo_{12}O_n$=$Te_3PMo_9V_3O_n$> $Te_2PMo_{11}VO_n$=$Te_{2.5}PMo_{10}V_2O_n$ Wu *et al.* (2012); Ding *et al.* (2016); Huynh *et al.* (2009b).

The selectivity to MAC increases considerably substituting protons with tellurium in a V–substituted molybdophosphoric system.

To evaluate the effect of both tellurium and vanadium, Ding et al., varied these metal ions over $Te_{(12-x)/4}PMo_{12-x}V_xO_m$ (x=0–3) and the maximum selectivities to MAA and MAC were 22 % and 34 %, respectively with $Te_{2.25}PMo_9V_3O_n$ at 390 °C Ding *et al.* (2016). These results confirmed that Te^{4+} improves the catalytic performance ; whereas, vanadium increases selectivity of MAC+MAA Ding *et al.* (2016). The conversion increased with temperature in the range of 370 °C to 410 °C over $Te_{2.25}PMo_9V_3O_n$ catalyst Ding *et al.* (2016). The selectivity to MAA increased gradually ; conversely, the selectivity to MAC decreased while the total yield (MAC+MAA) gradually increased with temperature (Fig. 3.17).

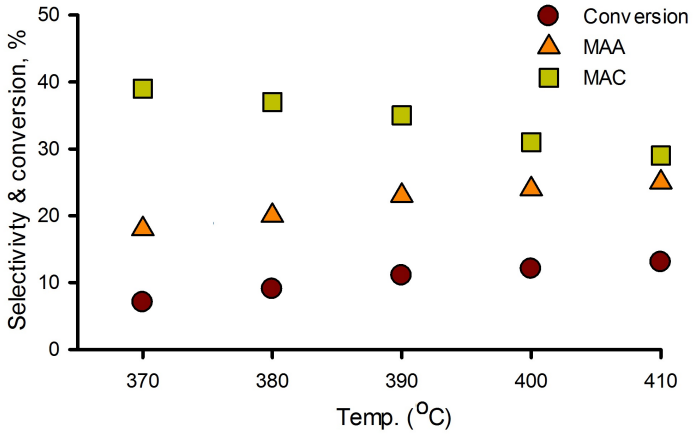

Figure 3.17 The effect of temperature on MAA and MAC selectivity and isobutane conversion over $Te_{2.25}PMo_9V_3O_n$ (isobutane/O_2/inert= 27 %/13 %/60 %) Ding *et al.* (2016)

Vanadium in the cesium salt catalyst containing tellurium increased conversion ; meanwhile, it decreased slightly MAA and MAC selectivity (Fig. 3.18)Huynh *et al.* (2009a). However, the maximum selectivity was obtained by changing the content of vanadium and tellurium in the catalyst and the optimum catalyst was $Cs_2Te_{0.3}V_{0.1}H_xPMo_{12}O_{40}$ Huynh *et al.* (2009a). The same catalyst but with less tellurium ($Cs_2Te_{0.2}V_{0.1}H_xPMo_{12}O_{40}$) achieved 49 % MAA+MAC selectivity at 6 % conversion and 362 °C Loridant *et al.* (2010).

Table 3.24 Effect of the tellurium ion in Keggin–structure or mixed oxides (⋆)

Catalyst	Temp., °C	Conversion, %	Selectivity, %			Sum of yields, %	Ref.
			MAA	MAC	CO_x	MAA+MAC	
$Cs_2Te_{0.3}(VO)_{0.1}H_xPMo_{12}O_{40}$	360	17.5	61	7	21	11.9	Huynh *et al.* (2009b)
$H_{1.8}Te_{0.6}PMo_{12}O_{40}$	355	6.3	27	22	37	3.1	Huynh *et al.* (2009a)
$H_1Te_1PMo_{12}O_{40}$	360	4.8	33	39	23	3.5	Huynh *et al.* (2009a)
$Te_{1.5}PMo_{12}O_{40}$	355	4	37	30	26	2.7	Huynh *et al.* (2009a)
$Cs_2Te_{0.05}H_xPMo_{12}O_{40}$	369	14.4	25	13	50	5.4	Huynh *et al.* (2009a)
$Cs_2Te_{0.2}H_xPMo_{12}O_{40}$	367	12	50	12	28	7.4	Huynh *et al.* (2009a)
$Cs_2Te_{0.5}H_xPMo_{12}O_{40}$	370	10.8	52	19	19	7.8	Huynh *et al.* (2009a)
$Cs_2Te_{0.3}V_{0.1}H_xPMo_{12}O_{40}$	350	16.1	54	11	26	10.5	Huynh *et al.* (2009a)
$Te_{1.5}PMo_{12}O_m$⋆	350	8	11	25	46	2.9	Wu *et al.* (2012)
$Te_2PMo_{11}VO_m$⋆	350	10.4	26	22	42	5	Wu *et al.* (2012)
$Te_{2.5}PMo_{10}V_2O_m$⋆	350	9.2	25	13	50	3.6	Wu *et al.* (2012)
$Te_3PMo_9V_3O_m$⋆	350	8.4	20	11	54	2.6	Wu *et al.* (2012)
$Te_3PMo_{12}O_m$⋆	390	9.3	9	28	51	3.4	Ding *et al.* (2016)
$Te_{2.75}PMo_{11}VO_m$⋆	390	9.8	14	28	48	4.1	Ding *et al.* (2016)
$Te_{2.5}PMo_{10}V_2O_m$⋆	390	10.5	15	29	46	4.7	Ding *et al.* (2016)
$Te_{2.25}PMo_9V_3O_m$⋆	390	11.8	22	34	36	6.6	Ding *et al.* (2016)

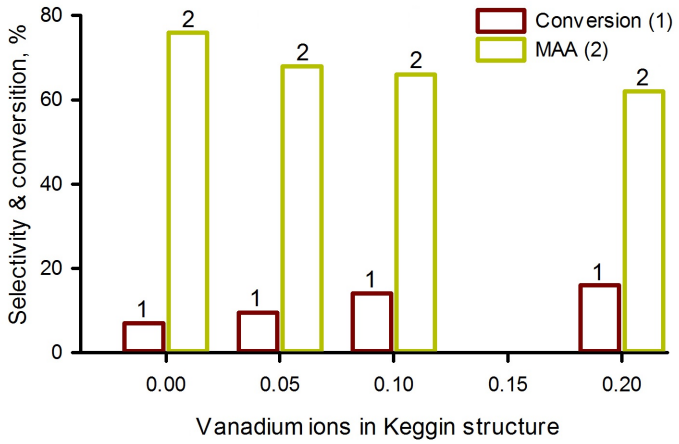

Figure 3.18 The effect of vanadium on conversion and selectivity of methacrylic acid in $Cs_2Te_{0.2}V_xH_yPMo_{12}o_{40}$ over isobutane/O_2/H_2O= 13.5 %/27 %/10 % Huynh *et al.* (2009a)

Catalysts that contain tellurium dehydrogenate isobutane to isobutene although it is unreported in the effluent— either because it oxidizes much faster than isobutane, or because the catalyst oxidizes isobutene at the surface of the polyoxometalates catalysts while multiple surface layers participated to the reaction (Scheme 3.15) Huynh *et al.* (2009a).

Effect of antimony on catalyst performance Inserting antimony into the Keggin structure ($H_xPMo_{12}SbO_y$) improved the catalyst performance for which the maximum selecti-

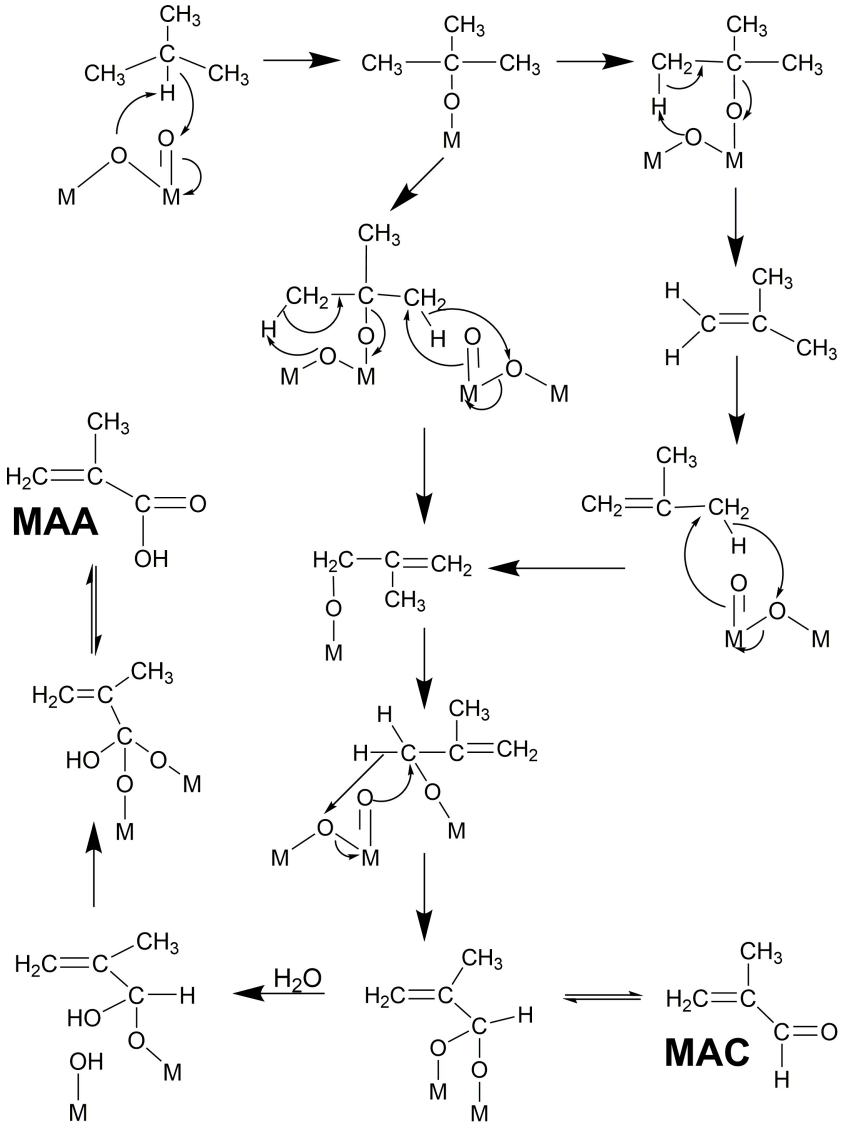

Schème 3.15 – Mechanism of oxidation of isobutane to Methacrylic acid and methacrolein over $Cs_2Te_{0.3}V_{0.1}H_xPMo_{12}O_{40}$ Huynh *et al.* (2009a). Reprinted with permission from ref. 157 Copyright 2009 Elsevier B.V.

vity of MAA and MAC was 50 % and 20 %, respectively and the conversion was 10 % at 340 °C Krieger et Kirch (1981). During calcination, antimony accelerates electron exchange $Sb^{3+}+2Mo^{6+}\rightarrow Sb^{5+}+2Mo^{5+}$ which decreases the oxidation state of molybdenum Cavani *et al.* (2001c). This ion exchange stabilizes the reduced molybdenum even under oxidizing conditions Cavani *et al.* (2001c). Cavani et al. inserted 0.23 Sb atoms per Keggin unit of $(NH_4)_3PMo_{12}O_{40}$ and MAA selectivity reached 45 % Cavani *et al.* (2001c, 1998). The activity of catalyst containing antimony was constant ; however, the selectivity was poor initially Cavani *et al.* (2003b). The redox reaction between the $PMo_{12}O_{40}{}^{3-}$ anion and Sb^{3+} generated active sites during calcination Cavani *et al.* (2003b, 2001c).

The polyoxometalate must work in a reduced state in order to be selective, while can be achieved either by operating under isobutane–rich conditions, or by doping the compound with an element like Sb, which is able to keep the compound in the reduced state even under isobutane lean (more oxidizing) conditions.

All studies confirm higher selectivity to MAA over Sb–catalysts compared to undoped catalysts under isobutane lean reaction conditions Cavani *et al.* (2003b). The selectivity of MAC was unchanged from 340 °C to 370 °C over the Sb–doped catalyst, while it decreased with temperature over undoped catalysts. Catalysts containing antimony are selective even at low isobutane concentrations Cavani *et al.* (1998).

Cavani et al. reported conversion as high as 70 % at a 1 % isobutane feed concentration (Fig. 3.19) Cavani *et al.* (2003b, 2001e). Increasing its partial pressure decreased conversion. The low selectivity under isobutane–lean conditions over catalyst containing antimony is due either to the high conversion (and consecutive oxidation of products) or because the higher catalyst oxidation state, and the weaker interaction between Sb^{3+} and the Keggin anion Cavani *et al.* (2003b, 2001e).

The reduced $(NH_4)_3PMo_{12}O_{40}/Sb_{0.23}O_x$ catalyst is highly selective under isobutane–lean conditions ; however, undoped catalysts are unselective under the same conditions Cavani *et al.* (2001e). Moreover, the selectivity of MAA increased a little in comparison with undoped catalysts under isobutane–rich conditions. In general the sum of MAA and MAC were almost constant with both Sb– doped and undoped catalysts Cavani *et al.* (2001e).

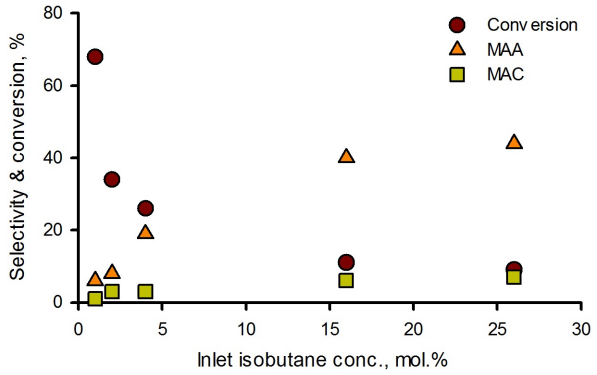

Figure 3.19 The effect of reactant concentration on conversion and selectivity or Sb–heteropolycompounds Cavani *et al.* (2003b)

Effect of other metal ions on catalyst performance Partially substituting copper in $Cs_2Cu_x^{2+}H_{1-2x}PMo_{12}o_{40}$ ($0<x<0.43$) increased catalyst activity up to x= 0.2. At higher cation content, the acidity of the catalysts decreased because of the decreasing proton content Langpape *et al.* (1999). However, copper had a negative effect on MAA selectivity Langpape *et al.* (1999).

Cesium ions in catalysts that contain copper ($Cs_yH_{0.5-y}Cu_{0.25}VO[PMo_{12}O_{40}]$) affected performance : Cu^{2+} changed both oxidative activity and methacrylic acid and methacrolein selectivity over $Cs_xH_{1-x}VO[PMo_{12}O_{40}]$ and $Cs_yH_{0.5-y}Cu_{0.25}VO[PMo_{12}O_{40}]$ catalysts as a function of the molar ratio of $nCs^+/(nCs^+ + nH^+)$ (Fig. 3.20) Liu-Cai *et al.* (2002). Higher Cs^+ ($Cs>0.5$) decreased the selectivity of MAA+MAC compared with Cu–free catalysts. Adding copper to the catalyst increased selectivity up to Cs= 0.8 and then it decreased (Fig. 3.20). A lower $nCs^+/(nCs^+ + nH^+)$ ratio may form oxygen vacancies favored by the presence of Cu^{2+} cations and the higher content of protons in the initial samples that increase activity. Lower cesium concentration in copper–catalysts accelerate the formation of oxygen vacancies, because the proton associated with oxygen of the heteropolyanion is absent Hodnett et Moffat (1984); Liu-Cai *et al.* (2002).

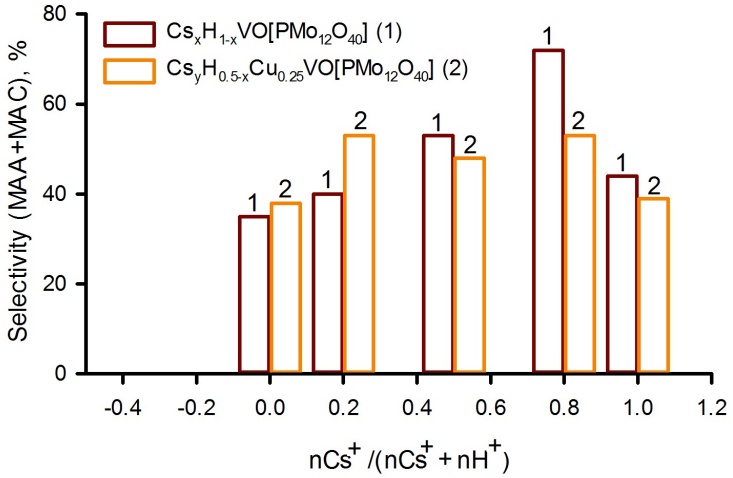

Figure 3.20 Selectivity of MAA+MAC over heteropolycompounds containing vanadium and cesium with/without copper over isobutane/O_2/H_2O= 26 %/13 %/12 % Liu-Cai *et al.* (2002)

The maximum selectivity to MAA+MAC was 45 % at a conversion of 22 % over Cu, As and V in cesium salted heteropoly catalysts (Cs :1.4/P :1.5/Mo :12/V :0.5/As :0.4/Cu :0.3) at 367 °C Schindler *et al.* (2003, 2001).

Mizuno et al. inserted metal ions (M) into the component $Cs_{2.5}M_{0.08}H_{0.34}PMo_{12}O_{40}$ where Mn^{2+} significantly increased the MAA+MAC yield; otherwise, Co^{2+}, Cu^{2+}, Hg^{2+}, Pt^{2+}, or Pd^{2+} substitution decreased the yields under oxygen–rich conditions (Table 3.25) Mizuno *et al.* (1996b, 1998).

Potassium had no effect in catalysts with/without iron for which the selectivity of MAC and MAA was the same at constant conversion under isobutane–rich conditions Busca *et al.* (1996). Busca *et al.* (1996) proposed a correlation between catalyst, reactant, and products in which the addition of iron affected the Mo ion redox properties, even though a direct participation of iron in the reaction mechanism cannot be excluded (Scheme 3.16) Busca *et al.* (1996).

The addition of arsenic obviously decreases catalytic activity and that the appropriate As modification can efficiently enhance the selectivity to MAA by restraining the split products. The optimal yield of MAA is achieved over $H_xFe_{0.12}Mo_{11}VPAs_{0.3}O_y$ at a conversion of 24 % and a MAA selectivity of 70 % Deng *et al.* (2005).

Effect of supports on catalyst performance Catalyst activity and product selectivity are sensitive to support and catalyst dispersion; for example, Jing et al. impregnated ($(NH_4)_3HPMo_{11}VO_{40}$–APMV) over commercial SiO_2, SBA–15, ZrO_2–grafted SBA–15, and

Table 3.25 Effect of metal ions in the Keggin–structure

Catalyst	Temp., °C	Conversion, %	Selectivity, %			Sum of yields, %	Ref.
			MAA	MAC	CO_x	MAA+MAC	
$H_xP_{1.1}Mo_{12}V_{1.1}Cu_{0.1}Cs_{1.1}O_y$	320	10.3	56	16	NA	7.4	Yamamatsu et Yamaguchi (1990)
$H_xP_{1.5}Mo_{12}V_1Cu_{0.2}Nd_{0.5}Cs_1O_y$	320	12.8	54	16	NA	8.9	Yamamatsu et Yamaguchi (1993)
$H_xP_{1.5}Mo_{12}V_{0.5}As_{0.4}Cs_{1.8}Cu_{0.3}O_y$	320	11.2	54	12	NA	7.3	Sun *et al.* (2014)
$H_xP_{1.5}Mo_{12}V_{0.5}As_{0.4}Cs_{1.4}Cu_{0.3}O_y$	330	25	3	43	NA	11.3	Sun *et al.* (2014)
$Cs_{2.5}Mn_{0.08}H_{0.34}PMo_{12}O_{40}$	340	21	20	11	60	6.5	Min et Mizuno (2001a); Mizuno *et al.* (1996b)
$Cs_{2.5}Cu_{0.08}H_{0.34}PMo_{12}O_{40}$	340	12	12	10	71	2.6	Min et Mizuno (2001a); Mizuno *et al.* (1996b)
$Cs_{2.5}Co_{0.08}H_{0.34}PMo_{12}O_{40}$	340	7	11	15	68	1.9	Min et Mizuno (2001a); Mizuno *et al.* (1996b)
$Cs_{2.5}Ni_{0.08}H_{0.34}PMo_{12}O_{40}$	340	24	27	6	59	8	Min et Mizuno (2001a); Mizuno *et al.* (1996b, 1994b)
$Cs_{2.5}Hg_{0.08}H_{0.34}PMo_{12}O_{40}$	340	15	10	10	73	2.4	Mizuno *et al.* (1996b)
$Cs_{2.5}Pd_{0.08}H_{0.34}PMo_{12}O_{40}$	340	8	0	1	98	0.1	Mizuno *et al.* (1996b)
$Cs_{2.5}Pt_{0.08}H_{0.34}PMo_{12}O_{40}$	300	34	0	0	100	0	Mizuno *et al.* (1996b)
$Cs_2Cu_{0.05}H_{0.9}PMo_{12}O_{40}$	340	7	7	16	64	1.6	Langpape *et al.* (1999)
$Cs_2Cu_{0.2}H_{0.6}PMo_{12}O_{40}$	340	7.5	6	15	72	1.6	Langpape *et al.* (1999)
$Cs_2Cu_{0.3}H_{0.4}PMo_{12}O_{40}$	340	6.6	6	16	72	1.4	Langpape *et al.* (1999)
$Cs_2Cu_{0.43}H_{0.14}PMo_{12}O_{40}$	340	5.9	5	15	76	1.2	Langpape *et al.* (1999)
$H_xFe_{0.12}PMo_{11}VAs_{0.2}O_z$	370	24.1	12	1	7	8	Deng *et al.* (2005)
$H_xFe_{0.12}PMo_{11}VAs_{0.3}O_z$	370	23.9	17	1	3	4.2	Deng *et al.* (2005)
$H_xFe_{0.12}PMo_{11}VAs_{0.4}O_z$	370	23.2	10	1	10	2.6	Deng *et al.* (2005)

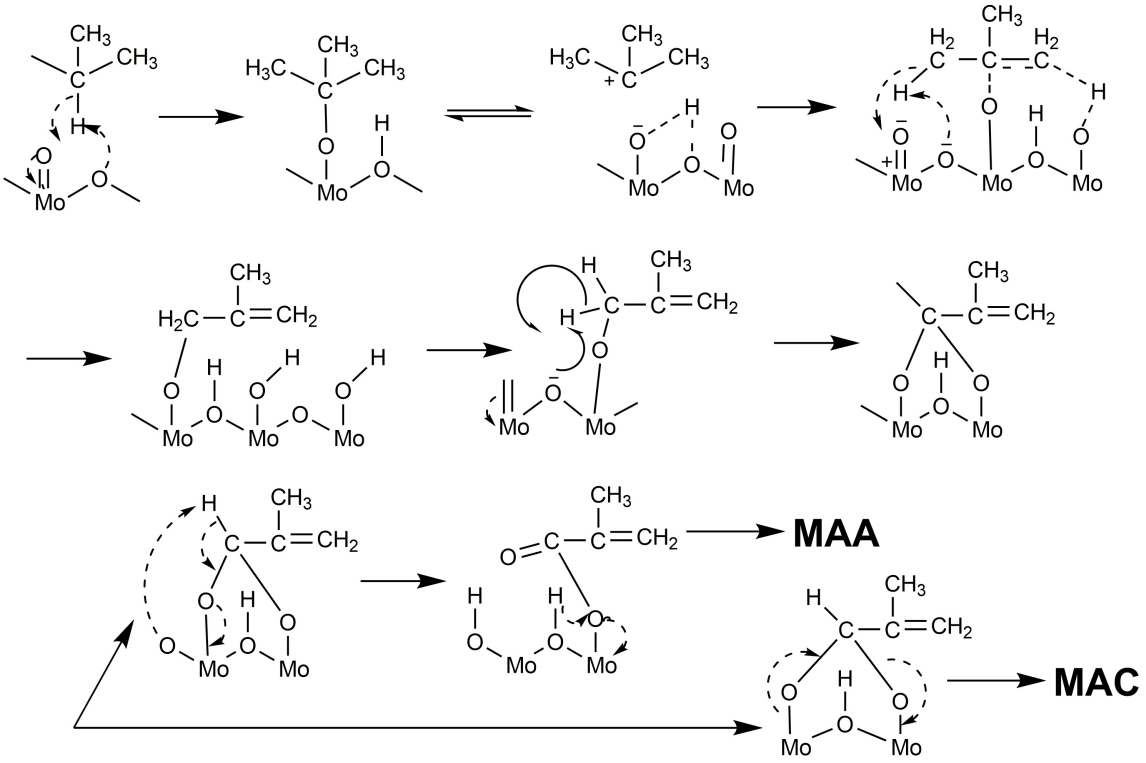

Schème 3.16 – Proposed mechanism for the oxidation of isobutane to MAA and MAC over $K_1(NH_4)_2PMo_{12}O_{40}$ at 350 °C Busca *et al.* (1996); Ballarini *et al.* (2007b). Reprinted with permission from ref. 84 Copyright 1996 Elsevier B.V.

$Cs_3PMo_{12}O_{40}$ (CPM) (Table 3.26). The conversion over non–supported catalysts (APMV) was 2.5 % and it rose to 15 % over CPM–supported catalyst Jing *et al.* (2013), meanwhile, the selectivity of MAA was 34 % and 42 % over bulk APMV and APMV/CPM, respectively Jing *et al.* (2013). The CPM–supported catalyst improved thermal decomposition stability and increased acid sites, which were necessary to convert alkanes to acids ; however, the active phase decomposed during the synthesis step with silica–based catalysts which resulted in poorer catalyst performance (Table 3.26) Kanno *et al.* (2010); Ballarini *et al.* (2007a); Nair *et al.* (2010).

Not only the type of support, but the concentration of the active phase also affects catalyst performance in the range of a mass fraction of 10 A to 50 APMV over $Cs_3PMo_{12}O_{40}$ Jing *et al.* (2014b). Impregnating more active phases increased the catalyst stability with respect to the structure (Table 3.27). The maximum reactant conversion was 15.3 % over catalyst at a mass fraction of 40 % ; otherwise, the highest selectivities of MAA and MAC—47 % and 11.4 %, respectively—were achieved for 50APMV/CPM Jing *et al.* (2014b).

Table 3.26 Effect of support on catalyst performance

Catalyst	Temp., °C	Conversion, %	Selectivity, %			Sum of yields, %	Ref.
			MAA	MAC	CO_x	MAA+MAC	
$H_{3.6}Cu_2PMo_{11}VO_{40}/SiO_2$	348	13	11	56	NA	8.7	Bielmeier *et al.* (1994)
$H_4PMo_{11}VO_{40}/Ta_2O_5$	350	28.5	13	41	NA	15.5	Sun *et al.* (2014)
APMV/SBA–15	340	5	10	18	42	1.4	Jing *et al.* (2013)
APMV/ZrO_2/SBA–15	340	6.6	2	10	63	0.7	Jing *et al.* (2013)
APMV/SiO_2	340	11.3	13	15	43	3.1	Jing *et al.* (2013)
APMV/CPM	340	15.3	42	10	31	8	Jing *et al.* (2013)
$P_1Mo_{11}V_1O_x$(50 wt.%)/H_2SO_4–$Ta_2O_5.nH_2O$	350	28.5	12	4	NA	15.5	Ushikubo (2003)
$P_1Mo_{10}V_2O_x$(50 wt.%)/H_2SO_4–$Ta_2O_5.nH_2O$	350	27.5	12	4	NA	15.2	Ushikubo (2003)
$P_1Mo_{11}V_1O_x$(50 wt.%)/$Ta_2O_5.nH_2O$	350	8.7	4	1	NA	4.5	Ushikubo (2003)
$P_1Mo_{11}V_1O_x$(50 wt.%)/diatomaceous earth	350	7.9	4	1	NA	4.7	Ushikubo (2003)

Table 3.27 Catalytic performance for isobutane oxidation over APMV/CPM catalysts at 340 °C Jing *et al.* (2014b)

Catalyst	Conversion, %	Selectivity, %			Sum of yields, %
		MAA	MAC	CO_x	MAA+MAC
10APMV/CPM	0	—	—	—	—
20APMV/CPM	14.7	33	9	38	6.2
40APMV/CPM	15.3	42	10	31	8
50APMV/CPM	14	47	11	27	8.1

APMV=$(NH_4)_3HPMo_{11}OV_{40}$

CPM=$Cs_3PMo_{12}O_{40}$

The surface acidic sites activate isobutane by forming C=C bonds via oxidative dehydrogenation Huynh *et al.* (2009a); Schindler *et al.* (2001). Moreover, they accelerate the oxidation of alkenes to the desired acid products; meanwhile, they desorb products from the catalyst surface and minimize re–oxidation to CO_x Jing *et al.* (2014b); Huynh *et al.* (2009a); Schindler *et al.* (2001). The conversion increased linearly from 280 °C to 350 °C and the maximum was 16 % at 350 °C (Fig. 3.21). The selectivity of MAA was almost constant with temperature; however, MAC selectivity decreased and the maximum was 29 % at 280 °C Jing *et al.* (2014b) (Fig. 3.21).

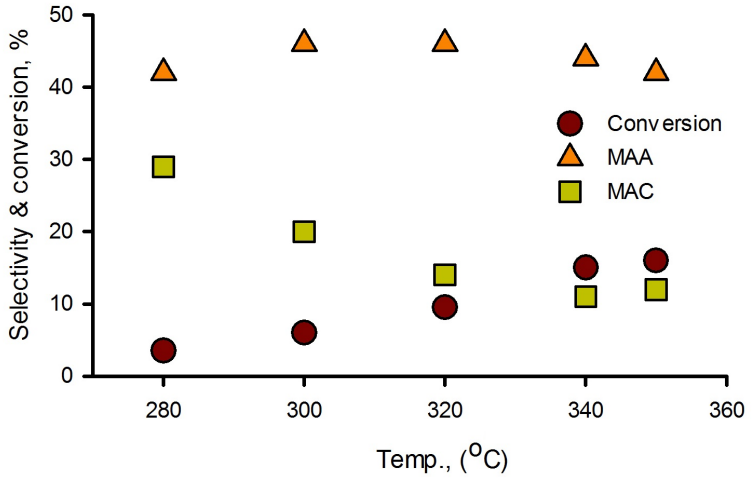

Figure 3.21 The effect of temperature on selectivity and conversion over 50APMV/CPM catalyst and isobutane/O_2/H_2O= 27 %/13.5 %/10 % Jing *et al.* (2014b)

$H_4PVMo_{11}O_{40}$ (H_4PVMo) dispersed over $Cs_3PMo_{12}O_{40}$ showed no activity (less than 0.2 %)

compared to $H_3PMo_{12}O_{40}$ Paul *et al.* (2010). However, the maximum MAA selectivity was 42 % at 4.6 % conversion. $H_4PVMo_{11}O_{40}$ over $HCs_3PVMo_{11}O_{40}$ at the same conditions had the highest activity compared to pure acid ($H_4PVMo_{11}O_{40}$) in which the conversion reached 11 %. In general, the reactant conversion and yield of the desired products increased according to : $H_4PVMo_{11}O_{40}$<$H_4PVMo_{11}O_{40}$/ $Cs_3PMo_{12}O_{40}$<$H_4PVMo_{11}O_{40}$/$HCs_3PVMo_{11}O_{40}$ Paul *et al.* (2010).

Loading $H_4PMo_{11}VO_{40}$ on SiO_2 increased the its activity compared to the bulk $H_4PMo_{11}VO_{40}$; the maximum conversion was 3.3 % with a mass fraction of 50 % $H_4PMo_{11}VO_{40}/SiO_2$ that was five–times higher than that of unsupported one Kanno *et al.* (2010). However, the MAA selectivity dropped Kanno *et al.* (2010), whereas the selectivity of MAA increased asymptotically over unsupported $H_4PMo_{11}VO_{40}$ after 50 min. In general, SiO_2 had a negative effect on selectivity to MAA ; it was equal to 75 % and 63 % for unsupported and supported catalysts, respectively Kanno *et al.* (2010).

Ushikubo activated P–Mo–V heteropolyacid compounds with hydrated tantalum oxide treated with sulfuric acid (H_2SO_4/TA) (Table 3.26). They proposed a mechanism in which catalyst removes H^- from isobutane to produce i–$C_4H_9^+$ because of the strong acid site on the hydrated tantalum oxide treated with sulfuric acid ; thereafter, this intermediate migrates to the surface of the heteropoly acid and oxidizes to MAA and MAC (Scheme 3.17) Ushikubo (2003).

Impregnating Keggin–type heteropolycompounds on high–surface–area silica gel (as a support) reduces the oxidative degradation of the MAA+MAC products by dispersing the heat of reaction. Furthermore the supported catalyst was more stable and performance was unchanged Ballarini *et al.* (2007a).

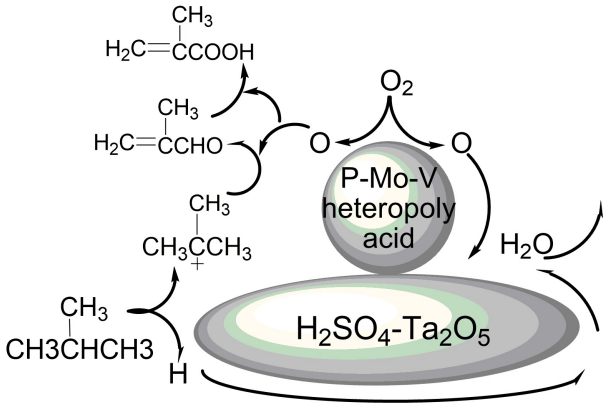

Schème 3.17 – Proposed mechanism over V–heteropolycompounds supported on Ta_2O_5 Ushikubo (2003). Reprinted with permission from ref. 200 Copyright 2003 Elsevier B.V.

Huynha et al. dispersed $Cs_2Te_{0.3}(VO)_{0.1}H_xPMo_{12}O_{40}$ (CsTeV active phase) over α–$La_2Mo_2O_9$ (LM) and β–$La_2Mo_{1.9}V_{0.1}O_{8.95}$ (LMV) for which the pure CsTeV phase was highly active with acceptable selectivity to MAA ; on the contrary, the pure LM and LMV phases were inactive and MAA selectivity was negligible. Increasing LM content up to 50 % in the CsTeV–LM, increased conversion slightly while the MAA reached a maximum of 50 % over LM (Fig. 3.22) Huynh *et al.* (2009b). Both activity and selectivity of desired products decreased with high LM content which was independent of the reaction temperature Huynh *et al.* (2009b).

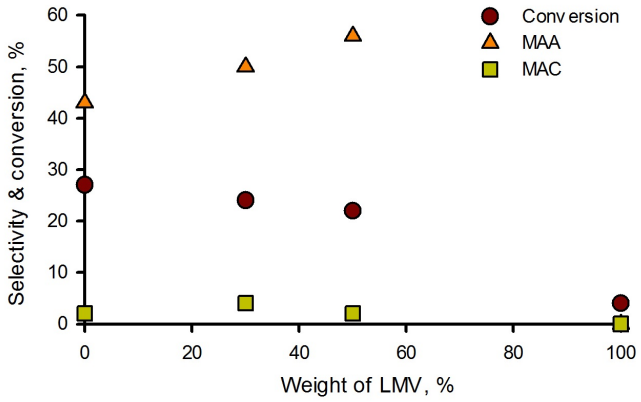

Figure 3.22 The effect of LM support in $Cs_2Te_{0.3}(VO)_{0.1}H_xPMo_{12}O_{40}$ on conversion and selectivity over isobutane/O_2/H_2O= 22.4 %/30.3 %/10 % Huynh *et al.* (2009b)

Based on these studies, the general mechanism assumes that isobutene and MAC are the main intermediates but they have not detected isobutene which may suggest that it reacts rapidly to MAC or it remains on the surface (Scheme 3.18) Costine et Hodnett (2005).

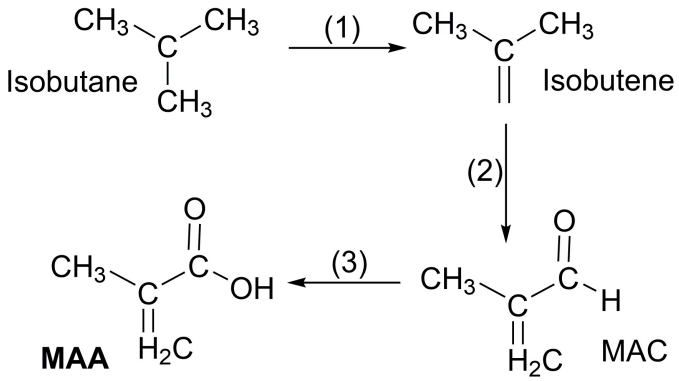

Schème 3.18 – Proposed oxidation network for isobutane to MAA and MAC Costine et Hodnett (2005)

In conclusion to maximize MAA selectivity, the following conditions should be met :

1. operate under reducing (isobutane–rich) conditions to improve selectivity ;
2. dope catalysts with metals (Sb, Fe, and etc.) to achieve stability ;
3. generate active sites during reaction, by partial structural decomposition of the POM.

Isobutane oxidation to MAC and MAA over mixed metal oxides

Mixed metal oxides are more selective to MAC than MAA and molybdenum is a key element to activate isobutane Guan *et al.* (2008d, 2009a, 2007a). Guan et al. investigated mixed metal oxides with the general formula of MoV_xTe_y and found that small amounts of vanadium improved catalyst selectivity to MAC Guan *et al.* (2008d, 2009a, 2007a). The selectivity of MAA and MAC increased continuously with vanadium but the maximum values were only 1.7 % and 27 %, respectively (V/Mo ratio of 0.3) Guan *et al.* (2008d). They claimed that V^{4+}/V^{5+} over the surface strongly affected MAC selectivity according to the redox reaction : $V^{5+}+Mo^{5+}\rightarrow V^{4+}+Mo^{6+}$ Guan *et al.* (2008d, 2007c). Tellurium increased MAC selectivity via oxidation of isobutane on the TeMo–containing crystalline phases (i.e. $TeMo_5O_{16}$) Guan *et al.* (2009a). The maximum conversion was 16 % with Te/Mo<0.17 ; whereas the maximum MAC selectivity was 44 % over $MoV_{0.3}Te_{0.25}$ at 420 °C. Tellurium had no effect on MAA selectivity (4 %) Guan *et al.* (2009a,c, 2008a,b, 2007a). Dispersion of mixed metal oxides over SiO_2, SBA−3 and $AlPO_4$ improved MAC selectivity without changing MAA selectivity dan Sun *et al.* (2011); Wang *et al.* (2012).

Antimony in mixed metal oxide structures had a negative effect on MAA ; however, it increased both selectivity to MAC and conversion Stuyven *et al.* (2014); Shishido *et al.* (2000). The maximum conversion (13 %) and MAC selectivity (37 %) were achieved with a Sb/Mo ratio of 0.1 and 0.5, respectively with $MoV_{0.3}Te_{0.23}Sb_x$ Guan *et al.* (2006, 2007b). Isobutane conversion increased with temperature and the yield of MAC+MAA increased from 3.3 % to 8.8 % up to 470 °C and then decreased at 480 °C on $MoV_{0.3}Te_{0.23}Sb_{0.5}$ (Fig. 3.23) Guan *et al.* (2006).

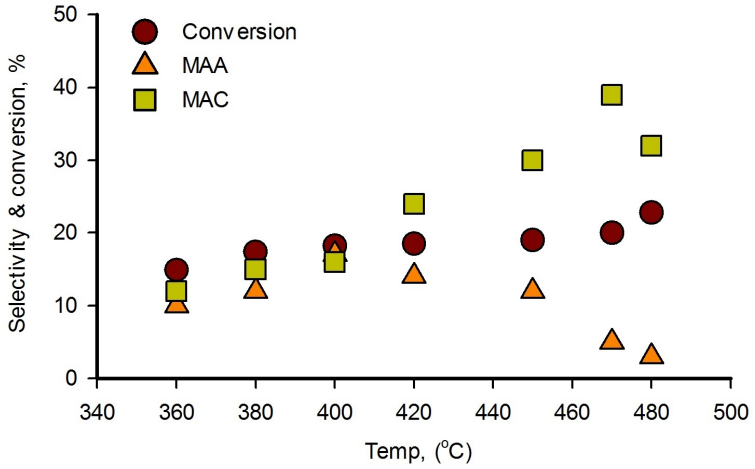

Figure 3.23 The effect of temperature on conversion and selectivity over $MoV_{0.3}Te_{0.23}Sb_{0.5}$ and isobutane/O_2/H_2O molar ratio of 1/1/1 Guan *et al.* (2006)

Adding antimony in the presence of phosphorous ($MoV_{0.3}Te_{0.23}P_{0.3}Sbx$) increased conversion to a maximum of 10 % (Sb/Mo= 0.1). Higher antimony content decreased conversion. The maximum MAC selectivity was 43 % when the Sb/Mo ratio was 0.15 Guan *et al.* (2007b, 2006). Guan et al. proposed introducing antimony into the TeMO phase (M=Mo, V and P) which promoted the oxidative dehydrogenation and accelerated the oxidation of reactants to isobutylene and MAC, and thereafter suppressed the sequential oxidation of MAC to MAA. The $MoV_{0.3}-Te_{0.23}P_{0.3}Sb_{0.1}$ catalyst achieved the best MAC+MAA selectivity (50 %) Guan *et al.* (2007b).

Inserting cerium into mixed metal catalysts (Mo−V−Te−Ce_x) improved catalyst performance where the maximum selectivity of MAA and MAC was 20 % and 33 %, respectively at a Ce/Mo ratio equal to 0.2 Guan *et al.* (2007c). Cerium ions may modify the redox properties Guan *et al.* (2007c). Three possible reaction pathways were proposed to model the reaction network ; inserting oxygen into the methyl C−H bond forming iso–butanol, this compound dehydrates to isobutylene or oxidizes to MAA and MAC. Direct oxidative dehydrogenation of isobutane to isobutylene, which thereafter oxidizes to MAA and MAC is the second pathway. In the third, oxygen inserts into the methane C−H bond resulting in tert-butanol which dehydrates to isobutylene or further oxidizes to acetone (Scheme 3.19) Guan *et al.* (2007c).

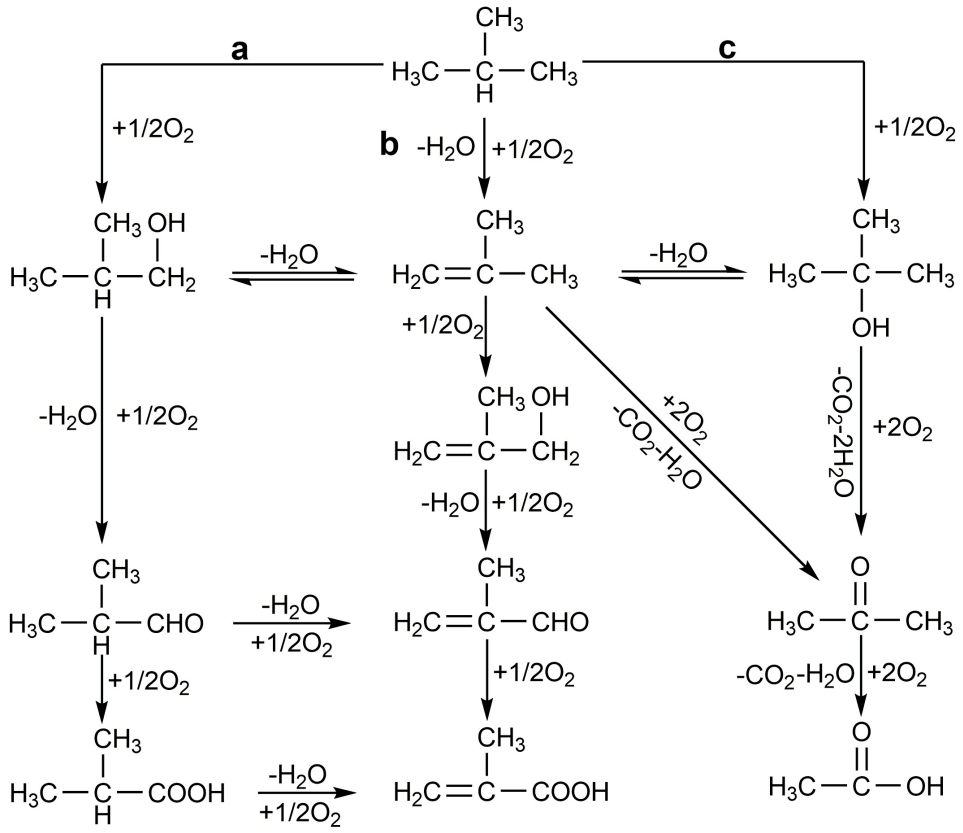

Schème 3.19 – Reaction mechanism over MoVTeCeO catalyst Guan *et al.* (2007c). Reprinted with permission from ref. 82 Copyright 2007 Elsevier B.V.

Hydrothermal synthesis of $MoV_{0.3}Te_{0.25}Sb_x$ improved MAC selectivity compared to the slurry method for which the maximum MAC selectivity was 49 % with Sb/Mo= 0.5. However, the selectivity of MAA decreased with increased antimony insertion where the conversion was almost constant Guan *et al.* (2009b).

Guan et al. proposed that the proper surface V^{5+}/V^{4+} ratio is an effective parameter to maximize the MAA+MAC selectivity over vanadium pyrophosphate–VPP Guan *et al.* (2009d, 2008c). Adding dodecyl amine (DA) as a surfactant in the VPP structure increased selectivity up to ratio of DA/VPP= 1 ; however, their selectivities decreased thereafter Guan *et al.* (2009d).

Most of these studies indicated that MAC and MAA selectivity were higher under isobutane–rich conditions—isobutane :dioxygen molar ratios greater than 2. The triangular diagram shows the feed composition adopted by various companies, with respect to the flammability region at room temperature (Fig 3.24) Ballarini *et al.* (2007b).

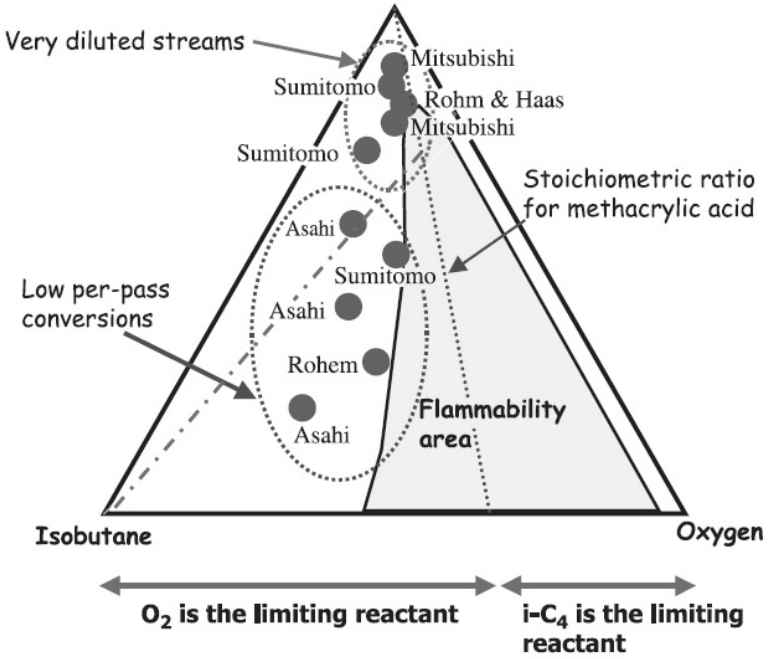

Figure 3.24 Isobutane flammability diagram Ballarini *et al.* (2007b). Reprinted with permission from ref. 14 Copyright 2007 Wiley

Although isobutane is a desirable feedstock for MAA, it must operate in the upper flammability region. To achieve high yield, the feed must be recylced Cavani *et al.* (2001f). Moreover, because the reaction is highly exothermic multi-tubular or fluidized bed reactors are required to control temperature. In the latter case, product combustion in the freeboard region above the catalyst bed may be problematic Edake *et al.* (2017a).

3.6.4 Oxidation of 2–methyl–1,3–propanediol

Recently, Pyo et al. proposed a bio–process in which 2–methyl–1,3–propanediol (2MPDO) oxidizes to 3–hydroxy–2–methylpropionic acid via 3–hydroxy–2–methylpropanal in micro–organisms and then this intermediate dehydrates to MAA and MAC over titanium dioxide at 210 °C Pyo *et al.* (2012). However, the productivity of this bioroute remains low and expensive due to the enzymes.

2MPDO is a co–product of 1,4–butanediol in the hydroformylation process of allyl alcohol and can be an attractive feedstock to produce MAA Dubois (2014); Mahboub *et al.* (2016a). Arkema France patented a process to oxidize 2MPDO to MAA over mixed oxides consisting of Cs, Mo, P, V, Sb and Cu, for which the maximum MAA selectivity was 24 % Dubois (2014).

Darabi et al., oxidized 2MPDO to MAA and MAC over Keggin–type heteropolyacids containing cesium (Cs), vanadium (V) and copper. The maximum selectivities to MAA and MAC were 41 % and 33 %, respectively, over $Cu_{0.5}(VO)O_x/Cs(NH_4)_2PMo_{12}O_{40}$ with 63 % 2MPDO conversion (Fig. 3.25). The MAA selectivity and conversion increased with time ; conversely, MAC selectivity decreased from 64 % to 33 % over 100 min Mahboub *et al.* (2016a,b).

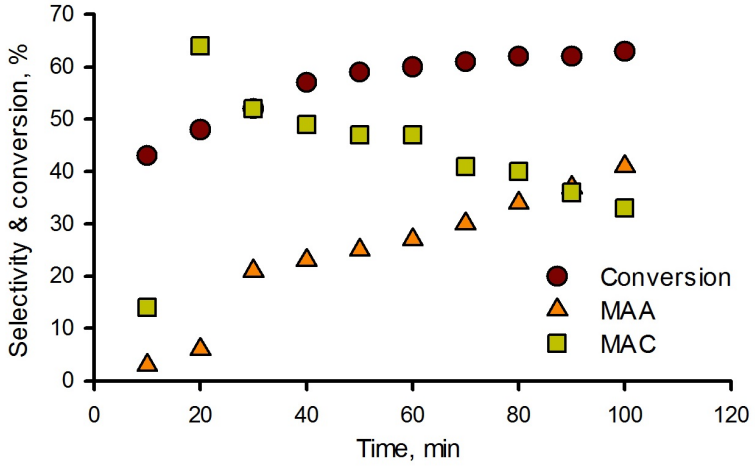

Figure 3.25 Selectivity of methacrylic acid and methacrolein and conversion of 2MPDO over $Cu_{0.5}(VO)O_x/Cs(NH_4)_2PMo_{12}O_{40}$ at 250 °C over isobutane/ O_2/ inert= 13 %/10 %/77 % Mahboub *et al.* (2016a)

In the first step, 2MPDO oxidizes to 3–hydroxy–2–methylpropanal, this intermediate dehydrates to MAC (as the main intermediate) in the second step. Finally MAC reacts with molecular oxygen over the catalyst surface forming MAA (Scheme 3.20) Mahboub *et al.* (2016a).

3.7 Producing MAA and MMA from renewable sources

Raw materials (C_1–C_4) to synthesize MAA (which then esterifies to MMA) are mainly petroleum–based. Renewable biomass is a potential source to produce these raw materials that could reduce the CO_2 burden to the atmosphere Dubois (2011a); Johnson *et al.* (2011). Haas et al. produced carboxylic acids from biochemicals such as lactic acid and citric acid Haas *et al.* (2014). The medium pH necessary for most fermentation processes is above the pK_a value of the carboxylic acid, therefore, carboxylic acid are produced as salts. Adding acids converts carboxylates to their free acids (Gypsum process) Haas *et al.* (2014); Baniel *et al.* (1996).

Several patents have been filed to derive at least one compound from bio sources Dubois et

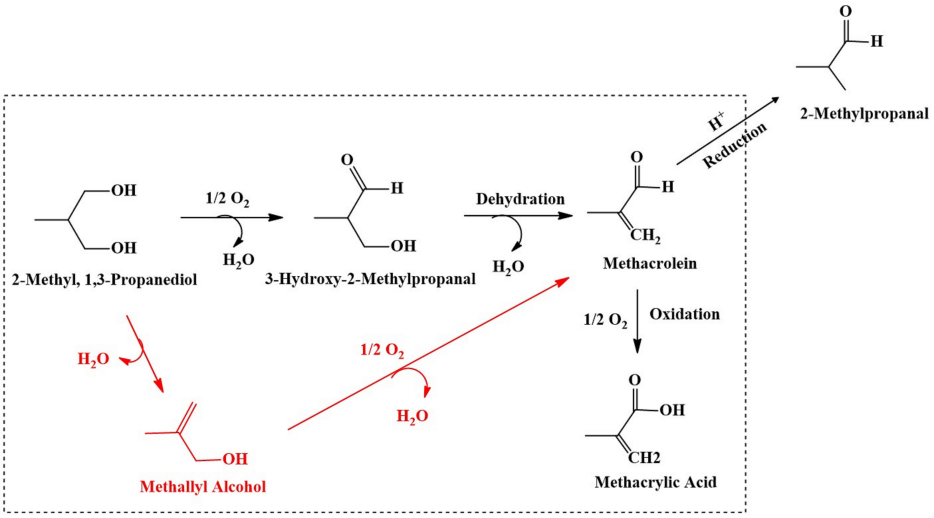

Schème 3.20 – Mechanism for oxidation of 2–methyl–1,3–propanediol to MAA and MAC over $Cs(NH_4)_2PMo_{12}O_{40}(VO)Cu_{0.5}$ at 250 °C Mahboub *et al.* (2016a)

Pirri (2012); Dubois (2011b,a); Dubois *et al.* (2011); Johnson *et al.* (2015). Dubois proposed beginning with MAC derived from biomass and oxidizing it to MAA, then esterifying the MAA to MMA Dubois (2011a). For the ACH route, fermenting plant crops gives ethanol and acetone (ABE process). Dubois et al., proposed producing acetone, cyanohydric acid, or methanol for the ACH route with biomass Dubois *et al.* (2011). Acetobutylic fermentation of C_5 and C_6 sugars produces an acetone–butanol mixture Dubois *et al.* (2011). Methane–oxidizing methylomonas biocatalyst (sp. DH–1) produce acetone Hur *et al.* (2017). The average productivity and specific productivity of acetone were $0.678\,\mathrm{mmol\,h^{-1}}$ and $0.141\,\mathrm{mmol\,h^{-1}\,g^{-1}}$cell, respectively. Hydrothermal liquefaction of sewage sludge or catalytic conversion of palm oil residues are other methods to produce acetone from bio–based matter. Ammoxidation of methane gives hydrocyanic acid.

For an ethylene route, wood gasification, for example, produces syngas as a feedstock for methanol to produce the ester or formaldehyde. The spent liquor and bleaching liquor from cellulose pulp industries are also potential sources for syngas Dubois (2011a). For the ethylene process, methyl propionate is the main intermediate which reacts with formaldehyde–methanol mixture to produce MMA. For this case, biomass can produce at least a fraction of one of the reactants Dubois (2011b). Dehydrating ethanol from ethanolic fermentation of plant matter produces ethylene Dubois (2011b). Acid catalysts transesterify vegetable oils to biodiesel and glycerol. Oxydehydrating the glycerol produces acrylic acid and proprionic acid and from there methyl proprionate.

For C_4 routes, distillation of fusel oils (fusel alcohols) upgrades biomass to isobutanol. Yeast ferments plant material to isobutanol. Isobutanol dehydrates to isobutene and in a subsequent

step partially oxidizes to MAC Dubois (2011a). Global Bioenergies developed technology to convert sugars to isobutene, while Syngip patented a process starting from CO_2. Ethanol or acetic acid are other primary feedstocks to isobutene ($ZA_xZr_yO_z$ catalyst) Sun *et al.* (2015a,b).

Lucite International UK Limited filed patents to produce MAA from base catalysed decarboxylation from itaconic, citraconic, or mesaconic acid Johnson *et al.* (2011, 2015, 2013); Eastham *et al.* (2015). Carlsson et al. reported 70 % yield of MAA from itaconic acid. They proposed a mechanism to decompose citric acid to itaconic acid and then MAA (Scheme 3.21). Carlsson *et al.* (1994).

Itaconic, citraconic or mesaconic acids are available from non–fossil fuel derived sources which are produced from a source of pre–acids, for instance, citric acid or isocitric acid. These pre–acids dehydrate and decarboxylate to itaconic, citraconic or mesaconic acids or from aconitic acid by decarboxylation Eastham *et al.* (2015). Fermenting sugars produce the citric acid and isocitric acid. The maximum selectivity of MAA was 40 %, 49 % and 52 % for citraconic acid, itaconic acid and mesaconic acid, respectively Eastham *et al.* (2015). Base catalysts decarboxylate these substrates best at temperatures above 250 °C (Table 3.28) Johnson *et al.* (2013, 2011, 2015).

Lucien et al., tested base-catalyzed decarboxylation of itaconic acid over transition metal catalysts in which the base part was 0.5M NaOH. The maximum yield of MAA was 65 % over Pd/C–NaOH catalyst at 250 °C where the conversion of itaconic acid was 97.3 % Notre *et al.* (2016).

One disadvantage of the biobased routes relates to the atom economy : the O/C of sugars is 1 but it is equal 0.5 for MAA. Furthermore, the process rejects 2 atoms of carbon per molecule of sugar ($C_6H_{12}O_6$). The molar mass of MMA is 100 g mol^{-1} compared 180 g mol^{-1} of glucose. Consequently, yield on a mass basis can be no better than 56 %.

Table 3.28 The effect of temperature on MAA yield for decarboxylation of itaconic, citraconic and mesaconic acids over NaOH Johnson *et al.* (2013, 2011, 2015)

Reactant	Catalyst type	Temp., °C	MAA yield, %
Itaconic acid	NaOH (0.5M)	250	19.25
Itaconic acid	NaOH (0.5M)	310	58.36
Itaconic acid	NaOH (0.5M)	330	56.74
Itaconic acid	NaOH (0.5M)	350	54.42
Citramalic acid	NaOH (0.005M)	250	33.52
Citramalic acid	NaOH (0.005M)	300	80.80

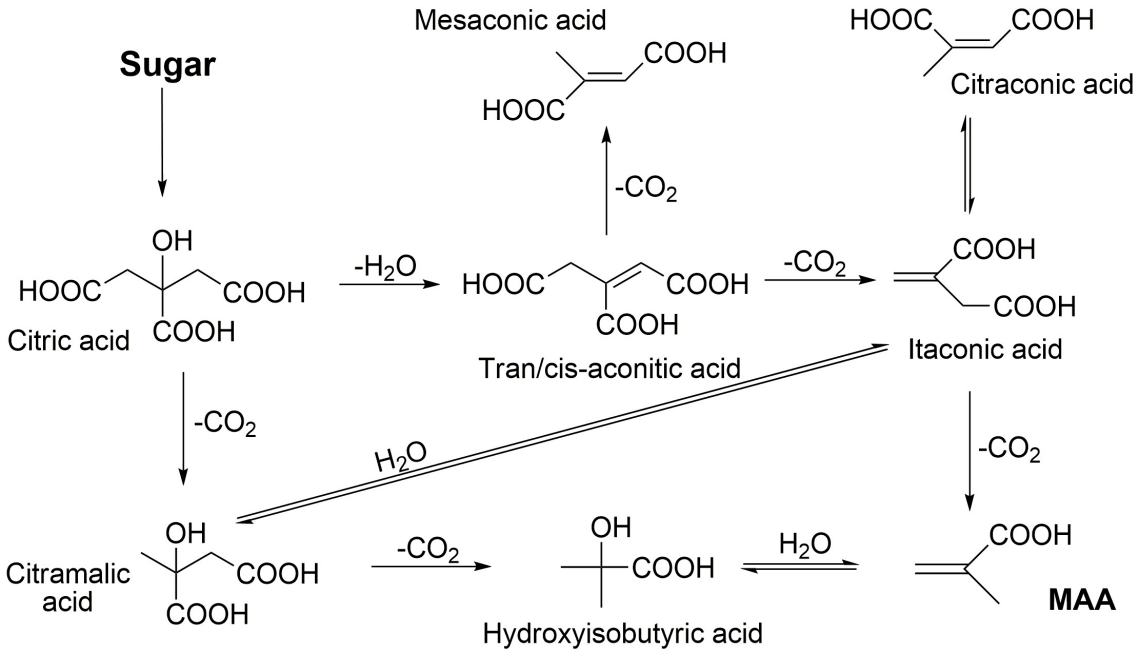

Schème 3.21 – Reaction network to produc MAA from sugar via citric acid Carlsson *et al.* (1994). Reprinted with permission from ref. 226 Copyright 1994 American Chemical Society

3.8 Producing MMA through PMMA depolymerization

Industrial PMMA scraps (off–spec products and cuttings), and some end–of–life PMMA products are collected and when appropriate ground and re–melted for injection or extrusion, or they are depolymerized above 350 °C. It is one of the very few polymers which unzips the chain via a radical mechanism to its monomer in high yield and high purity (more than 95 %) and has seen several decades of development. Cast sheets (produced by bulk polymerization of MMA with little or no additives) are the ideal source for the depolymerization. The installed capacity for PMMA depolymerization is not reported, but in Europe alone in early 2017 about 10 kt of capacity where available at three sites.

There has been several technology developments for PMMA recycling to the monomer (MMA), but still, the prevailing technology is the so–called molten lead bath process Domingo et Cabanero (1953) : PMMA is crushed to centimeter scale particles and then directly injected into molten lead Domingo et Cabanero (1953); Tatsumi *et al.* (1970). The PMMA depolymerizes above 400 °C. The produced gases contain mostly MMA which is cooled and purified by distillation. Some carbonaceous species form in the molten bath and, because of its density these impurities float on the surface, which is regularly scraped to remove them. This process is robust and produces refined MMA without any lead impurities. Because the reaction must be carried out in a controlled atmosphere, contaminates are not released to the environment.

The major issue is linked to the production of carbonaceous residue containing lead, which must be treated before disposal. This creates a constraint on the source of PMMA scrap that can be used. The performance of other molten metals and metal salts is inferieur to Pb Tatsumi *et al.* (1970).

Alternative technologies including dry distillation, reactive extrusion–depolymerization, fluid bed pyrolysis, direct heat transfer with superheated steam or a flame, and even microwaves have been tested (Fig. 3.26) Mannsfeld *et al.* (1966); Shapiro (1966).

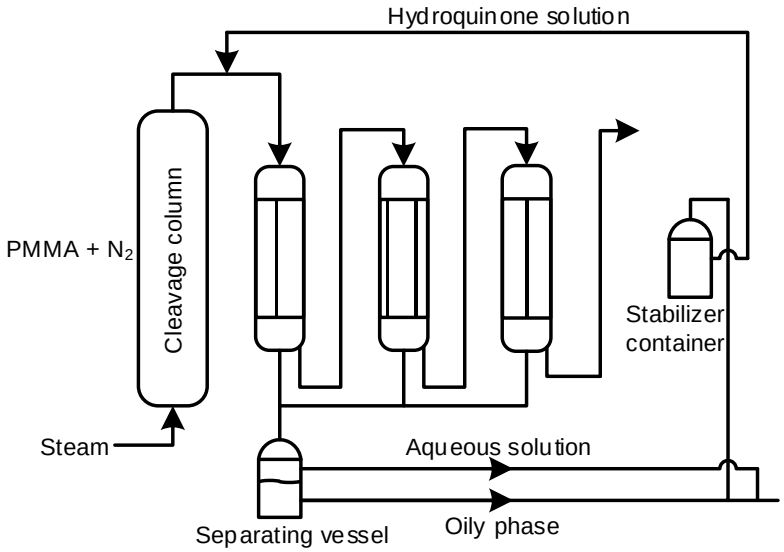

Figure 3.26 Flowsheet of the Superheated steam process Mannsfeld *et al.* (1966)

Dry distillation is probably the oldest process to treat PMMA in which scraps contact a heat source Rohm et GmbH (1935); Strain (1935). The main disadvantage is the inhomogeneous reactor temperature so carbon residues form near the wall.

In reactive extrusion, PMMA depolymerizes in an internally or externally heated single screw extruder or twin screw extruder Tokushige *et al.* (1973); Bruncke *et al.* (1995). The extruder discharges monomer through venting orifices and the monomer cools and condenses. PMMA depolymerizes under vacuum and more than 95 % of the recovered liquid is MMA Tokushige *et al.* (1973); Bruncke *et al.* (1995).

Mitsubishi Rayon operates a 2 kt per year PMMA fluidized bed pilot Sasaki *et al.* (2007). This technology was formerly investigated by ICI, Duvergier and Kaminsky et al. (Fig. 3.27) Kaminsky et Franck (1991); Vaughan et Highgate (1992) In this process, the heat transfer medium is hot sand that is circulated to be reheated in a separate vessel. The PMMA scraps are injected into the fluid bed, which the PMMA depolymerizes when it contacts the hot sand.

The carbonaceous materials produced and the PMMA residues are withdrawn with the sand then separated. The carbon deposits are burned and the hot sand is returned to the reactor. Several reactor configurations can be designed based on this principle. The major difficulties in this process include the fluidization gas selection and how to maintain fluidization over time. An inert gas to fluidized the bed dilutes the product stream, which then requires larger vessels and requires more energy. In several cases MMA was proposed as the fluidization gas, but this could reduce the product quality due to thermal degradation. In the fluidization process, the PMMA melts and then depolymerizes. If the amount of PMMA in the fluid bed becomes too large, molten particles agglomerate and render the bed unstable (bed collapse). As PMMA depolymerizes, the MMA vapor contributes to the fluidization of the bed. But plant start–up remains problematic and would need an inert gas.

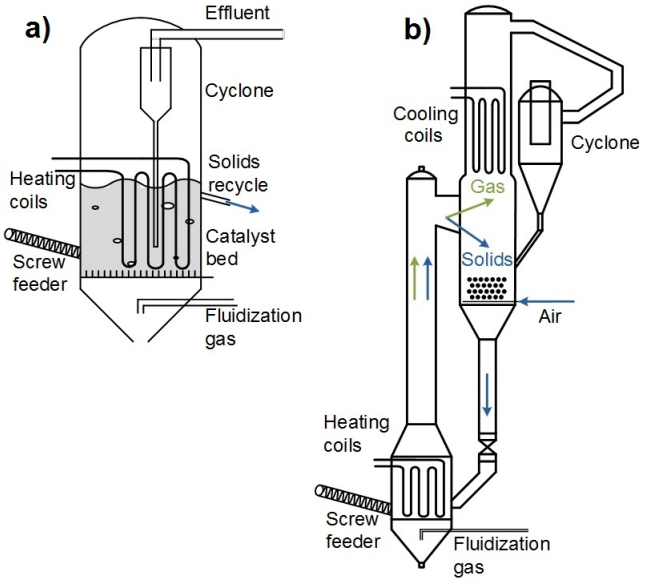

Figure 3.27 Fluidized bed processes to depolymerize PMMA. a) Turbulent fluidized bed (note that the cross-sectional area of the Duvergier process the vessel increases in proportion to increase in volumetric flow rate). Solids are withdrawn from the bed and carbon depostits combusted and returned. A screw feeder introduces polymer to the bed. b) Circulating fluidized bed. Carrier gas entrains solids through a riser to a regenerator/heat exchanger. Air combusts carbon that deposits on the solids and the heated particles return to the transport bed via a standpipe. Heating coils in the bed maintain the reactor at isothermal conditions.

More recently, Metallgesellscahft Aktiengesellschaft and Rohm GmbH Chemische Fabrik, investigated a process combining circulating hot sand as heat carrier (to reheat the sand) and a conveyor where the depolymerization takes place Fabrik et AG (1998). This process decouples the fluidization of the heat transfer media from the reaction itself.

3.9 Conclusions

Acetone–cyanohydrine, ethylene, and isobutylene will remain the primary feestocks to produce MAA and MMA in the near future but emerging technologies offer sustainable alternatives. Catalysis plays a prominent role in these alternative processes with respect to yield, purity, productivity, and economic viability. These new processes must improve on the ACH process with respect to the environmental deficiencies. Oxidation/esterification of light hydrocarbons (C_2–C_4) are furthest along the development path to compete with the ACH process, particularly isobutane. Based on hundreds of studies on this technology, Keggin–type heteropoly compounds are the most promising and achieve the highest selectivity at a respectable conversion.

Yield is sensitive to the type of metal ion inserted in the Keggin–type structure. Partial insertion of metal ions with H^+ has a positive effect on MAA selectivity mainly by accelerating MAC $\rightarrow$ MAA and charge exchange between cation and molybdenum. Cesium is the main cation that acts as a support and increases surface area and disperses the acid. Most of the research concentrates on metal cations—V^{5+}, Cu^{2+}, $Fe^{2+,3+}$, K^+, Te^{4+}, and Sb^{5+}—inserted in cesium salted Keggin–structures ($Cs_xH_{3-x}PMo_{12}O_{40}$)

Replacing some Mo with vanadium or adding vanadium in the Keggin–anion ($[PMo_{12}O_{40}]^{3-}$) also increases MAA selectivity. Catalyst performance is sensitive to hydrocarbon rich versus hydrocarbon lean conditions : MAA selectivity is higher inserting metal ions in cesium salted catalyst in i-C_4–rich conditions ; in i-C_4–lean conditions MAA selectivity is better adding metal ions to the pure acid ($H_3PMo_{12}O_{40}$) or inserting ammonium in the catalyst structure ($(NH_4)_xH_{3-x}PMo_{12}O_{40}$). Catalyst activity and conversion increase inserting metal ions in the Keggin structure in i-C_4–rich conditions ; however, under lean conditions, conversion was insensitive to cation insertion.

The best results were obtained under isobutane–rich conditions. Even at low conversion in this case, recovery and recycle of uncoverted isobutane is economically feasible, while the cost would be prohibitive to recover a mole fraction of 1 % isobutane at the outlet under lean conditions. The isobutane–lean conditions make sense only if very high conversion and yields can be achieved.

At the end, the oxidation state of the catalyst is a very important parameter. Several strategies have been defined to control it : pyridine addition, use Sb_2O_3 (to generate a redox couple with the HPA). Vanadium is an important element in catalyst formulation. Many authors have prepared HPVMo catalysts, but the V leaves the Keggin ion to sit next to it, so equally good catalyst can be prepared by impregnation of vanadyl ion on HPA catalysts.

The bio-based routes are furtherest from commercialization but are attractive despite the poor atom economy of sugar based processes.

3.9.1 Future perspectives for development

Partial oxidation of isobutane to MAA is the most attractive emerging technology for commercialization ; however, the partial oxidation step requires a high yield to be competitive versus alternatives. For example, indirect routes involving either dehydrogenating to isobutene followed by isobutene oxidation (this process has a low technology risk as it is now well established) or isobutane autoxidation to hydroperoxide of t-butyl, which is used as an oxidation agent of propylene to produce propylene oxide and generate t-butanol. The latter can be used as an isobutene substitute in the direct oxyesterification/oxidation to MMA or MAA but it relies on the propylene oxide market, and is therefore not the preferred option. The dehydrogenation route would require additional capital cost that might not be optimized for a small MAA unit. However dehydrogenation yields are rather good, and the cumulated yields of dehydrogenation and oxidation, would be anyway well above what has been achieved so far in direct isobutane oxidation.

Acknowledgments

The authors would like to thank CRIBIQ and MITACS for their financial support of this study.

Biographies

Mohammad Jaber Darabi Mahboub is a PhD candidate in prof. Gregory Patience's research group at Polytechnique Montreal. He received his B.Sc. and M.Sc. in Chemical Engineering at Ferdowsi University of Mashhad (Iran). He has completed experimental work on the partial oxidation of 2-methyl 1,3-propandiol and is modelling the kinetics in collaboration with Arkema, France.

Jean–Luc Dubois is Scientific Director at Arkema. He is in charge of Corporate R&D linked with Catalysis, Processes, Renewables and Recycling. He supervises the long–term projects in this area, and builds relationships with academic partners and companies for collaborative research. Graduated from the Hautes Etudes Industrielles (HEI), he did a Voluntary Service Overseas in Saudi Arabia at the KFUPM/RI. He obtained his PhD from the Institut Français du Pétrole for his work on Catalysts for Oxidative Coupling of Methane. After a Post-

Doctorate at the National Chemical Laboratory for Industry (Tsukuba, Japan), he began his industrial career as a Research Scientist at the R&D Centre of the refining company Elf-Antar-France (now TOTAL), and completed a two-year assignment in the laboratories of Japan Energy in a collaborative research project on hydrodesulphurization catalysts. He moved to the chemical division of the group, Elf-Atochem (now in-part Arkema) in 1997, and worked in R&D Centres in Saint-Avold and Pierre-Bénite (France), where he developed oxidation catalysts and initiate several research projects including dehydration of glycerol to acrolein/acrylic acid, oxidative coupling of alcohols, cross metathesis to monomers for polyamide, hydroformylation for monomers, reactive castor seed crushing to methyl–ester and detoxified seed meal. He is the author of more than 100 publications and 150 patent disclosures.

Fabrizio Cavani is Full Professor of Industrial Chemistry at the Department of Industrial Chemistry "Toso Montanari", University of Bologna. He received a PhD in Industrial Chemistry in 1986. Then he was hired by EniChem Synthesis, where he contributed to the development of a new process for cumene synthesis with H–β zeolite. In 1990 he joined the team of Prof. Ferruccio Trifirò at the University of Bologna. He is author of about 200 papers, more than 30 patents and a few books on Oxidation Catalysis.

Mohammad Rostamizadeh is an Assistant Professor of Chemical Engineering at Sahand University of Technology (Iran). He received his PhD in Chemical Engineering at the Iran University of Science and Technology (Iran) in 2014 working under the supervision of Prof. Abbas Taeb on the synthesis and characterization of zeolite nanocatalyst for methanol to olefin (MTO) reaction. During his doctoral studies, he joined the research group of Prof. Gregory S. Patience at Polytechnique Montreal as a visiting PhD student and worked on catalyst design and shaping for different processes.

Gregory S. Patience returned to academia in 2004 (Polytechnique Montreal) after 14 years at E. I. du Pont de Nemours. His industrial career involved roles in commercializing vanadium pyrophosphate catalyst (Delaware), designing and operating a circulating fluidized bed reactor to convert n-butane to maleic anhydride (Asutrias, Spain), and technical marketing and managing the Fibres Technology Laboratory (Geneva, Switzerland). He has authored books on communication and experimental methods and has contributed to 140 articles and a dozen patents. He was awarded a Canada Research Chair in High Temperature, High Pressure Heterogeneous Catalysis in 2017.

CHAPTER 4 ARTICLE 2 – GAS PHASE OXIDATION OF 2- METHYL-1, 3- PROPANEDIOL TO METHACRYLIC ACID OVER HETEROPOLYACID CATALYSTS

Mohammad Jaber Darabi Mahboub, Samira Lotfi, Jean-Luc Dubois, Gregory S Patience

Published : Catalysis Science & Technology, 6 (17), 2016, 6525–6535

4.1 Abstract

The acetone cyanohydrin process (ACH) to produce methyl methacrylate (MMA) relies on expensive and toxic feedstock and suffers from low yield. Methacrylic acid (MAA) esterification to MMA is an alternative to ACH. However, current processes to produce MAA require multi steps and catalysts lifetime are short. Here we report an alternative chemistry based on 2–methyl–1,3–propanediol (2MPDO) which is a co–product of the hydroformylation of allyl alchohol to 1–4 butanediol. Cesium salt of the Keggin type heteropoly acid (HPA) partially oxidized the 2MPDO to MAA. Inserting vanadium into the HPA reduced the Mo^{6+} to Mo^{5+}, and promoting it with copper increases selectivity to MAA but decreases conversion by 11 %. The HPA catalyst operated in a gas phase fluidized bed in which 0.3 mm nozzle atomized the 2MPDO liquid feed into the bed at 250 °C. The maximum selectivity to MAA and methacrolein (MAC) was 41 % and 33 %, respectively at 63 % conversion. In the first step, oxygen reacts with 2MPDO to form 3–hydroxy–2–methylpropanal. This intermediate dehydrates to methacrolein (MAC) in the second step, and finally in the third step oxygen reacts with MAC to form MAA. The main by-products were methane (gas phase) due to decomposition of reactant and 2–methyl–propanal (liquid phase) because of hydrogen transfer of MAC.

4.2 Introduction

Methyl methacrylate (MMA) is a monomer for poly–methyl–methacrylate (PMMA) (known as Plexiglas® or Altuglas® Jing *et al.* (2014b)) and a speciality chemical for paints and coatings Nagai (2001); Godfrey (1963); Kung (1994), polymers (MBS), a modifier for PVC, as a cement for total hip and knee replacements W.Dormer *et al.* (1998), and for bone inserts Smith *et al.* (1999). The current process is based on acetone cyanhydrin (ACH) that relies on hydrogen cyanide and concentrated sulfuric acid Mizuno et Yahiro (1998); Deng *et al.* (2005). Excess concentrated sulfuric acid generates large quantities of byproduct ammonium bisulfate Cavani (2010); Mizuno *et al.* (1996b); Knapp *et al.* (2001). Mitsubishi Gas Chemicals

developed an ACH process to address the environmental and toxic issues. Short catalyst lifetime and parasitic reactions remain to be solved Shuji *et al.* (1994); Kiochi (1999).

Methacrylic acid (MAA) is the principal substrate for MMA. Annual production has surpassed 4000 kt in 2002 and increases ata rate of 5 % per year Communities (2002). Ethylene and propylene are potential feedstock to produce MAA and would have alower environmental impact compared to the ACH process Nagai (2001); Mizuno et Yahiro (1998); Merger et Foerster (1984); Montag et Mckenna (1991); Drent et Budzelaar (1996); Visuvamithiran *et al.* (2013); McGarvey et Moffat (1991). Ethylene reacts with carbon monoxide and water to produce propionaldehyde, propionic acid, methyl propionate and methacrolein as intermediate products over Cs/SnO_2-SiO_2 catalystMontag et Mckenna (1991). Increasing catalyst activity to fully convert intermediate products is under investigationMerger et Foerster (1984); Montag et Mckenna (1991). Other chemistry that relies on CO and HCHO as a feedstock also involves a multiple steps and consequently investment costs are highDrent et Budzelaar (1996). The Lucite ALPHA process relies on ethylene, CO and CH_3OHDrent et Budzelaar (1996).

Oxidizing propylene in CO, H_2 and water is another alternativeNagai (2001). First propylene reacts to form isobutyric acid that further reacts to MAANagai (2001). High by–product selectivity, low yield isobutyric acid and short catalyst life time are the main drawbacks of this processMcGarvey et Moffat (1991). Moreover, separating isobutyric acid from MAA is challenging, which necessitates near complete conversion of isobutyric acidNagai (2001); McGarvey et Moffat (1991). These disadvantages impede the commercialization of this chemistry.

Direct oxidation of isobutane to MAA is an attractive process because the reaction is exothermic and it conserves carbon (atom economy). Inexpensive feedstock, reduced environmental impact (compared to the other processes), reduced inorganic waste and co–products, and a simple one–step process are advantages of this processSultan *et al.* (2004); Cavani *et al.* (2001f).

Selectivity to MAA with heteropoly compounds and vanadium pyrophosphate catalyst have reached 49 % after 90 h reaction time Sultan *et al.* (2004); Cavani *et al.* (2001f); Misono (2001); Kanno *et al.* (2010); Zhang *et al.* (2013); Paul *et al.* (2010); Jing *et al.* (2014a); Wang *et al.* (2016); He *et al.* (2015); Mizuno et Mison (1998); Mizuno *et al.* (1998). The process operates above the upper flammability region in oxygen lean condition, single pass conversion of the hydrocarbon is dictated by the oxygen concentration and as a consequence it is below 25 % Cavani *et al.* (2001f).

Recently, Pyo et al. Pyo *et al.* (2012) proposed a new approach to produce MAA from 2MPDO

which oxidized through bioconversion to 3–hydroxy–2–methylpropionic acid via 3–hydroxy–2–methylpropanal and the catalytic dehydration of the resulting acid in the presence of a micro–organism. Titanium dioxide (at 210 °C) converted the intermediate to MAA Pyo *et al.* (2012). The productivity of this bioroute remains low and expensive due to the enzymes. Arkema France applied for a patent in which MAA produced from 2MPDO over mixed oxides or heteropolycompounds consisting of Cs, Mo, P, V, Sb and Cu, and selectivity to MAA was 24 % Dubois (2014).

2MPDO is a co-product of 1,4–butanediol in the hydroformylation process of allyl alcohol and has not much application besides usual glycol application. It is an easily handled liquid and has an intermediate boiling point to decompose at mild temperature which can be a proper potential reactant to produce MAA Dubois (2014). In this study, we partially oxidized 2MPDO to MAA and MAC over heteropolyacids with cesium (Cs), vanadium (V) and copper (Cu).

4.3 Experimental

4.3.1 Catalyst preparation

We prepared several catalysts with several metal ions and concentrations (preliminary screening) and found that mixtures of cesium–ammonium in a Keggin structure in presence of vanadium and copper improved catalyst activity and selectivity. In the experimental design, we considered each metal ion as an independent factor at two levels, $2^3 = 8$ experiments (Table 1).

Preparing $Na_2HPMo_{12}O_{40}$ as a precursor.

Sodium molybdate (26.45 g) dissolved in 35 mL of distilled water. We added 0.656 ml H_3PO_4 (85 % by volume) dropwise to the solution followed by 97.4 mL of $HClO_4$ (70 % by volume) with the flow rate of 2 mL min^{-1} until phosphomolybdic acid disodium salt precipitated

Table 4.1 Factorial design—metal ion molar concentration and levels

Parameter	**Symbol**	**Min**	**Max**
Cesium (mole)	x	1	3
Vanadium (mole)	y	0	1
Copper (mole)	z	0	0.5
$Cs_x(NH_4)_{3-x}PMo_{12}O_{40}(VO)_yCu_z$	$2^3 = 8$		

(yellow solid). A sintered porous glass filter ($n°4$) separated the solids from the supernatant and subsequently the solids dried for 24 h at 100 °C Daubrege (1998). In this case we prepared 20 g of $Na_2HPMo_{12}O_{40}$.

$Cs_x(NH_4)_{3-x}PMo_{12}O_{40}(VO)_yCu_z$ catalyst.

A NH_4NO_3 solution (0.1M) dissolved 1.87 g $CsNO_3$ into which we added a $Na_2HPMo_{12}O_{40}$ solution (0.2M) at a flow rate of 2 mL min^{-1} while stirring vigorously until a fine precipitate formed. A centrifuge separated the precipitate from the supernatant and an oven dried the solids ($Cs_x(NH_4)_{3-x}PMo_{12}O_{40}$) for 16 h at 120 °C. 35 mL of deionized water dissolved 2.2 g of $VOSO_4 \cdot 5\,H_2O$ and 1.05 g of $Cu(NO_3)_2 \cdot 3\,H_2O$, which was then added with the flow rate of 2 mL min^{-1} to the solids. A Rota–evaporator homogenized the resulting thick slurry for 3 h. It then dried for 16 h at 120 °C in a ventilated oven, and calcined for 4 h with the temperature ramp of 2 °C min^{-1} at 350 °C under air atmosphere Daubrege (1998); Misono (2001); Okuhara *et al.* (2000); Okuhara (2002); Bruckner *et al.* (2007).

The catalyst powder belong to the Geldart Group B classification : We sieved it to reject particles smaller than 90 µm and greater than 150 µm. Catalyst particle density varied around 3000 kg m^{-3}.

4.3.2 Catalyst characterization

An Autosorb-1 nitrogen porosimeter measured the surface area and total pore volume. The sample degassed 3 h at 200 °C to evaporate residual water.

A TA-Q50IR TGA ramped the used and fresh catalyst samples to 1100 °C at 5 °C min^{-1} and measured the mass loss with time to assess thermal decomposition and coke formation. It maintained a continuous nitrogen flow equal to 20 mL min^{-1}.

A Philipps X'pert diffractometer scanned the catalyst samples with a Cu-Kα radiation source (1.542 Å at 50 kV and 40 mA) over 2θ (5° to 70°) to identify the crystalline structure.

Field Emission Scanning Electron Microscope (FE–SEM) (Jeol JSM-7600TFE) characterized the morphology of the fresh and used catalysts. An EDX detector identified the elemental distribution on the surface.

4.3.3 Reaction procedure

Fluidized bed micro reactors have several advanatages over fixed bed reactors to derive kinetics. Fluidized beds operate isothermally and radial gradients are minimal. Catalyst oxidation

states are uniform throughout the bed due to the continual mixing induced by bubbles. On the other hand, in fixed bed reactors, axial and radial concentration and temperature gradients can be significant particularly in the case of catalyst deactivation or coking Kaarsholm *et al.* (2007). Diluting the bed with inert powders attentuates these affects at the risk of adding uncontrolled parasitic reactions of intermediates. In micro fluidized bed reactors, bypassing is minimal since the bubble size are on the order of mm and we routinely approach 100 % conversion. Finally atomizing gases and liquids into fluidized beds ensures heat transfer rates several order of magnitude greater than in fixed beds.

Therefore, we conducted all experiments in a µ-fluidized bed reactor consisting of a 520 mm long quartz tube with an inner diameter of 8 mm (Fig. 4.1). A 20 µm ceramic disk distributed the gas across the diameter of the tube. It was placed 250 mm from the bottom of the tube. A three-zone furnace maintained the reactor under isothermal conditions and a thermocouple monitored the temperature. Mass flow controllers (from $20-200\,\mathrm{mL\,min^{-1}}$) metered the argon and oxygen flow rates and a syringe pump injected the liquid feed (2MPDO) to a nozzle that atomized the liquid with argon. An Omega pressure transducer (250 $\mathrm{mmH_2O}$ Full Scale) monitored the pressure drop across fluidized bed. Before each experiment, argon purged reactor while the furnace ramped the bed temperature to the desired temperature.

Heat tape traced the exit line to minimize product polymerization and condensation. A quench with distilled water trapped condensable products. A pump circulated the water solution from the bottom of the quench to the exit line of the reactor to improve the dissolution of the condensables. A Gas Chromatograph Mass Spectrometer (Agilent 7890A) (GC–MS) identified compounds from both the liquid and the gas and Pfeiffer Vacuum Thermostar on–line mass spectrometer (MS) monitored the gas effluent from the quench. High Performance Liquid Chromatograph (Varian Prostar) (HPLC) quantified condensable products and reactant in liquid phase. A filter at the gas exit line prevented fines from contaminating the on–line MS, GC–MS and GC (Brucker Gas Chromatograph Scion 456-GC).

The conversion of 2MPDO (X_{2MPDO}) as well as products selectivities(S_p) were calculated as followsLotfi *et al.* (2015) ;

$$X_{2MPDO}(mole\%) = \frac{n^{in}_{2MPDO} - n^{out}_{2MPDO}}{n^{in}_{2MPDO}} \times 100 \tag{4.1}$$

$$S_p(mole\%) = \frac{n_p}{n^{in}_{2MPDO} - n^{out}_{2MPDO}} \times \frac{z_p}{z_{2MPDO}} \times 100 \tag{4.2}$$

where n^{in}_{2MPDO} and n^{out}_{2MPDO} are the molar flow rates of 2MPDO at reactor entrance and exit. In Eq. (2), n_p is the molar stream of each product. z_p and z_{2MPDO} represent the number of

carbon atoms of the products and 2MPDO.

μ-fluidized beds have high heat and mass transfer rates compared to fixed bed but atomizing liquids into the small diameter tubes can agglomerate the solids Lotfi *et al.* (2015). To optimize the spray we tested the ratio of liquid 2MPDO to $Ar_{atomization}$, pressure drop, and nozzle spray configuration to avoid slumping the fluidized bed Liu *et al.* (2008). The best design consisted of atomizing the 2MPDO into a chamber below the nozzle rather than Ar atomizing the liquid at the nozzle tip. We fixed the $Ar_{atomization}$ flow rate to $20\,\mathrm{ml\,min^{-1}}$ and varied the liquid flow rate. At liquid injection rates greater than $0.05\,\mathrm{mL\,min^{-1}}$ the injector blocked. The nozzle tip diameter was 0.3 mm and the optimal liquid injection rate at 250 °C was $0.03\,\mathrm{mL\,min^{-1}}$. The heater maintained the top of the catalyst bed at 300 °C to minimize product condensation. We monitored the pressure drop of the bottom and top of the reactor to reach the uniform pressure fluctuation to calculate the U_{mf}.

Blank tests — injecting 2MPDO into the reactor empty — demonstrated the reactor was inert. Based on literature studies (Lotfi *et al.*, 2015), we set the reactor temperature and feed composition and tested the performance of the eight catalyst samples. We selected the catalyst with the highest yield to MAA and MAC to identify the optimum operating conditions.

4.4 Results and discussions

4.4.1 Catalyst morphology

HPAs containing cesium (Cs^+) have a higher specific surface area compared to the parent acid ($H_3PMo_{12}O_{40}$). Copper decreases surface area in all samples (Table 5.2). All the catalysts are micro–mesoporous materials with pore diameter of 15 Å to 40 Å. The used catalysts have a lower surface area, pore volume, and pore diameter compared with the fresh ones. The pore volume of the prepared catalysts is very low ($<0.20\,\mathrm{mL\,g^{-1}}$) and after the reaction dropped to $<0.15\,\mathrm{mL\,g^{-1}}$.

4.4.2 XRD specification

The main crystalline peaks before and after the reaction for three calcined catalysts are similar (Fig. 4.2). The catalysts have a crystalline cubic structure and the main diffraction peaks are at 2θ= 10.6°, 18.5°, 24.1°, 26.1°, 30.6°, 36.0° and 39.3°. Ammonium salts of 12–molybdophosphoric acid have the same pattern : the diffraction peaks at 2θ = 10.6°, 26.4° and 36.0° correlated to (110), (222) and (332) planes, respectively Nair *et al.* (2010).

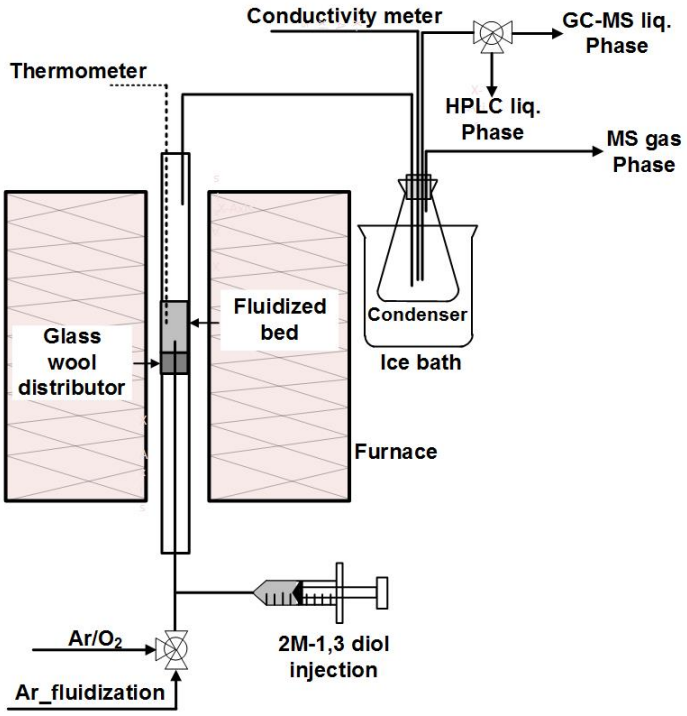

Figure 4.1 Schematic of the experimental set–up

Table 4.2 Specific surface area of fresh (S^1_{BET}) and used (S^2_{BET}) catalysts

Catalyst	abbreviation	S^1_{BET} (m^2/g)	S^2_{BET} (m^2/g)
$(NH_4)_3PMo_{12}O_{40}$	parent acid	9	–
$Cs(NH_4)_2PMo_{12}O_{40}$	$Cs-NH_4$	19	8
$Cs(NH_4)_2PMo_{12}O_{40}(VO)$	Cs_1-V	38	36
$Cs(NH_4)_2PMo_{12}O_{40}Cu_{0.5}$	Cs_1-Cu	19	5
$Cs(NH_4)_2PMo_{12}O_{40}(VO)Cu_{0.5}$	Cs_1-V-Cu	24	21
$Cs_3PMo_{12}O_{40}$	CPM	44	26
$Cs_3PMo_{12}O_{40}(VO)$	Cs_3-V	41	26
$Cs_3PMo_{12}O_{40}Cu_{0.5}$	Cs_3-Cu	26	19
$Cs_3PMo_{12}O_{40}(VO)Cu_{0.5}$	Cs_3-V-Cu	31	6

The general formula for catalyst and support is $Cs_x(NH_4)_{3-x}PMo_{12}O_{40}$. Substituting more cesium ($x \geq 2$) for ammonium decreases active phase concentration ($(NH_4)_3PMo_{12}O_{40}$). In this case, XRD is incapable of detecting the dispersed (active) phase, hence it only shows the body centered cubic phase which allocated to support Kendel et Brown (2011). XRD detects two phases related to the dispersed phase and support for $x<2$. In our experiments, all catalysts displayed the cubic phase associated with the pure alkaline heteropolysalts. Partially substituting NH_4^+ with Cs (e.g. Cs_1-V-Cu) formed a second phase (shown with circle in Fig. 4.2c and f).

The used catalysts maintained their Keggin structures : due to the structural decomposition of the catalyst (Cs_1-V-Cu, for example) MoO_3 forms (shown with star in Fig. 4.2f). However, there is no MoO_3 in Fig. 4.2d and e, which confirms that higher cesium concentrations thermally stabilize the catalyst.

4.4.3 TGA specification

CPM, Cs_3-V-Cu, and Cs_1-V-Cu catalysts lose mass during a temperature ramp (Thermogravimetric analysis) in two steps (Fig. 4.3) : physisorbed water escapes in the first step below 120 °C ; in the second step, ammonia evolves above 350 °C from the active phase which leads to a $H_3PMo_{12}O_{40}(VO)Cu_{0.5}$ dispersed over $Cs_3PMo_{12}O_{40}$. In parallel, the heteropoly-compound liberates acidic protons and forms a Keggin-structure Jing *et al.* (2013, 2014b). Catalyst containing P−Mo−V−O also decomposes to metal oxides such as VO_x, MoO_x, etc. Finally, P_2O begins to sublime which accounts for the further weight loss above 500 °C (Fig. 4.3) Jing *et al.* (2013, 2014b).

The thermal stability of the CPM was superior to either the Cs_1-V-Cu or the Cs_3-V-Cu. The weight loss increased in the following order : CPM (2.8 %) < Cs_3-V-Cu (5.2 %) < Cs_1-V-Cu (7.8 %). We observed the same pattern in the used catalysts : increasing the amount of Cs decreased the weight loss.

The fresh catalyst had more adsorbed water but the weight loss in the used catalyst was higher in the second step, (<320 °C), which we attribute to coke (or possibly adsorbed polymeric carbon). We confirmed that the mass loss in the TGA was due to carbon by measuring the CO and CO_2 signals during the regeneration step (3 % to 4 % of the mass of the catalyst was carbon).

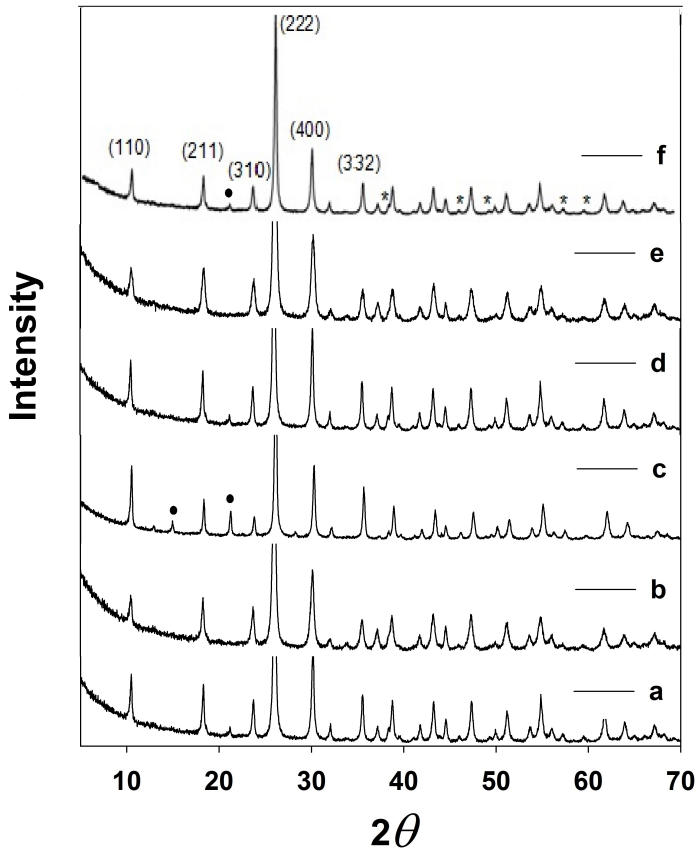

Figure 4.2 XRD diffractograms : a) CPM, b) Cs_3-V-Cu, c) Cs_1-V-Cu (d, e, and f refer to used catalysts, respectively).

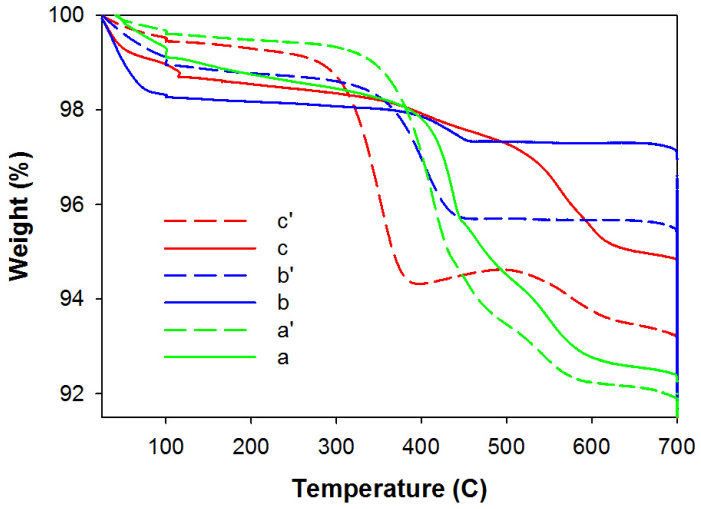

Figure 4.3 Thermogravimetric analysis : a) Cs_1-V-Cu, b) CPM, c) Cs_3-V-Cu ($a\prime$, $b\prime$, and $c\prime$ refer to used catalysts, respectively).

4.4.4 Morphological studies

The surface of the Cs_1-V-Cu before and after the reaction was rough with particle grains varying from 20 nm to 500 nm (Fig. 4.4). The surface did not sinter. EDX spectrum of used Cs_1-V-Cu (Fig. 4.5) confirms the presence of Cs, Mo, P, V, and Cu, while, the used catalyst shows some dark spots related to carbon (Fig. 4.4b).

4.4.5 Catalyst composition

We conducted the first series of experiments with 2 g of each catalyst at 350 °C and the feed composition of 26 %/ 13 %/61 % for 2MPDO/O_2/argon, respectively. The total feed flow at reaction temperature was 210 mL min^{-1}, and all experiments lasted 100 minutes. We assessed the effect of the metal ions in the HPA structure and temperature on selectivity to MAA and MAC with eight experiments (Table 5.3).

The maximum selectivity to MAA and MAC was 11 % and 23 %, respectively over Cs_1-V-Cu. The conversion of 2MPDO for all experiments was 100 %. Partial substitution of NH_4 with Cs in the Keggin structure and inserting of V, Cu as an oxidant and promoter, respectively, increased selectivity to MAA and MAC. Selectivity to MAA and MAC was lower for catalysts with higher Cs loading (e.g. CPM). Oxygen conversion ranged from 93 % to 100 %. Partial oxygen conversion is preferred to maintain the catalyst oxidation state and minimize coke from forming. At high temperature the 2MPDO formed methane (selectivity $\sim$ 40 %) rather than MAA and MAC. The catalyst color changed from green/yellow to black due to coke or reduction. The carbon and oxygen balances were in the range of 77 % to 89 % and 61 % to 103 % , presumable due to the coke.

Table 4.3 Selectivity of main products over catalysts at 350 °C

Catalyst	Selectivity (%)					Coke (%)	Carbon balance	O_2 balance
	MAA	MAC	CO_2	CO	CH_4			
$Cs-NH_4$	2	14	23	1	42	3	85	79
Cs_1-V	4	16	8	25	28	2	82	103
Cs_1-Cu	<1	13	4	33	32	2	86	99
Cs_1-V-Cu	11	23	21	—	32	2.5	89	96
CPM	—	3	7	27	39	3	79	73
Cs_3-V	1.3	12	21	<1	41	3	79	64
Cs_3-Cu	<1	9	20	1.5	43	4	77	61
Cs_3-V-Cu	3	15	7.5	22	37	3	87	84

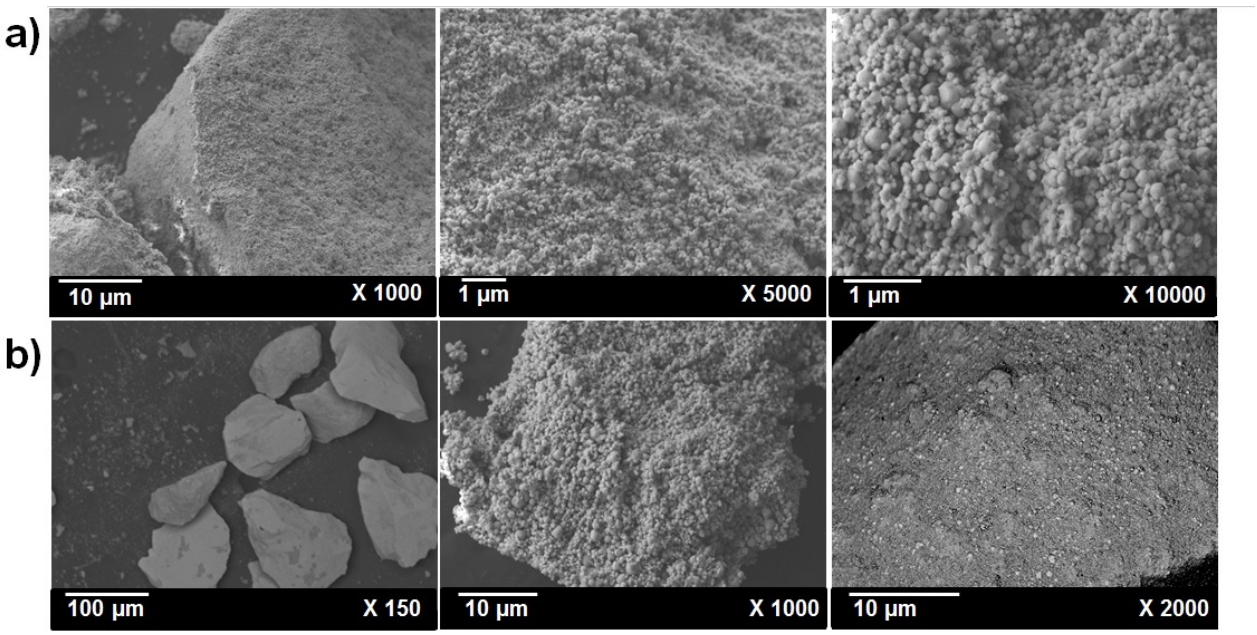

Figure 4.4 FE-SEM characterization for a) fresh C_1-V-Cu, b) used C_1-V-Cu

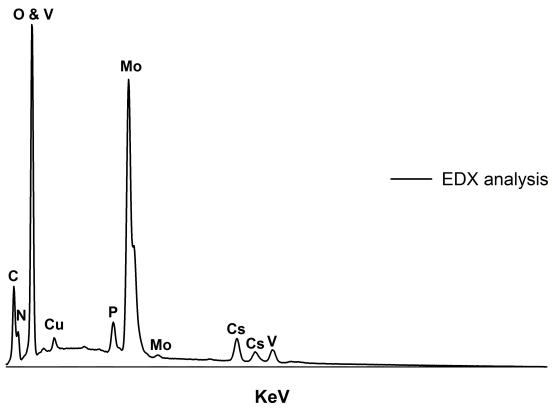

Figure 4.5 EDX spectrum of used Cs_1-V-Cu catalyst

At 250 °C with Cs_1-V-Cu, conversion decreased to 71 %. Coincidentally methane selectivity decreased to 26 % while the MAA and MAC selectivity rose to 14 % and 35 %, respectively.

4.4.6 Optimum catalyst composition and reaction conditions

The reaction time for each of the kinetic experiment (2 levels each for oxygen and 2MPDO at 250 °C) was 100 min. In this study we tried to find the proper catalyst composition (mixture of metal ions) to make sure which catalyst has a best performance on activity and selectivity. Then we investigated different feed compositions to reach the maximum selectivity and monitored the reactant conversion. After each test, an air stream dosed the catalyst at 320 °C for 20 min to remove coke (Table 5.4). The MS monitored the effluent concentration from which we derived the mass of carbon deposited (which helped close the mass balance).

Table 4.4 Catalyst evaluation in different reaction conditions at 250 °C

Run	Catalyst type	Feed Comp. (%)	Conversion (%)	Selectivity (%)			
		2MPDO/O_2/inert		MAA	MAC	CO_x	CH_4
1	CPM	10/10/80	74	< 1	9	42	40
2		10/13/77	76	< 1	6	66	26
3		13/10/77	69	1	13	47	37
4		13/13/74	88	< 1	11	48	37
5	Cs_3−V	10/10/80	77	3	13	47	31
6		10/13/77	82	2	7	64	17
7		13/10/77	72	5	11	51	28
8		13/13/74	75	2	15	53	26
9	Cs_3−Cu	10/10/80	69	3	7	49	33
10		10/13/77	80	< 1	5	60	28
11		13/10/77	77	3	9	55	29
12		13/13/74	72	< 1	9	56	30
13	Cs_3−V−Cu	10/10/80	71	11	22	43	13
14		10/13/77	81	5	14	55	17
15		13/10/77	78	13	31	39	14
16		13/13/74	82	9	27	41	19
17	Cs_1−V−Cu	10/10/80	71	31	39	23	5
18		10/13/77	81	23	29	37	9
19		13/10/77	63	41	33	21	4
20		13/13/74	74	30	44	22	4
21	Cs_1−V	10/10/80	73	26	41	26	3
22		10/13/77	77	18	22	53	7
23		13/10/77	61	35	37	28	1
24		13/13/74	73	27	43	29	1
25	Cs_1−Cu	10/10/80	72	14	51	26	3
26		10/13/77	69	11	31	51	8
27		13/10/77	69	15	48	33	3
28		13/13/74	81	11	37	45	4
29	Cs−NH_4	10/10/80	67	16	44	32	3
30		10/13/77	70	14	27	46	13
31		13/10/77	67	17	43	34	8
32		13/13/74	75	11	31	47	5

The maximum selectivity to MAA was 41 % and of reached 33 % for MAC at 250 °C over Cs_1−V−Cu (Table 4). Selectivity was lowest for the CPM and decreased with increasing oxygen concentration. Therefore, the presence of NH_4 in catalyst structure enhanced the selectivity which concluded that $(NH_4)_3PMo_{12}O_{40}$ acted as an active phase dispersed over support. We suspect that excess oxygen in the gas phase combusted the MAA and MAC.

2MPDO– as the feedstock– reacted with oxygen as well. Lower temperature (250 °C) and oxygen concentration (10 %) decreased the conversion to 63 %. The results again illustrate that the heteropoly compound catalyst containing cesium, ammonium, vanadium and copper acted as the best catalyst to produce MAA and MAC (Table 4).

The patent reports similar selectivity (37.5 %) for a catalyst containing Mo/V/P/Cu/Sb/Cs with a molar composition of 10/0.7/1.1/0.4/0.3/0.5 after 180 min at 315 °C and a molar feed ratio of 2MPDO/O_2/H_2O/inert of 1/2/10/12 Dubois (2014). Here, the best catalyst reaches a 10 % higher selectivity in about half the time Dubois (2014).

The selectivity to MAA over Cs_1-V-Cu increased steadily with time– on–stream (Fig. 4.6). After 30 min it reached 20 % then exceeded 40 % at 100 min. The MAC selectivity at the beginning of the reaction was higher than MAA and then it decreased (Fig. 4.7). We injected MAC as a reactant and did the reaction with the same conditions and it converted to MAA, CO and CO_2 which clearly showed that MAC is an intermediate step to produce MAA. 2MPDO conversion followed a similar trend as the MAA selectivity (Fig. 4.8). The conductivity meter monitored the products online and confirmed there was no product until 20 minutes after initialing the reaction ; the conductivity increased rapidly thereafter. Even after 100 min, the catalysts continue to activate and selectivity increases. However, the aim of this study screen catalysts to optimize its composition and later we study the reactor performance as a function of operating conditions.

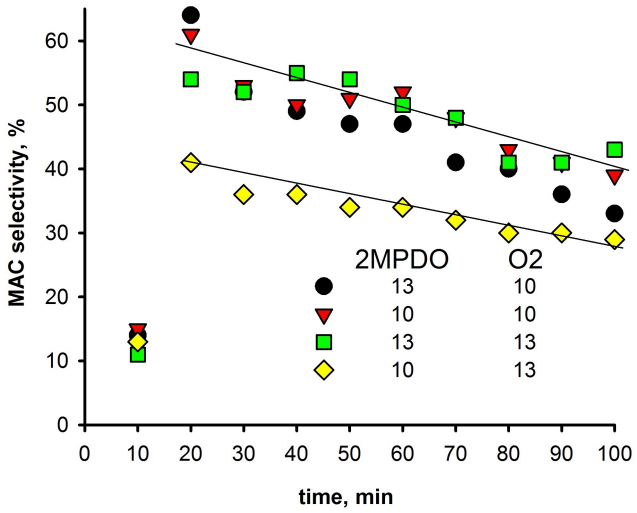

Figure 4.7 MAC selectivity in different reaction conditions over Cs_1-V-Cu catalyst

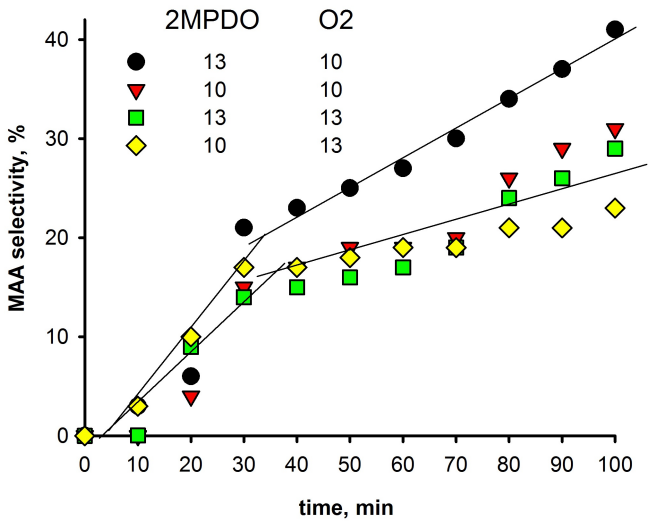

Figure 4.6 MAA selectivity in different reaction conditions over Cs_1-V-Cu catalyst

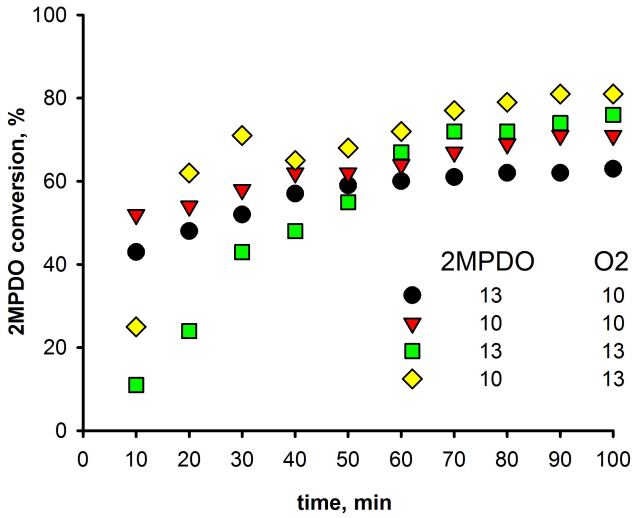

Figure 4.8 2MPDO conversion in different reaction conditions over Cs_1-V-Cu catalyst

GC–MS (Fig. 4.9a,b) and HPLC (Fig. 4.9c) samples confirmed the presence of MAA and MAC in liquid and gas phases and also confirmed that the MAA and MAC selectivity during the first 20 min were low. The HPLC and GC–MS detected traces of acrylic acid and displayed some unknown peaks as well (Fig. 4.9). CO_x selectivity reached 21 %. We were able to close a carbon mass balance to within 8 % (92 %–105 %) including the coke deposition. This difference was due to the unknown by-products formed during the reaction and appearing as minor peaks in the HPLC or GC–MS chromatogram (Fig. 4.9, Table 5.5). The oxygen balance was

in the range of 77 % –111 %. Methane was the main by-product which the selectivity was between 3 % and 39 %.

4.4.7 Evaluation of metals element in catalyst structure

We determined the effect of each cation elements in the catalyst structure to reach the maximum selectivity for desired products with *STATISTICA*® Software. The substitution of Cs^+ as cation for H^+ in $Na_2HPMo_{12}O_{40}$ formed an alkaline salt acting as a support over which the active phase was dispersed and thermally stabilizedSultan *et al.* (2004); Paul *et al.* (2010); Mizuno et Yahiro (1998). Therefore, it was the key parameter for the development of an active catalyst to partially oxdize 2MPDO. Moreover, adding Cs is known to increase the surface area of these catalysts Sultan *et al.* (2004). Partial substitution of ammonia with cesium and adding vanadium and copper enhanced the selectivity (Fig. 4.10).

Vanadium in the form of V^{5+} improved the catalyst activity and selectivitySultan *et al.* (2004); Cavani *et al.* (2001f); Jing *et al.* (2013). Ammonium ions reduced the active metal oxidation state that consequently increased MAA selectivity. Calcining at 350 °C partially vapourized ammonium creating vacancies and Mo reduced from 6+ to 5+Sultan *et al.* (2004); Jing *et al.* (2013). In other words, vanadium atoms were easily removed from the primary structure and participated in the reduction of the catalyst but had no effect on the activation of 2MPDO. Copper facilitated catalyzing the reduction of molybdenum which thus improved the activity and surface acidity of the catalyst Cavani *et al.* (2001f). However, copper did not have a significant effect on catalyst performance in the absence of ammonia in the catalyst structure. Vanadium had a positive effect on all catalysts. Fig. 4.10a shows that the catalyst with lower cesium in the presence of vanadium and copper have a higher selectivity corresponding with catalyst in higher cesium (Fig. 4.10b) which confirms the results of Table 4. Other words, complete substitution of cesium with ammonium had a negative effect on selectivity.

4.4.8 Possible mechanism

The products are detected by GC–MS and HPLC include methacrylic acid, methacrolein, 2–methyl propanal, methane, propanal, butanal and dioxane (Table 5). To account for the MAA and MAC, 2MPDO dehydrates to MAC which then oxidizes to MAA (Fig. 4.11). The HPLC and GC–MS did not detect 3-hydroxy-2-methylpropanal or methallyl alcohol ; however, Kishida et al. proposed the same mechanism for the dehydration of glycerol to lactic acid with 2–hydroxypropenal as an intermediate Kishida *et al.* (2005). Furthermore, hydroxypropanal is an intermediate in the oxidation of 1,3–propanediol to acrolein Díaz *et al.* (2010).

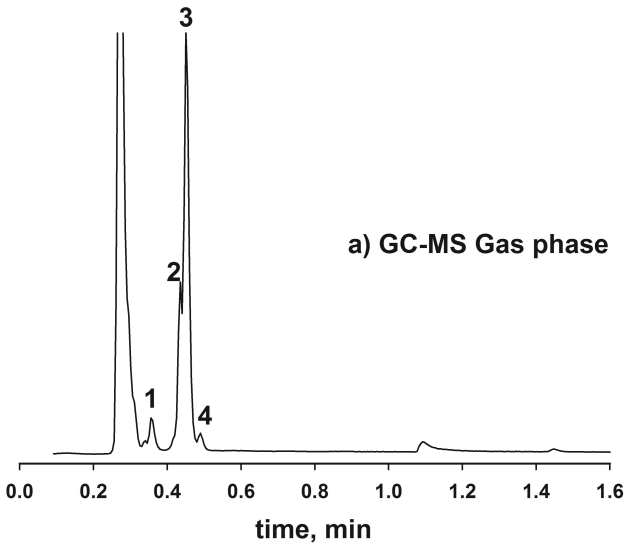
3
2
1
4
a) GC-MS Gas phase
0.0
0.2
0.4
0.6
0.8
1.0
1.2
1.4
1.6
time, min

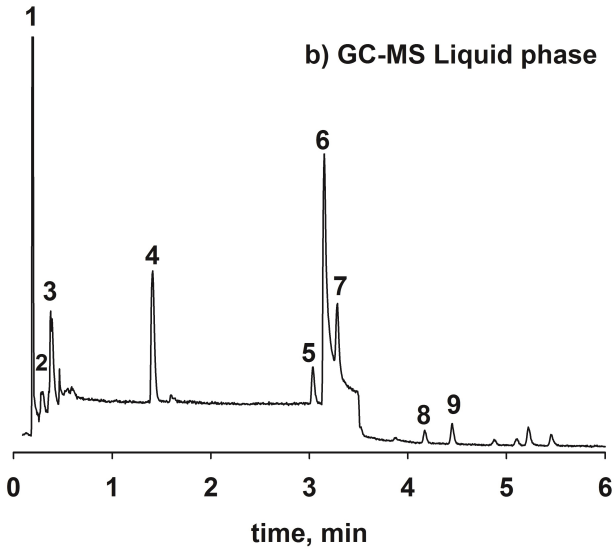
1
b) GC-MS Liquid phase
6
4
3
7
2
5
8
9
0
1
2
3
4
5
6
time, min

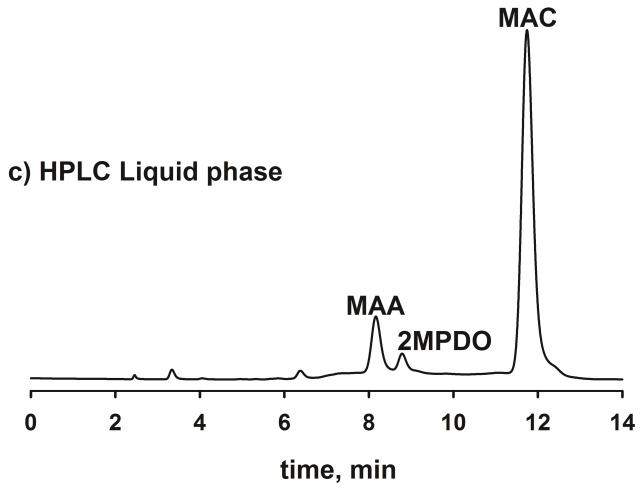

Figure 4.9 Analytical analysis of products a) GC–MS gas phase, b) GC–MS liquid phase, c) HPLC liquid phase

Table 4.5 Major products in liquid and gas phases detected by GC–MS

No.	Name	Phase	z/m (%)						structure
1	Nitrogen	Liquid	28, (M+, 100)	—	—	—	—	—	
2	Propanal	Liquid	58, (M+, 90)	39, (6.6)	29, (100)	—	—	—	
3	Methacrolein	Liquid	70, (M+, 100)	43, (24.5)	42, (21.5)	41, (91)	39, (78.7)	29, (14.3)	
4	Methacrylic acid	Liquid	86 (M+, 73.6)	69, (57.3)	59, (46.9)	43, (50.7)	41, (53.2)	45, (100)	
5	1,3,Dioxane,2-ethyl-5-methyl	Liquid	129, (M+, 12.8)	101, (100)	59, (63.3)	57, (34.7)	55, (88.2)	42, (28.9)	
6	2-methyl,1,3-propanediol	Liquid	90, (M+, 1.5)	57, (40.9)	43, (21.2)	42, (100)	41, (39.8)	39, (13.4)	
7	4-methyl-1,3-Dioxane	Liquid	102, (M+, 55.4)	55, (21.7)	42, (100)	41, (35.5)	39, (16.9)	31, (13.5)	
8	1,3-Dioxane,2-heptyl	Liquid	200, (M+, 1.2)	101, (100)	73, (33.1)	55, (75.5)	43, (34.7)	41, (18)	
9	2-methyl-propanal	Liquid	72, (M+, 61.3)	43, (100)	41, (28.4)	39, (14.2)	29, (37.4)	27, (19.3)	
1	Propanal	Gas	58 (M+, 90.6)	57, (25)	29, (100)	28, (71.2)	27, (54.8)	26, (17.8)	
2	2-methyl-propanal	Gas	72, (M+, 50.2)	43, (100)	41, (80.8)	39, (26.9)	29, (29.3)	27, (39.8)	
3	Methacrolein	Gas	70, (M+, 85)	42, (18.5)	41, (100)	40, (13.3)	39, (82.6)	38, (14.6)	
4	Butanal	Gas	72, (M+, 64.6)	70, (19.3)	57, (28.4)	44, (100)	42, (19.7)	41, (91.1)	

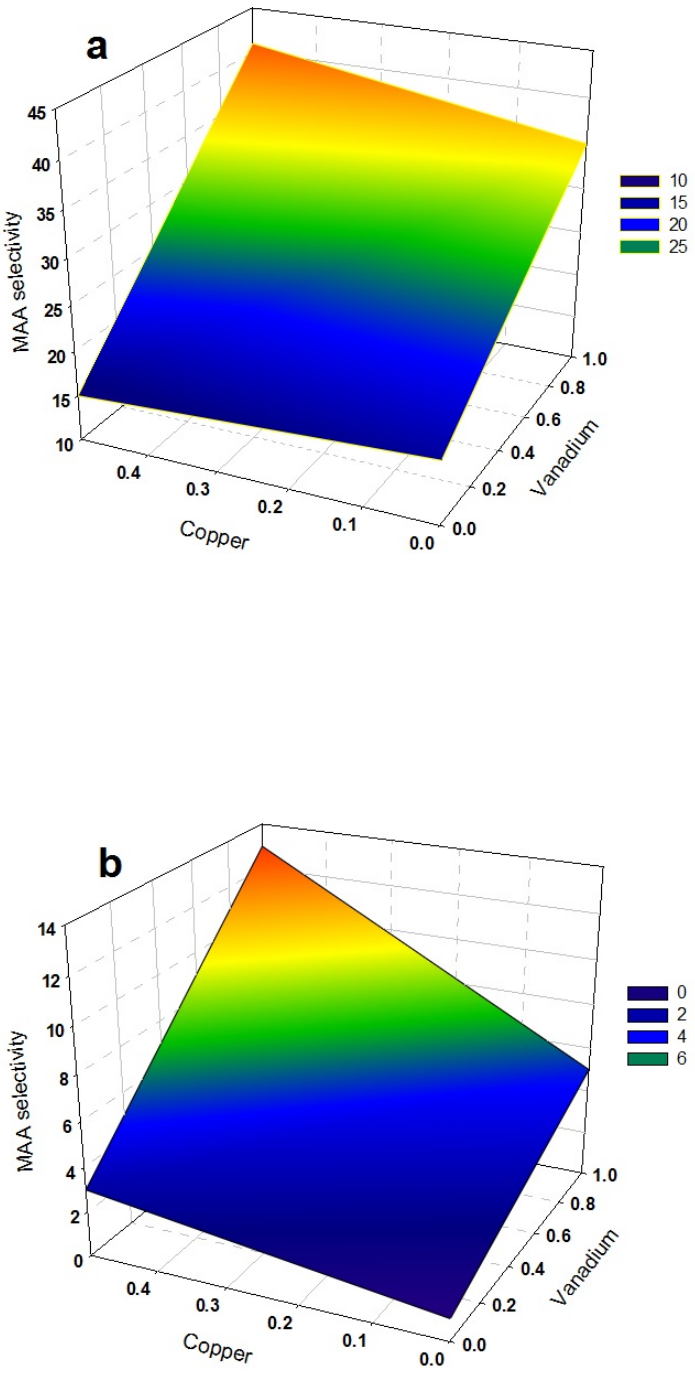

Figure 4.10 Cation element evaluation in catalyst performance with a) Lower Cs b) higher Cs

Therefore, we assume that first 2MPDO reacts to form 3–hydroxy–2–methylpropanal that dehydrates to MAC. To confirm 3–hydroxy–2–methylpropanal is a possible (and likely) intermediate, we added sulfuric acid to a mixture of methacrolein with water and held it at 90 °C. After 24 h we withdrew an aliquot and the GC-MS detected 3–hydroxy–2–methylpropanal. Hydrogen reacts with the MAC to form 2–methyl propanal, which is a major by-product. It is known that allylic alcohol oxidizes to acrolein Schulz et Cox (1993). Moreover, MAC and MAA re–oxidized to COx. Therefore, an alternative mechanism assumes that the 2MPDO dehydrates to 2-Methyl-2-propen-1-ol (β–Methallyl alcohol). Oxygen reacts with this intermediate to form MAC and water. Dioxane was also produced due to the cyclization of the starting material with itself, or with intermediates. Making a C_3 from a C_4 is not surprising since we have seen a lot of methane as a side product. Larger molecules produced due to some coupling reactions from the starting reactant leading to dioxane. However, these are generally present in small amount. From the same reaction mechanism (oxidation of isobutylene/isobutane to MAA), it is not uncommon to find smaller and larger molecules in oxidationCapua *et al.* (2007).

4.5 Conclusions

Catalysts containing cesium and ammonia in presence of vanadium and copper in Keggin structure had the best performance for this reaction. The selectivity to MAA increased with an decrease in oxygen concentration over a Cs_1-V-Cu catalyst and at the end of reaction, it reached 41 % and 33 % selectivity for MAA and MAC, respectively. The main by-products are methane (produced by thermal decomposition) and 2–methyl propanal which is produced by hydrogen spillover of MAC. The fluidized–bed reactor minimizes hot spots and homogeneous carbon distribution over the catalyst surface, it would be an ideal reactor type to regenerate the catalyst compared other conventional fixed beds.

4.6 Acknowledgements

The authors would like to thank MITACS and NSERC for their financial support of this study. Also, the great efforts of Dr. Cristian Neagoe and Davide Carnevali at Polytechnique Montreal for set-up, preparation, and analytic development are greatly appreciated.

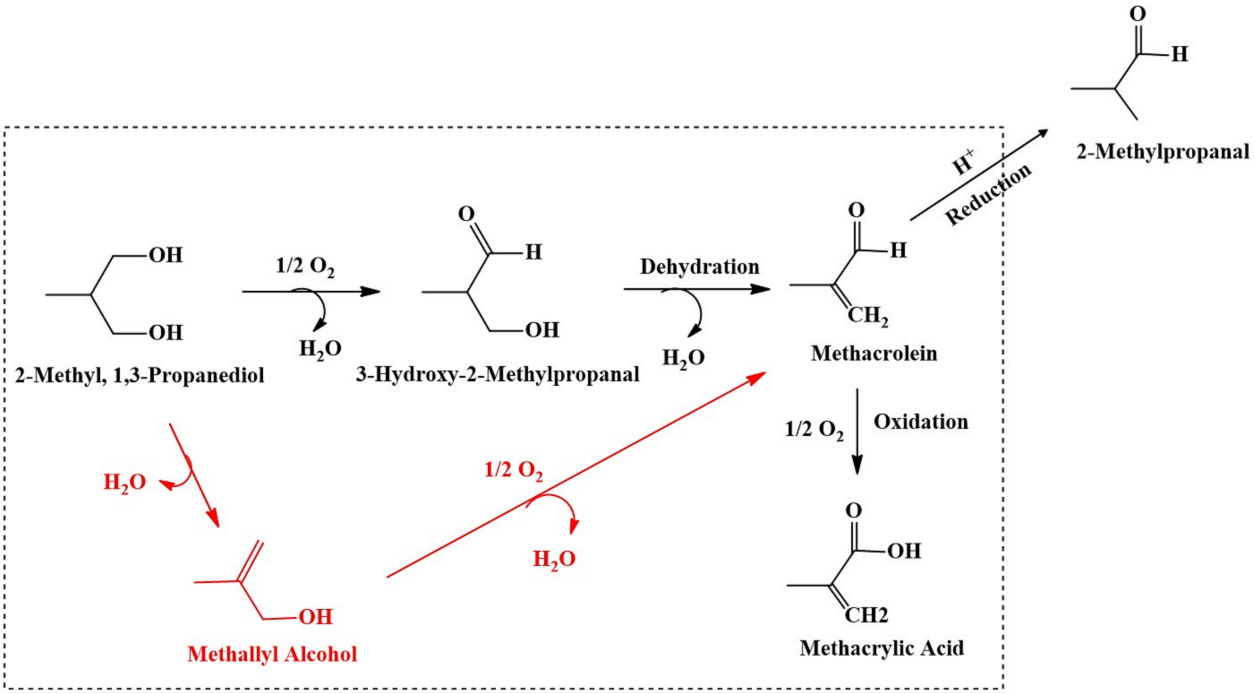

Figure 4.11 Expected reaction pathways for partial oxidation of 2MPDO

CHAPTER 5 ARTICLE 3 - PARTIAL OXIDATION OF 2–METHYL–1,3–PROPANEDIOL TO METHACRYLIC ACID : EXPERIMENTAL AND NEURAL NETWORK MODELING

Mohammad Jaber Darabi Mahboub, Mohammad Rostamizadeh, Jean-luc Dubois, Gregory S Patience

Published : RSC Advances, 6 (115), 2016, 114123–114134

5.1 Abstract

Methacrylic acid (MAA) is a specialty intermediate to produce methyl methacrylate (MMA), which is a monomer for poly methyl methacrylate. Current processes to MMA and MAA rely on expensive feedstocks and multi–step processes. Here we investigate the gas–phase oxidation of 2–methyl–1,3–propanediol (2MPDO) to MAA over heteropolycompounds as effective catalysts, finding that the maximum selectivity to MAA was 41 % with 63 % conversion of reactant at 250 °C over $Cs(NH_4)_2PMo_{12}O_{40}(VO)Cu_{0.5}$. Cesium (Cs) stabilized the catalyst structure at 250 °C, and vanadium (V) and copper (Cu) played a positive role as an oxidant and promoter, respectively. A 0.3mm nozzle atomized the liquid reactant over the catalyst surface into a µ–fluidized bed reactor. The proposed Artificial Neural Network (ANN) model predicts MAA selectivity based on 2MPDO and oxygen compositions and catalyst components (Cs, V, Cu) as independent factors. The model accounts for 97 % of the variance in the data (R^2=0.97). Vanadium as a catalyst component and oxygen concentration are the two most significant factors. Genetic algorithms (GA) coupled with ANN modeling optimized the input parameters to improve the selectivity. The selectivity to MAA over the optimized catalyst ($Cs(NH_4)_2PMo_{12}O_{40}(VO)Cu_{0.15}$) and optimum feed compositions (2MPDO/O_2/Ar= 13 %/10 %/77 %) was 43 % at 250 °C.

5.2 Introduction

Methyl methacrylate (MMA) is a constituent in paint, coating dispersion agents, modifiers for PVC, bone inserts and is a monomer for poly–methyl–methacrylate (PMMA)Nagai (2001); Godfrey (1963); Kung (1994); Smith *et al.* (1999); W.Dormer *et al.* (1998). One process to produce MMA is based on acetone and cyanohydrin but the reactants are expensive and it generates a high volume of byproducts Mizuno et Yahiro (1998); Deng *et al.* (2005); Cavani (2010); Mizuno *et al.* (1996b); Knapp *et al.* (2001). Methacrylic acid (MAA) is the principal

monomer to produce poly(methacrylic acid) ; however, it is a potentially economic feedstock to produce methyl methacrylate. Catalyst lifespan, multi–step reaction processes and low conversion impede the commercialization of the oxidation of light hydrocarbons (ethylene, propylene, isobutene and isobutane) to MAA Wood (2001); Nagai (2001); Mizuno et Yahiro (1998); Merger et Foerster (1984); Montag et Mckenna (1991); Drent et Budzelaar (1996); McGarvey et Moffat (1991); Sultan *et al.* (2004); Cavani *et al.* (2001f); Misono (2001); Kanno *et al.* (2010); Zhang *et al.* (2013); Paul *et al.* (2010); Mizuno et Mison (1998); Mizuno *et al.* (1998). Recently, we proposed the gas–phase partial oxidation of 2–methyl–1,3–propanediol (2MPDO) to MAA and methacrolein (MAC) rather than olefins. After 1 h time–on–stream, MAA selectivity in the fluidized bed reactor reached 41 %. Dubois (2014); Mahboub *et al.* (2016a).

Reaction conditions and catalyst compostion are the main factors to maximize MAA selectivity. Many studies compare the performance of metals versus non–metal ions in the catalyst. Keggin–type polyoxometalates containing phosphorus and molybdenum are the most active and selective heterogeneous catalysts for the oxidation of isobutane and 2MPDO to MAA Mahboub *et al.* (2016a); Dubois (2014); Nagai (2001); Merger et Foerster (1984); Paul *et al.* (2010); Ballarini *et al.* (2007a); McGarvey et Moffat (1991); Sultan *et al.* (2004); Cavani *et al.* (2001f); Misono (2001); Kanno *et al.* (2010); Zhang *et al.* (2013); Mizuno et Mison (1998); Mizuno *et al.* (1998). However, phosphomolybdic acid ($H_3PMo_{12}O_{40}$) is a poor and non–stable catalyst to oxidize lower alkanes Kozhevnikov *et al.* (1996), though inserting metal ions and protons into the catalyst structure enhanced catalyst performance Okuhara *et al.* (2000); Okuhara (2002); Lyons *et al.* (1999). Substituting Cs^+ with H^+ in $H_3PMo_{12}O_{40}$ enhances MAA+MAC yield Okuhara *et al.* (2000); Sultan *et al.* (2004); Mahboub *et al.* (2016a). Cesium forms an alkaline salt in the catalyst structure and acts as a support over which the active phase is dispersed and thermally stabilized Mizuno et Yahiro (1998); Misono (2001); Mizuno et Mison (1998); Paul *et al.* (2010); Okuhara (2002); Mahboub *et al.* (2016a). Ammonium ions increase the surface area and enhance MAA selectivity Jing *et al.* (2014b); Cavani *et al.* (2001f); Sultan *et al.* (2004); Jing *et al.* (2013). Vanadium in the form of V^{5+} reduces Mo^{6+} to Mo^{5+}, which improves or accelerates both the reduction and reoxidation steps and consequently increases catalytic activity Jing *et al.* (2013, 2014b); Mizuno et Mison (1998); Bruckner *et al.* (2007); Huynh *et al.* (2009a). Copper (Cu) acts as a promoter into the catalyst structure Mizuno *et al.* (1998); Mahboub *et al.* (2016a). Partially substituting iron in a Keggin anion decreases selectivity to MAA and conversion Knapp *et al.* (2001). However, it increases selectivity by inserting into the catalyst structure as a counter cation Knapp *et al.* (2001); Min et Mizuno (2001b); Etienne *et al.* (2003). Langpape et al. demonstrated that inserting iron into the acid structure of the support on the cesium salt increases selectivity

without changing the activity of the acid phase Langpape et Millet (2000). Tellurium as Te^{4+} is a counter–cation that enhances selectivity to MAA and MAC Huynh *et al.* (2009a,b). Hundreds of catalysts oxidize isobutane MAA and MAC (Table 5.1).

Identifying the optimal catalyst composition that maximizes yield and selectivity is time consuming Rostamizadeh et Rizi (2012). Combinational methods and Design Of Experiments (DOE) reduce the number of experiments and identify better experimental strategies to establish the best combination of promoters and dopants Rostamizadeh et Rizi (2012). Black box modeling and optimization such as response surface methodology (RSM), artificial neural networks (ANN) and genetic algorithms (GA) are capable of modelling and optimizing the composition of heterogeneous catalysts Hadi *et al.* (2016). ANN recognizes, classifies and generalizes patterns. It reduces experimental noise and can approximate the performance outside the range of the factor input space Rostamizadeh et Rizi (2012); Rostamizadeh *et al.* (2013). The technique does not require knowledge of the phenomenological equations the describe the process hydrodynamics or the reaction kinetics Rostamizadeh *et al.* (2013). ANN is widely applicable in science and technology fields such as economics, chemistry, separation, chemical engineering, reaction engineering, computer science, water and waste–water treatment Ahmadpour *et al.* (2014); Rashidi *et al.* (2015); Corma *et al.* (2005); Misra et Saha (2010); Hamzaoui *et al.* (2011); Shabanzadeh *et al.* (2015); Sarve *et al.* (2015); Adabi *et al.* (2015); Asfaram *et al.* (2016); Ahmadpour *et al.* (2013).

Rostamizadeh et al. applied ANN modeling to predict methanol conversion and propylene selectivity in the methanol to propylene reaction (MTP) in a fluidized bed reactor Rostamizadeh *et al.* (2014). Inputs included reaction conditions—temperature, flow rate, pressure, feed concentration—and catalyst composition—metal ion ratios. The close agreement between the results and the ANN model demonstrated the applicability of this approach to describe and predict complex catalytic processes.

Multi–layer feed–forward neural networks with a back propagation training algorithm, known as back propagation neural network (BPNN) or multi–layer perceptrons (MLPs) are well established models for engineering applications Rostamizadeh *et al.* (2013); Orkcu et Bal (2011).

BPNN consists of input data, hidden layers including neurons, and training data sets Rostamizadeh *et al.* (2013, 2014). It is necessary to normalize input values to start network training which acts as linear or nonlinear mathematical function to predict outputs. The training develops a model according to input data to generate a network Rostamizadeh *et al.* (2013, 2014). Mean squared error (MSE) and root mean squared error (RMSE) are the error functions in the algorithm to compare the model predictions and the experimental data

Table 5.1 Summary of MAA and MAC production over different kinds of catalysts

Used catalyst	Feed Comp. (v/v%) 2MPDO/O_2/Inert/Water	Conversion (%)	Temp. ($°C$)	Selectivity MAA	Selectivity MAC	Ref
$H_3PMo_{12}O_{40}$	26/13/49/12	4	340	4	12	Sultan *et al.* (2004)
$H_4PMo_{11}VO_{40}$	26/13/49/12	3	340	25	39	Sultan *et al.* (2004)
$Cs_{1.15}(NH_4)_{1.85}HPMo_{11}VO_{40}$	26/13/49/12	6	340	45	15	Sultan *et al.* (2004)
$(NH_4)_3PMo_{12}O_{40}$	26/13/49/12	4	340	33	21	Sultan *et al.* (2004)
$(NH_4)_3HPMo_{11}VO_{40}$	26/13/49/12	2	340	49	32	Sultan *et al.* (2004)
$Cs_{2.5}H_{0.5}PMo_{12}O_{40}$	17/33/50/0	16	340	24	7	Mizuno *et al.* (1996b)
$Cs_{2.5}Ni_{0.08}H_{0.34}PMo_{12}O_{40}$	17/33/50/0	24	340	27	6	Mizuno *et al.* (1996b)
$Cs_{2.5}Ni_{0.08}H_{1.34}PVMo_{11}O_{40}$	17/33/50/0	31	340	29	4	Mizuno et Yahiro (1998)
$Cs_2HPMo_{12}O_{40}$	17/33/50/0	11	340	34	10	Mizuno *et al.* (1998)
$Cs_2Te_{0.3}V_{0.1}H_xPMo_{12}O_{40}$	27/13.5/49.5/10	16	350	54	11	Huynh *et al.* (2009a)
$H_{1.8}Te_{0.6}PMo_{12}O_{40}$	27/13.5/49.5/10	6	355	27	22	Huynh *et al.* (2009a,b)
$Cs_2Fe_{0.2}H_{0.4}PMo_{12}O_{40}$	33.4/17.2/49.4/0	7	340	24	17	Langpape et Millet (2000)
$Fe_{0.85}H_{0.45}PMo_{12}O_{40}$	33.4/17.2/49.4/0	4	340	9	27	Langpape et Millet (2000)
$Cs_2HPMo_{12}O_{40}$	33.4/17.2/49.4/0	7	340	12	14	Langpape et Millet (2000)
$Cs_{1.5}Fe_{0.5}(NH_4)_2PMo_{12}O_{40}$	25/25/35/15	8	360	21	4	Knapp *et al.* (2001)
$Cs_{1.5}(NH_4)_2PMo_{11.5}Fe_{0.5}O_{39.5}$	25/25/35/15	8	360	15	4	Knapp *et al.* (2001)
$H_xFe_{0.12}Mo_{11}VPAs_{0.3}Oy$	29/29/42/0	24	370	70	4	Deng *et al.* (2005)
$Cs_{2.5}Fe_{0.08}H_{0.26}PMo_{12}O_{40}$	17/33/50/0	14	340	–	30	Min et Mizuno (2001b)
$H_4PVMo/Cs_3PMo_{12}O_{40}$	26/13/49/12	5	340	42	17	Paul *et al.* (2010)
$Fe_{0.5}(NH_4)_{2.5}PMo_{12}O_{40}$	26/13/49/12	6	350	32	14	Etienne *et al.* (2003)
$(NH_4)_3PMo_{12}O_{40}$	26/13/49/12	7	380	40	11	Cavani *et al.* (2001f)
$(NH_4)_3PMo_{12}O_{40}/Sb_{0.23}Ox$	26/13/49/12	6	350	45	12	Cavani *et al.* (2001f)
$(NH_4)_3HPMo_{11}VO_{40}$/CPM	27/13.5/49.5/10	15	340	42	10	Jing *et al.* (2013)
$(NH_4)_3HPMo_{11}VO_{40}/SiO_2$	27/13.5/49.5/10	11	340	13	15	Jing *et al.* (2013)
$(NH_4)_3HPMo_{11}VO_{40}$	27/13.5/49.5/10	3	340	34	20	Jing *et al.* (2013)
40 $(NH_4)_3HPMo_{11}VO_{40}$/CPM	27/13.5/49.5/10	15	340	42	10	Cavani *et al.* (2001f)
$(NH_4)_3PMo_{12}O_{40}$/Silica	26/13/49/12	10	350	37	3	Ballarini *et al.* (2007a)
$Cs(NH_4)_2PMo_{12}O_{40}(VO)Cu_{0.5}$	13/10/77/0	63	250	41	33	Mahboub *et al.* (2016a)

(Fig. 5.1)Hadi *et al.* (2016); Rostamizadeh *et al.* (2013, 2014).

$$MSE = \frac{1}{n}\sum_{i=1}^{n}(m_i - M_i)^2 \tag{5.1}$$

$$RMSE = \sqrt{\frac{1}{n}\sum_{i=1}^{n}(m_i - M_i)^2} \tag{5.2}$$

Coupling ANN and a genetic algorithm (GA) is an intelligent approach to optimize the catalyst design of any process. In fact, the ANN model can be a fitness function for checking the GA. Hadi et al. coupled ANN and GA to design and optimize M-Mn/ZSM-5 systems Hadi *et al.* (2016). Niaei et al. designed H-ZSM-5 catalyst for the methanol to gasoline (MTG) reaction with ANN-GA Mousavi *et al.* (2013).

Izadkhah et al. optimized Ag/ZSM-5 catalyst to eliminate volatile organic compounds (VOCs) by coupling the ANN-GA and included catalyst formulation, preparation conditions and loading of the metal atomic descriptors in their analysis Izadkhah *et al.* (2012). Omata et al. studied the methanol synthesis and applied ANN-GA to optimize the catalyst design (Cu-Zn-Al-Sc-B-Zr) and preparation conditions including calcination temperature and precipitant concentrations Omata *et al.* (2004). However, there are no existing studies that model catalyst design and optimize the operating conditions for the gas–phase oxidation of 2MPDO to MAA. In this study, we present the experimental and modeling results for this reaction. Ultimately, GA coupled with the proposed ANN model as a fitness function optimize the input parameters and predict the output value.

5.3 Experimental

5.3.1 $Cs_x(NH_4)_{3-x}PMo_{12}O_{40}(VO)_yCu_z$ Catalyst preparation

We prepared eight cesium (Cs) salted heteropoly catalysts containing vanadium (V) and copper (Cu) following a full factorial design (two–levels for each) to evaluate the catalyst performance (Table 5.2) Daubrege (1998). 20 g of $Na_2HPMo_{12}O_{40}$ dissolved in 25 mL of distilled water (as precursor) was added dropwise to a solution of $CsNO_3$–NH_4NO_3 (containing 1.87 g of $CsNO_3$ and 0.1M of NH_4NO_3) until a fine precipitate formed. We then filtered and dried the thick slurry for 16 h at 120 °C and recovered $Cs_x(NH_4)_{3-x}PMo_{12}O_{40}$ solid. Then 35 mL of dionized water dissolved 2.2 g of $VOSO_4 \cdot 5\,H_2O$ and 1.05 g of $Cu(NO_3)_2 \cdot 3\,H_2O$. A solid stick pulp formed while the solution was mixed. The rota–evaporator homogenized this pulp for 3 h. It then dried and calcined at 120 °C (12 h) and 350 °C (4 h) with a temperature

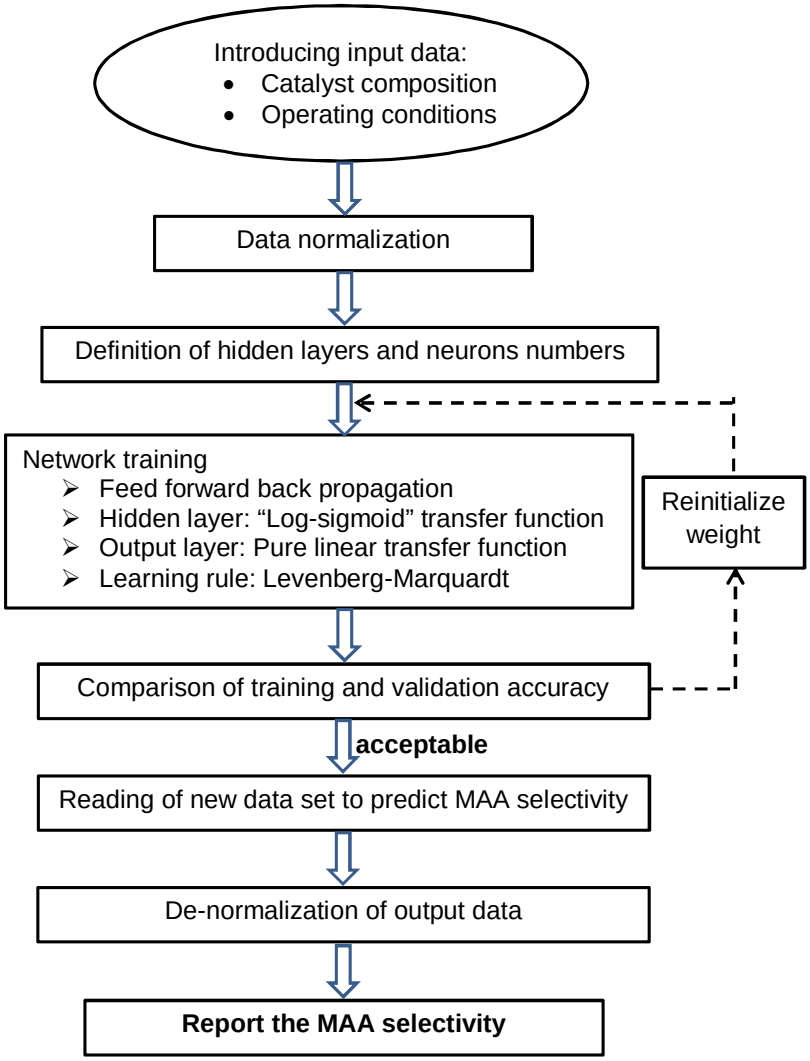

Figure 5.1 Neural network catalyst modeling flowchart

ramp of 2 °C min^{-1}, respectively, to provide $Cs_x(NH_4)_{3-x}PMo_{12}O_{40}(VO)_yCu_z$.

We synthesized eight catalysts following a full factorial design (2^3) and measured the MAA selectivity in a fluidized bed. We refer to these catalysts as $Cs_x-V_y-Cu_z$. For example, Cs_1-V-Cu is $Cs_1(NH_4)_2PMo_{12}O_{40}(VO)Cu_{0.5}$ and $Cs_1(NH_4)_2PMo_{12}O_{40}$ is $Cs-NH_4$. Five catalysts were synthesized twice and three catalysts were synthesized three times to check the reproducibility. The MAA selectivity for the three repeats was within ±5 %.

5.3.2 Catalyst characterization

An Autosorb-1 measured the surface area and total pore volume by N_2 adsorption/desorption after degassing the catalysts at 200 °C. A TA-Q50IR TGA analyzed the thermal decomposition of the catalysts and their stability, and also estimated the amount of coke that built up on the catalyst surface with time. An X'pert diffractometer (XRD) characterized the crystalline structure of the materials with Cu−Kα radiation (λ=1.542 Å) at 50 kV and 40 mA. A field Emission Scanning Electron Microscope (FE–SEM) (Jeol JSM-7600TFE) imaged the surface of the fresh and used catalyst samples. An EDX detector probed the existence of coke and metal elements on the surface.

5.3.3 Reaction conditions and procedure

A three-zone electrical furnace maintained the reactor— a µ-fluidized bed with an inner diameter of 8 mm, 520 mm long— temperature at 250 °C (Fig. 5.2). All experiments lasted 100 min and the total flow rate was 210 mL min^{-1}.

A ceramic disk distributed the O_2–Ar gas flow uniformly in the middle of the reactor to the 2 g of catalyst. Mass flow controllers metered the argon and a mixture of oxygen and argon and a thermocouple monitored the temperature. A syringe pump metered the fluid to the nozzle and an argon atomized the liquid 2MPDO.

Table 5.2 Parameters and their levels for catalyst design and operating conditions

	Parameters	Ranges and levels	
		-1	+1
Catalyst design	Cesium (x)	1	3
	Vanadium (y)	0	1
	Copper (z)	0	0.5
Reaction conditions	2MPDO (%)	10	13
	Oxygen (%)	10	13

To minimize slumping the fluidized bed and optimizing the spray, we tested liquid 2MPDO/Ar ratios, pressure drop, and nozzle spray configurations Liu *et al.* (2008); Mahboub *et al.* (2016a). Atomizing the 2MPDO into a chamber below the nozzle distributed the fluid better than atomizing the liquid at the nozzle tip with Ar. We calculated the U_{mf} by monitoring the pressure drop of the bottom and top of the reactor to reach the uniform pressure.

We varied the liquid flow rate and fixed the $\mathrm{Ar_{atomization}}$ flow rate ($20\,\mathrm{ml\,min^{-1}}$) to identify the optimum ratio for a 0.3 mm nozzle. At liquid flow rates greater than $0.05\,\mathrm{mL\,min^{-1}}$ the injector blocked. The optimal rate was $0.03\,\mathrm{mL\,min^{-1}}$ at 250 °C Mahboub *et al.* (2016a). The upper furnace zone maintained the reactor tube at 300 °C to minimize product condensation.

Argon purged the reactor while a furnace increased the temperature to the set point. Heat tape kept the exit line at 200 °C to prevent the product from polymerizing. Finally, the blank tests (empty bed) confirmed that the reactor was inert.

A quench condensed volatile compounds in distilled water. An HPLC measured the quantity and quality of all condensed products off–line and GC–MS measured the gas products. A mass spectrometer (MS) (Pfeiffer Vacuum Thermostar) monitored the gas phase composition on–line at a frequency of 1 Hz while a conductivity meter monitored the change in conductivity of the liquid phase on-line.

The factorial design for the feed composition considers two levels each for oxygen mole fraction (10 % and 13 %) and reactant mole fraction (10 % and 13 %). These narrow concentrations were based on earlier screening tests that identified these range of conditions as optimal (Table 5.2). Because the relative importance of these two factors were unknown we adopted a 2^2 factorial design rather than a mixture design. We varied the Ar flow rate in order to achieve the desired feed concentrations.

5.3.4 Computational method

The Genetic Algorithm method proposes approximate solutions for optimization problems. This technique is a global search method and a special class of evolutionary algorithms. Based on biological sciences, evolutionary processes can be translated to design strategies and effective search. The GA applies these strategies and determines an optimal solution for any multi–dimensional problems. The GA as a search algorithm mimics the behavior of natural selection. Population generation of possible solutions by the GA leads to the best solution of problems which is the maximum of a function. Through mutation and crossover processes, better solutions are found from the current possible solutions. The process is repeated to find

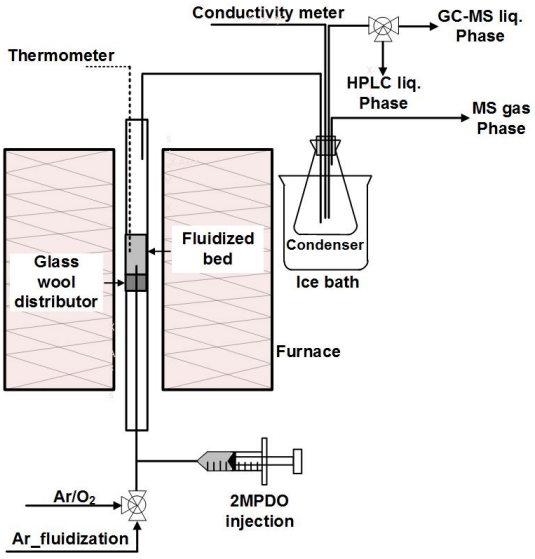

Figure 5.2 Schematic of the experimental set–up Mahboub *et al.* (2016a)

an acceptable solution. Here, in order to find the optimal catalyst design, we coupled the ANN model with the GA. The GA provided virtual catalysts, and the ANN model acted like a virtual catalyst test setup, which evaluated the fitness of the GA (in terms of selectivity to MAA). 2MPDO and oxygen concentrations as well as the three metal ions (Cs, V and Cu) comprise the six genes of each chromosome in the GA structure. The optimal GA procedure is :

1. Generate a random initial population of chromosomes.
2. Calculate MAA selectivity for all chromosomes by the ANN model.
3. Select the best pairs.
4. Perform the crossover.
5. Perform the mutation.
6. Evaluate the termination criteria (convergence of population, termination of the number of generation, lack of changes in fitness value). If these are acceptable, then the program ends, otherwise it goes back to stage 2.
7. The optimization was carried out by GA codes available in the optimization tool box in $MATLAB^{®}$.

The optimal parameters of the GA are shown in Table 5.3. Other parameters were held at their default values or types Hadi *et al.* (2016).

Table 5.3 Optimal GA parameters applied in optimization procedure Hadi *et al.* (2016)

Parameter	Value or type
Population type	Double vector
Crossover fraction	0.8
Fitness scaling	Rank
Mutation	Gaussian
Selection	Stochastic uniform
Crossover function	Scattered

5.4 Results and discussions

5.4.1 Catalyst composition and reaction conditions evaluation

We tested four feed compositions over eight catalysts at 250 °C to measure the product selectivity after 100 min. We maintained the oxygen at a mole fraction of 0.1 and 0.13 to simulate a recycle process (with partial oxygen conversion). HPLC detected MAA, MAC, 2–methylpropanal and unreacted hydrocarbon as the main products in the liquid phase. The MS detected CO_2, CO, CH_4 and unreacted O_2 in the gas phase. A stream of oxygen diluted in argon (21 %) regenerated the used catalyst at 320 °C to remove coke and the MS recorded the CO_2, CO and O_2 signals to qualify the carbon and hydrogen and close the mass balance.

The maximum selectivity to MAA and MAC was 41 % and 33 %, respectively over Cs_1-V-Cu at 2MPDO/O_2/Ar= 13 %/10 %/77 % (Fig. 5.3). Lower oxygen concentrations reduced the oxidation rate of acid products to CO_x, but overall conversion was lower.

Among the eight catalyst compositions, those containing both cesium and ammonium, and vanadium and copper (Cs_1-V-Cu) performed the best : and the least 2MPDO conversion (63 %) (Fig. 5.4). The CPM catalyst was almost unselective to MAA, and its selectivity to MAC was 6 %.

Partial cesium insertion into the Keggin-structure had a positive effect on thermal stability and catalyst activity. The complete substitution of Cs with ammonium had a negetive effect on performance, due to the complete elimination of the active phase ($(NH_4)_3PMo_{12}O_{40}$). Vanadium as an oxidant and copper as a promoter increased selectivity to desired products (Fig. 5.4).

Vanadium and copper have a synergistic effect on conversion in catalysts with cesium and ammonium. Neither have an effect on catalysts without ammonium. Ammonium attenuates the catalyst activity : CPM catalyst (no ammonium) produces CO_2 and methane.

In the first 20 min MAA selectivity was below 13 % which was confirmed by the conductivity

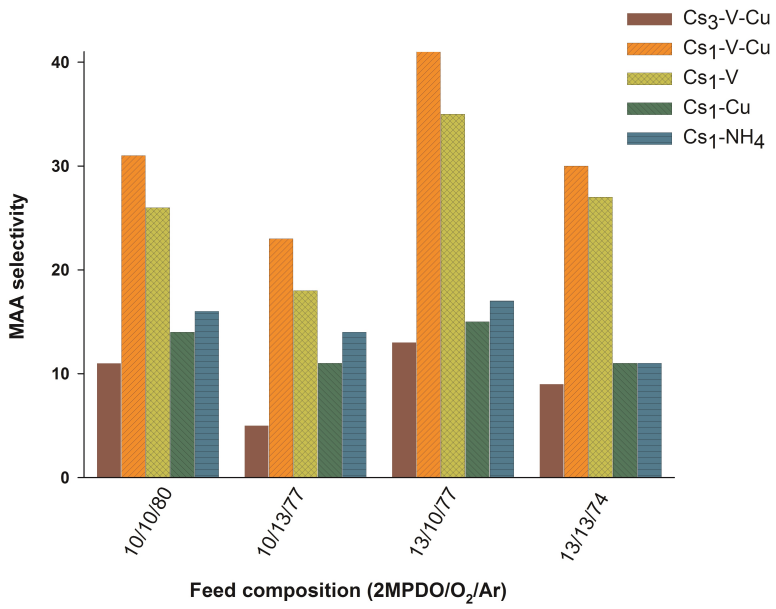

Figure 5.3 Feed compositions evaluation over prepared catalysts at 250 °C

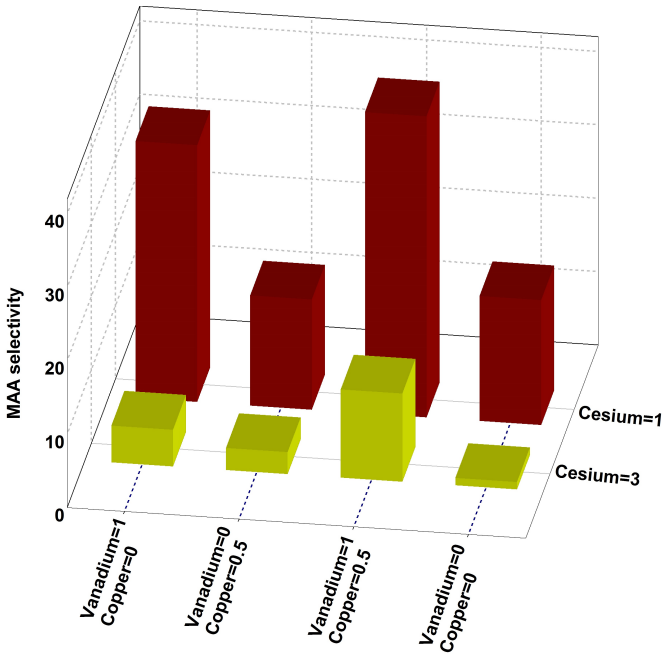

Figure 5.4 Effect of catalyst composition on MAA selectivity with 2MPDO/O_2/Ar= 13 %/10 %/ 77 % at 250 °C

of the quench. It increased sharply to 41 % thereafter (Fig. 5.5). Coke forms on non-selective sites in the glycerol dehydration to acrolein thereby increasing selectivity (and yield) with time (Dalil *et al.*, 2015). Conversely, MAC selectivity is higher at the beginning and then decreases with time, which confirms that MAC is an intermediate to produce MAA. The selectivity to CO_2 decreases slightly and reaches 15 % at 100 min. CO and CH_4 selectivities are invariant at 6 % and 4 %, respectively (Fig. 5.5).

These trends, confirmed by monitoring the conductivity of products online, showed low values in the first 20 min, and then a sharp increasing trend (Fig. 5.6). In general, the carbon balance was from 92 % to 105 %. Methane and 2–methylpropanal were the main by-products in gas and liquid phases, respectively.

5.4.2 Modeling

We manipulated the catalyst composition and reaction conditions to enhance MAA selectivity. Metal ions such as Cs, V and Cu influenced selectivity to MAA, in addition to the reaction feed composition, which were 2MPDO and oxygen concentrations. Here we optimized and simulated the catalyst components (Cs, V and Cu) to maximize the MAA selectivity by employing an ANN and GA hybrid system. The predictive ability of ANN varies with its topology, training algorithms and transfer functions. However, there is no proper method to categorize the optimal combination of these factors ; therefore, we optimized the factors by trial and error. Table 5.4 illustrates the input and output parameters with min and max values.

We tested various ANN topologies and algorithms to optimize both catalyst content and feed concentration for this reaction. The number of catalyst design and operational conditions determine the number of input neurons. Rostamizadeh et al. claim that ANN efficiency decreases with the increase of neurons in the hidden layer (more than 20) and also the number of hidden layers Rostamizadeh *et al.* (2014). However, Hadi et al. illustrated that

Table 5.4 Input and output parameters and their levels

	Parameter	**Symbol**	**Min**	**Max**
Input	Cs	X	1	3
	V (mole)	Y	0	1
	Cu (mole)	Z	0	0.5
	2MPDO (vol. %)	P	10	13
	Oxygen (vol. %)	O_2	10	13
Output	MAA selectivity (%)	S	0.8	41

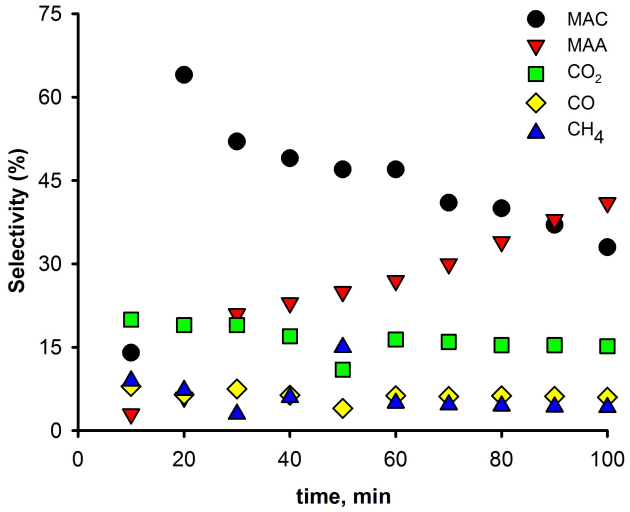

Figure 5.5 Gas and liquid selectivities versus time (2MPDO/ O_2/Ar= 13 %/10 %/77 % at 250 °C over Cs_1-V-Cu)

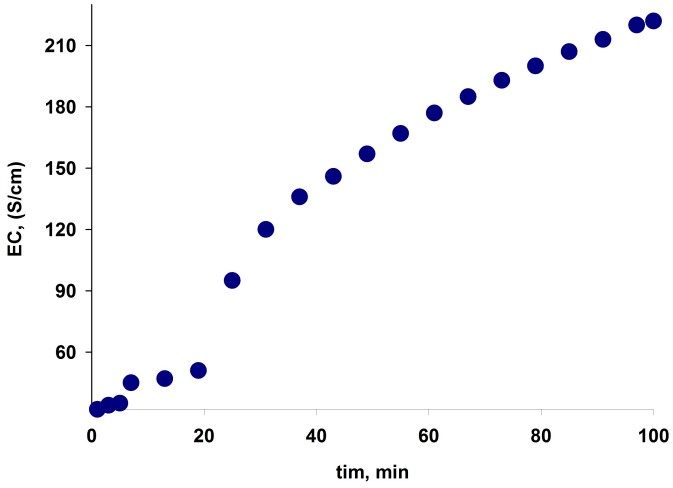

Figure 5.6 Electro conductivity profile with 2MPDO/O_2/Ar=13 %/10 %/77 % over Cs_1-V-Cu at 250 °C

an ANN topology with a low number of neurons in its hidden layer failed to verify the link between input and output factors Hadi *et al.* (2016). We conducted several topologies and began with four neurons in the hidden layer, and then added neurons to enlarge the network until reaching the best results without over fitting. An ANN structure with one hidden layer including ten neurons was suitable (Fig. 5.7). Network training applied to 70 % of the data sets and testing utilized 30 % of them. Among the tested structures, one hidden layer including ten neurons provided the highest accuracy for train and test data (Fig. 5.8).

Proper algorithm coupling with optimal topology provides the ANN with high accuracy to predict the experimental data. We investigated the effect of various algorithms such as gradient descent with adaptive (GDA), resilient back propagation (RP), gradient descent with momentum (GDM), Levenberg-Marquart (LM) and gradient descent (GD). Among these algorithms, the LM algorithm was the most accurate for both training and test data (R^2=0.97). BPNN with one hidden layer (6-10-1) consisting of log-sigmoid (LS) and pure linear (PL) transfer functions and the LM algorithm is an optimum ANN structure to predict the selectivity of MAA (Fig. 5.9). The ANN prediction results (as output) plotted versus the experimental data show are well correlated ($R^2 = 0.97$) (Fig. 5.10).

Sensitivity analysis

The cosine amplitude method (CAM) examined the impact of input independent variables (catalyst composition and operating conditions) on the output dependent variable (MAA selectivity). The CAM method expressed all of the data pairs to construct a data array X in common X–space : Each of the elements, X_i, in the data array X is a vector of lengths of m, that is :

$$X = X_1, X_2, X_3, ..., X_m \tag{5.3}$$

Each of the data pairs specifies a point in m-dimensional space in m-coordinates to describe the points completely.

$$X_i = X_{1i}, X_{2i}, X_{3i}, ..., X_{mi} \tag{5.4}$$

A pairwise comparison of two data samples of X-space (x_i and x_j) provided each element of a relation– r_{ij}– where the strength of the relation between the data pairs is measured by the membership value expressing that strength [$r_{ij} = \mu R(x_i, y_j)$]. The CAM calculates r_{ij} from the following equation :

$$r_{ij} = \frac{\sum_{k=1}^{m} x_{ik} \times x_{jk}}{\sqrt{\sum_{k=1}^{m} x_{ik}^2 \times \sum_{k=1}^{m} x_{jk}^2}} \tag{5.5}$$

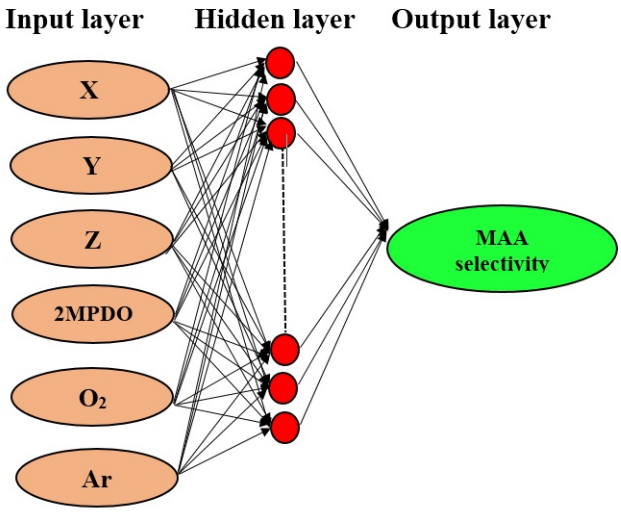

Figure 5.7 Optimum ANN structure

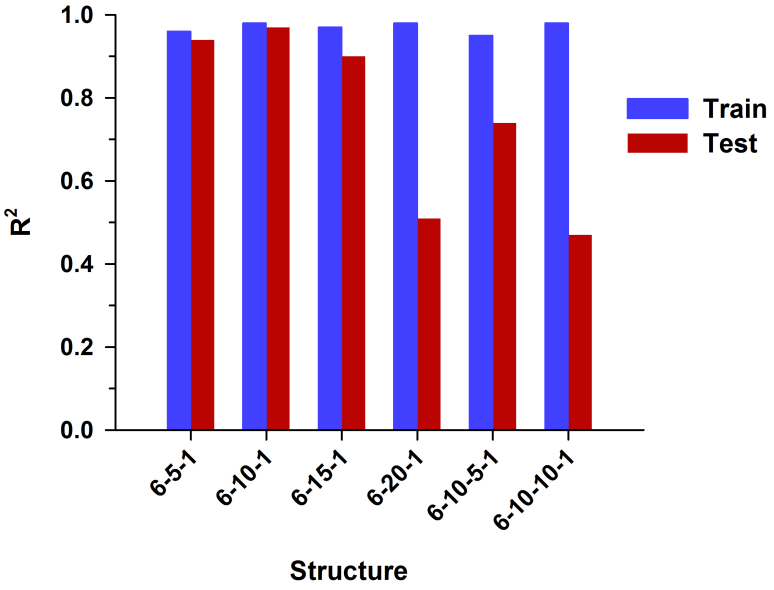

Figure 5.8 Results of different ANN structure

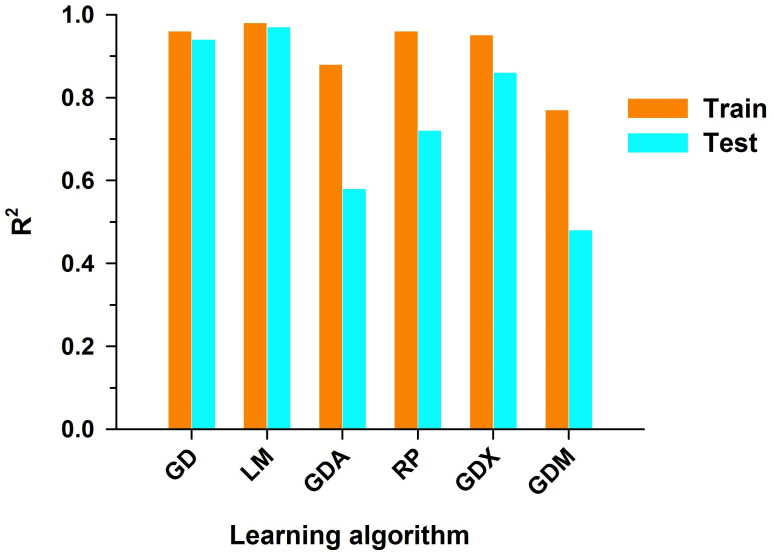

Figure 5.9 Comparison of different train algorithm

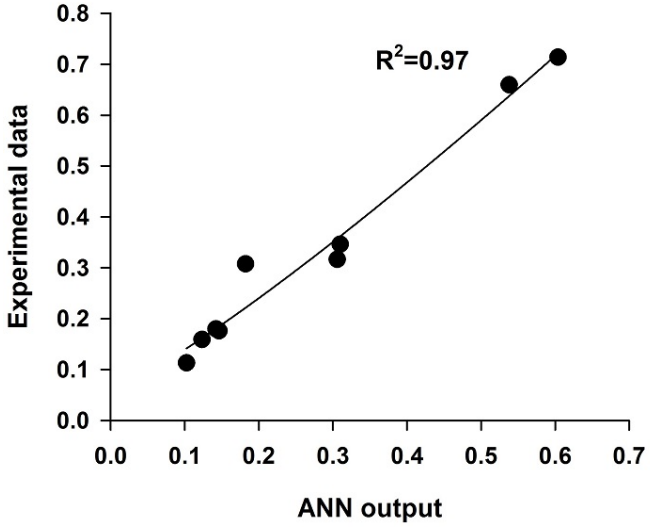

Figure 5.10 Correlation of the experimental and predicted data

Selectivity to MAA depends on all of the independent variables (Fig. 5.11). In catalyst design, vanadium had a higher effect compared to other elements, followed by copper and cesium. Argon depended on the concentration of hydrocarbon and oxygen ; therefore, oxygen affected the MAA selectivity more than 2MPDO.

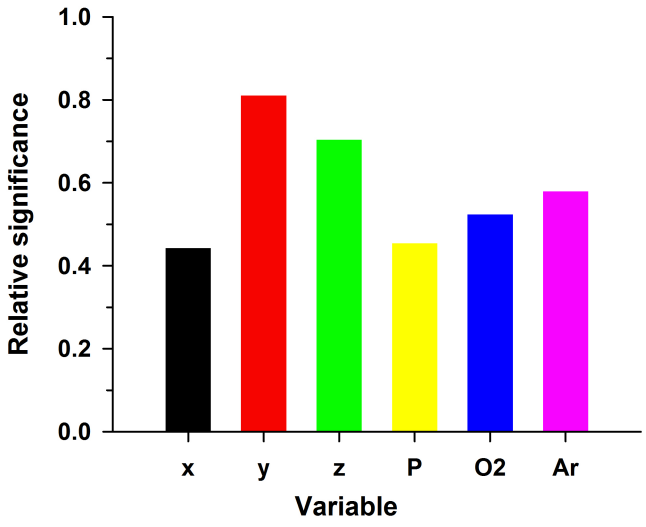

Figure 5.11 Significance of input parameters

Effects of pair parameters on selectivity using ANN

The optimum neural network predicts the MAA selectivity from different inputs in the domain of the training data set. The concentration of argon depends on oxygen and 2MPDO concentrations. The selectivity and yield to MAA reach maximum (41 % and 63 %, respectively) with the lowest partial pressure of oxygen and the highest 2MPDO concentration (Fig. 5.12). The oxidation rate of MAA and MAC decreases with decreasing oxygen. In this case, with higher hydrocarbon concentration (13 % 2MPDO/10 % oxygen), the reaction is under reducing condition and oxygen acts as a limiting reagent. Therefore, we suspect that under reducing condition we have two types of active sites on the catalyst surface that produce MAA and MAC. Less coke forms and a some of the active phase oxidizes the reactant to CO_x. Conversely, under oxidizing conditions, we propose additional active sites produce CO_x. 2MPDO – as the feedstock – reacted with oxygen as well which produce also CO_x. MAA selectivity was 31 %, with 10 % 2MPDO and 10 % oxygen. Selectivity was insensitive to 2MPDO concentration but it decreases almost proportionately with increasing oxygen, which was substantiated by the ANN modelling (Fig. 5.12). ANN modeling confirmed that

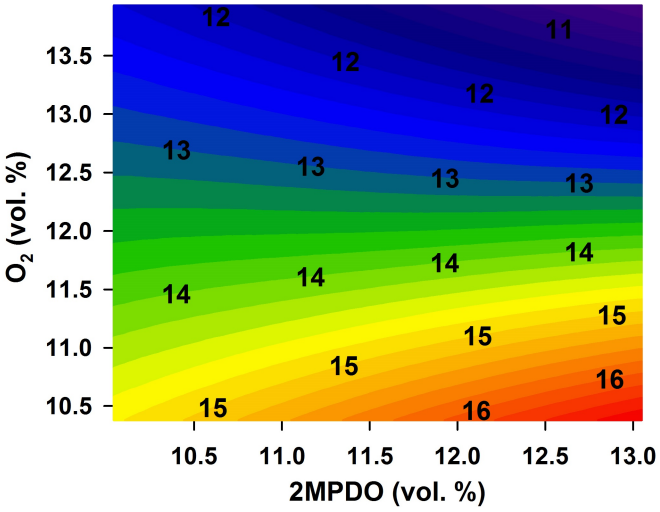

Figure 5.12 The effects of 2MPDO and O_2 on MAA selectivity

all metal ions had a positive effect on selectivity, particularly with both NH_4^+ and Cs in the Keggin structure (Figs. 5.13). However, the effect of each ion was different depending on what other ions were present. The change of colours in the contour plots represent the change of MAA selectivity : the dark blue represents the lowest selectivity and the red represents the highest selectivity. The model illustrated that selectivity was higher with catalysts where Cs partially substituted NH_4^+ compared to a complete substitution of ammonium with cesium (Fig. 5.13a and b). The effect of vanadium and copper was more obvious with lower cesium concentrations. For example, with complete substitution of cesium with ammonium (Cs=3), MAA selectivity was independent of vanadium ; however, with lower cesium concentrations (Cs=1), the vanadium concentration had an effect on selectivity (Figs. 5.13a). The ANN showed that completely substituting ammonium with cesium decreased selectivity which agrees with the experimental measurements. This observation confirms that cesium is in the catalyst structure ($Cs_3PMo_{12}O_{40}$) and plays a role as a support that disperses the $(NH_4)_3PMo_{12}O_{40}$ active phase. Also inserting vanadium in the catalyst structure enhanced MAA selectivity but only in the presence of both cesium and ammonium (Fig. 5.13a). Vanadium was an oxidant in the catalyst and reduced Mo^{6+} to Mo^{5+}.

Copper had a marginal effect as a promoter over a range of Cs/NH_4^+ ratios (Fig. 5.13b and c). MAA selectivity is essentially constant regardless of the Cu substitution at a Cs/NH_4^+ ratio equal to 1. At higher ratios, selectivity increases slightly with higher Cu substitutions. At a Cs/NH_4^+=2, MAA selectivity doubled when the vanadium substitution increased from 0 to 0.5 (Fig. 5.13a) while it only increased from 12 % to 13 % for copper (Fig. 5.13b). Finally, the predicts that are correlated positively : increasing the substitution rate of each increases

the selectivity (Fig. 5.13c).

5.4.3 Optimization

The ANN-GA determined that the optimal catalyst composition contains an equal moles concentration cesium, vanadium and 0.15 mole fraction of copper with respect to Cs and V : $Cs(NH_4)PMo_{12}O_{40}(VO)Cu_{0.15}$. Furthermore, the optimal feed concentration is 13 %/10 %/77 % for 2MPDO/O_2/Ar (Table 5.5). The ANN–GA accurately predicts the experimental selectivity (42 % vs 43 % for the model) which confirms the developed model is valid. It predicts that the selectivity of optimum catalyst component with 1 :1 :0.15 (Cs :V :Cu) would be 43 % with the same conversion (63 %) than the 1 :1 :0.5 catalyst was tested.

5.4.4 Catalyst characterization

Nitrogen adsorption/desorption analysis

The analysis of the first eight catalysts showed that the Cs^+ increased the specific surface area of HPA catalysts compared to the parent acid ; conversely, copper decreased the surface area Mahboub *et al.* (2016a). The surface area ranged form $19\,m^2\,g^{-1}$ to $44\,m^2\,g^{-1}$ Mahboub *et al.* (2016a). The optimized sample (before and after reaction) represents a hysteresis loop at a relative pressure of 0.6–1, confirming type V isotherms and illustrates that this catalyst is a micro–mesoporous material (Fig. 5.14). The surface area and pore volume of the optimized catalyst is $31\,m^2\,g^{-1}$ and $<0.21\,mL\,g^{-1}$, respectively, and after reaction it dropped to $24\,m^2\,g^{-1}$ and $<0.19\,mL\,g^{-1}$.

XRD specification

The curves and crystalline peaks are the same for the optimized catalyst before and after reaction (Fig. 5.15). Each curve represents a peak in Fig. 5.15. The catalyst before and after reaction has a cubic lattice of ammonium oxonium molybdenum oxide phosphate ($(NH_4)_{2.6}(H_3O)_{0.4}(PO_4Mo_{12}O_{36})$) with a=b=c=11.7 Å. The thickness of each curve is the same in different positions, which suggests that the catalyst is homogeneous and all the me-

Table 5.5 Optimum catalyst and feed conditions and selectivity to MAA

Catalyst component (mol)			Feed concentration (%)			Selectivity to MAA (%)	
Cesium (x)	Vanadium (y)	Copper (z)	2MPDO	O_2	Ar	Experimental	Predicted
1	1	0.15	13	10	77	42	43

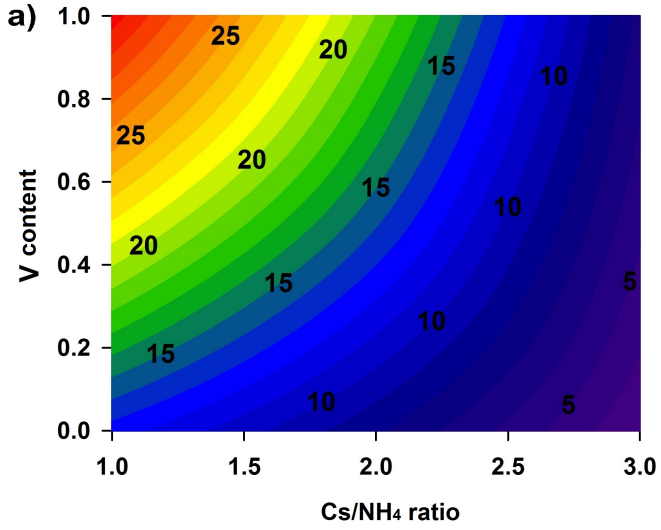
a)
V content
Cs/NH4 ratio
1.0
0.8
0.6
0.4
0.2
0.0
1.0
1.5
2.0
2.5
3.0
25
20
15
10
5

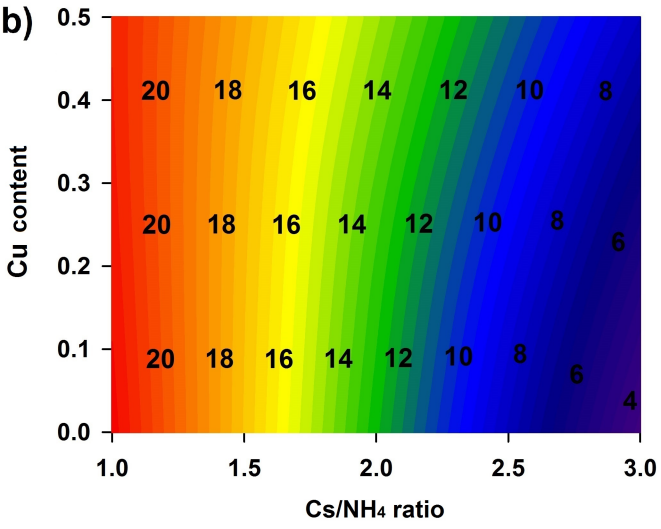
b)
Cu content
Cs/NH4 ratio
0.5
0.4
0.3
0.2
0.1
0.0
1.0
1.5
2.0
2.5
3.0
20
18
16
14
12
10
8
6
4

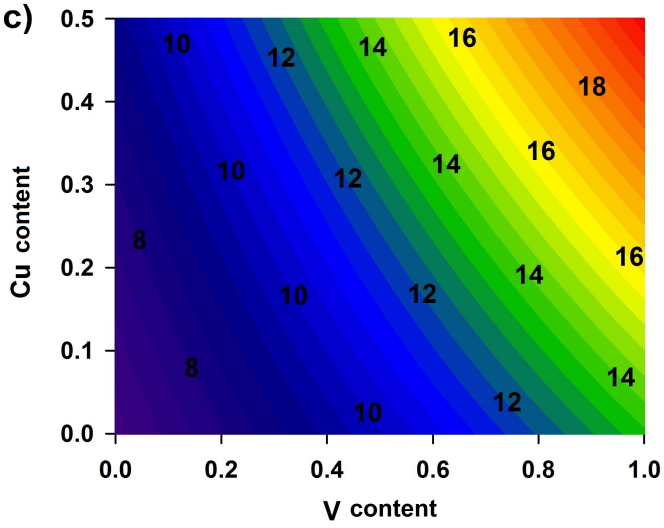

Figure 5.13 Effects of pair parameters on MAA selectivity

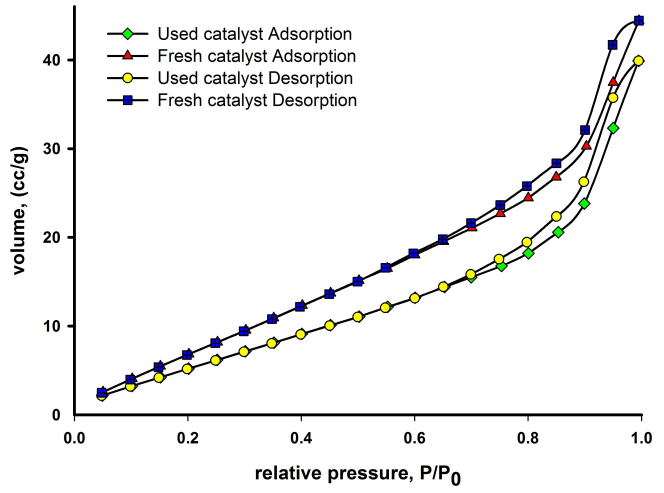

Figure 5.14 Specific surface are of fresh and used catalysts

tal ions dispersed uniformly. The main diffraction peaks are at 2θ= 10.6°, 18.5°, 24.1°, 26.1°, 30.6°, 36.0°, 39.3°, 43.9°, 47.9°, 55.5° and 62.1°, which correlate to (110), (211), (310), (222), (400), (332), (510), (440), (532), (550) and (732), respectively.

Morphological analysis

The surface of the optimized catalyst before and after reaction was rough, with particle grains varying from 20 nm to 500 nm (Fig. 5.16). The surface did not sinter ; however, higher zoom (X 50000) shows spherical particles cover the surface. The EDX spectrum of the catalyst (Fig. 5.16a and b) confirms the presence of Cs, Mo, P, V, and Cu, while the used catalyst also shows the presence of carbon.
Elemental analysis of the catalyst before and after reaction also confirms carbon deposition on the surface, with an increase in mass fraction from 3.2 % to 19.5 %. A small fraction of NH_4^+ remains after calcination in the catalyst (a mass fraction of 0.001) but none remains after reaction. Map analysis using an EDX detector illustrated that all ions dispersed uniformly over the catalyst surface.

5.5 Conclusions

A Keggin structure with cesium, vanadium and copper demonstrated the best performance for maximum selectivity to MAA (41 %) with 63 % conversion. MAA selectivity increased with a decrease in oxygen concentration due a drop in conversion. Methane and 2–methylpropanal (produced by thermal decomposition of the reactant and hydrogen transfer of MAC, respectively) are the main by-products. We propose a powerful ANN model to predict MAA selectivity in a fluidized bed reactor based on oxygen and 2MPDO concentration and catalyst composition. BPNN with one hidden layer (6-10-1) consisting of log-sigmoid (LS) and pure linear (PL) transfer functions and the LM algorithm is an optimum ANN structure for predicting MAA selectivity. Sensitivity analysis illustrates that the vanadium content in the catalyst structure and oxygen concentration are the most significant inputs. A genetic algorithm optimized the parameters, and the predicted selectivity to MAA was 43 % over the optimal catalyst ($Cs(NH_4)_2PMo_{12}O_{40}(VO)Cu_{0.5}$) with 2MPDO/$O_2$/Ar= 13 %/10 %/77 %. At the end, we tested the optimum catalyst and the selectivity to MAA was 42 % which confirmed the model predictions.

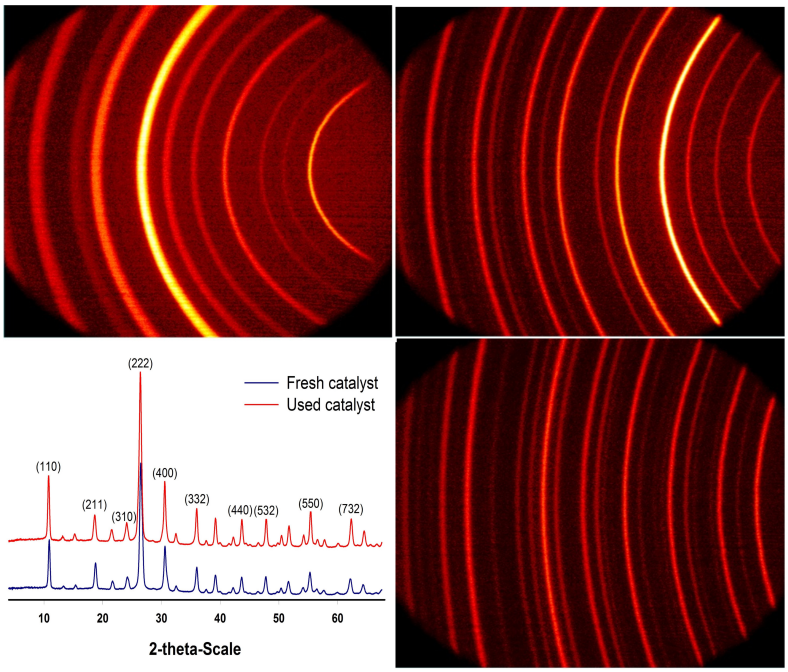

Figure 5.15 XRD diffractograms of fresh and used catalysts

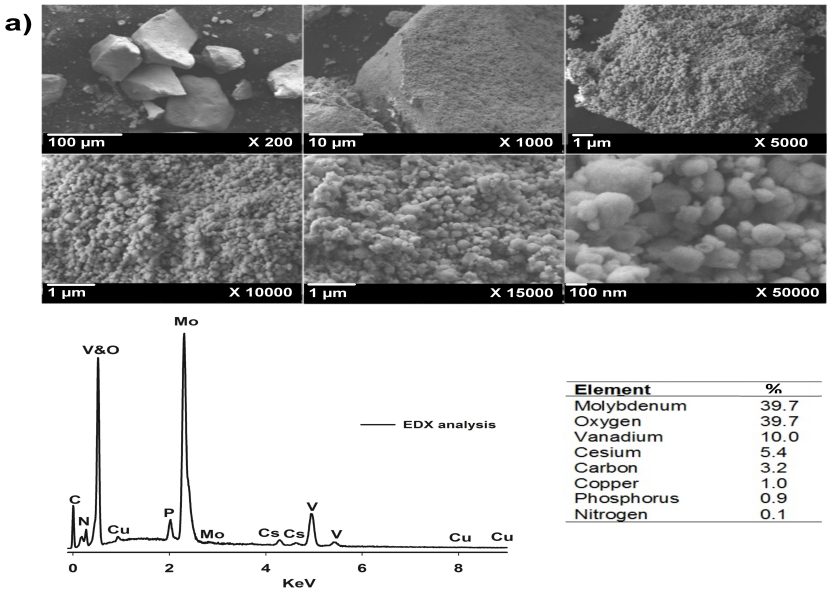

Element	%
Molybdenum	39.7
Oxygen	39.7
Vanadium	10.0
Cesium	5.4
Carbon	3.2
Copper	1.0
Phosphorus	0.9
Nitrogen	0.1

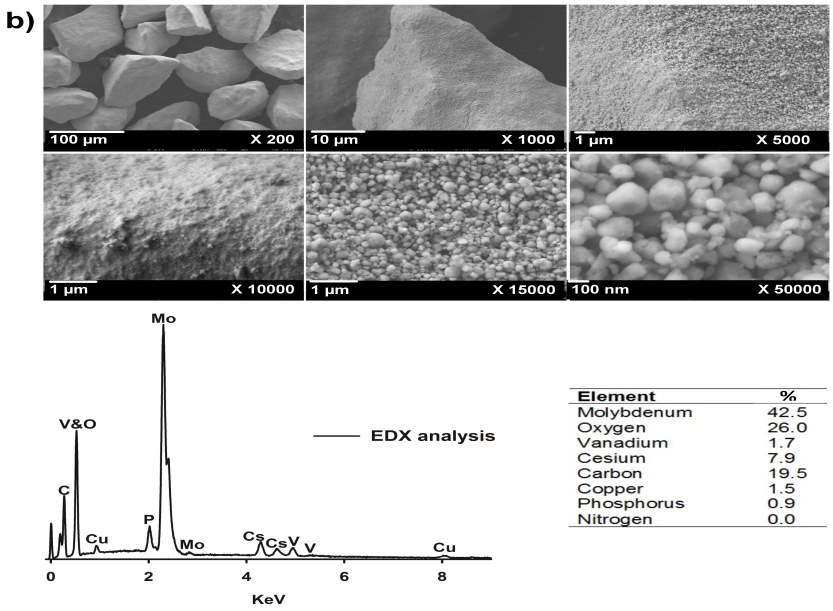

Figure 5.16 FE-SEM and EDX characterization for a) fresh and b) used optimized catalysts and their elemental analysis. The table caption in the figures report the elemental mass fraction in %

5.6 Acknowledgements

The authors would like to thank MITACS and NSERC for their financial support of this study. Also, the great efforts of Dr. Cristian Neagoe and Davide Carnevali at Polytechnique Montreal for set-up, preparation, and analytic development are greatly appreciated.

CHAPTER 6 ARTICLE 4 - Cs, V, Cu KEGGIN–TYPE CATALYSTS PARTIALLY OXIDIZE 2–METHYL–1,3–PROPANEDIOL TO METHACRYLIC ACID

Mohammad Jaber Darabi Mahboub, Jordan Wright, Daria C Boffito, Jean-Luc Dubois, Gregory S Patience

Published : Applied Catalysis A : General, 554, 2018, 105–116

6.1 Abstract

Heteropoly acids are among the best catalysts to produce carboxylic acids from light hydrocarbons. The Keggin structure maintains metals at a high oxidation particularly in the presence of cesium, vanadium, and copper. They effectively catalyze the partial oxidation of 2–methyl–1,3–propanediol (2MPDO)—a co-product in the hydroformylation of allyl alchol to 1–4 butanediol. Converting 2MPDO to methacrylica acid would improve the economics of this route to 1–4 butanediol. Here, we establish the relationship between heteropoly acid performance and calcination temperature at 300 °C and 350 °C. The molybdenum oxidation state was higher after the high temperature treatment but it reduced to a greater extent during reaction (from Mo^{6+} to Mo^{5+}). The higher extent of reduction confirms the higher $O^{2-} \rightarrow Mo^{6+}$ charge–transfer in the Keggin anion. Maximum MAA and MAC selectivities were 61 % and 28 %, respectively at 250 °C after 480 min over cycling oxidation–reduction and 2MPDO/O_2/Ar= 13/10/77 as the best reaction condition and feed composition. Though, the route of direct dehydration of 2MPDO (C−OH bond cleavage) followed by oxidation to MAC is the most direct path to the products detected, we propose a mechanism that passes through the homolitic dissociation of the tertiary C−H bond, in reason of the very similar bonding energies.

6.2 Introduction

Polymethyl methacrylate (PMMA) is a specialty polymer for computer screens, electronics, automotives and household fixtures which methyl methacrylate (MMA) is the main monomer of PMMA. Acetone-cyanohydrin (ACH) is a common process to produce MMA Nagai (2001); Deng *et al.* (2005). However, current ACH process is coupled with acrylonitrile plants that supply HCN. On purpose HCN production to account for an expanding market above that expected for acrylonitrile requires dedicated facilities for this toxic compound Cavani (2010);

Mizuno *et al.* (1996b); Knapp *et al.* (2001). Oxidizing light olefins to methacrylic acid (MAA)– as an alternative feedstock for MMA– reduces the deficiencies of the current process Montag et Mckenna (1991); Drent et Budzelaar (1996); Zhou *et al.* (2015). MAA yield per pass from ethylene and propylene are low and the process involves multiple steps that include CO and HCHO as reactants Nagai (2001); Mizuno et Yahiro (1998); Montag et Mckenna (1991); Drent et Budzelaar (1996); Visuvamithiran *et al.* (2013). Similarly, yields from oxidizing isobutene to MAA are low which negatively impact the economics Nagai (2001); Mizuno et Yahiro (1998); Montag et Mckenna (1991); Visuvamithiran *et al.* (2013). The single–step oxidation of isobutane to MAA is an interesting alternative because the feedstock cost is low and it replaces multiple reactions steps with a single step Sultan *et al.* (2004); Cavani *et al.* (2001f); Misono (2001); Kanno *et al.* (2010); Zhang *et al.* (2013); Paul *et al.* (2010). However, single pass conversion is less than 10 %, yields are low and reaction times are long (Fig. 6.1) Jing *et al.* (2014a); Cavani *et al.* (2001f). For gas phase partial oxidation of isobutane to MAA, Keggin–type polyoxometalates (POMs) as heterogeneous catalysts containing phosphorus and molybdenum are the most active and selective catalysts Min et Mizuno (2001b); Ishikawa et Ueda (2016); Sushkevich *et al.* (2016); Karcz *et al.* (2017). Substituting H^+ with Cs^+ in $H_3PMo_{12}O_{40}$ forms an active phase ($H_3PMo_{12}O_{40}/Cs_3PMo_{12}O_{40}$) that thermally stabilizes the catalyst structure and improves the MAA yield Okuhara *et al.* (2000); Sultan *et al.* (2004); Mahboub *et al.* (2016a). Cesium forms an alkaline salt that acts as a support and disperses the active phase Mizuno et Yahiro (1998); Misono (2001); Mizuno et Mison (1998); Paul *et al.* (2010); Okuhara (2002). Ammonium ions increase the surface area, which the reduction of the HPA by ammonia issued from the decomposition of the ammonium cations increases MAA selectivity Jing *et al.* (2014b); Cavani *et al.* (2001f); Sultan *et al.* (2004); Jing *et al.* (2013). Replacing one molybdenum atom by a vanadium in the catalyst structure forms

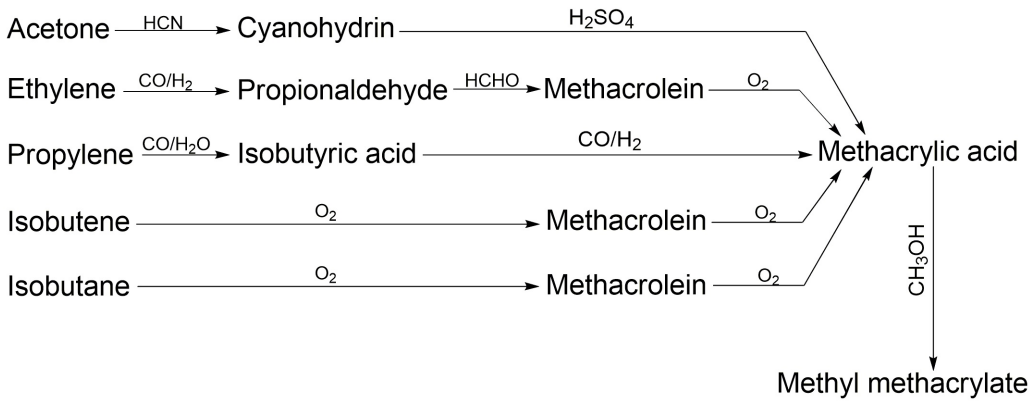

Figure 6.1 All routes to produce MMA/MAA

($H_4PMo_{11}VO_{40}$) and increases the reduction and reoxidation rates, which improves activity selectivities to MAA and MAC Mizuno et Mison (1998); Bruckner *et al.* (2007); Huynh *et al.* (2009a); Jing *et al.* (2013, 2014b); Ren *et al.* (2016). Some studies showed that vanadium in the form of VOx accelerates dehydrogenation of isobutane to isobutene which then it converts to MAA and MAC Wang *et al.* (2016); Zhang *et al.* (2016). Huynh et al. inserted vanadium to reduce acetic acid selectivity and carbon oxides from MAA and MAC decomposition Huynh *et al.* (2009a,b). Copper catalyzes the reduction of molybdenum, which improves the activity and surface acidity of the catalyst Mizuno *et al.* (1998); Mahboub *et al.* (2016a).

Mixed metal oxides with Cs, Mo, P, V, Sb and Cu partially oxidize 2–methyl–1,3– propanediol (2MPDO) to MAA (selectivity= 24 %) Dubois (2014). In a micro-fluidized bed reactor, the heteropolycompound $Cs_x(NH_4)_{3-x}PMo_{12}O_{40}(VO)Cu_y$ ($Cu_{0.5}(VO)O_x/Cs(NH_4)_2PMo_{12}O_{40}$ where vanadium and copper atoms were placed in secondary structure of Keggin–type in contact with oxygen) improves selectivity to MAA versus mixed metal oxides, vanadium pyrophosphate (VPP), tungsten oxide, and pure Keggin-type structure ($H_3PMo_{12}O_{40}$) and reaches 41 % at 250 °C after 100 min Mahboub *et al.* (2016a,b).

Catalyst activity depends on composition, morphology (metal ions and type of support), and reaction conditions (temperature, pressure, flow regime). Catalyst preparation conditions—precipitation versus impregnation, calcination temperature and ramp, time, gaseous environment—affect activity and morphology. Vanadium pyrophosphate catalysts are particularly sensitive to over-oxidation in its topotactic transformation from the hemi-hydrate to the pyrophosphate Patience *et al.* (2007), for example.

Here we compare the activity and selectivity of $Cs(NH_4)_2PMo_{12}O_{40}(VO)Cu_{0.5}$ (Cs−V−Cu) precursor and the catalyst calcined at 300 °C and 350 °C. We tested catalysts performance with oxygen and hydrogen and cycling between the two atmospheres.

6.3 Experimental

6.3.1 Catalyst preparation

MAA yields were highest for a Keggin type heteropoly compound containing vanadium and copper where cesium substituted ammonium with the formula of $Cs(NH_4)_2PMo_{12}O_{40}(VO)Cu_{0.5}$ Mahboub *et al.* (2016a,b). Above 400 °C, the Keggin–structure is destroyed, so for the first series of tests, we prepared three catalysts : uncalcined, and samples calcined at 300 °C and 350 °C. Adding vanadium or replacing it with molybdenum improves the catalyst redox as vanadium atoms are easily removed from the primary structure and participate in reducing the catalyst. Consequently, both catalyst activity and selectivity improve. Copper acts as a

promoter and facilitates molybdenum reduction in the catalyst, which improves activity and increases surface acidity Mahboub *et al.* (2016a).

$Na_2HPMo_{12}O_{40}$ was the precursor for all catalysts. Ammonium nitrate (0.1M) dissolved 1.87 g $CsNO_3$ while a magnet stirred the solution vigorously in a 100 mL beaker at 40 °C. A pump fed $Na_2HPMo_{12}O_{40}$ (0.2 M) to the beaker at 2 mL min^{-1} until a fine precipitate formed. After separating the precipitate from supernatant, the solids dried 16 h at 120 °C to form 27 g of $Cs(NH_4)_2PMo_{12}O_{40}$. A solution containing 2.2 g $VOSO_4 \cdot 5\,H_2O$ and 1.05 g $Cu(NO_3)_2 \cdot 3\,H_2O$ (dissolved in 35 mL dionized water) were added to $Cs(NH_4)_2PMo_{12}O_{40}$ and formed thick slurry that a rota–evaporator homogenized for 3 h. The slurry dried for 16 h at 120 °C in a ventilated oven, and calcined for 4 h at 300 °C and 350 °C in air. The temperature ramp on the over was 2 °C min^{-1}. The three catalysts we designate as $Cs{-}V{-}Cu \cdot non$, $Cs{-}V{-}Cu \cdot 300$ and $Cs{-}V{-}Cu \cdot 350$.

6.3.2 Catalyst characterization

Standard techniques such as nitrogen porositmetry (Quantachrome, Autosorb–1), X-Ray diffraction (Philipps X'pert diffractometer), thermogravimetric analysis (TA–Q50IR TGA), and Field Emission Scanning Electron Microscope (Jeol JSM-7600TFE) with an EDX detector were used to measure bulk and surface catalyst properties Mahboub *et al.* (2016a). PerkinElmer Spectrum 65 FT-IR Spectrometer (KBr) recorded the IR spectra from 1800 cm^{-1} to 500 cm^{-1} with a resolution of 4 cm^{-1}. The reference peak was the central $P{-}O$ bond of the Keggin unit since it did not react. Renishaw inVia Raman Microscope equipped with a RenCam CCD detector measured the Raman spectra of fresh and used samples. The 514 nm Ar laser focused on the sample with a 50× objective lens using a Leica microscope. We sampled each catalyst at three point to verify the homogeneity. A Cary 6000i UV-Vis-NIR from 200 nm to 800 nm with a 60 mm integrating sphere recorded UV–Vis diffuse reflectance spectra of the samples at room temperature. A Bruker Avance 600 Spectrometer equipped with a 4 mm probe analyzed the ^{1}H (600 MHz) and ^{31}P (242.9 MHz) MAS–NMR spectra at a spin rate of 14 kHz. Anti–ring and single-pulse excitation sequences were used for ^{1}H and ^{31}P spectra, respectively. Ammonium dihydrogen phosphate was the chemical shift reference for the ^{31}P spectrum. X–ray photoelectron spectroscopy (XPS) (VG ESCALAB 3 MKII) analyses the elemental surface of catalyst with the Al Kα as a source. It penetrates less than 10 nm. The detection limit of elements over the surface is around 0.1 %.

6.3.3 Reaction conditions and procedure

All experiments were conducted in a 8 mm by 520 mm quartz tube containing 2 g of catalyst operating in the bubbling fluidized bed flow regime. A mixture of argon–oxygen (21 %) fluidized the catalyst particles (with a diameter from 90 µm to 150 µm). A 20 µm ceramic disk 250 mm from the bottom of the tube distributed the gas uniformly to the catalyst. A three-zone furnace maintained the reactor under isothermal conditions and a thermocouple monitored the bed temperature. Mass flow controllers (from $20-200\,\mathrm{mL\,min^{-1}}$) adjusted the argon, hydrogen and oxygen flow rates. An HPLC pump injected the liquid reactant (2MPDO) to the bottom of nozzle which argon cofed to the tube and mixed together before nozzle tip and argon atomized the liquid. Argon purged the reactor while the furnace ramped the temperature to 250 °C.

Heat tape maintained the temperature of the exit line above 100 °C. A gas chromatograph-mass spectrometer (Agilent 7890A) (GC–MS) analysed a slip stream of this lie while the rest entered a water quench to trap the condensible vapours. A conductivity meter in the quench monitored the acid production and the GC–MS and a High Performance Liquid Chromatograph (Varian Prostar) (HPLC) quantified condensible liquid phase. Aliquots from the quench were withdrawn at 20 min intervals. A pump circulated the quench solution from the bottom to the exit line to increase the gas-liquid contacting time to maximize product dissolution. A Pfeiffer Vacuum Thermostar on–line mass spectrometer (MS) monitored the gas phase composition at a frequency of 1 Hz.

The conversion of 2MPDO (X_{2MPDO}) as well as product selectivities (S_{p}) were calculated as follows Edake *et al.* (2017b) ;

$$X_{\mathrm{2MPDO}} = \frac{n^{\mathrm{in}}_{\mathrm{2MPDO}} - n^{\mathrm{out}}_{\mathrm{2MPDO}}}{n^{\mathrm{in}}_{\mathrm{2MPDO}}} \times 100 \tag{6.1}$$

$$S_{\mathrm{p}} = \frac{n_{\mathrm{p}}}{n^{\mathrm{in}}_{\mathrm{2MPDO}} - n^{\mathrm{out}}_{\mathrm{2MPDO}}} \times \frac{z_{\mathrm{p}}}{z_{\mathrm{2MPDO}}} \times 100 \tag{6.2}$$

Where $n^{\mathrm{in}}_{\mathrm{2MPDO}}$ and $n^{\mathrm{out}}_{\mathrm{2MPDO}}$ are the molar flow rates of 2MPDO at reactor entrance and exit. In Eq. (2), n_{p} is the molar stream of each product. z_{p} and z_{2MPDO} represent the number of carbon atoms in the products and 2MPDO Mahboub *et al.* (2016a).

In the first experimental series (12 experiments), we partially oxidized the 2MPDO over all catalysts with four different feed compositions (Table 6.1). In this case, we purged the catalyst bed with oxygen–argon for 2 h at 250 °C and then the reactant and oxygen react over the catalyst surface for 100 min. The catalyst calcined at 350 °C produced more MAA than the other two so we tested its stability for 480 min over the optimum feed composition.

In the next series of tests (three experiments), a 25 mL stream of hydrogen (STP) reduced the catalysts for 12 h at 250 °C before the oxidation tests with 2MPDO. Again, for this test, the catalyst calcined at 350 °C produced more MAA so we tested this catalyst in forced concentration cycling conditions with 20 min O_2/Ar followed by 2 min H_2/Ar. For all experiments, the carbon balance was in the rang of 91–107 % and the oxygen balance ranged from 72 to 110 %.

6.4 Results and discussion

6.4.1 Catalyst characterization

The specific surface area of the catalyst calcined at 350 °C is double that of the uncalcined precursor but it loses 33 % after reaction (Table 6.2). The hysteresis in the nitrogen adsorption–desorption curves suggest that these catalysts are micro-mesoporous materials Mahboub *et al.* (2016a). The pore radius also decreases after reaction but the initial pore radius is independent of whether the catalyst was calcined or not. The pore volume was slightly higher for the calcined catalysts but it also dropped after reaction.

XRD

Large, sharp peaks of the X-ray diffractograms at 2θ= 10.6°, 26.4° and 30.6° confirm the Keggin–type crystalline structure (body–centered cubic with Å=11.4) of ammonium oxonium molybdenum oxide phosphate (as the main crystal). The minor peak at 2θ= 18.5° is attributable to Mo_4O_{11} and the peaks at 2θ= 26.1° and 2θ= 39.3° correspond to $(V_{0.07}Mo_{0.93})_5O_{14}$ Guan *et al.* (2008d). The main diffraction peaks are the same for the calcined and uncalcined

Table 6.1 Reaction experimental design for each series

Reaction type	Catalyst type	Feed Comp. (%) 2MPDO/O_2/Ar	Purging with O_2 (120 min)	Purging with H_2 (120 min)	Switching O_2-H_2 (Each 20 min)	Rxt. time (min)
Oxidation	Cs−V−Cu · non Cs−V−Cu · 300 Cs−V−Cu · 350	10/10/80 13/10/77 10/13/77 13/13/74	✓			100
Long term oxidation reaction	Cs−V−Cu · 350	13/10/77	✓			480
Reduction	Cs−V−Cu · non Cs−V−Cu · 300 Cs−V−Cu · 350	13/10/77		✓		100
Long term oxidation-reduction	Cs−V−Cu · 350	13/10/77			✓	480

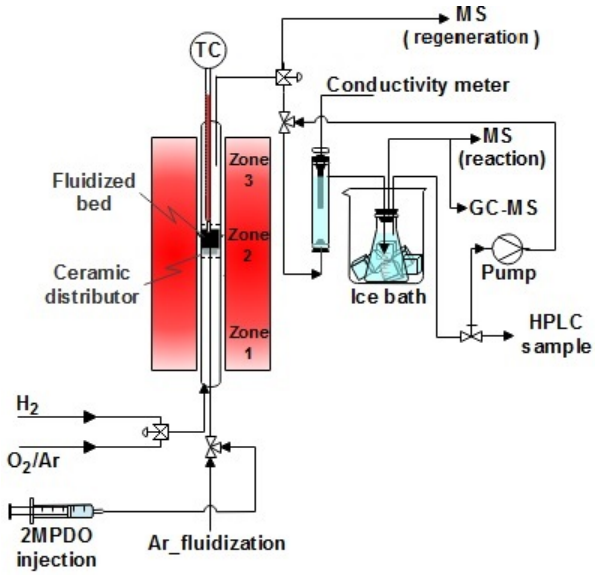

Figure 6.2 Experimental set–up with an 8 mm diameter quartz tube housed in a 3 zone electrical furnace. The injection line diameter was 1.6 mm (OD). During the regeneration step, the effluent bypassed the quench and absorbent. The MS detected no water during the regeneration step.

Table 6.2 Textural characteristics of catalysts

Catalyst	$S_{\mathrm{BJH}}(m^2g^{-1})$	Pore volume (cm^2g^{-1})	Pore radius (Å)
Cs-V-Cu.non	11	0.149	15.1
Cs-V-Cu.300	19	0.151	15.3
Cs-V-Cu.350	24	0.156	15.3
Used Cs-V-Cu.350*	17	0.13	13.8

*= After 480 min reaction at 250 °C

catalysts for which 2θ= 10.6°, 18.5°, 24.1°, 26.1°, 30.6°, 39.3°, 43.9°, 47.9°, 55.5° and 62.1° correspond to (110), (211), (310), (222), (400), (332), (440), (532), (550) and (732), respectively (Fig. 6.3) Mahboub *et al.* (2016b); Nair *et al.* (2010). The XRD spectra for all three catalysts before and after reaction are indistinguishable. The calcination temperature either doesn't affect catalyst crystallization or XRD cannot detect the differences.

XRD only shows the body centered cubic phase as it is impossible to distinguish the dispersed (active—$(NH_4)_3PMo_{12}O_{40}$ and $Cu_{0.5}(VO)O_x$) from the support ($(Cs)_3PMo_{12}O_{40}$) Kendel et Brown (2011). Substituting cesium with ammonium shifted the peaks to lower angles and because Cs has a larger ionic radius compared to $NH_4{}^+$, the inter-planar spacing (d–spacing) is expanded Jing *et al.* (2014b). The narrow peaks also confirm that the catalysts structure are well crystallized Mahboub *et al.* (2016b).

The used catalysts maintained their Keggin structure ; however, some MoO_3 crystals (shown with $\star$ in Fig. 6.3) over used catalysts are evident, which is due to thermal decomposition of catalyst after 480 min.

FT–IR

The intense peaks of the FT–IR spectra at 1063 cm^{-1}, 966 cm^{-1}, 866 cm^{-1}, and the very broad band centered around 795 cm^{-1} represent ν(P-O), ν(Mo=O_t), corner–sharing ν(Mo–O_b–Mo), and edge–sharing ν(Mo–O_t–Mo), respectively, which confirm the Keggin structure of all Cs−V−Cu catalysts before and after reaction (Fig. 6.4, Table 6.3) Mizuno *et al.* (1996b); Busca *et al.* (1996). The characteristic weak peak around 1411 cm^{-1} assigned to the ammonia cation with the exception of the uncalcined sample where the band was shifted to 1404 cm^{-1}. This deviation and the corresponding weak shoulder around 1383 cm^{-1} are caused by free ammonia groups that are later desorbed by calcination Jing *et al.* (2014a). Very weak characteristic bands around 595 cm^{-1} for all samples corresponded to MoO_3 species, suggesting that some structural decomposition occurred before reaction Ballarini *et al.* (2007a). However, this trace decomposition was undetectable by XRD for the fresh samples.

The increase of peak intensity at 593 cm^{-1} after the reaction, for the Cs−V−Cu.300, corresponds to more MoO_3, whereas, a related decrease of band intensities corresponding to the ν(Mo=O) and edge–sharing ν(Mo–O_t–Mo) of the Keggin unit indicates the catalyst decomposes during reaction. However, this result appears due to trace fluctuations in the ν(P-O) bond caused by the decreased thermal stability of Cs−V−Cu.300 compared to Cs−V−Cu.350 (confirmed by TGA). (The spectra of used Cs-V-Cu.300 are omitted from Fig. 6.4).

The spectra of the Cs−V−Cu.350 before and after reaction demonstrate the opposite rela-

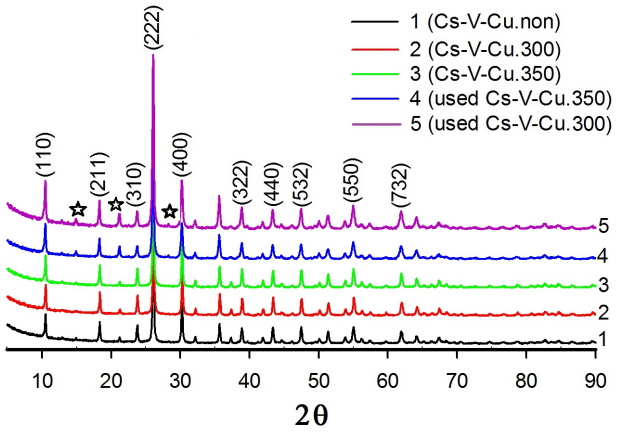

Figure 6.3 XRD characterization of fresh catalysts and used Cs−V−Cu.350 after 480 min at 250 °C with 2MPDO/O_2/Ar= 13 %/10 %/77 %

tionship. The peaks corresponding to the ν(Mo=O_t) and edge–sharing ν(Mo–O_t–Mo) of the Keggin unit increase in intensity. There is also a notable decrease in the intensity of the peak indicative of corner-sharing ν(Mo–O_b–Mo) at 866 cm^{-1}. This result is caused by catalyst decomposition and simultaneous formation of MoO_3 crystals during reaction, as they share the ν(Mo=O_t) and edge–sharing ν(Mo–O_t–Mo) bands of the Keggin structure. In unexpected contrast, the intensity of the ammonium band increased a little, which suggests the active phase forms during reaction Cavani *et al.* (2001d).

A weak band around 1035 cm^{-1} is typical of V−O stretching vibrations in the spent catalyst sample. The band develops due to the reduction of V^{5+} during the reaction and the formation of VO^{2+} thereafter Jing *et al.* (2014b). Furthermore, a weak band develops around 628 cm^{-1} which we assign to binary Cu−O bonds formed during reaction. This band is not well–documented, but lies near the theoretical vibrational frequency of the binary Cu−O bond calculated at 640 cm^{-1} via the Hooke's Law model of bond vibration with a force constant 3.08 mdyn $Å^{-1}$ for binary Cu−O.

Table 6.3 FT–IR vibration wave numbers

Catalyst	Wave number (cm^{-1})				
	N−H	P−O	Mo−O_t	Mo−O_b−Mo	Mo−O_t−Mo
Cs−V−Cu.non	1404	1063	966	866	798
Cs−V−Cu.300	1413	1063	967	866	799
Cs−V−Cu.350	1416	1063	967	867	798
used Cs−V−Cu.300	1415	1063	966	867	795
used Cs−V−Cu.350	1413	1063	966	867	793

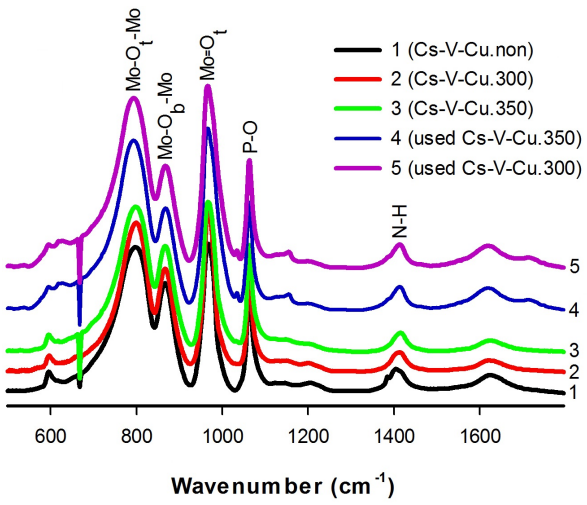

Figure 6.4 FT–IR characterization of fresh catalysts and used Cs−V−Cu.350 after 480 min at 250 °C with 2MPDO/O_2/Ar= 13 %/10 %/77 %

Raman spectroscopy

Raman spectra characterization (the same as FT–IR) confirms the main bands of the Keggin structure for all samples with 982, 965 (shoulder), 872, and a broad band at 605 cm^{-1} which are assigned to ν_s(Mo=O), ν_{as}(P−O), ν_{as}(Mo−O_b−Mo) and ν_{as}(Mo−O_c−Mo), respectively (Fig. 6.5) Jing *et al.* (2014b). The spectra of the fresh calcined and uncalcined catalysts illustrate a weak band around 815 cm^{-1}, ascribed to MoO_3. This agrees with the FT-IR results suggesting structural decomposition during preparation. FT-IR and Raman are sensitive techniques capable of detecting tiny amounts of MoO_3, none of which was detected by XRD for the fresh calcined and uncalcined catalysts. The higher intensity and more obvious shoulder of V_2O_5 for Cs−V−Cu.350 indicates stronger interaction between vanadium and oxygen into the Keggin structure. Therefore, the stronger bond of vanadium and oxygen (V_2O_5) justifies the better performance of this catalyst.

The wide spectra from 1380 to 1600 cm^{-1} for the used Cs−V−Cu · 350 indicates the presence of amorphous carbon which is heterogeneously distributed over the catalyst surface. The broad 600-700 cm^{-1} band is actually due to the overlapping of peaks at 605 and 645 cm^{-1} corresponding to the original ν_{as}(Mo−O_c−Mo) of the Kegging structure and MoO_3, respectively. This, along with the increase in intensity of the 815 cm^{-1} band, indicates partial structural decomposition after reaction, in agreement with the FT-IR results (Fig. 6.5).

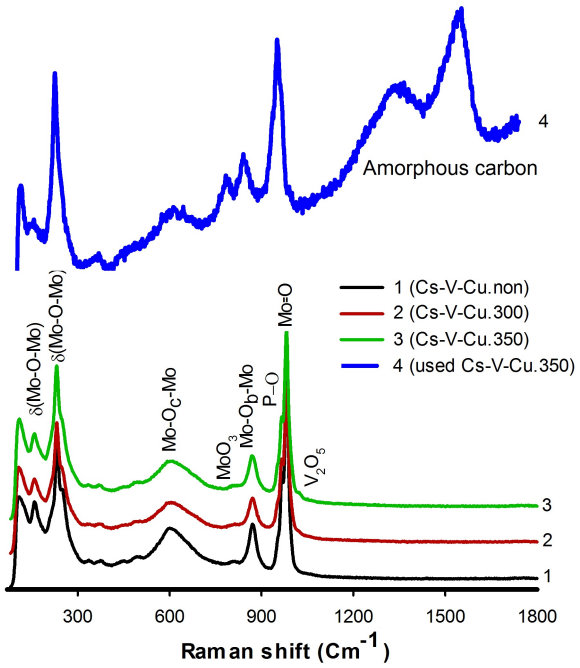

Figure 6.5 Raman spectroscopy characterization of fresh catalysts and used Cs-V-Cu. 350 after 480 min at 250 °C with 2MPDO/O_2/Ar= 13 %/10 %/77 %

UV-vis

UV-Vis diffuse reflectance spectra of catalysts before and after reaction show broad, intense absorption bands from 200 nm to 600 nm (Fig. 6.6). Several components associated with the various $O^{2-} \rightarrow Mo^{6+}$ charge–transfers in the Keggin anion constitute these broad spectra Cavani *et al.* (2001f) : the low-energy charge-transfer band is due to oxidation potential of the oxometal. Crystallinity of the compound as a structure of catalyst and also the function of the cationic composition of the Keggin structure result in the absorption band above 400 nm Cavani *et al.* (2001f). The broad band centered at ca. 700 nm that occurs in the spectra of the spent Cs−V−Cu.350 catalyst shows the intervalence charge–transfers energies of molybdenum species ; indicating that octahedral Mo^{5+} developed during reaction and confirmed the catalyst reduction after 480 min Ballarini *et al.* (2007a). The notable broadening and intensity increase of this band in the spectrum of the spent Cs−V−Cu calcined at 350 °C compared to its low-temperature counter-part indicate increased charge mobility within the Keggin anion. Therefore, Cs−V−Cu.350 reduced more than Cs−V−Cu.300 compared to the corresponding fresh ones which resulted in better performance of Cs−V−Cu.350 for MAA and MAC selectivities. Among the fresh samples, the Cs−V−Cu.350 shows a higher extent of reduction compared to the other samples which confirms the higher effective redox reaction between molybdenum and vanadium ($Mo^{5+}+V^{5+} \rightarrow Mo^{6+}+V^{4+}$) (confirmed by XPS).

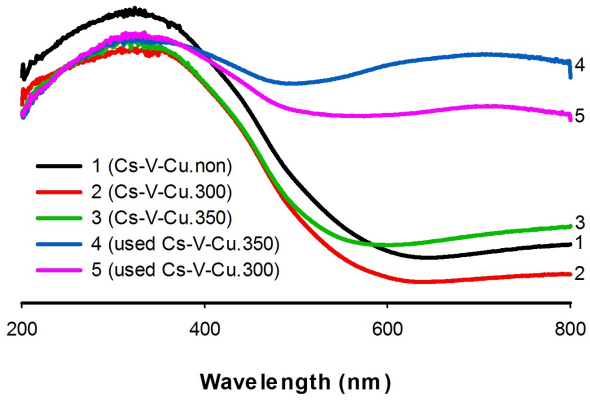

Figure 6.6 UV-Vis characterization of fresh catalysts and used Cs−V−Cu.350 after 480 min at 250 °C with 2MPDO/O_2/Ar= 13 %/10 %/77 %

NMR

^{1}H and ^{31}P MAS-NMR spectra measure the quality and degree of hydration of the Keggin structure over the catalysts' life cycle for fresh and used Cs−V−Cu.350. The ^{31}P MAS-NMR spectra of the catalysts show the Keggin structure of the samples (Fig. 6.7a). One sharp peak, observed for every sample at ca. δ=-4.0 ppm, corresponds to the $[PMo_{12}O_{40}]^{3-}$ anion ; however, the presence of other weak peaks in the spectra of the uncalcined and spent catalyst suggest complexities in the catalyst structure which depend on the degree of hydration and cationic interactions Guan *et al.* (2007a); Damyanova *et al.* (2003). Mizuno et al. reported the formation of $[PMo_{12}O_{40}]^{3-}$ by thermal treatment of $H_3PMo_{12}O_{40}$ Mizuno *et al.* (1996b); Mizuno et Yahiro (1998). Therefore this peak for phosphorus asserts the formation of salted cesium 12-molybdophosphoric acid in presence of vanadium and copper ($Cs(NH_4)_2PMo_{12}O_{40}(VO)Cu_{0.5}$) after treatment in air at 250 °C. The ^{1}H MAS-NMR spectra of the catalysts show one common peak for the ammonium cation at ca. δ= 5.8 ppm Chernyak *et al.* (2013). This shoulder disappears with calcination temperature, as evidenced by the gradual decrease in intensity from the uncalcined sample to the catalyst treated at 350 °C (Fig. 6.7b). This shoulder disappears entirely from the catalyst calcined at 350 °C after reaction but only partially from the spent catalyst which was calcined at 300 °C.

TGA

The TG curve of the thermal decomposition of Cs−V−Cu shows four steps from 50 °C to 600 °C. In the first two steps, physisorbed water is released (< 100 °C), followed by a comparably small amount of bound water between 100 and 200 °C. Between 250 and 450 °C, the anhydrous Cs−V−Cu salt decomposes to V and Mo oxides. By analogy with a previous study,

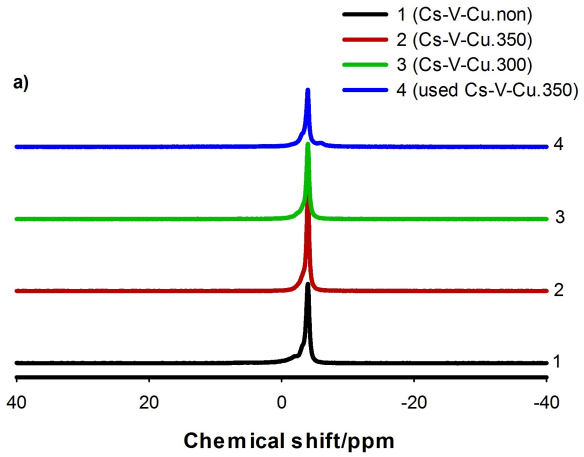

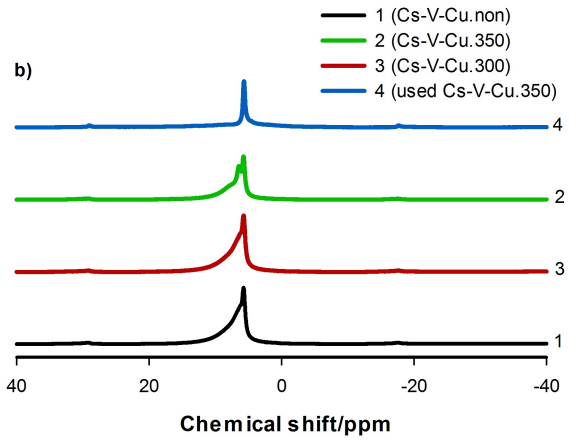

Figure 6.7 a) ^{31}PNMR b) ^{1}HNMR characterization of fresh catalysts and used Cs−V−Cu.350 after 8 h at 250 °C with 2–methyl–1,3–propanediol/O_2/Ar= 13 %/10 %/77 %

this begins with the decomposition of the ammonium cation above 350 °C resulting in ammonia evolution, the formation of $H_3PMo_{12}O_{40}$ and $Cu_{0.5}(VO)O_x$ dispersed over $Cs_3PMo_{12}O_{40}$, and simultaneous elimination of acidic protons Mahboub *et al.* (2016a). The result is a lacunary Keggin structure that further decomposes to the aforementioned oxides (Fig. 6.8). The weight loss may also be due to CuO reducing to Cu_2O on heating. Cs−V−Cu.350 loses 6.5 % of its mass while the Cs−V−Cu.300 lost 7 %. While both spent samples lost more mass than their fresh counterpart due to coke built-up from the reaction, the spent Cs−V−Cu calcined at 300 °C decreased sharply at 550 °C, followed by a plateau (Fig. 6.8). Jing et al. claim that above 550 °C, P_2O_5 sublimes and this sublimation is more obvious for catalyst calcined at lower temperature (300 °C) Jing *et al.* (2014b).

FE-SEM

High resolution FE–SEM shows that the elements are distributed evenly for all catalysts with a rough texture at low magnification. At high magnification, the roughness is obviously due to 200 nm to 500 nm particles that cover the surface. (Fig. 6.9). Surface elemental analysis (EDX spectrum) confirms the presence of Cs, Mo, P, V, and Cu (Fig. 6.9). Used catalysts also have a strong carbon peak due to coke.
The map elemental analysis at higher resolution also indicates that nitrogen is more evenly distributed on the catalyst calcined at 350 °C, which correlates with its superior performance.

XPS

High resolution X-ray photoelectron spectroscopy confirms the oxidation state of Cs, P, Mo, and C elements on the surface. The uncalcined sample contains Mo3d 5/2 level at binding energies of 231.7, 232.7 and 234.7 eV, with intensities corresponding to 1.9 % at., 11.5 % at. and 4.5 % at. of the total count, respectively. The first binding energy is attributable to Mo^{5+} while the second is attributable to the crystalline phase of Mo^{6+}. The last one (234.7 eV) has a higher binding energy compared to the normal molybdenum which we suppose it is due to the higher electro–negativity of the atoms surrounding Mo or it might be due to water trap for uncalcined sample. The calcined samples have two binding energies at 231.9 and 233 eV which are assigned to Mo^{5+} and Mo^{6+}, respectively.

The atomic ratio of Mo^{6+}/Mo^{5+} for calcined samples is higher than uncalcined one (12.4, 9.9 and 8.4 % for Cs−V−Cu.350, Cs−V−Cu.300 and Cs−V−Cu.non, respectively) which confirms that calcination oxidizes the coordinatively unsaturated Mo^{5+} to Mo^{6+} in the crystalline phase. Higher atomic ratio of molybdenum (compared to other metal cations) for all

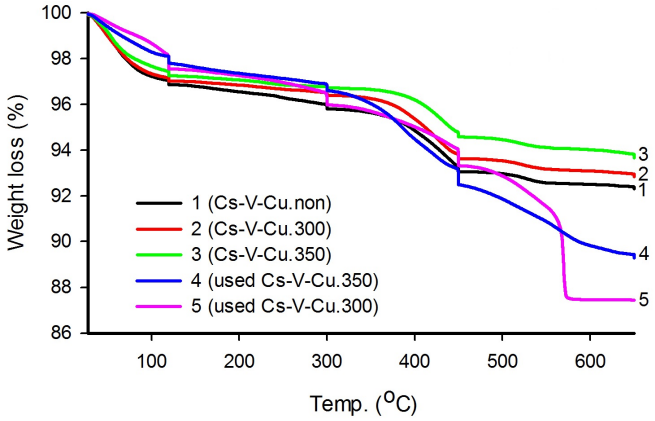

Figure 6.8 Thermal decomposition of fresh catalysts and used Cs−V−Cu.350 after 480 min at 250 °C with 2MPDO/O_2/Ar= 13 %/10 %/77 % under oxygen flow

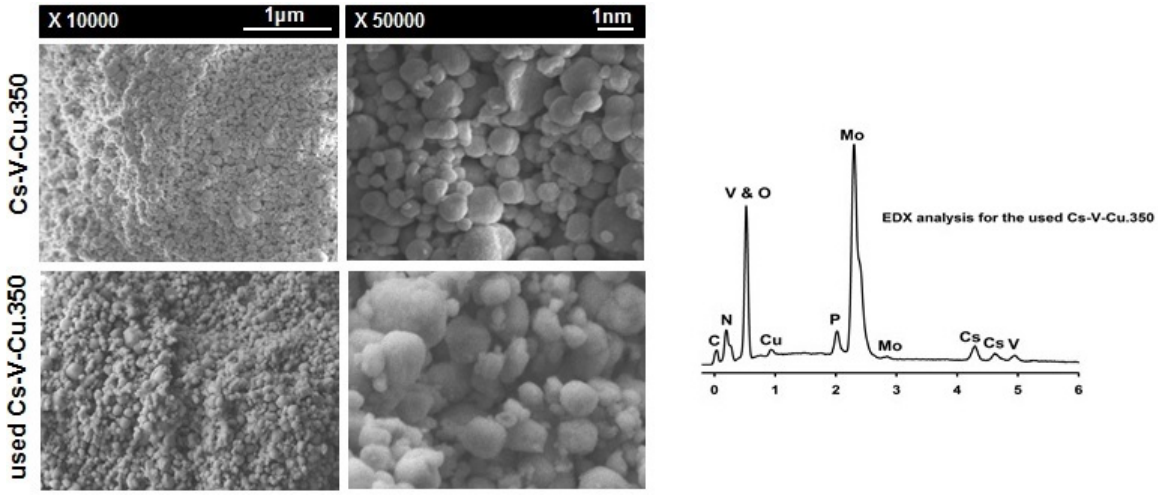

Figure 6.9 Morphology of fresh catalysts and used Cs−V−Cu.350 after 480 min at 250 °C with 2MPDO/O_2/Ar= 13 %/10 %/77 % under oxygen flow

catalysts before and after the reaction confirms that the surface is enriched in molybdenum (Table 6.4).

All samples before and after reaction have similar binding energies (~ 132 eV) for phosphorous (P2p) in the form of PO_4 which confirms that this atom is mainly present as P^{5+}. Cesium also shows the same binding energy before and after reaction equal to 724 eV–Cs^{1+} (Fig. 6.11– used Cs−V−Cu · 350 sample).

We expect to find binding energies for vanadium (V2p 3/2) between 512 eV to 518 eV but no peak is evident in that region of the spectrum, which suggests that its surface concentration is less that 0.1 at. %. So oxidation state for vanadium is unknown. The same applies for copper and nitrogen : binding energies for copper lie between 932 eV to 954 eV, N1s binding energies are 400 eV, but it overlaps Mo3p 3/2.

The Auger electron peaks for cesium at 933 cm^{-1} overlaps with the main copper peak so to identify copper we rely on its secondary peak. The XPS identified the secondary peak in the hydrogenated sample but it was absent in the original sample. Most of the oxygen before and after reaction is oxygen connected to metal cations in the form of O^{2-} (530.7 eV). There is a small portion for oxygen with a lower electron density than O^{2-} ions (531.7 eV) and oxygen in nonequivalent oxygen sites (around 529.8 eV) (Fig. 6.11– used Cs−V−Cu · 350 sample).

XPS detected small portions of C−OH or C−O−C at 532.8 eV and O−C in ester with binding energy of 533.9 eV in the used catalyst. These species may form when the samples were exposed to air. The oxidation state of the Mo changes with time on stream as the surface Mo^{6+}/Mo^{5+} atomic ratios of the used catalysts are much lower than those of the corresponding fresh catalysts (Table 6.4). The reduction of molybdenum for Cs−V−Cu.350 is higher than Cs−V−Cu.300, which suggests that a lower oxidation Mo is desirable. Finally, the analysis of used samples illustrate the presence of carbon on the surface due to coke formation (Fig. 6.11e) (We put the XPS results for used Cs−V−Cu.350 as an example).

Table 6.4 XPS data for fresh catalysts and used Cs−V−Cu.350 after 480 min at 250 °C with 2MPDO/O_2/Ar= 13/10/77 under oxygen flow

Sample	Binding energy (eV)					Surface composition (at %)					SOS*
	Cs $3d_5$	P 2p	Mo 3d	O 1s	C 1s	Cs	P	Mo	O	C	Mo^{6+}/Mo^{5+}
Cs-V-Cu.non	725.1	135	233.9	531.6	—	4.5	1.5	17.9	76.1	—	8.4
Cs-V-Cu.300	723.8	133.9	233	530.7	—	4.1	2.1	17.5	76.3	—	9.9
Cs-V-Cu.350	724.5	134.8	233.6	531.4	—	4.3	2.3	17.4	76.0	—	12.4
Used Cs-V-Cu.300	723.7	133.8	232.8	531.6	284.8	0.2	0.3	3.0	34.7	61.7	8.7
Used Cs-V-Cu.350	723.6	133.7	232.7	531.5	284.8	0.4	0.6	5.1	42.8	51.1	9.0

*SOS = Surface oxidation state

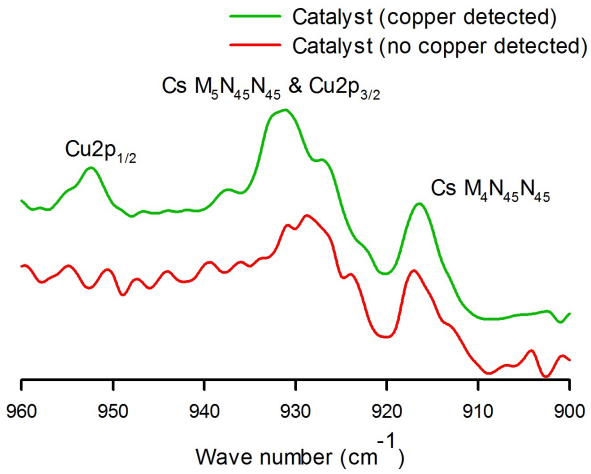

Figure 6.10 Cs-V-Cu.350 XPS spectra before hydrogenation (lower red line) and after hydrogenation (upper green line). Auger electrons mask the primary Cu peak at 932 cm^{-1} ($Cu2p_{3/2}$)after hydrogenation but the secondary peak $Cu2p_{1/2}$ is clearly evident. The secondary Cu peak is absent in the catalyst spectra before before hydrogenation.

6.4.2 Catalytic activity

Calcination temperature

Among the three catalysts (uncalcined, calcined at 300 °C, and calcined at 350 °C), after 100 min time–on–stream at 250 °C, Cs−V−Cu.350 was the most selective and produced the most MAA, with a yield greater than 24 % (Table 6.5, Fig. 6.12). The maximum selectivity to MAA and MAC was 41 % and 33 %, respectively. The uncalcined catalyst has the poorest performance towards MAA and MAC selectivity. Calcining the catalyst decreases activity while increasing selectivity, which is standard for many oxidation catalysts Patience *et al.* (2007). MAA yield decreases with increasing 2MPDO conversion which this decreasing trend is more obvious for uncalcined catalyst and is minimum for Cs−V−Cu · 350. Higher calcination temperature improves catalyst performance and product selectivity which directly relates to oxidation state of metal ions into the catalyst structure and redox reaction between the Keggin–anion and cations. More carbon oxides formed during the oxidation step with the catalyst calcined at 350 °C compared to sample calcined at 350 °C and for this reason 2MPDO conversion was higher but oxygen conversion is lower, which is counterintuitive. XPS results showed that calcining samples increased the Mo^{6+}/Mo^{5+} ratio where higher calcination temperature resulted in higher ratio. Therefore, we suppose that calcining reduces vanadium from V^{5+} to V^{4+} while the Mo^{5+} oxidizes to Mo^{6+} in the Keggin structure (V^{5+}+Mo^{5+} → V^{4+}+Mo^{6+}) which is consistent with previous reports. The XPS spectra confirmed that V^{4+}

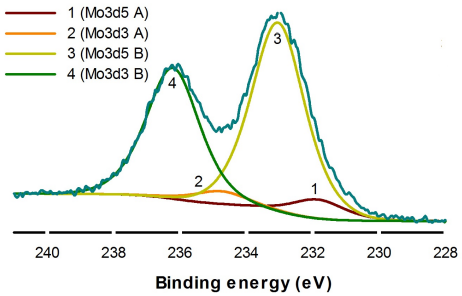

(a) Molybdenum ion.

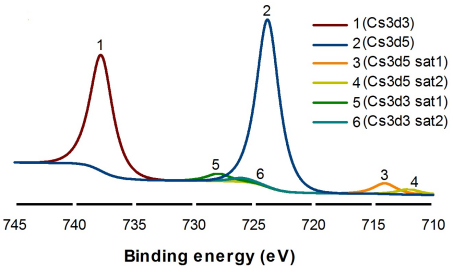

(b) Cesium ion.

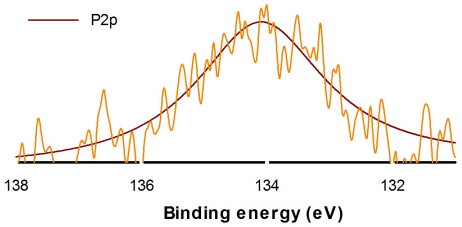

(c) Phosphorous ion.

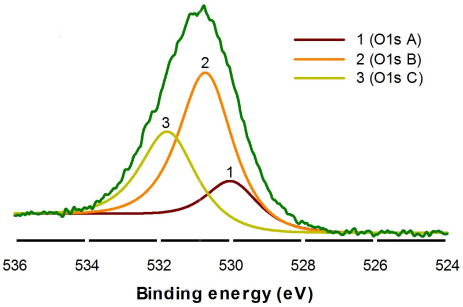

(d) Oxygen ion.

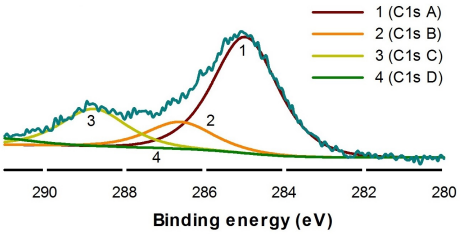

(e) Carbon deposition on surface.

Figure 6.11 High resolution elemental surface analysis by XPS for used Cs−V−Cu.350

leaves the Keggin ion (primary structure) and forms VO^{2+} as part of the secondary structure due to the partial structural decomposition of the polyoxometalate during the heat treatment. This compound maintained the reduced state even while calcining in air and during reaction (based on XPS analysis). The XPS results indicate that the average oxidation state (based on Mo^{6+}/Mo^{5+} atomic ratio) of Cs−V−Cu.350 is higher than Cs−V−Cu.300, which correlates with the improved performance. The XPS analysis and UV–Vis data demonstrate that used catalyst calcined at 350 °C becomes more reduced compared to the used catalyst calcined at 300 °C. The Mo^{6+}/Mo^{5+} for the Cs–V–Cu.350 decreased 27 % after reaction whereas, the oxidation state of Cs–V–Cu.300 decreased by less than 10 %. These data confirm that MAA and MAC selectivity increase over Cs–V–Cu.350 because of the higher reduction and ion exchange between molybdenum and other elements (vanadium and oxygen).

Raman spectroscopy confirms that the V_2O_5 bond in Cs−V−Cu.350 reduced the molybdenum more compared to the other samples. Higher calcination temperature shows a redox reaction couple between the primary structure ($PMo_{12}O_{40}{}^{3-}$) and cation ions. Although the crystallinity of the uncalcined catalyst is the same as the calcined catalysts, its performance is poorer potentially because the catalyst is not sufficiently reduced to form the active phase.

The maximum error of instruments for all experiments (based on repeated experiments) was 3 %. Therefore, the difference between selectivity for all samples at the different feed composition is due to calcination temperature. The selectivity of MAA and MAC is the same for the uncalcined catalyst (Cs−V−Cu.non) and the selectivity to methane is highest, which demonstrates that it is very active (Fig. 6.13). The selectivity for MAA is highest for the calcined catalysts followed by : MAA>MAC>CO_x>CH_4. MAC and methane selectivity are the same (32 % and 5 %, respectively) for the calcined catalysts (Fig. 6.13).

Time–on–stream oxidation

During the first 20 min, the Cs−V−Cu.350 catalyst is non-selective and as it activates with time, MAA selectivity increases, MAC decreases. High throughput experimental methods might have rejected the catalyst. The trend in yield of the desired product is uncharacteristic of vanadium pyrophosphate catalysts (VPP) for butane oxidation to maleic anhydride (2 % n-butane in air) Patience *et al.* (2007). Whereas both selectivity and activity increase with time for the Cs−V−Cu.350, VPP catalysts lose activity and gain selectivity during the activation period (24 h). Only as the phosphorous volatilizes due to the high temperature (< 400 °C) does the VPP lose selectivity and gain in activity. Some studies on partial oxidation of isobutane to MAA over molybdenum based catalysts show the same trend for both selectivity and activity because of in–situ reduction of Mo and to the partial decomposi-

Table 6.5 Calcination temperature and feed composition on catalyst performance at 250 °C after 100 min time–on–stream

Run	Catalyst	Feed composition 2MPDO/O_2/Ar	2MPDO Conv. (%)	O_2 Conv. (%)	Selectivity (%)			
					MAA	MAC	COx	CH_4
1	Cs−V−Cu.300	10/10/80	67	90	31	35	22	6
2		10/13/77	79	81	23	34	25	8
3		13/10/77	60	91	37	32	22	5
4		13/13/74	76	83	30	39	23	3
5	Cs−V−Cu.350	10/10/80	71	85	32	39	23	5
6		10/13/77	81	80	28	29	37	9
7		13/10/77	63	91	41	33	21	4
8		13/13/74	74	92	34	44	22	4
9	Cs−V−Cu.non	10/10/80	76	77	17	27	29	18
10		10/13/77	84	80	11	13	47	18
11		13/10/77	78	97	19	20	30	22
12		13/13/74	81	95	18	27	35	15

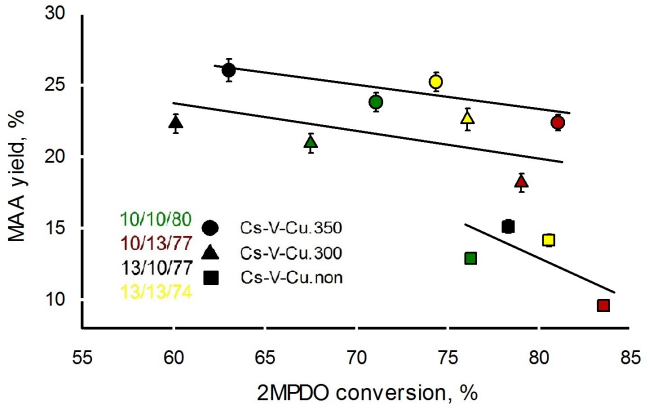

Figure 6.12 Selectivity versus conversion over different catalysts and feed compositions at 250 °C at 100 min

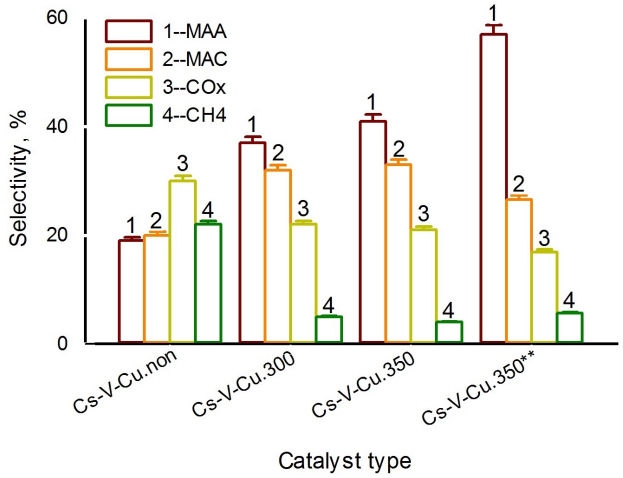

Figure 6.13 Products selectivity vs. catalyst type for 2MPDO/O_2/Ar= 13 %/10 %/77 % at 250 °C after 100 min (** : Cs−V−Cu.350 performance after 480 min)

tion of the catalyst and generation of more active Mo species in the cationic position of the polyoxomtalate Cavani *et al.* (2003b, 2001b, 2003a).

In the first 10 min, Cs−V−Cu · 350 catalyst combusts 45 % of the 2MPDO and not until 100 min time-on-stream does the MAA yield improve to 25 %. After 8 h the selectivity to MAA reaches 57 % and a yield of 38 % (Figs. 6.14,6.15). However, during the initial 100 min, the selectivity to MAC decreases from above 40 % to 26 % at the end of the test. The increase in MAA yield is several fold larger than the drop in the MAC yield. The catalyst does convert MAC to MAA but this reaction rate must be slower than the direct route from 2MPDO to MAA. Evidence for this lies in CO_2, CO, and CH_4. MAC in the product gas confirms that it formation rate is on the same order of magnitude as its reaction rate.

At temperatures above 250 °C oxygen and 2MPDO react catalytically to MAA, MAC, carbon oxides and methane (Eqs. 6.3–6.5). The decrease in MAC yield correlates most with the decrease in yield of carbon oxides and methane. During the last 8 h, selectivity to MAC and CO_x and CH_4 decrease : The MAC selectivity dropped from 57 % to 26 % while the CO_2 selectivity reached 17 % at the end of the test and CH_4 selectivity was 5.5 % (Fig. 6.14).

In fact, the catalyst combusted the 2MPDO up to 10 min after beginning to inject the solution and the CO_2/CO was 0.7. The CO_x selectivity was 45 %. CH_4 selectivity was 25 % at the beginning but after 10 min it dropped and the CO_x/CH_4 ratio remained constant at 3 thereafter. The methyl group of the C_4 compounds hydrogenates to methane while the

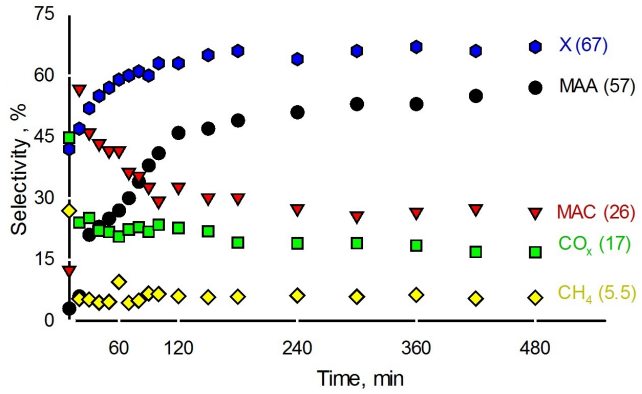

Figure 6.14 Conversion and product selectivity over Cs−V−Cu · 350 at 250 °C and 2MPDO/O_2/Ar= 13/10/77 during 8 h after oxidation which X shows the 2MPDO conversion trend

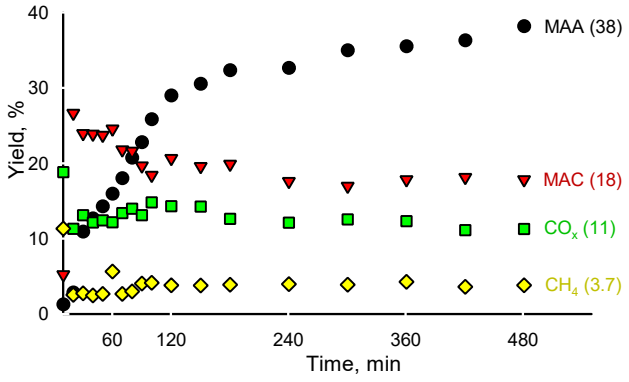

Figure 6.15 Yield as a function of time over Cs−V−Cu · 350 at 250 °C and 2–methyl–1,3–propanediol/O_2/Ar= 13/10/77 during 8 h after oxidation

remaining 3 carbons form CO_2 and CO.

$$C_3H_5(CH_3)(OH)_2 + 0.5O_2 \longrightarrow C_2H_2(CH_3)CHO + 2H_2O \tag{6.3}$$

$$C_3H_5(CH_3)(OH)_2 + O_2 \longrightarrow C_2H_2(CH_3)COOH + 2H_2O \tag{6.4}$$

$$C_3H_5(CH_3)(OH)_2 + 3O_2 \longrightarrow 2CO_2 + CO + CH_4 + 3H_2O \tag{6.5}$$

During the first 2 h, the selectivity of MAA triples and the MAC drops by 50 %, while the carbon oxides and methane increase by 30 %. So, the marginal increase in carbon oxides and methane corresponds to the increase in MAA but the series decomposition rate is an order of magnitude slower. After 2 h, the selectivity of MAA continues to rise but the selectivity to MAC, CO_x, and CH_4 drops but the yield is essentially constant. The oxygen conversion was high compared to 2MPDO (Table 6.5) which confirms that the reaction is limited by O_2 availability. Byproducts yield vs O_2 conversion shows that the yield of CO_2 is almost invariant with oxygen conversion ; however, the yields of CO and CH_4 increase with increasing of oxygen conversion up to 77 % and then they are almost constant with increasing conversion (Fig. 6.16). The MAA selectivity changes in three stages : in the first 30 min, it is below 6 % ; it increases sharply in the second stage between 30 min to 120 min ; and, it increases slightly thereafter up to 480 min where it increased from46 % to 57 %. The change in MAA selectivity correlates with the drop in MAC selectivity but this relationship is not substantiated in the graph of yield versus time-on-stream since MAC yield decreases 10 % over the first 2 h whereas the yield of MAA increases to 38 % (Fig. 6.15). Moreover, 2MPDO conversion increases and there is a constant trend for other byproducts, which confirms that 2MPDO converts directly to MAA over the catalyst surface. If the carbon oxides and methane come predominantly from MAC, then an increase in MAC yield would necessarily increase the yield of these byproducts, which is not the case. Therefore, at least two catalytic sites must be active in the process.

The change in the conductivity of the quench confirms that the product selectivity toward MAA increases with time as the rate of change was low during the first 100 min and increased thereafter at a steady rate. MAC contributes less to the conductivity compared to MAA.

The favoured path to MAA is via 2MPDO directly rather than via MAC. At the same reaction conditions ($MAC/O_2/Ar$=13/10/77 at 250 °C and after 100 min), MAA yield and selectivity were lower with MAC as the reactant versus 2MPDO. We propose the general mechanism in which 2MPDO reacts to form both MAC and MAA. MAC is the main intermediate that oxidizes to MAA and CO_x. 2MPDO forms CH_4 catalytically (Fig. 7.7).

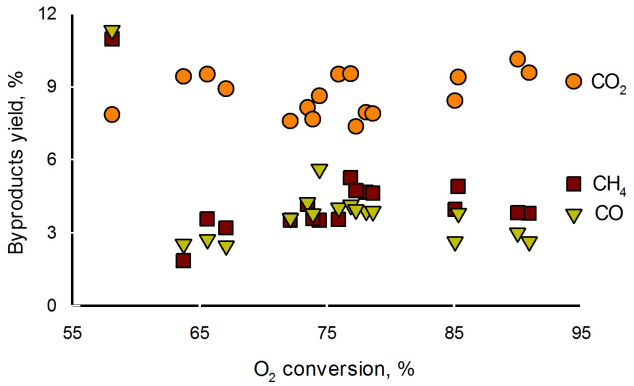

Figure 6.16 By–products selectivity versus oxygen conversion for 2MPDO/O_2/Ar= 13 %/10 %/77 % at 250 °C after 480 min over Cs−V−Cu.350

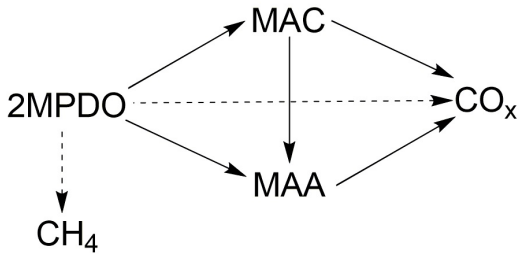

Figure 6.17 The general mechanism to produce MAA from 2MPDO

Hydrogen pretreatment after calcination

To test whether or not the Mo oxidation state was a factor in the low initial MAA selectivity, we reduced the three uncalcined and calcined catalysts in hydrogen ($40\,mL\,min^{-1}$) for 12 h at 250 °C. We then fed 2MPDO/O_2/Ar=13 %/ 10 %/77 %. Consistent with the experiments with the reduction step, the performance of the Cs−V−Cu · 350 was the best and the initial selectivities were low : reducing the catalyst had no apparent effect on the initial selectivity. After 100 min, the maximum MAA and MAC selectivities were 43 % and 37 %, respectively, over Cs−V−Cu.350 which is similar to the calcined only catalyst (Cs−V−Cu.350) of 41 % and 33 %, respectively (Fig. 6.18). The CO_x and CH_4 selectivities were also similar for the two cases. Much like the non-reduced catalysts, the performance of the Cs−V−Cu.non was the poorest.

There is lower oxygen connected to metal cations over the reduced catalyst surface compared oxygen with lower electron density than O^{2-} and oxygen in sites with higher covalence of the metal–O bond. Moreover, for reduced catalyst, XPS detected the vanadium and copper in the first 10 nm of the surface ; whereas, for the non–reduced catalyst, XPS did not detect these metal ions. Higher vanadium and copper over catalyst surface may accelerate ion transfer among metal ions and also oxidation–reduction of molybdenum and vanadium. FT–IR analysis illustrates a broad pick for a Mo−O_t−Mo and a small shoulder for Mo−O_b−Mo which confirm weaker bond between molybdenum and oxygen and sharper pick for which can be a proof for slight better performance of reduced catalyst.

6.4.3 Long time-on-stream oxidation-reduction sequence

The experimental protocol for this series of tests was to dose the catalyst with 2MPDO and oxygen (2MPDO/O_2/Ar=13/10/77) for 20 min and then reduce in hydrogen ($40\,mL\,min^{-1}$) for 2 min (stop injecting 2MPDO and switch oxygen to hydrogen) at 250 °C. The trend of the selectivity over 8 h was the same as the non-reduced catalyst : initial selectivity of MAA was low while the initial MAC selectivity was high. The MAA selectivity was slightly higher and 2MPDO conversion was the same. MAC selectivity was 2 % higher and consequently, the CO_x and methane were lower. Consistent with the 100 min test after 12 h of reduction, hydrogen has no effect on catalyst performance, thus the increase in catalyst performance with time on stream must be due to the carbon-catalyst moieties on the surface, which happen to be inert with respect to hydrogen (Fig. 6.19).

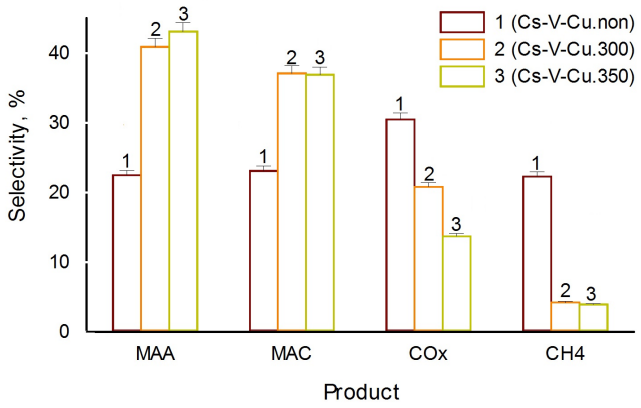

Figure 6.18 Selectivity of products over reduced catalysts at 250 °C and 2MPDO/O_2/Ar= 13/10/77 after 100 min

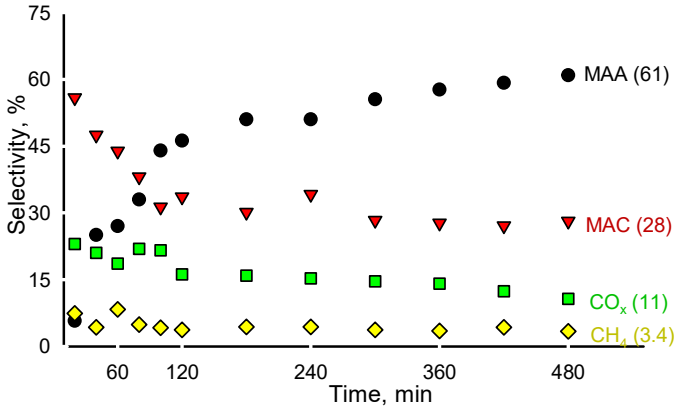

Figure 6.19 Product selectivity over Cs−v−Cu · 350 at 250 °C and 2MPDO/O_2/Ar= 13/10/77 after 480 min over oxidation–reduction condition

Mechanism

Cavani et al. reported the mechanism of the selective oxidation of isobutane to methacrylic acid catalyzed by Keggin–type polyoxometalates Cavani *et al.* (2001f). Here, we designed experiments at high conversion and partial 2MPDO conversion to identify the reaction steps and study the relationship between catalyst structure and products. At the same feed concentration over 0.5 g of catalyst (rather than 2 g) and 200 °C (rather than 250 °C) the main product was MAC with some 3–hydroxy–2–methylpropanal, 3–hydroxy–2–methylpropionic acid, acetic acid, 2–methylpropanal and isopropyl alcohol (Fig. 6.20). However, we did not detect MAA because MAC oxidizes to MAA above 200 °C. In 2MPDO the C−H and the C−OH single bond homolitic dissociation energy of the tertiary carbon and the carbon bearing the alcoholic function, respectively, is comparable (400 kJ mol^{-1} vs. 393 kJ mol^{-1}). Therefore the cleavage of these two bonds is equally likely. Though, the route of direct dehydration of 2MPDO followed by oxidation to MAC seems the most direct path to the products detected, we also propose a mechanism that passes through the homolitic dissociation of the C−H bond, in reason of the very similar bonding energies. The two mechanisms may be therefore parallel. The quantification of the respective contributions needs further data collection. We propose a mechanistic model for the gas–phase oxidation of 2MPDO to MAA and MAC over a Keggin-type catalyst with molybdenum and oxygen on the surface (XPS results) (Fig. 6.21). Equally to the activation of isobutane, the rate limiting step is the abstraction of a hydride ion (H^-) from the tertiary carbon, which gives a tertiary carbocation passing through an alkoxide–type intermediate (I). The bond C−H is weaker than C−C and C−O. In a second step (II), an adjacent Mo oxidized surface site abstracts an H^+ species from the carbon bearing the alcoholic function of the 2MPDO yielding another alkoxide–type intermediate connected to the catalyst surface via a Mo−O−C bridge. This species is in equilibrium with a dialkoxy species, where the H of the alcoholic function migrates in correspondence of the carbocation. This latter dialkoxy species is common intermediate to both methacrolein and methacrylic acid (steps IIIa and IIIb in Fig. 6.21). In case of methacrolein, the surface sites involved re-oxidize yielding the intermediate 3–hydroxy–2–methylpropanal. In previous experiments, we confirmed that the 3-hydroxy-2-methylpropanal is a possible intermediate by adding sulfuric acid (as a catalyst) to a mixture of MAC with water Mahboub *et al.* (2016a). After 24 h, the GC-MS detected 3-hydroxy-2-methylpropanal peak Mahboub *et al.* (2016a). 3–hydroxy–2–methylpropanal dehydrates to methacrolein (IIIa). For methacrylic acid, the surface site further reduces to yield 3–hydroxy–2–methylpropionic acid, which then dehydrates to MAA (IIIb).

Pyo et al. reported the oxidation of 2MPDO to MAA in a two–step process where enzymes

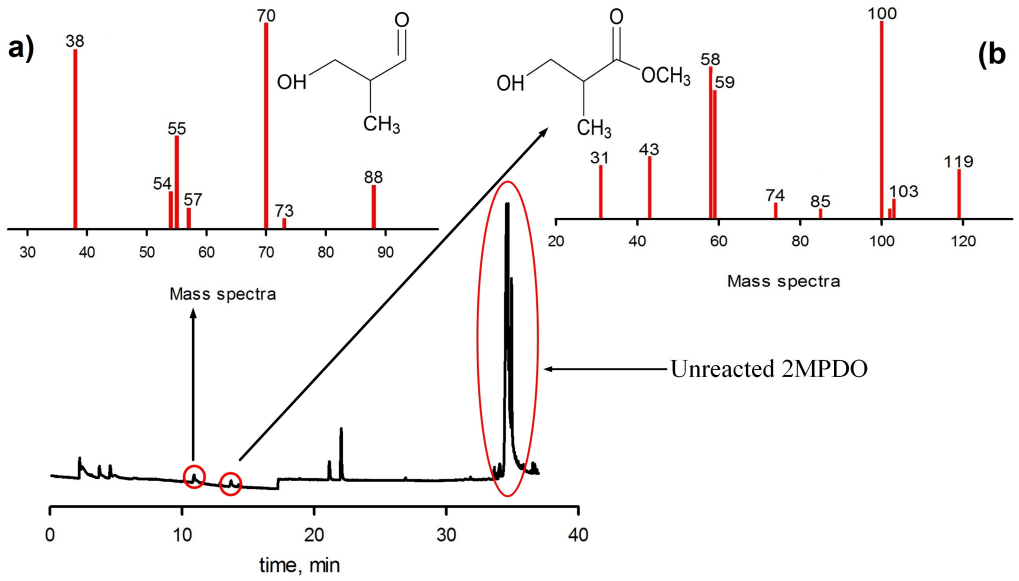

Figure 6.20 GC-MS analysis to detect a) 3–hydroxy–2–methylpropanal and b) 3–hydroxy–2–methylpropionic acid at low 2MPDO conversion

first convert 2MPDO to methacrolein and then TiO_2 oxidizes it to the final product Pyo *et al.* (2012). We also report the gas–phase dehydration to the same intermediate (Fig. 6.21). However, Brønsted and Lewis acid sites may promote the dehydration keeping the intermediates anchored to the catalyst surface without desorbing any oxidized compound in the gas-phase, except for the two products (MAA and MAC). In this case, there are 3-hydroxy-2-methylpropanal and 3–hydroxy–2–methylpropionic acid in the products at low conversion, whereas, as soon as conversion increases they are converted to MAC and MAA. In our case, we speculate that, being the starting material already oxidized and acid–catalyzed dehydration. Oxygen in the gas–phase re–oxidizes the catalyst according to the redox mechanism Paul *et al.* (1997). However, the product selectivity changes over time (Fig. 6.14, 6.15). In particular, while MAA selectivity increases, MAC selectivity decreases together with CO_x. All Keggin–type heteropolyacids present an unsteady behaviour at the beginning of the reaction Cavani *et al.* (2000). During the equilibration period, the catalyst undergoes a decrease in the Mo^{6+}/Mo^{5+} (Table 6.4) even under oxidizing conditions Cavani *et al.* (2001f). The progressive increase in the extent of the reduction of the catalyst should accompany with a progressive increase of the partial oxidation products, MAA and MAC and a decrease in CO_x selectivity. At the beginning of the reaction MAA overoxidizes to CO_x on the catalyst and decomposes to CH_4. The trend of CO_x in fact increases in the first 120 minute. After the equilibration time of 120 minute, the activity of the catalyst towards complete oxidation reduces, privileging the one towards partial oxidation. At this point the MAA selectivity stabilizes

together with CO_x (Fig. 6.15). The catalyst cracks 50 % of 2MPDO to one mole of methane, 2 mole of CO and 1 mole of CO_2. The route of the direct dehydration of 2MPDO followed by oxidation to MAC and then oxidizing MAC to MAA is likely mechanism, since dehydration is easier than a C−H activation, which opens the possibility two parallel mechanisms. The respective contributions of the different process routes require clarification in future work.

6.5 Conclusions

Higher calcination temperature increases MAA selectivity, whereas the maximum selectivity for MAC and MAC was 41 % and 33 %, respectively at 250 °C over 2MPDO/O_2/Ar= 13/10/77 after 100 min over Cs−V−Cu.350. Over higher temperature, more ammonium ions evaporate from the catalyst structure and therefore, it's crystallinity reforms by providing V_2O_5 and stabilizes with more vacancies. Over Cs−V−Cu.350, there is a higher reduction of molybdenum (Mo_6^+ to Mo_5^+) by vanadium compared to Cs−V−Cu.300. Time–on-stream reaction shows that the catalyst (Cs−V−Cu.350) is active up to 480 min and over the steady–state situation the selectivity of MAA is 57 %. The MAA selectivity increases over reduced catalysts because hydrogen consumes the oxygen of the catalyst's surface and then during the reaction some molecular oxygen as a co–feed is adsorbed by the catalyst which prevents re–oxidation of desired products. The oxidation–reduction condition maximized the selectivity to MAA (61 %) after 480 min over Cs−V−Cu.350.

6.6 Acknowledgements

The authors recognize MITACS and CRIBIQ for their financial support of this study.

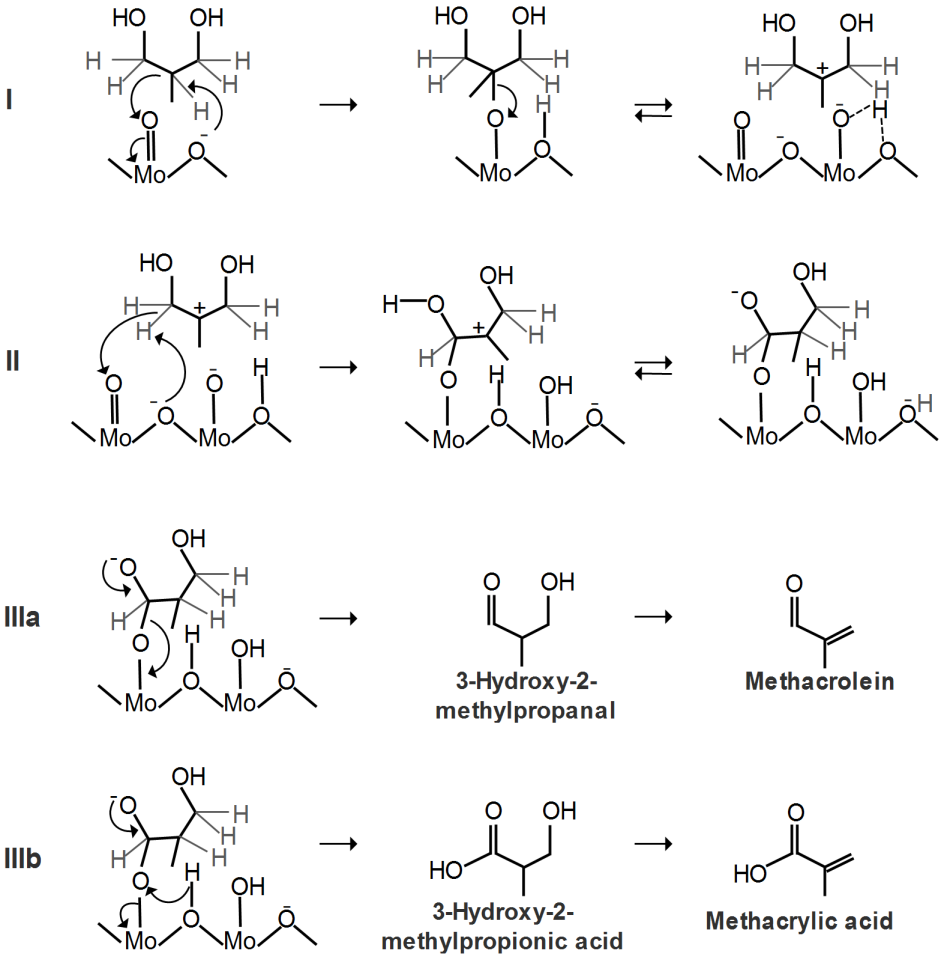

Figure 6.21 Proposed mechanism based on the correlation between catalyst structure and reaction

CHAPTER 7 ARTICLE 5 - OXIDATION KINETICS OF 2–METHYL–1,3 PROPANEDIOL TO METHACRYLIC ACID

Mohammad Jaber Darabi Mahboub, Olga Chub, Jean–Luc Dubois, Gregory S Patience

Submitted to : Chemical Engineering journal (2018)

7.1 Abstract

Methacrylic acid (MAA) is a specialty monomer for poly methyl methacrylate (PMMA). Partial oxidation of 2–methyl–1,3–propanediol (2MDPO) to MAA is an alternative to commercial technology with fewer process steps, less costly and toxic feedstocks and longer catalyst lifetime. Here we evaluated 2MPDO and oxygen concentrations, reaction temperature, and contact time on product selectivity and 2MPDO conversion over $VOCu_{0.5}/Cs(NH_4)_2PMo_{12}O_{40}$. Higher temperature increases selectivity and conversion ; MAA selectivity reached 46 % at 69 % 2MPDO conversion. Higher 2MPDO to O_2 ratio favors higher MAA selectivity due to methacrolein (intermediate) oxidation to MAA (means higher ratio favors consecutive oxidation) or lower combustion of MAA to CO_x. Shorter contact times decrease MAA selectivity. The Mars van Krevelen model characterizes the experimental data better than either the Langmuir-Hinshelwood or Eley-Rideal models : The reaction sequence involves both direct and indirect reactions in which 2MPDO goes to methacrolein (MAC) as an intermediat and then it oxidizes to MAA (indirect) and/or 2MPDO directly oxidizes to MAA but the indirect reaction rate to MAA is 50 times faster than the direct reaction rate. The reaction order to both 2MPDO and oxygen is one, and reacting of 2MPDO over the oxidized sites to form products is the rate–limiting step.

7.2 Introduction

Methyl methacrylate (MMA) polymerizes to poly–methyl–methacrylate (PMMA), which is a transparent non-crystalline vitreous thermoplastic known as Altuglas (Arkema), Plexiglass (Arkema and Evonik), and Lucite (Mitsubishi) Nagai (2001); Godfrey (1963); Kung (1994). The monomer has also diverse applications in the paints and coatings and medical industries Smith *et al.* (1999); W.Dormer *et al.* (1998); Ballard *et al.* (2017); Cao *et al.* (2018). Acetone–cyanohydrin (ACH) is the prevalent commercial route to produce MMA in which acetone reacts with hydrogen cyanide to form MMA via cyanohydrin as an intermediate Zhou *et al.* (2017b). Highly toxic and expensive reactants and a large volume of byproduct ammonium

bisulphate are the main drawbacks of this process Mizuno et Yahiro (1998); Deng *et al.* (2005); Cavani (2010); Mizuno *et al.* (1996b); Knapp *et al.* (2001).

Ethylene, propylene and isobutene are promising alternative feedstocks to produce PMMA but the technology hurdles that so far discourage investment include catalyst stability and high capital associated with the multiple reaction trains Nagai (2001); Mizuno et Yahiro (1998); Montag et Mckenna (1991); Drent et Budzelaar (1996); McGarvey et Moffat (1991); Edake *et al.* (2017b); Aworinde *et al.* (2018). Isobutane partially oxidizes to MAA and MAC in a single–step but conversion is unacceptably low Sultan *et al.* (2004); Cavani *et al.* (2001f); Misono (2001); Kanno *et al.* (2010); Zhang *et al.* (2013); Paul *et al.* (2010); Mizuno et Mison (1998); Mizuno *et al.* (1998). Heteropolycompounds (Keggin–type) are selective catalysts to form MAA and MAC Ma *et al.* (2017); Zhou *et al.* (2017a). Several studies tested various operating conditions and feed composition for the partial oxidation of isobutane and confirmed that it follows Mars van Krevelen mechanism Sultan *et al.* (2004); Paul *et al.* (1997); Schindler *et al.* (2001). Gas–phase partial oxidation of 2–methyl–1,3–propanediol (2MPDO) over Keggin–type heteropolycompounds containing cesium, vanadium and copper is an interesting approach that promises high MAA+MAC selectivity and reactant conversion after 1 h time–on–stream Mahboub *et al.* (2016a,b); Dubois (2014). Previous studies identified factors to maximize MAA selectivity over $VOCu_{0.5}/Cs(NH_4)_2PMo_{12}O_{40}$Mahboub *et al.* (2016a,b).

Here we measure the 2MPDO partial oxidation kinetics and derive a mechanistic model that accounts for the effect of feed composition, temperature, and contact time.

7.3 Experimental

7.3.1 Synthesis of $VOCu_{0.5}/Cs(NH_4)_2PMo_{12}O_{40}$ Catalyst

Cesium nitrate (1.87 g) dissolved in 0.1 mol L of NH_4NO_3 under vigorous stirring in 100 mL of distilled water at 40 °C. $Na_2HPMo_{12}O_{40}$ (2 mL min^{-1}) reacted with the solution to form a fine precipitate. Filtering and drying this precipitate for 16 h at 120 °C provided $Cs(NH_4)_2PMo_{12}O_{40}$ solid Mahboub *et al.* (2016a). We then dissolved 2.2 g of $VOSO_4 \cdot 5\,H_2O$ and 1.05 g of $Cu(NO_3)_2$ in 35 mL of deionized water. This solution was added dropwise to 27 g of $Cs(NH_4)PMo_{12}O_{40}$ to form a sticky pulp. A rota–evaporator homogenized the pulp for 3 h. Finally, the catalyst dried in air at 120 °C (12 h) and calcined at 350 °C (4 h) to form $VOCu_{0.5}/Cs(NH_4)_2PMo_{12}O_{40}$.

7.3.2 Reaction conditions and procedure

The experimental design consists of three hydrocarbon and oxygen concentrations (10 %, 13 % and 16 %) at 200 °C, 250 °C, 285 °C, and 320 °C and a residence time (τ) of 0.18 s and 0.36 s. We completed a full factorial design with 72 experiments in a µ-fluidized bed with an inner diameter of 8 mm and 520 mm long. Each experiment lasted 100 min. Mass flow controllers metered the gas to the reactor and a thermocouple monitored temperature (Fig. 7.1) Mahboub *et al.* (2018). An HPLC pump introduced the liquid into a 1/16" tube and a supplementary argon stream atomized the liquid at the nozzle tip inserted directly into the catalyst bed. Before running a test, argon purged the reactor while the furnace brought it to the desired temperature. Heat tape maintained the exit line at 200 °C to minimize product condensation. A 150 mL distilled water quench trapped all condesables. An online conductivity meter monitored the composition of samples that we withdrew from the vessel. An online mass spectrometer (MS) (Pfeiffer Vacuum Thermostar) tracked the noncondensable fraction and periodically we measured the gas phase composition by GC–MS.

7.3.3 Kinetic parameter estimation

Carbon and oxygen balances ranged from 95 % to 100 %. The two main products were MAA and MAC and their selectivity were calculated based on moles of carbon at the outlet with respect to 2MPDO in the inlet. We consider CO_x was a byproduct from 2MPDO, MAA, and MAC complete oxidation. We report kinetic rate constants with respect to a reference temperature of 653 K :

$$k_j = k_{j,653}[\frac{-Ea_j}{R}(\frac{1}{T} - \frac{1}{653})]$$

We minimize the following objective function (ϕ) to estimate the kinetic parameters that R^2 represents the coefficient of determination for the main products selectivity and reactants conversion Lorences *et al.* (2003) :

$$\phi = 3 - R^2_{X,2MPDO} - R^2_{S,MAA} - R^2_{S,MAC}$$

$$R^2_{X,2MPDO} = 1 - \frac{\sum (X_{2MPDO,calc} - X_{2MPDO,exp})^2}{\sum (X_{2MPDO,exp} - \bar{X}_{2MPDO,exp})^2}$$

$$R^2_{S,MAA} = 1 - \frac{\sum (S_{MAA,calc} - S_{MAA,exp})^2}{\sum (S_{MAA,exp} - \bar{S}_{MAA,exp})^2}$$

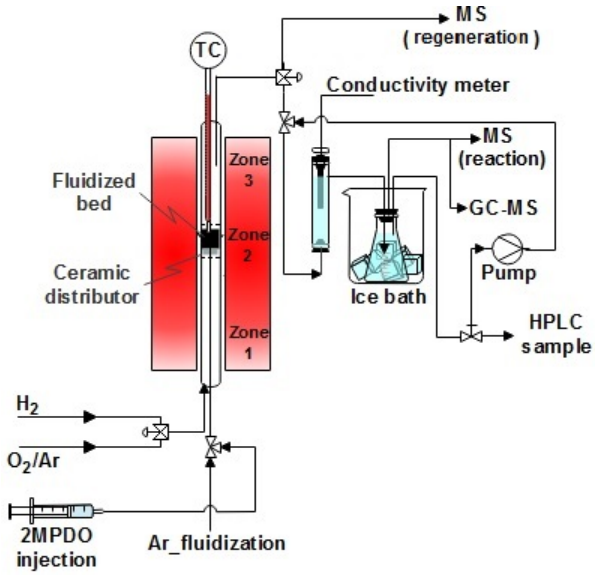

Figure 7.1 Schematic of the experimental set–up Mahboub *et al.* (2018)

$$R^2_{S,MAC} = 1 - \frac{\sum (S_{MAC,calc} - S_{MAC,exp})^2}{\sum (S_{MAC,exp} - \bar{S}_{MAC,exp})^2}$$

We chose 2MPDO conversion, methacrylic acid and methacrolein selectivities as the three factors to minimize in the objective function.

7.4 Results and discussion

Selectivity of MAA over $VOCu_{0.5}/Cs(NH_4)_2PMo_{12}O_{40}$ varied from 4 % to 46 % and the range for MAC was similar from 16 % to 63 % (Table 7.1 and Fig. 7.5). The CO/CO_2 ratio remained below 1 for almost all experiments. Experiments in which the CO/CO_2 was below 0.2 had correspondingly higher CH_4 selectivities that hovered around 8 % to 10 %. Low CO/CO_2 is a sign that most reactions are taking place on the catalyst surface and not the gas phase. The range of CO_2 selectivity was 12 % to 31 %, while it was 5 % to 15 % for CO, and 2 % to 14 % for CH_4. Coke accumulated on the catalsty and varied between 1 % to 5 % of the total carbon reacted. After each experiment, oxygen regenerates the catalyst and the MS monitors the carbon oxides concentration from which we calculate the carbon deposition over the surface.

Table 7.1 Experimental Data. Contact time for Experiments 1–27 was at τ= 0.36 s and τ= 0.18 s for Experiments 28–54.

Feed comp. (mol %) $C_4/O_2/H_2O$/inert	Temp. °C	Conversion, %	Selectivity, %		
			MAA	MAC	CO_x
2.2/7/33.5/57.3	280	8	56	7	25
2.2/7/33.5/57.3	300	17	53	13	19
2.2/7/33.5/57.3	340	47	18	3	36
2.2/13.7/33.5/50.6	300	22	51	0	23
2.2/20.7/33.5/43.6	300	28	34	0	28
2.2/13.7/33.5/50.6	300	12	58	0.4	21
2.2/13.7/33.5/50.6	300	11	51	14	19

7.4.1 Effect of feed compositions and temperature on selectivity at high conversion

In the range of 250–320 °C, MAA selectivity increased with temperature for all feed compositions and reached a maximum of 46 % at 320 °C, τ= 0.36 s and a 2MPDO/O_2 ratio of 13 %/10 %. Oxidizing MAC–as the main intermediate–to MAA at higher temperature accounts for this trend (Figs. 7.2-7.3). There is no specific tendency for all feed compositions because of complexity of the system by production–consumption of byproducts at different temperatures. The selectivity to MAA for 2MPDO/O_2= 13 %/10 % is much higher than other feed compositions at the same temperature and contact time. We supposed that hydrocarbon occupies more active sites and produce more desirable products ; meanwhile, minimizes carbon deposition. Lower oxygen concentration (10 %) yields higher MAA selectivity for all 2MPDO concentrations because the combustion of the product acids decreases with decreasing oxygen concentration (Fig. 7.2). The selectivity at 2MPDO/O_2= 10 %/16 % was almost the same at 250 °C and 285 °C and increased a little at 320 °C. At the same temperature, higher oxygen concentration was unfavorable because of the further oxidation of MAA to CO_x.

Conversely, MAC selectivity has a decreasing trend with temperature whereas it is maximum at 250 °C. Higher 2MPDO concentration favors MAC in which the maximum selectivity reaches 52 % at 2MPDO/O_2= 16 %/16 % and the lowest was 16 % at 2MPDO/O_2= 10 %/13 %. The selectivity to MAC at 2MPDO/O_2= 13 %/10 % is lower compared to others and trend confirms that MAC is an intermediate for this reaction and higher temperature favors oxidizing MAC to MAA.

CO_x selectivity is greatest at the highest oxygen concentration at all temperatures (Fig. 7.4).

The data suggest that CO_x mostly comes from MAC combustion. The selectivity to desired products (MAA and MAC) is lower at shorter residence time ; however, the selectivity to byproducts (CO_x and CH_4) is higher at shorter residence time. Oxygen conversion is higher than 2MPDO conversion for all feed compositions and temperatures. 2MPDO conversion increases with decreasing its concentration which is maximum with 10 % 2MPDO in inlet. There is no trend for oxygen conversion based on its concentration ; however, it decreases for lower oxygen concentrations in comparison with 2MPDO in feed composition (Figs. 7.2-7.4). Increasing the temperature (from 250 °C to 320 °C) has a little effect on 2MPDO and O_2 conversion. In conclusion, lower temperature (250 °C) and oxygen concentration (10 %) decreased the 2MPDO conversion down to 63 % at τ=0.36 s. Decreasing residence time to 0.18 s, decreases both 2MPDO and O_2 conversions for all experiments (Figs. 7.2-7.4).

The effect of both temperature and feed gas concentrations on 2MPDO conversion and MAA selectivity shows that at all temperature and feed gas concentrations, the MAA selectivity decreases with increasing 2MPDO conversion (Fig. 7.2). MAA selectivies are highest at about 46 % conversion with 13 % 2MPDO in the feed.

MAA selectivity is greatest at higher temperatures, indicating that 2MPDO mainly forms MAC rather than MAA then MAC oxidizes further to MAA ; higher temperature favors latter reaction. At each feed composition, MAA selectivity decreases with increasing 2MPDO conversion. Both selectivity and conversion increase with temperature. MAA selectivity varies almost linearly with 2MPDO conversion : at any inlet gas composition, its selectivity decreases linearly with increasing conversion.

The slope of the curve decreases smoothly from reducing conditions to an oxidizing environment. Selectivity to MAA decreases with increasing oxygen concentrations at all temperatures whereas, conversion decreases. Highly reducing conditions favor MAA selectivity ; however, selectivity reached a maximum with 13 % 2MPDO in the feed. Conversion is 10 fold lower at τ=0.18 s compared to τ=0.36 s ; however, MAA varies little (Fig. 7.2). The relationship between the reaction conditions and conversion is more complex : under highly oxidizing conditions (low 2MPDO concentration), 2MPDO is the limiting reagent and, therefore, conversion is limited by the contact time and temperature ; under reducing conditions (2MPDO= 16 %), oxygen is the limiting reagent.

MAC selectivity is more sensitive to temperature than MAA. On the contrary, conversion is less sensitive to temperature. Selectivity is independent of oxygen concentration at a constant 2MPDO concentration (Fig. 7.3). At a constant oxygen feed concentration, increasing 2MPDO decreases both MAC selectivity and 2MPDO conversion. At 200 °C, MAC selectivity is virtually independent of operating conditions and is steady around 55 % ; in the

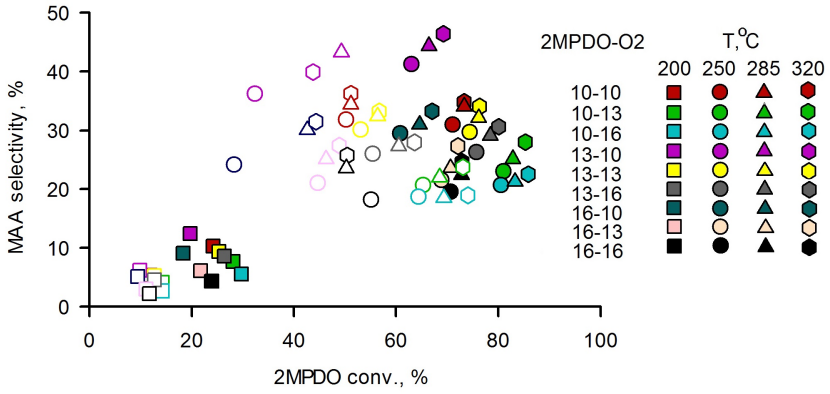

Figure 7.2 2MPDO conversion versus MAA selectivity as a function of temperature feed composition and contact time : τ= 0.36 s filled symbols and τ= 0.18 s hollow symbols.

range 250 °C to 320 °C, it varies from 16 % to 52 %. 2MPDO conversion is lower at shorter contact time but MAC selectivity is independent of contact time (Fig. 7.3). The relationship between CO_x and 2MPDO conversion is completely different than the MAA and MAC selectivities. At 250 °C, CO_x selectivity varies from 20 % to 32 %, while it is 20 % lower starting from 250 °C. At higher temperature and a constant feed composition, CO_x selectivity increases with increasing temperature. At the same oxygen concentration, increasing 2MPDO concentration decreases 2MPDO conversion more than CO_x selectivity. CO_x selectivity is independent of 2MPDO concentration.

7.4.2 Selectivity and conversion at 200 °C

MAA selectivity and 2MPDO conversion are lowest at 200 °C. MAA selectivity is three times higher at 250 °C while MAC is 20 % higher below 250 °C. Lower temperature favors MAC while high temperature favour MAA, which suggests 2MPDO oxidation to MAC is the first step in the mechanism. The MAA and MAC selectivity trends versus feed composition are the same from $\geq$ 250 °C (Fig. 7.5a). The selectivity to MAA decreases steadily with increasing oxygen in feed for both contact times. MAC selectivity increases with increasing oxygen concentration (Fig. 7.5a).

Decreasing residence time decreased MAC selectivity 6 %, but it increased CO_x selectivity 3 %. It means that CO_x is forming as byproduct since MAC selectivity is high. MAA selectivity is independent of residence time at 200 °C. 2MPDO conversion decreased around 40 % reducing residence time from τ=0.36 s to 0.18 s. Both 2MPDO and O_2 conversion increased with oxygen concentration. O_2 conversion decreased with increasing 2MPDO from 10 % to 13 % and thereafter was invariant with more 2MPDO in inlet (Fig. 7.5b). Although it is unu-

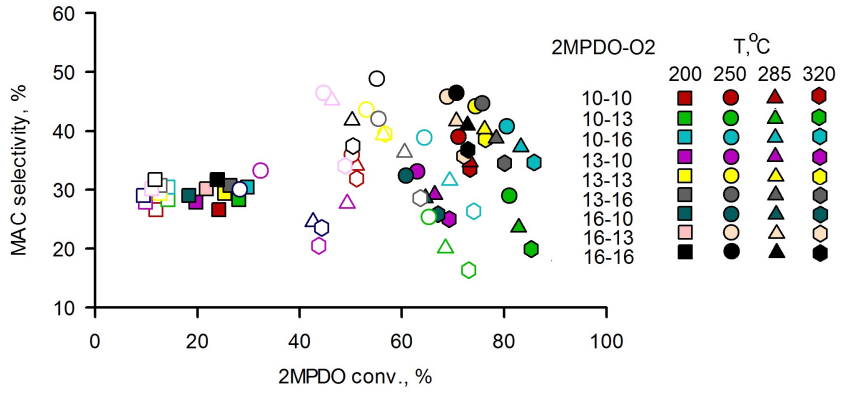

Figure 7.3 2MPDO conversion versus MAC selectivity as a function of temperature feed composition and contact time : τ= 0.36 s filled symbols and τ= 0.18 s hollow symbols.

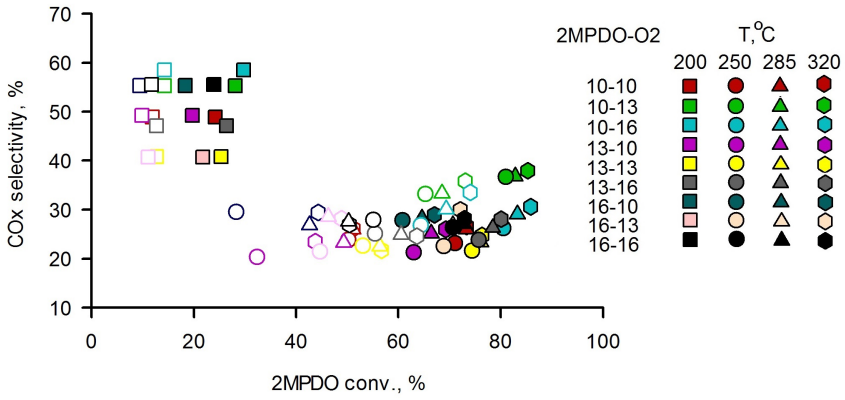

Figure 7.4 2MPDO conversion versus CO_x selectivity as a function of temperature feed compostion and contact time : τ= 0.36 s filled symbols and τ= 0.18 s hollow symbols.

sual, decreasing CO_x production justifies this unusual trend. 2MPDO conversion decreased a little with increasing 2MPDO concentration at the same oxygen inlet feed concentration. Oxygen conversion was high compared to 2MPDO, which suggests that the reaction rate is limited by O_2 availability.

During the first 30 min time–on–stream at 200 °C, MAA selectivity remained below 3 % but increased steadily thereafter to exceed 12 % at 100 min. Conversely, MAC selectivity was 85 % at 20 min then dropped to 60 % (Fig. 7.6). CO_2 selectivity increased slightly with time and reached 15 % at 100 min. CO and CH_4 selectivities were invariant at 6 % and 4 %, respectively (Fig. 7.6). MAC yield correlated with the increased yield of carbon oxides and MAA.

7.4.3 Kinetic Modelling

We completed a full factorial experimental design with $VOCu_{0.5}/Cs(NH_4)_2\ PMo_{12}O_{40}$ in a 8 mm diameter fluidized bed reactor (Table 7.1). The factors included 2MPDO and oxygen partial pressure (three levels each), temperature (four levels), and contact time (two levels). We monitored the non-condensable gas phase concentration continuously and withdrew liquid samples periodically : liquid-phase species concentrations reached steady state at about 100 min. The stoichiometric reactions for 2MPDO, MAA, and MAC are :

$$2\,\mathrm{MPDO} + 0.5\mathrm{O_2} \longrightarrow \mathrm{MAC} + 2\mathrm{H_2O} \tag{7.1}$$

$$2\,\mathrm{MPDO} + \mathrm{O_2} \longrightarrow \mathrm{MAA} + 2\mathrm{H_2O} \tag{7.2}$$

$$\mathrm{MAC} + 0.5\mathrm{O_2} \longrightarrow \mathrm{MAA} \tag{7.3}$$

The reaction network includes intermediates and byproducts (Fig. 7.7) and is based on the abstraction of four hydrogen atoms with/without oxygen insertion into the four–carbon skeleton.

The kinetic model assumes product concentrations are negligible initially compared to the reactants. We tested Langmuir–Hinshelwood, Eley–Rideal, and Mars van Krevelen expressions involving oxidized sites Hachemi et Murzin (2018); Morin *et al.* (2018). We fit the experimental data to models assuming that either the adsorption of reactant, reaction, or desorption of products is rate–limiting .

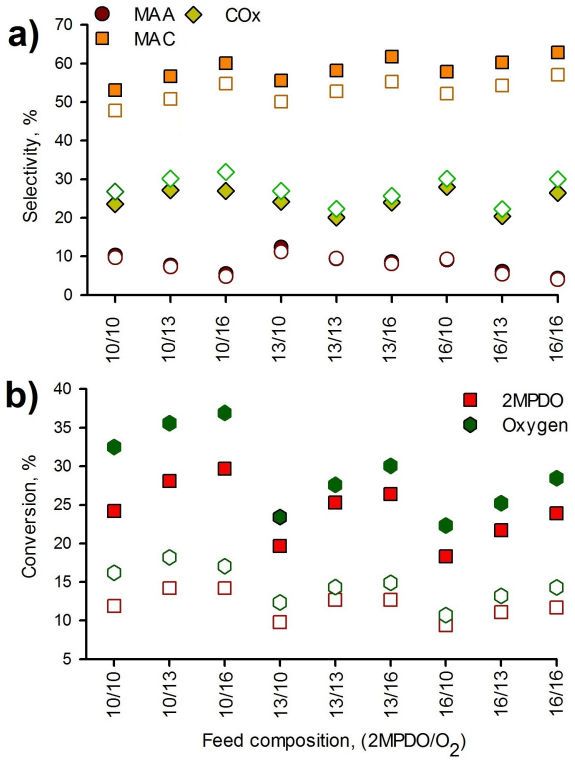

Figure 7.5 Product selectivity (a) and reactant conversion (b) at 200 °C as a function of composition and contact time : τ= 0.36 s (filled symbols) and τ= 0.18 s (hollow symbols).

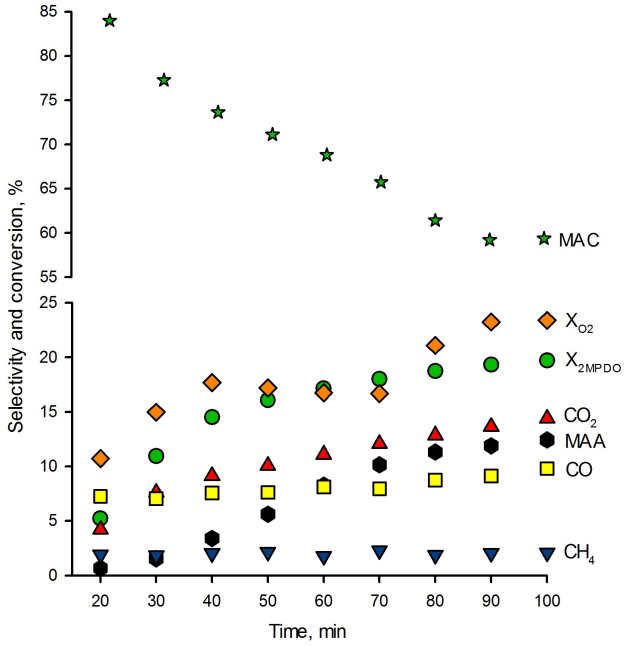

Figure 7.6 Selectivity and conversion with time over 2MPDO/O_2/Ar= 13 %/10 %/77 %

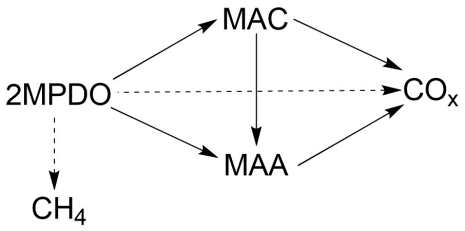

Figure 7.7 The reaction mechanism for main products and byproducts

Langmuir–Hinshelwood mechanism

In this mechanism, 2MPDO and oxygen adsorb on neighboring sites, X, thus forming adsorbed species 2MPDO* and O* (dissociative adsorption) :

$$2\text{MPDO} + X \longrightarrow 2\text{MPDO}^* \tag{7.4}$$

$$\text{O}_2 + 2X \longrightarrow 2\text{O}^* \tag{7.5}$$

$$2\text{MPDO}^* + \beta\text{O}^* \longrightarrow products + (1+\beta)X \tag{7.6}$$

In scenario 1 the adsorbed species react on the active sites, X : 2MPDO occupies one site and oxygen dissociates on two sites. The adsorbed species combine to form an adsorbed product MAA*, MAC*, or CO$_x$*. A fraction of the MAC* species desorbs to gaseous MAC and another fraction reacts to form MAA*. Finally, MAA* desorbs leaving the site vacant (X) (supplementary materials, Table 7.3). Expressions for each of the rate limiting steps become :

1) 2MPDO adsorption : $r = \frac{k_1' P_{2MPDO}}{[1+(K_2 P_{O2})^{\frac{1}{2}}]}$

2) adsorption of O$_2$ over the active site : $r = \frac{k_2' P_{O2}}{[1+K_1 P_{2MPDO}]^2}$

3) surface reaction : $r = \frac{k_3' P_{2MPDO} P_{O2}^{\frac{1}{2}}}{[1+K_1 P_{2MPDO}+(K_2 P_{O2})^{\frac{1}{2}}]^2}$ or $r = \frac{k_3' P_{2MPDO} P_{O2}}{[1+K_1 P_{2MPDO}+(K_2 P_{O2})^{\frac{1}{2}}]^3}$

In scenario 2, the partially reacted species desorb and react in the gas phase. This scenario gives the same rate expressions for adsorption of 2MPDO and O$_2$, and surface reaction steps as scenario 1 ; however, there is an additional model involving surface reaction :

$r = \frac{k_3' P_{2MPDO} P_{O2}^{\frac{1}{2}}}{[1+K_1 P_{2MPDO}+(K_2 P_{O2})^{\frac{1}{2}}]}$.

Eley–Rideal model

The Eley–Rideal assumes that 2MPDO adsorbs on an active site to form an activated adsorbed species 2MPDO* and molecular oxygen reacts with this species directly. We tested scenarios in which reactants form gas phase molecular (scenario 3) or 2MPDO* in presence of molecular oxygen produces adsorbed products (except for MAC) and then MAA* and $CO_x{}^*$ desorb from the same sites into the gas phase (scenario 4) :

$$2\text{MPDO} + X \longrightarrow 2\text{MPDO}^* \tag{7.7}$$

$$2\text{MPDO}^* + \text{O}_2 \longrightarrow products + X \tag{7.8}$$

In the former 2MPDO absorbs on an active site to form 2MPDO*. Molecular oxygen reacts with this species to form MAC which desorbs from the site immediately. In the competitive reaction path, one atom of oxygen produces the active specie of O* that partially reacts with molecular MAC to form MAA and a vacant site. In the parallel reaction path, 2MPDO* reacts with O_2 to form molecular MAA. The 2MPDO* species also forms $CO_x{}^*$ which desorbs from the surface. MAA and MAC also react further with adsorbed oxygen O* to produce CO_x.

Scenario 4 is similar to scenario 3 but 2MPDO*, MAA*, and MAC* combust to CO_x on the surface :

1) adsorption of 2MPDO over the active site : $r = k_1^{'} P_{2MPDO}$

2) surface reaction : $r = \frac{k_2^{'} P_{2MPDO} P_{O2}}{[1+K_1 P_{2MPDO}]}$

Mars van Krevelen mechanism

This model assumes a redox couple in which 2MPDO reacts with oxidized sites, X, thereby reducing them to V. Molecular oxygen re–oxidizes the reduced sites (V). In scenario 5, 2MPDO reacts with oxidized sites on the surface and desorbs as the products while in scenario 6, 2MPDO reacts directly with oxidized sites to products :

$$2\text{MPDO} + X \longrightarrow products + V \tag{7.9}$$

$$V + \text{O}_2 \longrightarrow X \tag{7.10}$$

So, 2MPDO adsorbs and reacts with X–(with the concentration of C_X) and forms adsorbed

species–2MPDO*– (with the concentration of $C_{2MPDO-S}$). MAC* forms MAA and reduced sites. Reactants and products also produce coke ($C_v^{C_4}$) over the reduced sites. Molecular oxygen finally reforms the reduced site to oxidized sites. Further, we assumed that the reaction are irreversible :

$K_{C_X} = \frac{k_{11}P_{O2}}{(\alpha\, k_1 P_{2MPDO})}$ Which $C_X = K_{C_X} \times C_V$

$K_{C_{2MPDO-S}} = \frac{(\alpha\, k_1 k_{11} P_{2MPDO} P_{O2})}{(\beta\, k_2 + \gamma\, k_3 + \eta\, k_5)(\alpha\, k_1 P_{2MPDO})}$ Which $C_{2MPDO-S} = K_{C_{2MPDO-S}} \times C_V$

$K_{C_V^{C4}} = \frac{(\tau\, k_8 P_{2MPDO} + k_{11} P_{O_2} - k_{11} P_{2MPDO} P_{O_2})}{k_{12} P_{O2}}$ Which $C_V^{C4} = K_{C4} \times C_V$

$\Longrightarrow C_V = \frac{1}{(1 + K_{C_X} + K_{C_V^{C4}} + K_{C_{2MPDO-S}})}$

$\Longrightarrow C_{2MPDO-S} = \frac{K_{C_{2MPDO-S}}}{(1 + K_{C_X} + K_{C_V^{C4}} + K_{C_{2MPDO-S}})}$

$\Longrightarrow C_V^{C4} = \frac{K_{C_V^{C4}}}{(1 + K_{C_X} + K_{C_V^{C4}} + K_{C_{2MPDO-S}})}$

$\Longrightarrow C_X = \frac{K_{C_X}}{(1 + K_{C_X} + K_{C_V^{C4}} + K_{C_{2MPDO-S}})}$

Therefore for each step of reaction as a rate–limiting step, we have :

1) Adsorption of 2MPDO over the portion (α) of oxidized sites (X) :

$r = \frac{k_1 P_{O2}}{[1 + K_1 \frac{P_{O2}}{P_{2MPDO}} + K_2 \frac{P_{2MPDO}}{P_{O2}} - K_4]}$

2) Reaction of adsorbed 2MPDO over the oxidized sites to MAA, MAC, and COx :

$r = \frac{k'}{[1 + K_2 \frac{P_{O2}}{P_{2MPDO}} + K_3 \frac{P_{2MPDO}}{P_{O2}}]}$

3) Reaction of 2MPDO over the reduced sites (V) to form coke :

$r = \frac{k_8' P_{2MPDO} + k_{11} P_{O2}}{[1 + K_2 \frac{P_{O2}}{P_{2MPDO}} + K_3 \frac{P_{2MPDO}}{P_{O2}} - K_4]}$

In scenario 6, instead of 2MPDO reacting with oxidized sites (2MPDO*), it reacts directly to products that desorb directly into the gas phase. All the other steps are the same as scenario 5 (supplementary materials). Then we have :

$K_{C_X} = \frac{k_{10} P_{O2}}{(\alpha\, k_1 + \beta\, k_2 + \phi\, k_6) P_{2MPDO}}$ Which $C_X = K_{C_X} \times C_V$

$K_{C_V^{C4}} = \frac{\tau\, k_9 P_{2MPDO}}{k_{11} P_{O2}}$ Which $C_V^{C4} = K_{C_V^{C4}} \times C_V$

$\Longrightarrow C_V = \frac{1}{(1 + K_{C_X} + K_{C_V^{C4}})}$

$\Longrightarrow C_V^{C4} = \frac{K_{C_V^{C4}}}{(1 + K_{C_X} + K_{C_V^{C4}})}$

$\Longrightarrow C_X = \frac{K_{C_X}}{(1 + K_{C_X} + K_{C_V^{C4}})}$

The kinetic reaction rate models for adsorbing 2MPDO over the oxidized sites to produce MAA, MAC, and CO_x and reacting oxygen over the reduced sites are the same as scenario 5. The only difference is having another model for burning coke over the sites with oxygen to form CO_x :

$r = \frac{k_9' P_{2MPDO}}{[1 + K_2 \frac{P_{O2}}{P_{2MPDO}} + K_3 \frac{P_{2MPDO}}{P_{O2}}]}$

7.4.4 Hydrodynamic Modeling

To adequately interepret reaction rate data requires a basic understanding of gas and solids transport characteristics. The advantage of fluidized bed reactors to study kinetics is that the solids are completely backmixed—the oxidation state, adsorbed species concentrations, and coke concentration are the same throughout the bed. In fixed bed reactors, coke build up on the catalyst and oxidations states have strong radial and axial gradients Kaarsholm *et al.* (2007). On the other hand, bubbles complicate the hydrodynamics of the gas-phase and thus require more attention to establish the prevailing contact efficiency. Gas transient step response techniques measure the residence time distribution that assess potential non-uniformities. We installed a four–way valve and fed a constant flow of argon to the reactor, and then switched argon to air at time "0"—heavyside unit step function' (Fig. 7.8) Lorences *et al.* (2006). The mass spectroscopy monitored the oxygen concentration online at a frequencey of 2 Hz. As the air sweeps across the catalyst, the oxygen concentration increases gradually to its steady–state value.

We evaluated the hydrodynamics in a first series of experiments at room temperature in the 8 mm ID quartz reactor at a gas velocity of 23, 33, 49, and 58 mm s^{-1}. To minimize

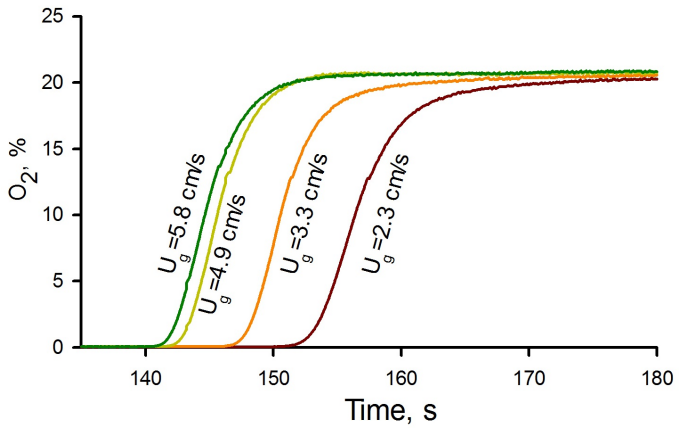

Figure 7.8 Oxygen breakthrough curves as a function of the gas velocity

the freeboard contribution to dispersion, we placed the MS capillary 1 and 2 cm above the catalyst surface. We conducted a second set of experiments at reaction temperature (250 °C) and the gas velocities were the same as in the first series and the identical location for the capillary tip. In a third series of tests, we decreased the catalyst mass 50 % while maintaining the same velocities, temperatures, and capillary positions. We evaluated the transport effects due to the connecting tubing with the empty reactor. All tests were repeated two times at each gas velocity, and the reproducibility was very good. Axial dispersion is quite low as the reactor operates close to the minimum fluidization velocity and so the gas phase is close to plug flow like a fixed bed. The minimum bubbling velocity is 3.3 cm s^{-1} (U_{mf}) and kinetic experiments we ran at velocities within $2 \times U_{\mathrm{mf}}$.

n–CSTR in Series Model

The tanks–in–series model is an good first approximation to characterize the gas-phase hydrodynamics and it agrees well with the axial–dispersion model for Peclet numbers above 5 (i.e. moderate deviation from plug flow). A tracer mass balance around tank j yields the following equation Lorences *et al.* (2006) :

$$C_j = \frac{Q}{V_j} e^{-tQ/V_j} \int_0^t C_{j-1} e^{tQ/V_j} dt$$

where Q is the flow velocity and V_j the volume of tank j. All tanks have the same volume and then we have :

$$\frac{Q}{V_j} = \frac{n}{t_m}$$

where n is the number of tanks and t_m is the mean residence time. The residence time distribution for the whole system is obtained from a mass balance for n tanks Lorences *et al.* (2006) :

$$F(t) = 1 - e^{-nt/t_m}[1 + \frac{nt}{t_m} + \frac{1}{2!}(\frac{nt}{t_m})^2 + ... + \frac{1}{(n-1)!}(\frac{nt}{t_m})^{(n-1)}]$$

$$E(t) = \frac{t^{n-1}}{(n-1)!t_{mi}^n}e^{-t/t_{mi}}$$

The number of tanks varies between 42 at low gas velocities (fixed–bed operation) and 5 at high gas velocities (bubbling bed) Table 7.2. The significance of the assumed number of tanks in series has profound implications when the conversion of the limiting reagent approaches 100 %. At conversions in the range of 35 %, predictions of a plug–flow model (infinite number of tanks in series) differ from those of a CSTR (one tank in series) by only 6 %.

7.4.5 Estimation of kinetic parameters

We estimated activation energies and rate constants for each kinetic model while taking into account the reactor hydrodynmics. The Mars van Krevelen mechanism fit the experimental data best as the ϕ function was lowest compared to all other models (Table 7.3). Kinetic models assuming reactant adsoprtion as the rate limiting step fit the experimental data poorest with objective functions ϕ exceeding 2 in the case of the Langmuir and Eley-Rideal models. The objective function for models that assume surface reaction as the rate limiting step are lower but even so, they exceed 1.5 in the case of the Langmuir expressions. For one of the Eley-Rideal models $\phi < 1$ with R^2 better than 0.5 for the three species—MAA, MAC, and 2MPDO. The Mars van Krevelen model has the lowest ϕ at 0.64 and the final expression of the form :

Table 7.2 n–CSTR in Series Model Parameters

U_g	σ^2	t_m	n	Pe
2.3	24.5	20.5	42	83
3.3	13.3	20.3	31	59
4.9	11.7	19.4	13	24
5.8	8.5	13.9	5	8

Table 7.3 The R values for all possible mechanisms

Mechanism	Rate limiting	Reaction mechanism	R^2_{MAA}	R^2_{MAC}	R^2_{2MPDO}	ϕ
Langmuir	Adsorption of 2MPDO[1&2]	$2\,\mathrm{MPDO} + \mathrm{X} \underset{k'}{\overset{k}{\rightleftharpoons}} 2\,\mathrm{MPDO}^*$	0.39	0.20	0.33	2.08
	Adsorption of O_2[1&2]	$\mathrm{O_2} + 2\,\mathrm{X} \underset{k'}{\overset{k}{\rightleftharpoons}} 2\,\mathrm{O}^*$	0.27	0.52	0.42	2.79
	Reaction to MAC[1&2]	$2\,\mathrm{MPDO}^* + \mathrm{O}^* \underset{k'}{\overset{k}{\rightleftharpoons}} \mathrm{MAC}^* + 2\,\mathrm{H_2O} + \mathrm{X}$	0.48	0.61	0.47	1.54
	Reaction to MAA[1&2]	$2\,\mathrm{MPDO}^* + 2\,\mathrm{O}^* \underset{k'}{\overset{k}{\rightleftharpoons}} \mathrm{MAA}^* + 2\,\mathrm{H_2O} + 2\,\mathrm{X}$	0.57	0.39	0.44	1.6
	Reaction of MAC to MAA[2]	$\mathrm{MAC} + \mathrm{O}^* \underset{k'}{\overset{k}{\rightleftharpoons}} \mathrm{MAA} + \mathrm{X}$	0.33	0.47	0.41	1.79
Eley–Rideal	Adsorption of 2MPDO[3&4]	$2\,\mathrm{MPDO} + \mathrm{X} \underset{k'}{\overset{k}{\rightleftharpoons}} 2\,\mathrm{MPDO}^*$	0.11	0.13	0.09	2.67
	Surface reaction[3&4]	$2\,\mathrm{MPDO}^* + \mathrm{O_2} \underset{k'}{\overset{k}{\rightleftharpoons}} \mathrm{MAC} + 2\,\mathrm{H_2O} + \mathrm{O}^*$	0.19	0.27	0.26	2.28
Mars van Krevelen	Adsorption	$2\,\mathrm{MPDO} + \alpha\,\mathrm{X} \rightarrow \alpha\ 2\,\mathrm{MPDO}^*$	0.71	0.72	0.54	1.03
	Surface reaction	$2\,\mathrm{MPDO}^* + \rightarrow \mathrm{MAA}$ or MAC or COx + V	0.74	0.81	0.58	0.87
	Coke formation	$2\,\mathrm{MPDO} + \tau\ \mathrm{V} \rightarrow \tau\ \mathrm{S}^{C_4} + \mathrm{H_2O}$	0.61	0.69	0.55	1.15
	Adsorption & reaction	$2\,\mathrm{MPDO} + \mathrm{X} \rightarrow \mathrm{MAA}$ or MAC or COx + V	0.81	0.96	0.56	0.67
	Coke formation	$2\,\mathrm{MPDO} + \tau\,\mathrm{V} \rightarrow \tau\,\mathrm{S}^{C_4} + \mathrm{H_2O}$	0.23	0.27	0.19	2.31

1 & 2 : the first and second scenarios
3 & 4 : the third and fourth scenarios

$$r = \frac{k'}{[1+K_2\frac{P_{O_2}}{P_{2MPDO}}+K_3\frac{P_{2MPDO}}{P_{O_2}}]} \longrightarrow r = \frac{k' P_{O_2} P_{2MPDO}}{[K_2 P_{O_2}+K_3 P_{2MPDO}]}$$

where K_2=K_o and K_3=K_r, and k'=$K_o \times K_r$

We normalized the total number of active sites to equal 1 and assumed the number of sites was independent of temperature. The $E_r = 170\,\mathrm{kJ\,mol^{-1}}$ and $E_o = 160\,\mathrm{kJ\,mol^{-1}}$.

The best fit values of the kinetic constants suggest that 2MPDO first reacts to MAC which then forms MAA or combusts (Fig. 7.12). The reaction rate of these reactions are about the same. 2MPDO does form MAA directly but the reaction rate to MAC is four times greater. The MAA combustion rate to carbon oxides is negligible as its reaction rate is several orders magnitude lower than that of MAC to COx (Table 7.5). The regression model for MAA selectivity accounts for 80 % (Figs. 7.9) of the variance in the data and it accounts for 96 % of the variance in the MAC selectivity (Figs. 7.10 but for fit is not as convincing for the 2MPDO (Figs. 7.11). The data cover a broad range of temperatures but perhaps too broad : the fit between experimental selectivity and model predictions are poor at low temperature. Some catalytic systems have very different reaction mechanisms at low temperature versus high temperatureGodefroy *et al.* (2010). Here we excluded methane that simplifies the modelling but introduces some error.

7.5 Conclusions

Poly methyl methacrylate (PMMA) is a specialty commercial polymer with boundless applications for everyday life, including medical fields for ophtalmology, for example. Its high transparency and good mechanical properties makes it an attractive alternative to replace glass in application require impact resistant, low weight, and safety. PMMA annual production surpasses 2.8 million tonne and its increasing demand motivates industry to develop clean technologies based on renewable resources. 2MPDO is a co–product of 1,4–butanediol in the hydroformylation process of allyl alcohol and can be an attractive feedstock to produce MAA and replace current technologies that suffer from low yield, short catalyst life time, and

Table 7.4 Kinetic constants for Mars van Krevelen based on 2MPDO consumption

Temperature, °C	K_r, $\mathrm{mol\,s^{-1}atm^{-1}}$	K_o, $\mathrm{mol\,s^{-1}atm^{-1}}$
200	1.46×10^{-7}	7.55×10^{-7}
250	2.55×10^{-7}	1.30×10^{-6}
285	5.03×10^{-7}	2.29×10^{-6}
320	6.97×10^{-7}	3.44×10^{-6}

Table 7.5 Reaction rate constant and activation energy of each step of the proposed model

i	k_i	E_{ai}
1	5.8×10^{-1}	23.1
2	247×10^{-1}	9.4
3	2.3×10^{-1}	25.6
4	1.9×10^{-1}	25.3
5	252×10^{-1}	8.9
6	4.3×10^{-3}	27.7

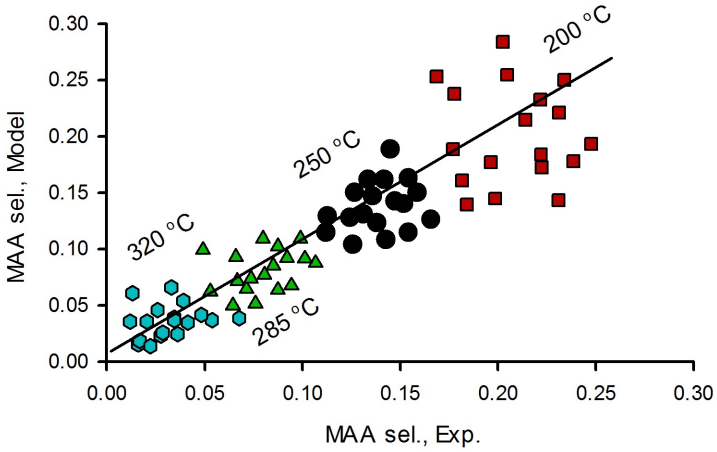

Figure 7.9 MAA selectivity analysis (model vs experimental)

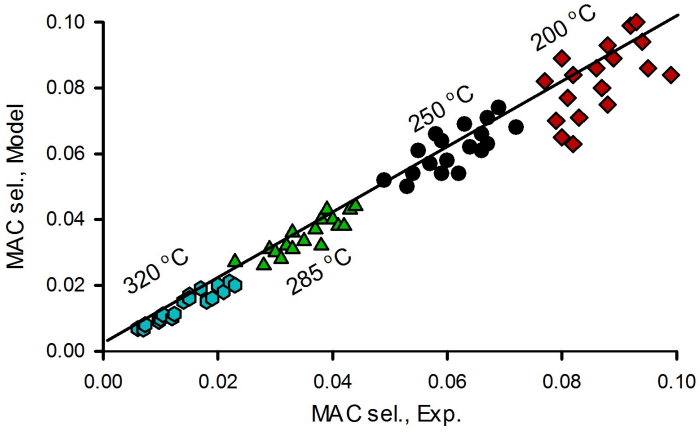

Figure 7.10 MAC selectivity analysis (model vs experimental)

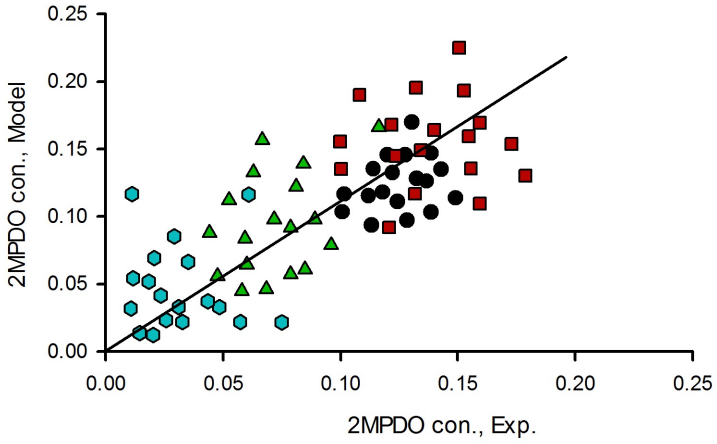

Figure 7.11 2MPDO conversion analysis (model vs experimental)

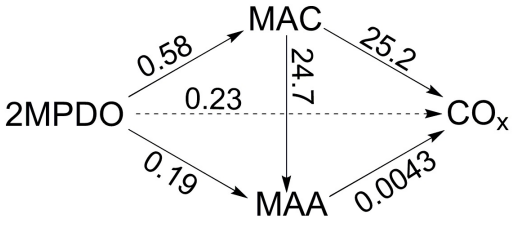

Figure 7.12 Reaction scheme with the reaction constants

toxic feedstocks.

We evaluated the effect of operation conditions such as temperature, feed compositions, contact time to evaluate the significance of each parameter on selectivity and conversion. After about 100 min most concentrations approached steady state. Above 250 °C), both MAC and 2MPDO oxidize to MAA at commercially relevant reaction rates. 2MPDO/O_2 ratio has a greater effect on MAA+MAC selectivity than temperature : Higher ratios improve MAA and MAC selectivities and productivity. Coke forms with time, therefore, to maintain activity requires a periodic regeneration step like a redox reaction configuration where catalyst cycles between net reducing and net oxygen environments.

We tested the Langmuir–Hinshelwood, Eley–Rideal, and Mars van Krevelen kinetic models. The Mars van Krevelen mechanism fit the experimental data best, which confirms that a redox reactor configuration would be ideal for this system. The re–oxidation step is faster than the reduction step by 2MPDO. The reaction network for the partial oxidation of 2MPDO includes five reaction steps : 2MPOD predominately forms MAC in the first step and MAC is more reactive than either 2MPDO or MAA as it combusts readily to CO_x. MAA is more stable and its oxidation kinetics to CO_x are negligible at low temperature.

7.6 Acknowledgements

The authors thank MITACS and CRIBIQ for their financial support of this study. They also recognize the helpful discusions on modelling with Seyed Mahdi Jazayeri.

Nomenclature

MAA = methacrylic acid
MAC = methacrolein
D = axial dispersion, m^2s^{-1}
n = number of tanks in the n–CSTR in series model
Pe = Peclet number of axial dispersion
r_i = reaction rate, $mol\,s^{-1}m^{-3}$
E_{aj} = activation energy, $kJ\,mol^{-1}$
k_i = reaction rate constant, various units
$R^2_{X,2MPDO}$ = coefficient of determination for 2MPDO conversion
$R^2_{S,MAA}$ = coefficient of determination for MAA selectivity
$R^2_{S,MAC}$ = coefficient of determination for MAC selectivity
R^2_{S,CO_x} = coefficient of determination for CO_x selectivity

S_i = selectivity to compound i
T = reaction temperature, K
t_m = mean residence time, s
U_{mf} = minimum fluidization velocity, $\mathrm{m\,s^{-1}}$
U_g = gas linear velocity, $\mathrm{m\,s^{-1}}$
X = butane conversion, %
P_i = partial pressure of reactants
P_j = partial pressure of products
F_i = gas flow rate of reactants, $\mathrm{mL\,min^{-1}}$
X= active (oxidized) sites over different mechanisms (eqs 4–11)
V = reduced sites over different mechanisms (eqs 9–10)
C_X= concentration of oxidized sites for Mar van Krevelen mechanism
C_V= concentration of reduced sites for Mar van Krevelen mechanism
C_{2MPDO}= concentration of sites occupied by 2MPDO for Mar van Krevelen mechanism
C_V^{C4}= concentration of sites occupied by coke for Mar van Krevelen mechanism
K_r= reaction rate constant for reduction step of Mar van Krevelen mechanism
K_o= reaction rate constant for oxidation step of Mar van Krevelen mechanism

Greek Symbols

ϕ = objective function for modeling
β= a portion of active sites occupied by oxygen that reacts with adsorbed 2MPDO in eq 6
τ= contact time

CHAPTER 8 GENERAL DISCUSSION

Methyl methacrylate (MMA) is a specialty chemical that widely uses as an additive in paints and coatings and electronics. It is a modifier for PVC and also acts as bone inserts in medicine. However, the main application of MMA is producing poly–methyl–methacrylate (PMMA). PMMA is highly demand specialty chemical that its consumption surpassed 2.8 million tonne annually. The increasing demand of PMMA therefore affects the demand on MMA and will surpass 4.8 million metric tonne by 2020 with annual growth in demand of more than 0.2 million tonnes (5 % to 6 %) Nagai et Ui (2004); Program (2006); Schunk et Brem (2011); Global Market Analysts (2016). Due to the increasing demand for PMMA, the price of bulk MMA increased by 10 % annually Jing (2012).

The increasing demand on these chemicals motivates industry and academia to propose a new approach or improve the current technologies to maximize productivity and decrease the price of final product.

Acetone cyanhydrin (ACH) is the current dominant process to produce MMA which hydrogen cyanide and concentrated sulfuric acid are the main reactants Mizuno et Yahiro (1998); Deng *et al.* (2005). However, expensive and toxic raw materials and producing large quantities of byproduct (ammonium bisulfate) are the significant problems of this technology. Although, Mitsubishi Gas Chemicals developed an ACH process to address the environmental and toxic issues, it still suffers from short catalyst lifetime and parasitic reactions Shuji *et al.* (1994); Kiochi (1999).

Oxidizing light hydrocarbons (C_2–C_4) to MAA– as the principal substrate for MMA– reduces the deficiencies of the ACH process Montag et Mckenna (1991); Drent et Budzelaar (1996); Zhou *et al.* (2015). However, the proposed routes from these feedstock also suffer from low yield, multiple steps, and short catalyst lifetime. Oxidation of isobutane to MAA is an attractive process because of inexpensive feedstock, lower environmental impact, and a simple one–step process Sultan *et al.* (2004); Cavani *et al.* (2001f). Selectivity to MAA with heteropoly compounds and vanadium pyrophosphate catalyst have reached 49 % after 90 h reaction time Kanno *et al.* (2010); Zhang *et al.* (2013); Paul *et al.* (2010); Jing *et al.* (2014a); Wang *et al.* (2016); He *et al.* (2015). However, this process operates above the upper flammability region in oxygen lean condition and the hydrocarbon conversion is below 25 % Cavani *et al.* (2001f). Therefore, extra separation steps are necessary to separate unreacted isobutane from products.

2MPDO is a co–product of 1,4–butanediol in the hydroformylation process of allyl alcohol and

has not much application besides usual glycol application. It is an easily handled liquid and has an intermediate boiling point to decompose at mild temperature which can be a proper potential reactant to produce MAA. Therefore, gas–phase partial oxidation of 2MPDO can be a promising alternative approach to replace with the current technologies. The process of converting 2MPDO to valuable chemicals includes heterogeneous catalysis and fluidized bed reactor.

This thesis addresses various aspects of oxidation processes :

1. catalyst synthesis and characterization ;
2. optimizing catalyst structure and preparation conditions ;
3. catalytic reactions in fluidized bed reactors ;
4. optimizing the reaction conditions ;
5. analyzing the correlation between catalyst structure and reaction mechanism ;
6. kinetic modeling.

To have a deep vision about a recent progresses to produce MAA and MMA and also to clarify why the new approach is necessary, we comprehensively studied "Catalysis for the synthesis of methacrylic acid and methyl methacrylate" as a review paper (Chapter 2).

Synthesis of a new catalyst type and proposing a new process that converts 2MPDO to high selective products is challenging. In order to carry through this, we first investigated a gas-solid-liquid system and we injected the pure 2MPDO directly over the catalyst surface into a micro–fluidized bed that a 0.3 mm nozzle atomized the 2MPDO liquid feed into the bed. Blocking the injector in less than 10 min after running the experiments was the first challenge of the process. At low fluidization gas flow rate (less that $20\,\mathrm{mL\,min^{-1}}$, the injection line blocked because of agglomeration over the catalyst surface.

We tested several catalysts (such as VPP, mixed–metal oxides, zeolite, and heteropoly compounds) and found that Keggin–type heteropoly compounds including cesium, vanadium, and copper is an active catalyst to partially oxidize 2MPDO to MAA where MAC is the main intermediate. As the screening tests, 2MPDO injected continuously from the bottom of the reactor at 350 °C and 2MPDO/O_2= 13 %/10 % over 2 g of catalyst.

Keggin–type catalyst in form of pure acid ($H_3PMo_{12}O_{40}$) was non–selective to MAA that the main products were MAC and CO_x and the selectivity to MAA was less than 2 %. Small amounts of propanal, 2-Methylpropanal, butanal, and acetic acid were also detected in exit. Therefore, we inserted different metal ions to improve its performance. We replaced cesium and ammonium with hydorgen with different concentrations and inserted vanadium and copper in various amounts to find the optimum catalyst structure. $Cs(NH_4)_2PMO_{12}O_{40}(VO)Cu_{0.5}$

was the optimum catalyst structure and the maximum selectivity to MAA and MAC reached to 11 % and 23 %, respectively at 350 °C. The cesium salt of a Keggin–type heteropoly acid (HPA) partially oxidized 2MPDO to MAA. The substitution of Cs^+ as a cation for H^+ in $H_3PMo_{12}O_{40}$ formed an alkaline salt acting as a support over which the active phase was dispersed and thermally stabilized. However, substituting more cesium ($x > 2$) for ammonium decreased the active phase concentration and catalyst performance. Inserting vanadium into the HPA reduced the Mo^{6+} to Mo^{5+}, and promoting it with copper increased the selectivity to MAA but decreased the conversion by 11 %. In this condition, lots of coke and CO_x formed that decreased catalyst performance (Chapters 3 & 4).

To address catalyst productivity, we tested different feed compositions and temperatures and the maximum selectivity to MAA and MAC reached to 41 % and 33 %, respectively at lower temperature (250 °C). From the initial results we proposed that oxygen reacts with 2MPDO to form 3–hydroxy–2–methylpropanal. This intermediate dehydrates to MAC in the second step, and finally in the third step, oxygen reacts with MAC to form MAA. To check the carbon balance, we regenerated the used catalyst with higher oxygen concentration and monitored MS signals for CO_x (Chapters 3 & 4).

Although opearting conditions affect catalyst performance, catalyst synthesis changes also the productivity of the process or even might change the reaction path. Then, we evaluated the effect of calcination temperature– as one of the significant parameters on catalyst synthesis– to see how this parameter affects MAA+MAC selectivity. The keggin–structure decomposes to its metal oxides at temperature above 450 °C that limits us to work at lower calcination temperature. We calcined catalysts at 300 °C and 350 °C and compared their performance with uncalcined catalyst. Higher calcination temperature illustrated better performance for MAA and MAC selectivities that maximum MAA and MAC selectivities were 61 °C and 28 °C, respectively, at 250 °C after 480 min over cycling oxidation–reduction and $2MPDO/O_2/Ar=13/10/77$ as the best reaction condition and feed composition.

We characterized catalyst structure with several techniques to understand how higher temperature treatment changes catalyst performance. Large, sharp peaks of the X–ray diffractograms at $2\theta = 10.6°$, 26.4°, and 30.6° confirmed the Keggin–type crystalline structure (body–centered cubic with Å= 11.4) of ammonium oxonium molybdenum oxide phosphate (as the main crystal).

FT–IR and Raman techniques detected the higher intensity and more obvious shoulder of V_2O_5 for catalyst calcined at 350 °C that indicate stronger interaction between vanadium and oxygen into the Keggin structure. Therefore, the stronger bond of vanadium and oxygen (V_2O_5) justified the better performance of catalyst treated at higher temperature.

The Raman spectroscopy analysis showed the intervalence charge–transfers energies of molybdenum species ; indicating that octahedral Mo^{5+} developed during reaction and confirmed the catalyst reduction after 480 min. Therefore, catalyst calcined at 350 °C reduced more than catalyst calcined at 300 °C compared to the corresponding fresh ones which resulted in better performance of catalyst for MAA and MAC selectivities. The atomic ratio of Mo^{6+}/Mo^{5+} for calcined samples was higher than uncalcined one which confirms that calcination oxidize the coordinatively unsaturated Mo^{5+} to Mo^{6+} in the crystalline phase (Chapter 5).

XPS results showed that calcining samples increased the Mo^{6+}/Mo^{5+} ratio where higher calcination temperature resulted in higher ratio. Therefore, we suppose that calcining reduces vanadium from V^{5+} to V^{4+} while the Mo^{5+} oxidizes to Mo^{6+} in the Keggin structure. The XPS results indicated that the average oxidation state (based on Mo^{6+}/Mo^{5+} atomic ratio) of catalyst calcined at 350 °C was higher than other catalyst, which correlates with the improved performance.

At the end, based on the XPS analysis, we proposed a mechanism which correlates catalyst structure and products. In 2MPDO the C−H and the C−OH single bond homolytic dissociation energy of the tertiary carbon and the carbon bearing the alcoholic function, respectively, is comparable (400 kJ mol^{-1} vs. 393 kJ mol^{-1}). Therefore the cleavage of these two bonds is equally likely. Though, the route of direct dehydration of 2MPDO followed by oxidation to MAC seems the most direct path to the products detected, we also propose a mechanism that passes through the homolytic dissociation of the C−H bond, in reason of the very similar bonding energies.

At the last step of this research, we tried to find the best kinetic model which present the experimental data. We tested three mechanisms and found that Mars and Van Krevelen is the best model for redox reaction. Reacting of 2MPDO over the oxidized sites to form products is the rate–limiting step of this reaction network (Chapter 6).

CHAPTER 9 CONCLUSION

9.1 Conclusion

The main objective of this work was the partial oxidation of 2–methyl–1,3–propanediol to methacrylic acid in a gas-solid fluidized bed reactor in the presence of heterogeneous catalyst.

Our first target was to synthesize, or introduce, an active catalyst that breaks C−H bond and be selective to methacrylic acid. For the first time, we tested Keggin–type heteropoly compounds including transition metal oxides such as vanadium, molybdenum, and copper in oxidation of 2MPDO to MAA and MAC. Product selectivity and yield depended upon the type of metal oxides and their concentration in catalyst structure and also the conditions of catalyst synthesis. Acid type of Keggin–structure ($H_3PMo_{12}o_{40}$) was non selective to MAA ; however, adding vanadium and molybdenum improved catalyst performance and showed a good activity in oxidation of 2MPDO to MAA and MAC.

In parallel, we explored a gas-solid fluidized bed that reduced issues of catalytic degradation of 2MPDO to CO_x. This system prevented also fast catalyst deactivation and agglomeration. First, we studied a gas-solid reactor with a pure 2MPDO sprayed on the surface of the bed. Howver, because of agglomeration, we tested different feed compositions, flow rates, and pressure drop to find the optimum conditions to have the best atomization. It helped us to run the experiments for 480 min without injector blockage. We tested different injector and reaction configuration to maximize productivity such as the place of gas distributer, and system isolation.

To improve catalyst performance we tested different reaction conditions, temperatures, and contact time. The trend of MAA selectivity and conversion were the same as by increasing selectivity, the conversion increased. MAC was the main intermediate in which the selectivity to MAC decreased with time. It confirmed that MAA was formed from two parallel mechanisms.

A detailed kinetic model can properly predict partial oxidation of 2MPDO over this type of catalyst. We estimated the reaction rate constant for each step and those data can be used for reactor scale up.

In this study, we found that the introduce gas-solid system in able to oxidize 2MPDO to methacrylic acid in a micro–fluidized bed reactor over Keggin–type heteropoly compounds in the presence of vanadium, molybdenum and copper. Using heterogeneous catalysts has advantageous such as easy separation, and less catalyst consumption and coke removal is

easier in the fluidized-bed reactors. It should be noted that, the test occurred at a medium temperature, and atmospheric pressure and reaction rate was fast.

9.2 Recommendations for future research

Gas–solid oxidation of 2MPDO was presented for the first time as a possibility in the conversion of 2MPDO to specialty chemicals such as MAA and MAC.

All experiments were run in a micro–fluidized bed reactor. The agglomeration of catalysts is the main problem in small reactor systems, and injecting liquid solution adds a level of complexity to this system. The ability to run a series of experiments in a large–scale reactor will be a big step in scaling up.

The second step is inserting other metal ions into the Keggin–type that we just tested three ions (V, Mo, and Cu). Adding another ions such as iron, potassium and nickel would be useful to see whether they affect catalyst performance or no. Moreover we evaluated the catalyst performance by synthesizing the catalyst at different calcination temperatures. Evaluating other parameters such as calcination atmosphere (air, nitrogen or argon), calcination temperature ramp, and even method of catalyst synthesis affects the catalyst performance and productivity. Therefore, we suggest to study these parameters as a future research.

We changed the feed composition in limited ranges and injected pure 2MPDO. Applying a wider range for feed composition in present of water as a co–feeding might affect the selectivity to MAA and MAC.

At the end we suggest to run the reaction for a longer time–on–stream whereas the longest run for this research was 480 min.

REFERENCES

Antoine Aboukais and Denise Ghoussoub and Emilie Blouet–Crusson and Monique Rigole and Michel Guelton (1994). Oxidative dehydrogenation of isobutyric acid on $H_4PVMo_{11}O_{40}$, $NaxH_{4\text{-}x}PVMo_{11}O_{40}$ and $Cu_yH_{4\text{-}2y}PVMo_{11}O_{40}$ heteropolyacid catalysts supported on silica. *Applied Catalysis A : General*, *111*(2), 109–118.

Mahdi Adabi and Reza Saber and Majid Naghibzadeh and Farnoush Faridbod and Reza Faridi–Majidi (2015). Parameters affecting carbon nanofiber electrodes for measurement of cathodic current in electrochemical sensors : an investigation using artificial neural network. *RSC Advances*, *5*(99), 81243–81252.

Ali Ahmadpour and Neda Jahanshahi and Sajjad Rashidi and Naser Chenarani and Mohammad Jaber Darabi Mahboub (2014). Application of artificial neural networks and adaptive neuro–fuzzy inference systems to predict activated carbon properties for methane storage. *Adsorption Science & Technology*, *32*(4), 275–290.

Ali Ahmadpour and Ahmad Okhovat and Mohammad Jaber Darabi Mahboub (2013). Pore size distribution analysis of activated carbons prepared from coconut shell using methane adsorption data. *Journal of Physics and Chemistry of Solids*, *74*(6), 886–891.

Mamoru Ai (2005). Formation of methyl methacrylate by condensation of methyl propionate with formaldehyde over silica-supported cesium hydroxide catalysts. *Applied Catalysis A : General*, *288*(1), 211–215.

Mamoru Ai (2006). Formation of methyl methacrylate from methyl propionate and methanol. *Catalysis today*, *111*(3), 398–402.

Mamoru Ai and Fujihashi Hideyuki and Hosoi Sanae and Yoshida Akiyo (2003). Production of methacrylic acid by vapor-phase aldol condensation of propionic acid with formaldehyde over silica-supported metal phosphate catalysts. *Applied catalysis A : general*, *252*(1), 185–191.

Ali M. Alsalme and Paul V. Wiper and Yaroslav Z. Khimyak and Elena F. Kozhevnikova and Ivan V. Kozhevnikov (2010). Solid acid catalysts based on $H_3PW_{12}O_{40}$ heteropoly acid : Acid and catalytic properties at a gas–solid interface. *Journal of Catalysis*, *276*(1), 181–189.

Yukio Aoki (1998). Ammoxidation catalyst composition. US5780664.

Atsushi Aoshima and Yoshio Suzuki and Setsuo Yamamatsu and Tatsuo Yamaguchi (1985). Method for preparing carboxylic esters. US4518796.

A. Asfaram and M. Ghaedi and M. H. Ahmadi Azqhandi and A. Goudarzic and M. Dastkhoona (2016). Statistical experimental design, least squares–support vector machine (ls–svm) and artificial neural network (ann) methods for modeling the facilitated adsorption of methylene blue dye. *RSC Advances*, *6*(46), 40502–40516.

Kunai Atsutaka and Kitano Tomoyuki and Kuroda Yasushi and Li–Fen Jiang and Sasaki Kazuo (1990). Pd/SiO_2 catalyst for oxidation of benzene to phenol. *Catalysis Letters*, *4*(2), 139–144.

Samson M. Aworinde and Artur M. Schweidtmann and Alexei A. Lapkin (2018). The concept of selectivity control by simultaneous distribution of the oxygen feed and wall temperature in a microstructured reactor. *Chemical Engineering Journal*, *331*, 765–776.

Karl Baer and Peter Bassler and Gerd Duembgen and Gerd Fouquet and Richard Krabetz and Franz Merger and Friedbert Nees (1985). Catalyst for the preparation of methyl methacrylate. US4520125.

Samira Bagheri and Nurhidayatullaili M. Julkapli and Sharifah B. Abd Hamid (2014). Titanium dioxide as a catalyst support in heterogeneous catalysis. *The Scientific World Journal*, *2014*, 727496.

Torsten Dr. Balduf (2008). Process for preparation of methyl methacrylate by esterification during oxidation. EP 1994978 A1.

Nicholas Ballard and Miren Aguirre and Alexandre Simula and Jose R. Leiza and Steven van Es and José M. Asua (2017). Nitroxide mediated suspension polymerization of methacrylic monomers. *Chemical Engineering Journal*, *316*, 655–662.

Nicola Ballarini and F. Candiracci and Fabrizio Cavani and H. Degrand and Jean-Luc Dubois and Giuseppe Lucarelli and Marta Margotti and A. Patinet and Anne Pigamo and Ferruccio Trifirò (2007a). The dispersion of keggin–type p/mo polyoxometalates inside silica gel, and the preparation of catalysts for the oxidation of isobutane to methacrolein and methacrylic acid. *Applied Catalysis A : General*, *325*(2), 263–269.

Nicola Ballarini and Fabrizio Cavani and Helene Degrand and Eric Etienne and Anne Pigamo and Ferruccio Trifirò and Jean-Luc Dubois (2007b). *The Oxidation of Isobutane to Methacrylic Acid : An Alternative Technology for MMA Production. In Methods and Reagents for Green Chemistry : An Introduction.* John Wiley & Sons, Inc., Hoboken, New Jersey, première édition.

Abraham M. Baniel and Aharon M. Eyal and Joseph Mizrahi and Betty Hazan and Rod R. Fisher and Jeffrey J. Kolstad and Brenda F. Stewart (1996). Lactic acid production, separation and/or recovery process. US 5510526 A1.

Renaud Bayer and Catherine Marchal–Roch and Feng Xian Liu and Andre Teze and Gilbert Herve (1996). Catalysis of the oxidation of isobutyric acid by vanadyl, copper and mixed vanadyl–copper salts of $H_3[PMo_{12}O_{40}]$ and $H_4[PMo_{11}VO_{40}]$. *Journal of Molecular Catalysis A : Chemical*, *114*(1), 277–286.

Siegmund Besecke and Guenter Schroeder and Hermann–Josef Siegert and Wolfgang Gaenzler (1984). Method for making isobutyric acid. US4452999.

Ernst Bielmeier and Thomas Haeberle and Hermann–Josef Siegert and Wilhelm Gruber (1995). Process for producing methacrylic acid and methacrolein by oxidation of isobutane with molybdenum heteropoly acid catalyst. US5380932.

Ernst Dr Bielmeier and Thomas Dr Haeberle and Hermann–Josef Dr Siegert and Wilhelm Dr Gruber (1994). Catalytic oxidation of isobutane to methacrylic acid and methacrolein. DE4240085A1.

Li Bin and Yan Ruiyi and Wang Lei and Diao Yanyan and Li Zengxi and Zhang Suojiang (2014). Sba-15 supported cesium catalyst for methyl methacrylate synthesis via condensation of methyl propionate with formaldehyde. *Industrial & Engineering Chemistry Research*, *53*(4), 1386–1394.

S. Breiter and H.–G. Lintz (1995). Partial oxidation of isobutene to methacrolein on biw/fecomok mixed oxide catalysts. *Chemical Engineering Science*, *50*(5), 785–791.

Franz J. Broecker and Gerd Duembgen and Gerd Fouquet and Richard Krabetz and Franz Merger and Friedbert Nees (1987). Preparation of methyl methacrylate from methacrolein. US4638085.

Angelika Bruckner and Gudrun Scholz and Detlef Heidemann and Martin Schneider and Daniel Herein and Ursula Bentrup and Muermans Kant (2007). Structural evolution of $H_4PVMo_{11}O_{40} \cdot xH_2O$ during calcination and isobutane oxidation : New insights into vanadium sites by a comprehensive in situ approach. *Journal of Catalysis*, *245*(2), 369–380.

Claus Dipl Ing Bruncke and Bernd–Michael Dipl Ing Graefe and Angelika Dipl Chem Heilmann and Thomas Dipl Ing Dr Krumsdorf (1995). Thermal conversion of plastics into useful gaseous and liq. prods. US3959357A.

G. Busca and F. Cavani and E. Etienne and E. Finocchio and A. Galli and G. Selleri and F. Trifirò (1996). Reactivity of keggin–type heteropolycompounds in the oxidation of isobutane to methacrolein and methacrylic acid : Reaction mechanism. *Journal of Molecular Catalysis A : Chemical*, *114*(1–3), 343–359.

Yun–Li Cao and Lei Wang and Bao–Hua Xu and Suo–Jiang Zhang (2018). The chitin/keggin–type heteropolyacid hybrid microspheres as catalyst for oxidation of methacrolein to methacrylic acid. *Chemical Engineering Journal*, *334*, 1657–1667.

Yun–Li Cao and Lei Wang and Li–Long Zhou and Guang–Jin Zhang and Bao–Hua Xu and Suo–Jiang Zhang (2017). $Cs(NH_4)_xH_{3-x}PMo_{11}VO_{40}$ catalyzed selective oxidation of methacrolein to methacrylic acid : Effects of NH^{4+} on the structure and catalytic activity. *Industrial & Engineering Chemistry Research*, *56*(3), 653–664.

Anna Di Capua and Jean-Luc Dubois and Michel Fournier (2007). Fine analysis of by-products of the selective oxidation of isobutane into methacrolein and methacrylic acid over mo–v–p catalyst. *Journal of Molecular Catalysis A : Chemical*, *263*(1–2), 62–69.

Magnus Carlsson and Christine Habenicht and Lance C. Kam and Michael Jerry Jr. Antal and Nanying Bian and Rebecca J. Cunningham and Maitland Jr. Jones (1994). Study of the sequential conversion of citric to itaconic to methacrylic acid in near-critical and supercritical water. *Industrial & Engineering Chemistry Research*, *33*(8), 1989–1996.

Gilbert B Carpenter (1933a). Preparation of carboxylic acids. US1924763.

Gilbert B Carpenter (1933b). Process for the production of carboxylic acids. US1924766.

Fabrizio Cavani (1998). Heteropolycompound-based catalysts : A blend of acid and oxidizing properties. *Catalysis Today*, *41*(1), 73–86.

Fabrizio Cavani (2010). Catalytic selective oxidation : The forefront in the challenge for a more sustainable chemical industry. *Catalysis Today*, *157*(1–4), 8–15.

F. Cavani and E. Etienne and R. Mezzogori and A. Pigamo and F. Trifirò (2001a). Improvement of catalytic performance in isobutane oxidation to methacrylic acid of keggin–type phosphomolybdates by preparation via lacunary precursors : nature of the active sites. *Catalysis Letters*, *75*(1–2), 99–105.

F. Cavani and E. Etienne and R. Mezzogori and A. Pigamo and F. Trifiró (2001b). Improvement of catalytic performance in isobutane oxidation to methacrylic acid of keggin–type phosphomolybdates by preparation via lacunary precursors : nature of the active sites. *Catal. Lett.*, *75*, 99–105.

Fabrizio Cavani and Roberto Mezzogori and Anne Pigamo and Ferruccio Trifirò (2000). Synthesis of methacrylic acid by selective oxidation of isobutane, catalysed by keggin–type polyoxometalates : relationship between catalytic performance, reaction conditions and chemicalphysical features of the catalyst. *Comptes Rendus de l'Académie des Sciences–Series IIC–Chemistry*, *3*(6), 523–531.

F. Cavani and R. Mezzogori and A. Pigamo and F. Trifirò (2001c). Improved catalytic performance of keggin-type polyoxometalates in the oxidation of isobutane to methacrylic acid under hydrocarbon-lean conditions using antimony-doped catalysts. *Chemical Engineering Journal*, *82*(1–3), 33–42.

F. Cavani and R. Mezzogori and A. Pigamo and F. Trifiró (2001d). Modification of redox and catalytic properties of keggin–type, sb-doped p/mo polyoxometalates in the selective oxidation of isobutane to methacrylic acid : control of preparation conditions. *Studies in Surface Science and Catalysis*, *140*(1), 141–152.

F. Cavani and R. Mezzogori and A. Pigamo and F. Trifirò (2001e). Modification of redox and catalytic properties of keggin-type, sb-doped p/mo polyoxometalates in the selective oxidation of isobutane to methacrylic acid : control of preparation conditions. *Studies in Surface Science and Catalysis*, *140*(1), 141–152.

F. Cavani and R. Mezzogori and A. Pigamo and F. Trifiró (2003a). Chemical–physical characterization of fe–doped, keggin–type p/mo polyoxometalates, catalysts for the selective oxidation of isobutane to methacrylic acid. *Appl. Catal. A*, *256*, 275–290.

F. Cavani and R. Mezzogori and A. Pigamo and F. Trifirò (2003b). Combined effects of sb-doping and of preparation via lacunary precursor for p/mo-based, keggin-type polyoxometalates, catalysts for the selective oxidation of isobutane to methacrylic acid. *Topics in Catalysis*, *23*(1–4), 119–124.

Fabrizio Cavani and Roberto Mezzogori and Anne Pigamo and Ferruccio Trifirò and Eric Etienne (2001f). Main aspects of the selective oxidation of isobutane to methacrylic acid catalyzed by keggin–type polyoxometalates. *Catalysis Today*, *71*(1–2), 97–110.

F. Cavani and A. Tanguy and F. Trifirò and M. Koutrev (1998). Effect of antimony on the chemical-physical features and reactivity in isobutyric acid oxidehydrogenation of keggin-type heteropolycompounds. *Journal of Catalysis*, *174*(2), 231–241.

Gianni Cavinato and Luigi Toniolo (2014). Carbonylation of ethene catalysed by pd(ii)–phosphine complexes. *Molecules*, *19*(9), 15116–15161.

A. V. Chernyak and A. V. Chub and E. A. Sanginov and P. Yu (2013). An nmr study of nanostructured ammonium 12–phosphotungstate. *Russian Chemical Bulletin*, *62*(8), 1798–1802.

Alessandro Chieregato and Jose M. Lopez Nieto and Fabrizio Cavani (2015). Mixed-oxide catalysts with vanadium as the key element for gas-phase reactions. *Coordination Chemistry Reviews*, *301–302*(1), 3–23.

Huang Chuanjing and Guo Wen and Yi Xiaodong and Weng Weizheng and Wan Huilin (2007). Effect of preparation condition on the performance of silica–supported MoVTeO catalysts for selective oxidation of propane to acrolein. *Catalysis Communications*, *8*(2), 162–166.

European Communities (2002). European union risk assessment report : Methacrylic acid.

Douglas Considine (2006). *Van Nostrands scientific encyclopedia*. John Wiley & Sons, Inc.

Vicente Cortés Corberán and Avellino Corma and Gojko Kremenić (1984). Partial oxidation of isobutene over molybdenum trioxide (MoO_3)–uranium trioxide (UO_3)–silicon dioxide catalysts. a reaction network. *Industrial & Engineering Chemistry Product Research and Development*, *23*(4), 546–552.

A. Corma and J.M. Serra and P. Serna and S. Valero and E. Argente and V. Botti (2005). Optimization of olefin epoxidation catalysts with the application of high–throughput and genetic algorithms assisted by artificial neural networks (softcomputing techniques). *Journal of Catalysis*, *229*(2), 513–524.

A. Costine and B.K. Hodnett (2005). Factors limiting selectivity in C_3 and C_4 amm(oxidation) reactions. *Applied Catalysis A : General*, *290*(1–2), 9–16.

Marjan Dalil and Davide Carnevali and Jean–Luc Dubois and Gregory S. Patience (2015). Transient acrolein selectivity and carbon deposition study of glycerol dehydration over WO_3/TiO_2 catalyst. *Chemical Engineering Journal*, *270*(1), 557–563.

S. Damyanova and L. Dimitrov and R. Mariscal and J.L.G. Fierro and L. Petrov and I. Sobrados (2003). Immobilization of 12–molybdophosphoric and 12-tungstophosphoric acids on metal-substituted hexagonal mesoporous silica. *Applied Catalysis A : General*, *256*(1), 183–197.

Xiao-dan Sun and Xiao-dong Yi and Wei-qi Hua and Hao Jin and Wei-zheng Weng and Hui-lin Wan (2011). Selective oxidation of isobutane to methacrolein over movte mixed oxide supported on sba–3 and SiO_2. *Fuel Processing Technology*, *92*(8), 1662–1669.

Franck Daubrege (1998). Systeme catalytique contenant de loxygene, du molybdene et du phosphore, et son application a loxydeshydrogenation dacides carboxyliques satures ou de leurs esters, ainsi qua loxydation dalcanes. FR2756500 A1.

He Dayun and Wu Jinglin and Zhong Bangke (2000). Oxidation of isobutene catalyzed by heteropoly compounds. *Journal of Natural Gas Chemistry*, *9*(3), 217–222.

Qian Deng and Shaoliang Jiang and Tiejun Cai and Zhenshan Peng and Zhengjun Fang (2005). Selective oxidation of isobutane over $H_xFe_{0.12}Mo_{11}VPAs_{0.3}O_y$ heteropoly compound catalyst. *Journal of Molecular Catalysis A : Chemical*, *229*(1–2), 165–170.

Yanyan Diao and Ruiyi Yan and Suojiang Zhang and Pu Yang and Zengxi Li and Lei Wang and Haifeng Dong (2009). Effects of pb and mg doping in Al_2O_3–supported pd catalyst on direct oxidative esterification of aldehydes with alcohols to esters. *Journal of Molecular Catalysis A : Chemical*, *303*(1–2), 35–42.

Yanyan Diao and Pu Yang and Ruiyi Yan and Li Jiang and Lei Wang and Heng Zhang and Chunshan Li and Zengxi Li and Suojiang Zhang (2013). Deactivation and regeneration of

the supported bimetallic pd–pb catalyst in direct oxidative esterification of methacrolein with methanol. *Applied Catalysis B : Environmental*, *142–143*, 329 – 336.

Eva Díaz and María Eugenia Sad and Enrique Iglesia (2010). Homogeneous oxidation reactions of propanediols at low temperatures. *ChemSusChem*, *3*(9), 1063–1070.

Wenli Ding and Lulu Liu and Fanpeng Shang and Jing Hu and Qiubin Kan and Jingqi Guan (2016). Preparation of $Te_{(12-x)}/4\,PMo_{12-x}V_xO_n$ mixed oxides from heteropolycompound precursors for selective oxidation of isobutane. *Catalysis Communications*, *18*(1), 81–84.

Segui Esteban Domingo and Alarcon Bienvenido Cabanero (1953). Process and device for the regeneration of monomers starting from polymethacrylate and, more especially, methyl polymethacrylate. US2858255A.

Dmitry E. Doronkin and Tuhin Suvra Khan and Thomas Bligaard and Sebastian Fogel and Par Gabrielsson and Soren Dahl (2012). Sulfur poisoning and regeneration of the ag/γ–Al_2O_3 catalyst for H_2–assisted scr of NOx by ammonia. *Applied Catalysis B : Environmental*, *117–118*, 49 – 58.

Eite Drent (1988). Process for the carbonylation of acetylenically unsaturated compounds. US4739109.

Eite Drent and Peter Arnoldy and Petrus H. M. Budzelaar (1994). Homogeneous catalysis by cationic palladium complexes. precision catalysis in the carbonylation of alkynes. *Journal of Organometallic Chemistry*, *475*(1–2), 57–63.

Eite Drent and Peter H. M. Budzelaar (1996). Palladium–catalyzed alternating copolymerization of alkenes and carbon monoxide. *Chemical Reviews*, *96*(2), 663–682.

Jean–Luc Dubois (2011a). Method for manufacturing a biomass-derived methyl methacrylate. US 20110301316 A1.

Jean–Luc Dubois (2011b). Method for manufacturing a biomass-derived methyl methacrylate. US 20110287991 A1.

Jean–Luc Dubois (2014). Method for producing methacrolein and/or methacrylic acid. WO2014/033413A1.

Jean–Luc Dubois and Jean Francois Crolzy and Lucie Campora and Camille Croizy and Pauline Croizy (2011). Biomass–derived methyl methacrylate and corresponding manufacturing method, uses and polymers. US 20110318515 A1.

Jean–Luc Dubois and Rosangela Pirri (2012). Impact additives. US 20120046416 A1.

Gerd Duembgen and Gerd Fouquet and Richard Krabetz and Ekhart Lucas and Franz Merger and Friedbert Nees (1985). Process for the preparation of α–alkylacroleins. US4496770.

Tran Ngoc Dung and Besson Michèle and Descorme, Claude and Fajerwerg Katia and Louis Catherine (2011). Influence of the pretreatment conditions on the performances of ceo 2–supported gold catalysts in the catalytic wet air oxidation of carboxylic acids. *Catalysis Communications*, *16*(1), 98–102.

Graham Ronald Eastham and David William Johnson and Adrianus Johannes Jozef Straathof and Marco Wilhemus Fraaije and Remko Tsjibbe Winter (2013). Process for the production of methyl methacrylate. WO2013179005A1.

Graham Ronald Eastham and David William Johnson and Mark Waugh (2015). Process for the production of methacrylic acid and its derivatives and polymers produced therefrom. US 20150094438 A1.

N.J. Van Eck and Ludo Waltman (2010). Software survey : Vosviewer, a computer program for bibliometric mapping. *Scientometrics*, *84*, 523–538.

Mahesh Edake and Marjan Dalil and Mohammad Jaber Darabi Mahboub and Jean–Luc Dubois and Gregory S Patience (2017a). Catalytic glycerol hydrogenolysis to 1, 3–propanediol in a gas–solid fluidized bed. *RSC Advances*, *238*, 3853–3860.

Mahesh Edake and Marjan Dalil and Mohammad Jaber Darabi Mahboub and Jean–Luc Duboisb and Gregory S. Patience (2017b). Catalytic glycerol hydrogenolysis to 1,3–propanediol in a gas–solid fluidized bed. *RSC Advances*, *1*(7), 3853–3860.

Eric Etienne and Fabrizio Cavani and Roberto Mezzogori and Ferruccio Trifirò and G. Calestani and Leon Gengembre and M. Guelton (2003). Chemical–physical characterization of fe–doped, keggin–type p/mo polyoxometalates, catalysts for the selective oxidation of isobutane to methacrylic acid. *Applied Catalysis A : General*, *256*(1), 275–290.

Rohm GmbH Chemische Fabrik and Metallgesellschaft AG (1998). Method for depolymerizing polymethylmethacrylate. US6469203B1.

Hong-Yu Fan and Chuan Shi and Xiao–Song Li and Shuo Zhang and Jing–Lin Liu and Ai–Min Zhu (2012). In–situ plasma regeneration of deactivated au/TiO_2 nanocatalysts during CO oxidation and effect of N_2 content. *Applied Catalysis B : Environmental*, *119–120*, 49–55.

Ioana Fechete and Ye Wang and Jacques C. Vedrine (2012). The past, present and future of heterogeneous catalysis. *Catalysis Today*, *189*(1), 2–27.

Teresita F. Garetto and Carlos I. Vignatti and Armando Borgna and Alberto Monzon (2009). Deactivation and regeneration of pt/Al_2O_3 catalysts during the hydrodechlorination of carbon tetrachloride. *Applied Catalysis B : Environmental*, *87*(3–4), 211–219.

Global Market Analysts, Inc. (2016). Methyl methacrylate market trends. http ://www.strategyr.com/MarketResearch/ Methyl Methacrylate MMA Market Trends.asp.

Antoine Godefroy and Gregory S. Patience and Roberta Cenni and Jean–Luc Dubois (2010). Regeneration studies of redox catalysts. *Chemical Engineering Science*, *65*(1), 261–266.

John J. Godfrey (1963). Production of methyl methacrylate. US3075001 A.

Makarand R Gogate and James J Spivey and Joseph R Zoeller (1997). Synthesis of methyl methacrylate by vapor phase condensation of formaldehyde with propionate derivatives. *Catalysis today*, *36*(3), 243–254.

Jingqi Guan and Mingjun Jia and Shubo Jing and Zhenlv Wang and Lihong Xing and Haiyan Xu and Qiubin Kan (2006). Selective oxidation of isobutane to methacrolein over mo–v–te–sb mixed oxide catalysts with different antimony contents. *Catalysis Letters*, *108*(3-4), 125–129.

Jingpi Guan and ShuBo Jing and Shujie Wu and Haiyan Xu and Zhenlv Wang and Qiubin Kan (2007a). Selective oxidation of isobutane over mo-v-te mixed oxide catalysts with different tellurium contents. *Reaction Kinetics and Catalysis Letters*, *90*(1), 27–33.

Jingqi Guan and Ke Song and Haiyan Xu and Zhuqian Wang and Yuanyuan Ma and Fanpeng Shang and Qiubin Kan (2009a). Oxidation of isobutane and isobutene to methacrolein over hydrothermally synthesized mo–v–te–o mixed oxide catalysts. *Catalysis Communications*, *10*(1), 528–532.

Jingqi Guan and Hongsu Wang and Ke Song and Chen Xu and Zhuqian Wang and Qiubin Kan (2009b). Selective oxidation of isobutane over hydrothermally synthesized mo–v–te–sb–o mixed oxide catalysts. *Catalysis Communications*, *10*(1), 1437–1440.

Jingqi Guan and Hongsu Wang and Ying Yang and Bo Liu and Xiaofang Yu and Yuanyuan Ma and Qiubin Kan (2009c). Effect of ph on the catalytic properties of mo–v–te–p–o catalysts for selective oxidation of isobutane. *Catalysis letters*, *131*(1), 512–516.

Jingqi Guan and Zhuqian Wang and Chen Xu and and Ying Yang and Bo Liu and Xiaofang Yu and Qiubin Kan (2009d). Partial oxidation of isobutane over vanadium phosphorus oxides. *Catalysis Letter*, *128*(1), 356–362.

Jingqi Guan and Shujie Wu and Mingjun Jia and Jiahui Huang and Shubo Jing and Haiyan Xu and Zhenlv Wang and Wanchun Zhu and Haijun Xing and Hongsu Wang and Qiubin Kan (2007b). Effect of antimony doping on the catalytic behavior of mo–v–te–p mixed oxide catalysts in oxidation of isobutane. *Catalysis Communications*, *8*(8), 1219–1223.

Jingqi Guan and Shujie Wu and Hongsu Wang and Shubo Jing and Guojia Wang and Kaiji Zhen and Qiubin Kan (2007c). Synthesis and characterization of movteceo catalysts and

their catalytic performance for selective oxidation of isobutane and isobutylene. *Journal of Catalysis*, *251*(2), 354–362.

Jingqi Guan and Chen Xu and Bo Liu and Ying Yang and Yanyan Ma and Qiubin Kan (2008a). Partial oxidation of isobutane over hydrothermally synthesized mo-v-te-o mixed oxide catalysts. *Catalysis letters*, *126*(1), 301–307.

Jingqi Guan and Cheng Xu and Zhuqian Wang and Ying Yang and Bo Liu and Fanpeng Shang and Yanqiu Shao and Qiubin Kan (2008b). Selective oxidation of isobutane and isobutene to methacrolein over te–mo mixed oxide catalysts. *Catalysis letters*, *124*(1), 428–433.

Jingqi Guan and Haiyan Xu and Shubo Jing and Shujie Wu and Yuanyuan Ma and Yanqiu Shao and Qiubin Kan (2008c). Selective oxidation of isobutane and isobutene over vanadium phosphorus oxides. *Catalysis Communications*, *10*(3), 276–280.

Jingqi Guan and Haiyan Xu and Ke Song and Bo Liu and Fanpeng Shang and Xiaofang Yu and Qiubin Kan (2008d). Selective oxidation and oxidative dehydrogenation of isobutane over hydrothermally synthesized mo–v–o mixed oxide catalysts. *Catalysis Letter*, *126*(1), 293–300.

Thomas Haas and Thomas Tacke and Achim Marx and Alexander Schraven and Olivier Zehnacker and Eva Maria Wittmann (2014). Method for the production of free carboxylic acids. US 8703451 B2.

Imane Hachemi and Dmitry Yu. Murzin (2018). Kinetic modeling of fatty acid methyl esters and triglycerides hydrodeoxygenation over nickel and palladium catalysts. *Chemical Engineering Journal*, *334*, 2201–2207.

Naser Hadi and Aligholi Niaeia and Seyed Reza Nabavi and Reza Alizadeh and Masoud Navaei Shirazi and Behrang Izadkhah (2016). An intelligent approach to design and optimization of m–mn/h–zsm–5 (m :Ce, Cr, Fe, Ni) catalysts in conversion of methanol to propylene. *Journal of the Taiwan Institute of Chemical Engineers*, *59*(1), 173–185.

Gary P Hagen (1984). Process for preparation of alpha, beta-unsaturated aldehydes using ams–1b borosilicate crystalline molecular sieve. US4433174.

Dong Haifeng and Li Zengxi and Wang Zhengping and Cheng Weiguo and Zhao Wei and Zhang Xiangping and Zhang Suojiang (2006). Oxidative esterification of methacrolein to methyl methacrylate over pd–pb/Al_2O_3 catalysts. *Journal of chemical industry and engineering–china*, *57*(6), 1346–1355.

Y. El. Hamzaoui and J.A. Hernandez and S. Silva–Martinez and A. Bassam and A. Alvarez and C. Lizama–Bahenaa (2011). Optimal performance of cod removal during aqueous treat-

ment of alazine and gesaprim commercial herbicides by direct and inverse neural network. *Desalination*, *277*(1–3), 325–337.

Li He and Li Fu and Yingzhan Tang (2015). Catalytic performance of a novel cr/znallao catalyst for oxidative dehydrogenation of isobutane. *Catalysis Science & Technology*, *5*(2), 1115–1125.

Niizuma Hiroshi and Miki Toshiro and Kojima Shiro and Azuma Kishiro and Kato Hiroyuki and Murakami Yuichi and Ito Tsutomu (1987). Process for the production of acrylic acid or methacrylic acid. US4677225.

B.K. Hodnett and J.B. Moffat (1984). Application of temperature-programmed desorption to the study of heteropoly compounds : Desorption of water and pyridine. *Journal of Catalysis*, *88*(2), 253–263.

Tung–Li Huang and Keith R. Cliffe and Jordan M. MacInnes (2000). The removal of ammonia from water by a hydrophobic catalyst. *Environmental Science & Technology*, *34*(22), 4804–4809.

Dong Hoon Hur and Thu Thi Nguyen and Donghyuk Kim and Eun Yeol Lee (2017). Selective bio-oxidation of propane to acetone using methane-oxidizing methylomonas sp. dh–1. *Journal of Industrial Microbiology & Biotechnology*, *44*, 1097–1105.

Que–Lam Huynh and Jean–Marc Millet (2005). Characterization of iron counter–ion environment in bulk and supported phosphomolybdic acid based catalysts. *Journal of Physics and Chemistry of Solids*, *66*(5), 887–894.

Quyet–Thang Huynh and Y. Schuurman and P. Delichere and S. Loridant and Jean marc M. Millet (2009a). Study of Te and V as counter–cations in keggin type phosphomolybdic polyoxometalate catalysts for isobutane oxidation. *Journal of Catalysis*, *261*(2), 166–176.

Quyet–Thang Huynh and A. Selmi and G. Corbel and P. Lacorre and Jean marc M. Millet (2009b). Atypical synergetic effect between te– and v–substituted phosphomolybdic cesium salt and lamox–type phases for the oxidation of isobutane into methacrylic acid. *Journal of Catalysis*, *266*(1), 64–70.

Nobuyuki Ichikuni and Yuma Nakao and Kazuya Ishizuki and Takayoshi Hara and Shogo Shimazu (2013). Effect of local structure of Mo oxide on selective photo–oxidation of propane to acetone. *Catalysis Letters*, *143*, 154–158.

Sebastian Illies and Bettina Kraushaar-Czarnetzki (2016). Processing study on the stability of heteropoly acid catalyst in the oxidation of methacrolein to methacrylic acid. *Industrial Engineering Chemistry Research*, *55*(31), 8509–8518.

Kei Inumaru and Akiko Ono and Hiroshi Kubo and Makoto Misono (1998). Catalysis by heteropoly compounds part 39 : The structure and redox behaviour of vanadium species in

molybdovanadophosphoric acid catalysts during partial oxidation of isobutane. *Journal of Chemical Society, Faraday Transactions*, *94*(12), 1765–1770.

Satoshi Ishikawa and Wataru Ueda (2016). Microporous crystalline mo–v mixed oxides for selective oxidations. *Catalysis Science & Technology*, *6*, 617–629.

B. Izadkhah and S.R. Nabavi and A. Niaei and D. Salari and T. Mahmuodi Badiki and N. Çaylak (2012). Design and optimization of bi–metallic ag–ZSM_5 catalysts for catalytic oxidation of volatile organic compounds. *Journal of Industrial and Engineering Chemistry*, *18*(6), 2083–2091.

L. Jalowiecki-Duhamel and A. Monnier and Y. Barbaux and G. Hecquet (1996). Oxidation of isobutane on a heteropolycompound hydrogen reservoir. *Catalysis Today*, *32*(1), 237–242.

Machek Jaroslav and Tichý Jan and Švachula Jan (1993). Catalytic oxidation of isobutyraldehyde over a molybdenum–vanadium oxide catalyst. *Reaction Kinetics and Catalysis Letters*, *49*(1), 209–214.

Fangli Jing (2012). Innovative keggin–structure polyoxometalate–based catalysts for the selective oxidation of isobutane into methacrylic acid. PhD thesis : University of Lille1.

Fangli Jing and Benjamin Katryniok and Elisabeth Bordes–Richard and Sébastien Paul (2013). Improvement of the catalytic performance of supported $(NH_4)_3HPMo_{11}VO_{40}$ catalysts in isobutane selective oxidation. *Catalysis Today*, *203*(1), 32–39.

Fangli Jing and Benjamin Katryniok and Franck Dumeignil and Elisabeth Bordes-Richard and Sébastien Paul (2014a). Catalytic selective oxidation of isobutane over $Cs_x(NH_4)_{3-x}HPMo_{11}VO_{40}$ mixed salts. *Catalysis Science & Technology*, *4*(9), 2938–2945.

Fangli Jing and Benjamin Katryniok and Franck Dumeignil and Elisabeth Bordes-Richard and Sèbastien Paul (2014b). Catalytic selective oxidation of isobutane to methacrylic acid on supported $(NH_4)_3HPMo_{11}VO_{40}$ catalysts. *Journal of Catalysis*, *309*(1), 121–135.

David William Johnson and Graham Ronald Eastham and Martyn Poliakoff and Thomas Andrew Huddle (2011). A process for the production of methacrylic acid and its derivatives and polymers produced therefrom. EP 2643283 B1.

David William Johnson and Graham Ronald Eastham and Martyn Poliakoff and Thomas Andrew Huddle (2013). Process for the production of methacrylic acid and its derivatives and polymers produced therefrom. US 20130303713 A1.

David William Johnson and Graham Ronald Eastham and Martyn Poliakoff and Thomas Andrew Huddle (2015). Method of producing arcylic and methacrylic acid. US 8933179 B2.

John A Jung and Jimmy Peress (1981). Preparation of carboxylic acids using a BF_3 catalyst complex. US4256913.

Li Junhui and Tai Jianren and Davis Robert J (2006). Hydrocarbon oxidation and aldol condensation over basic zeolite catalysts. *Catalysis today*, *116*(2), 226–233.

Mads Kaarsholm and Finn Joensen and Jesper Nerlov and Roberta Cenni and Jamal Chaouki and Gregory S. Patience (2007). Phosphorous modified ZSM−−5 : Deactivation and product distribution for MTO. *Chemical Engineering Science*, *62*(18–20), 5527–5532.

W. Kaminsky and J. Franck (1991). Monomer recovery by pyrolysis of poly(methyl methacrylate) (pmma). *J. Anal. Appl. Pyrolysis*, *19*, 311–318.

Mitsuru Kanno and Toshiya Yasukawa and Wataru Ninomiya and Ken Ooyachi and Yuichi Kamiya (2010). Catalytic oxidation of methacrolein to methacrylic acid over silica-supported 11–molybdo–1–vanadophosphoric acid with different heteropolyacid loadings. *Journal of Catalysis*, *273*(1), 1–8.

Robert Karcz and Piotr Niemiec and Katarzyna Pamin and Jan Poltowicz and Joanna Krysciak–Czerwenka and Bogna D. Napruszewska and Alicja Michalik–Zym and Malgorzata Witko and Renata Tokarz–Sobieraj and Ewa M. Serwicka (2017). Effect of cobalt location in keggin–type heteropoly catalysts on aerobic oxidation of cyclooctane : Experimental and theoretical study. *Applied Catalysis A : General*, *542*, 317–326.

Shane Kendel and Trevor Brown (2011). Comprehensive study of isobutane selective oxidation over group i and ii phosphomolybdates : Structural and kinetic factors. *Catalysis Letters*, *141*(12), 1767–1785.

Shane M. Kendell and Trevor C. Brown and Robert C. Burns (2008). Accurate low–pressure kinetics for isobutane oxidation over phosphomolybdic acid and copper(ii) phosphomolybdates. *Catalysis Today*, *131*(1–4), 526–532.

Jae Jin Kim and Wha Young Lee and Yun–ku Rhee (1985). Oxidation of methacrolein and isomerization of n–butene over heteropoly compounds. *Chemical Engineering Communications*, *34*(1–6), 49–63.

Kida Kiochi (1999). Production of methyl methacrylate. EP0941984 A2.

Hisanori Kishida and Fangming Jin and Zhouyu Zhou and Heiji Enomoto (2005). Conversion of glycerin into lactic acid by alkaline hydrothermal reaction. *Chemistry Letters*, *34*(11), 1560–1561.

Carlos Knapp and Toshiaki Ui and Koichi Nagai and Noritaka Mizuno (2001). Stability of iron in the keggin anion of heteropoly acid catalysts for selective oxidation of isobutene. *Catalysis Today*, *71*(1–2), 111–119.

Ivan Kozhevnikov and K.R. Kloetstra and A. Sinnema and Henny Zandbergen and H. van Bekkum (1996). Study of catalysts comprising heteropoly acid $H_3PW_{12}O_{40}$ supported on

mcm–41 molecular sieve and amorphous silica. *Journal of Molecular Catalysis A : Chemical*, *114*(1–3), 287–298.

Ivan V. Kozhevnikov (1998). Catalysis by heteropoly acids and multicomponent polyoxometalates in liquid–phase reactions. *Chemical Reviews*, *98*, 171–198.

Harold Krieger and Lawrence Samuel Kirch (1979). Process for the production of (meth)acrylic acid by the catalytic vapour phase oxidation of isobutane or propane. EP0010902A1.

Harold Krieger and Lawrence S. Kirch (1981). Process for the production of unsaturated acids. US4260822A.

Harold H. Kung (1994). Oxidative dehydrogenation of light (C_2 to C_4) alkanes. *Advances in Catalysis*, *40*(1), 1–38.

Ikuo Kurimoto and Hideto Hashiba and Hideo Onodera and Yukio Aoki (1989). Catalyst for the production of methacrylic acid. US5153162A.

M. Langpape and J.M.M. Millet and U.S. Ozkan and P. Delichere (1999). Study of cesium or cesium-transition metal-substituted keggin-type phosphomolybdic acid as isobutane oxidation catalysts : Ii. redox and catalytic properties. *Journal of Catalysis*, *182*(1), 148–155.

Martin Langpape and Jean–Marc M Millet (2000). Effect of iron counter–ions on the redox properties of the keggin–type molybdophosphoric heteropolyacid : Part i. an experimental study on isobutane oxidation catalysts. *Applied Catalysis A : General*, *200*(1–2), 89–101.

Nathalie Laronze and Catherine Roch-Marchal and Nathalie Guillou and F.X Liu and Gilbert Herve (2003). Solid–state chemistry of ammonium and cesium 1–vanado–11–molybdophosphate and ammonium 12–molybdosilicate : application to oxidation catalysis. *Journal of Catalysis*, *220*(1), 172–181.

Kwan Young Lee and Syoichi Oishi and Hiroshi Igarashi and Makoto Misono (1997). Acidic cesium salts of molybdovanadophosphoric acids as efficient catalysts for oxidative dehydrogenation of isobutyric acid. *Catalysis Today*, *33*(1), 183–189.

Sungchul Lee and Gayatri Keskar and Changchang Liu and William R. Schwartz and Charles S. McEnally and Ju-Yong Kim and Lisa D. Pfefferle and Gary L. Haller (2012). Deactivation characteristics of ni/CeO_2−−Al_2O_3 catalyst for cyclic regeneration in a portable steam reformer. *Applied Catalysis B : Environmental*, *111–112*, 157–164.

Jiang Li and Diao Yanyan and Han Junxing and Yan Ruiyi and Zhang Xiangping and Zhang Suojiang (2014). Mgo–sba–15 supported pd–pb catalysts for oxidative esterification of methacrolein with methanol to methyl methacrylate. *Chinese Journal of Chemical Engineering*, *22*(10), 1098–1104.

W. Li and K. Oshihara and W. Ueda (1999). Catalytic performance for propane selective oxidation and surface properties of 12–molybdophosphoric acid treated with pyridine. *Applied Catalysis A : General*, *182*(2), 357–363.

Wen Li and Wataru Ueda (1997). Catalytic oxidation of isobutane to methacrylic acid with molecular oxygen over activated pyridinium 12–molybdophosphate. *Catalysis Letters*, *46*(3), 261–265.

Tzong–Bin Lin and Dong–Lin Chung and Jen–Ray Chang (1999). Ethyl acetate production from water–containing ethanol catalyzed by supported pd catalysts : Advantages and disadvantages of hydrophobic supports. *Industrial & Engineering Chemistry Research*, *38*(4), 1271–1276.

L. Lioyd (2011). *Handbook of industrial catalysts*. CSpringer.

Shizhe Liu and Lu Chen and Guowei Wang and Jianwei Liu and Yanan Gao and Chunyi Li and Honghong Shan (2016). Effects of cs–substitution and partial reduction on catalytic performance of keggin-type phosphomolybdic polyoxometalates for selective oxidation of isobutane. *Journal of Energy Chemistry*, *25*(1), 85–92.

Xinhua Liu and Guangwen Xu and Shiqiu Gao (2008). Micro fluidized beds : Wall effect and operability. *Chemical Engineering Journal*, *137*(2), 302–307.

Feng Xian Liu-Cai and Charlotte Pham and Farida Bey and Gilbert Herve (2002). Oxidation of isobutane catalyzed by vanadyl, copper and cesium substituted $H_3PMo_{12}O_{40}$. *Reaction Kinetics and Catalysis Letters*, *75*(2), 305–314.

Maria J. Lorences and Jean–Philippe Laviolette and Gregory S. Patience and Monica Alonso and Fernando V. Diez (2006). Fluid bed gas rtd : Effect of fines and internals. *Powder Technology*, *168*(1), 1–9.

María J. Lorences and Gregory S. Patience and Fernando V. Díez and and José Coca (2003). Butane oxidation to maleic anhydride : Kinetic modeling and byproducts. *Industrial & Engineering Chemistry Research*, *42*(26), 6730–6742.

Stephane Loridant and Quyen Huynh and Jean–Marc M. Millet (2010). Specific insight of active sites in $Cs_2TexVyPMo_{12}O_{40}$ catalysts efficient for selective oxidation of isobutane by operando resonance raman spectroscopy. *Catalysis Today*, *155*(3–4), 214–222.

Samira Lotfi and Daria C. Boffito and Gregory S. Patience (2015). Gas–phase partial oxidation of lignin to carboxylic acids over vanadium pyrophosphate and aluminum–vanadium–molybdenum. *ChemSusChem*, *8*(20), 3424–3432.

Mikhail V. Luzgin and Alexander G. Stepanov and Alain Sassi and Jean Sommer (2000). Formation of carboxylic acids from small alkanes in zeolite h–zsm–5. *Chemistry–A European Journal*, *6*, 2368–2376.

Mikhail V. Luzgin and Karine Thomas and Jacob van Gestel and Jean–Pierre Gilson and Alexander G. Stepanov (2004). Propane carbonylation on sulfated zirconia catalyst as studied by 13c mas nmr and ftir spectroscopy. *Journal of Catalysis*, *223*, 290–295.

James E. Lyons and Anthony F. Volpe and Paul E. Ellis and Swati Karmakar (1999). Conversion of alkanes to unsaturated carboxylic acids over heteroploy acids supported on polyoxometallate salts. US5990348 A.

Tianlin Ma and Jianfei Ding and Rong Shao and Wei Xu and Zhi Yun (2017). Dehydration of glycerol to acrolein over wells–dawson and keggin type phosphotungstic acids supported on mcm–41 catalysts. *Chemical Engineering Journal*, *316*, 797–806.

Mohammad Jaber Darabi Mahboub and Samira Lotfi and Gregory S. Patience and Jean–Luc Dubois (2016a). Gas phase oxidation of 2–methyl 1,3 propanediol to methacrylic acid over heteropolyacid catalysts. *Catalysis Science & Technology*, *6*(17), 6525–6535.

Mohammad Jaber Darabi Mahboub and Mohammad Rostamizadeh and Jean-Luc Dubois and Gregory S. Patience (2016b). Partial oxidation of 2–methyl–1,3–propanediol to methacrylic acid : Experimental and neural network modeling. *RSC Advances*, *6*(115), 114123–114134.

Mohammad Jaber Darabi Mahboub and Jordan Wright and Daria Boffito and Jean–Luc Dubois and Gregory S. Patience (2018). Cs, v, cu keggin–type catalysts partially oxidize 2–methyl–1,3–propanediol to methacrylic acid. *Applied Catalysis A : General*, *554*(1), 105–116.

Sven-Peter Mannsfeld and Klaus–Jurgen Paulsen and Erich Buchholz (1966). Production of monomeric cleavage products by thermal decomposition of polymers. US3494958A.

Catherine Marchal–Roch and Nathalie Laronze and Nathalie Guillou and Andre Teze and Gilbert Herve (2000). , mixed ammonium–cesium and cesium salts derived from $(NH_4)_5[PMo_{11}VIVO_{40}]$ as isobutyric acid oxidation catalysts part ii. synthesis, characterization and catalytic activity in the oxidative dehydrogenation of isobutyric acid of mixed ammonium—cesium and cesium salts. *Applied Catalysis A : General*, *203*(1), 143–150.

IHS Markit (2016). Chemical economics handbook : Methyl methacrylate. https ://www.ihs.com/products/methyl–methacrylate–chemical– economics–handbook.html.

Neema A. Mashayekhi and Mayfair C. Kung and Harold H. Kung (2014). Selective oxidation of hydrocarbons on supported au catalysts. *Catalysis Today*, *238*, 74–79.

Sami Matar and Lewis F. Hatch (2001). *Chemistry of Petrochemical Processes : C_4 Olefins and Diolefins-Based Chemicals (Chapter 9)*. Elsevier, Hoboken, New Jersey, seconde édition.

G.B. McGarvey and J.B. Moffat (1991). The oxidative dehydrogenation of isobutyric acid to methacrylic acid on ion exchange modified 12–heteropoly oxometalates. *Journal of Catalysis*, *132*(1), 100–116.

Franz Merger and Hans–Juergen Foerster (1983). Preparation of alpha–alkylacroleins. US4408079.

Franz Merger and Hans–Juergen Foerster (1984). Process for the preparation of alpha–alkyl acroleines. EP0058927B1.

G. Mestl and T. Ilkenhans and D. Spielbauer and M. Dieterle and O. Timpe and J. Krohnert and F. Jentoft and H. Knozinger and R. Schlogl (2001). Thermally and chemically induced structural transformations of keggin-type heteropoly acid catalysts. *Applied Catalysis A : General*, *210*(1–2), 13–34.

Yuji Mikami and Akio Takeda and Motomu Oh–Kita (1999). Catalyst used in production of carboxylic acid esters and process for producing these esters. US5892102.

Jean-Marc M Millet and Jacques C Védrine (2001). Importance of site isolation in the oxidation of isobutyric acid to methacrylic acid on iron phosphate catalysts. *Topics in Catalysis*, *15*(2–4), 139–144.

Joon–Seok Min and Noritaka Mizuno (2001a). Effects of additives on catalytic performance of heteropoly compounds for selective oxidation of light alkanes. *Catalysis Today*, *71*(1–2), 89–96.

Joon–Seok Min and Noritaka Mizuno (2001b). Iron as an effective additive for enhancement of catalytic performance of cesium hydrogen salt of molybdophosphoric acid for selective oxidation of isobutane, propane, and ethane under oxygen–rich and –poor conditions and the catalyst design. *Catalysis Today*, *66*(1), 47–52.

Makoto Misono (2001). Unique acid catalysis of heteropoly compounds (heteropolyoxometalates) in the solid state. *Chemical Communications*, *1*(13), 1141–1152.

Janardan Misra and Indranil Saha (2010). Artificial neural networks in hardware : a survey of two decades of progress. *Neurocomputing*, *74*(1–3), 239–255.

Takanori Miyake and Tetsuo Asakawa (2005). Recently developed catalytic processes with bimetallic catalysts. *Applied Catalysis A : General*, *280*(1), 47–53.

Masahiko Mizuno and Tateo Seo and Tetsuya Suzuta (2008). Methyl methacrylate production process. EP20070740948.

Masahiko Mizuno and Tateo Seo and Tetsuya Suzuta (2009). Production method of methyl methacrylate. US20090209782A1.

Noritaka Mizuno and Wonchull Han and Tetsuichi Kudo (1998). Selective oxidation of ethane, propane, and isobutane catalyzed by copper–containing $Cs_{2.5}H_{1.5}PVMo_{11}O_{40}$ under oxygen–poor conditions. *Journal of Catalysis*, *178*(1), 391–394.

Noritaka Mizuno and Makoto Mison (1998). Heterogeneous catalysis. *Chemical Reviews*, *98*(1), 199–218.

Noritaka Mizuno and To-oru Hirose and Masaki Tateishi and Masakazu Iwamoto (1994a). Synthesis of $[PW_9O_{37}(Fe_{3-x}Ni_x(OAc)_3)]_9^{(+x)}$- (x= predominantly 1) and oxidation catalysis by the catalyst precursor. *Journal of Molecular Catalysis*, *88*(2), L125–L131.

Noritaka Mizuno and Dong-Jin Suh and Wonchull Han and Tetsuichi Kudo (1996a). Catalytic performance of $Cs_{2.5}Fe_{0.08}H_{1.26}PVMo_{11}O_{40}$ for direct oxidation of lower alkanes. *Journal of Molecular Catalysis A : Chemical*, *114*(2), 309–317.

Noritaka Mizuno and Masaki Tateishi and Masakazu Iwamoto (1994b). Enhancement of catalytic activity of $Cs_{2.5}Ni_{0.08}H_{0.34}PMo_{12}O_{40}$ by V^{5+}–substitution for oxidation of isobutane into methacrylic acid. *Applied Catalysis A : General*, *118*(1), L1–L4.

Noritaka Mizuno and Masaki Tateishi and Masakazu Iwamoto (1995). Pronounced catalytic activity of $Fe_{0.08}Cs_{2.5}H_{1.26}PVMo_{11}O_{40}$ for direct oxidation of propane into acrylic acid. *Applied Catalysis A : General*, *128*(2), L165–L170.

Noritaka Mizuno and Masaki Tateishi and Masakazu Iwamoto (1996b). Oxidation of isobutane catalyzed by $Cs_xH_{3-x}PMo_{12}O_{40}$–based heteropoly compounds. *Journal of catalysis*, *163*(1), 87–94.

Noritaka Mizuno and Hidenori Yahiro (1998). Oxidation of isobutane catalyzed by partially salified cesium molybdovanadophosphoric acids. *The Journal of Physical Chemistry B*, *102*(2), 437–443.

Ruth A. Montag and Stephen T. Mckenna (1991). Catalyst for production of alpha,beta–ethylenically unsaturated monocarboxylic acid. EP0255395B1.

Mathieu Morin and Sébastien Pécate and Mehrdji Hémati (2018). Kinetic study of biomass char combustion in a low temperature fluidized bed reactor. *Chemical Engineering Journal*, *331*, 265–277.

Y. Moro-oka and N. Miura and N. Fujikawa and Y.-C. Kim and W. Ueda (1993). Selective oxidation and ammoxidation of propane to form acrolein and acrylonitrile. *Studies in Surface Science and Catalysis*, *75*(1), 1983–1986.

Seyed Mahdi Mousavi and Aligholi Niaei and Dariush Salari and Parvaneh Nakhostin Panahi and Masoud Samandari (2013). Modelling and optimization of mn/activate carbon nanocatalysts for no reduction : comparison of rsm and ann techniques. *Environmental Technology*, *34*(11), 1377–1384.

Rajesh Munirathinam and Jurriaan Huskens and Willem Verboom (2015). Supported catalysis in continuous flow microreactors. *Advanced Synthesis and Catalysis*, *357*(6), 1093–1123.

Koichi Nagai (2001). New developments in the production of methyl methacrylate. *Applied Catalysis A : General*, *221*(1–2), 367–377.

Kiochi Nagai and Toshiaki Ui (2004). Trends and future of monomer– mma technologies. Sumitomo Chemical Co., Ltd.

Hari Nair and Jeffrey T. Miller and Eric A. Stach and Chelsey Baertsch (2010). Mechanism of dynamic structural reorganization in polyoxometalate catalysts. *Journal of Catalysis*, *270*(1), 40–47.

Hiroyuki Naitou and Takashi Karasuda and Tomoki Fukui (2010). Process for producing catalyst for methacrylic acid production, catalyst for methacrylic acid production, and process for producing methacrylic acid. US7662742.

Velinov Nikolay and Koleva Kremena and Tsoncheva Tanya and Manova Elina and Paneva Daniela and Tenchev Krassimir and Kunev Boris and Mitov Ivan (2013). Nanosized $Cu_{0.5}Co_{0.5}Fe_2O_4$ ferrite as catalyst for methanol decomposition : effect of preparation procedure. *Catalysis Communications*, *32*, 41–46.

Jerome Emile Lucien Le Notre and Elinor Lindsey Scott and Roeland Leo Croes and Jacobus Van Haveren (2016). Process for the production of methacrylic acid. US 20160207867 A1.

Motomu Oh–Kita and Yoshiyuki Taniguchi (1992). Preparation of catalysts for producing methacrolein and methacrylic acid. US5166119A.

Toshio Okuhara (2002). Water–tolerant solid acid catalysts. *Chemical Reviews*, *102*(10), 3641–3665.

Toshio Okuhara and Noritaka Mizuno and Makoto Misono (1996). Catalytic chemistry of heteropoly compounds. *Studies in Surface Science and Catalysis*, *41*(1), 113–252.

Toshio Okuhara and Hiromu Watanabe and Toru Nishimura and Kei Inumaru and Makoto Misono (2000). Microstructure of cesium hydrogen salts of 12-tungstophosphoric acid relevant to novel acid catalysis. *Chemistry of Materials*, *12*(8), 2230–2238.

Kohji Omata and Yuhsuke Watanabe and Masahiko Hashimoto and Tetsuo Umegaki and Muneyoshi Yamada (2004). Simultaneous optimization of preparation conditions and composition of the methanol synthesis catalyst by an all–encompassing calculation on an artificial neural network. *Industrial & Engineering Chemistry Research*, *43*(13), 3282–3288.

Hasan Orkcu and Hasan Bal (2011). Comparing performances of backpropagation and genetic algorithms in the data classification. *Expert Systems with Applications*, *38*(4), 3703–3709.

Gregory S. Patience and Richard E. Bockrath and John D. Sullivan and Harold S. Horowitz (2007). Pressure calcination of vpo catalyst. *Industrial & Engineering Chemistry Research*, *46*(13), 4374–4381.

Sébastien Paul and Wei Chu and Manzoor Sultan and Elisabeth Bordes–Richard (2010). Keggin–type $H_4PVMo_{11}O_{40}$-based catalysts for the isobutane selective oxidation. *Science China Chemistry*, *53*(9), 2039–2046.

Sébastien Paul and Véronique Le Courtois and Dominique Vanhove (1997). Kinetic investigation of isobutane selective oxidation over a heteropolyanion catalyst. *Industrial Engineering Chemistry Research*, *36*(8), 3391–3399.

Zhenshan Peng and Changlin Yu and Tiejun Cai and and Qian Deng (2004). Selective oxidation of isobutene over $CsFeCoBiMnMoO_x$ mixed oxide catalyst. *Journal of Natural Gas Chemistry*, *13*(3), 172–176.

Reddy K Hari Prasad and Anand Nair and Prasad PS Sai and Rao, KS Rama and Raju B David (2011). Influence of method of preparation of co–cu/mgo catalyst on dehydrogenation/dehydration reaction pathway of 1, 4–butanediol. *Catalysis Communications*, *12*(10), 866–869.

PERP Program (2006). Methyl methacrylate new report alert. Nexant Chem Systems.

T. Punniyamurthy and Subbarayan Velusamy and Javed Iqbal (2005). Recent advances in transition metal catalyzed oxidation of organic substrates with molecular oxygen. *Chemical Reviews*, *105*, 2329–2364.

Sang–Hyun Pyo and Tarek Dishisha and Secil Dayankac and Jargalan Gerelsaikhan and Stefan Lundmark and Nicola Rehnberg and Rajni Hatti–Kaul (2012). A new route for the synthesis of methacrylic acid from 2–methyl–1,3–propanediol by integrating biotransformation and catalytic dehydration. *Green Chemistry*, *14*(7), 1942–1948.

Pillai Unnikrishnan R. and Sahle–Demessie Endalkachew (2004). Selective oxidation of alcohols by molecular oxygen over a pd/mgo catalyst in the absence of any additives. *Green Chemistry*, *6*, 161–165.

Sajjad Rashidi and Ali Ahmadpour and Neda Jahanshahi and Mohammad Jaber Darabi Mahboub and Hamed Rashidi (2015). Application of artificial intelligent modeling for predicting activated carbons properties used for methane storage. *Separation Science & Technology*, *50*(1), 110–120.

Li–Ke Ren and Hua–Qing Yang and Chang–Wei Hu (2016). Theoretical study of the catalytic oxidation mechanism of 5–hydroxymethylfurfural to 2,5–diformylfuran by pmo–containing keggin heteropolyacid. *Catalysis Science & Technology*, *6*, 3776–3787.

Catherine Roch-Marchal and Nathalie Laronze and Nathalie Guillou and Andre Teze and Gilbert Herve (2000a). Study of ammonium, mixed ammonium-cesium and cesium salts derived from $(NH_4)_5[PMo_{11}VIVO_{40}]$ as isobutyric acid oxidation catalysts : Part i : Syntheses, structural characterizations and catalytic activity of the ammonium salts. *Applied Catalysis A : General*, *199*(1), 33–44.

Catherine Roch-Marchal and Nathalie Laronze and Richard Villanneau and Nathalie Guillou and Andre Teze and Gilbert Herve (2000b). Effects of NH_4^+, Cs^+, and H^+ counterions of the molybdophosphate anion in the oxidative dehydrogenation of isobutyric acid. *Journal of Catalysis*, *190*(1), 173–181.

Rohm and Haas GmbH (1935). Method of producing monomeric methacrylic acid esters. GB460009A.

Mohammad Rostamizadeh and Daria Camilla Boffito and Gregory S. Patience and Abbas Taeb (2014). Neural network modeling of methanol to propylene over p–zsm–5 in a fluidized bed. *Journal of Chemical and Process Engineering*, *1*(1), 201–208.

Mohammad Rostamizadeh and Mashallah Rezakazemi and Kazem Shahidi and Toraj Mohammadi (2013). Gas permeation through H_2–selective mixed matrix membranes : Experimental and neural network modeling. *International Journal of Hydrogen Energy*, *38*(2), 1128–1135.

Mohammad Rostamizadeh and S. Mohammad Hashemi Rizi (2012). Predicting gas flux in silicalite–1 zeolite membrane using artificial neural networks. *Journal of Membrane Science*, *403*(404), 146–151.

Mohammad Rostamizadeh and Abbas Taeb (2015). Highly selective me–zsm–5 catalyst for methanol to propylene (mtp). *Journal of Industrial and Engineering Chemistry*, *27*, 297 – 306.

Mohammad Rostamizadeh and Abbas Taeb (2016). Synthesis and characterization of hzsm–5 catalyst for methanol to propylene (mtp) reaction. *Synthesis and Reactivity in Inorganic, Metal–Organic, and Nano–Metal Chemistry*, *46*(5), 665–671.

Nooshin Saadatkhah and Marco G. Rigamonti and Daria C. Boffito and He Li and Gregory S. Patience (2017). Spray dried SiO_2WO_3/TiO_2 and SiO_2 vanadium pyrophosphate core–shell catalysts. *Powder Technology*, *316*, 434–440.

Antaram N. Sarve and Mahesh N. Varma and Shriram S. Sonawane (2015). Response surface optimization and artificial neural network modeling of biodiesel production from crude mahua (madhuca indica) oil under supercritical ethanol conditions using CO_2 as co–solvent. *RSC Advances*, *5*(85), 69702–69713.

Akinobu Sasaki and Nobuyuki Kikuya and Takashi Ookubo and Masahiro Hayashida (2007). Recovery method of pyrolysis product of resin. US8304573B2.

Gotz–Peter Schindler and Carlos Knapp and Toshiaki Ui and Koichi Nagai (2003). Enhancing the productivity of isobutane selective oxidation over a mo-v-p-as-cs-cu-o heteropoly acid catalyst. *Topics in Catalysis*, *22*(1–2), 117–121.

Gotz-Peter Schindler and Toshiaki Ui and Koichi Nagai (2001). Kinetics of isobutane selective oxidation over mo-v-p-as-cs-cu-o heteropoly acid catalyst. *Applied Catalysis A : General*, *206*(2), 183–195.

Kirk H. Schulz and David F. Cox (1993). Oxidation, reduction, and isomerization of allyl alcohol and 1–propanol over Cu_2O(100). *The Journal of Physical Chemistry*, *97*(1), 647–655.

Stephan Schunk and Nadine Brem (2011). Routes to methacrylic acid via partial oxidation. Royal Society of Chemistry.

Parvaneh Shabanzadeh and Rubiyah Yusof and Kamyar Shameli (2015). Modeling of biosynthesized silver nanoparticles in vitex negundo l. extract by artificial neural network. *RSC Advances*, *5*(106), 87277–87285.

Carl L Shapiro (1966). Method of and apparatus for depolymerizing acrylate resins. US2412296A.

Satoshi Shinachi and Mitsunori Matsushita and Kazuya Yamaguchi and Noritaka Mizuno (2005). Oxidation of adamantane with 1 atm molecular oxygen by vanadium-substituted polyoxometalates. *Journal of Catalysis*, *233*(1), 81–89.

Tetsuya Shishido and Atsushi Inoue and Tsuyoshi Konishi and Ikuya Matsuura and Katsuomi Takehira (2000). Oxidation of isobutane over mo-v-sb mixed oxide catalyst. *Catalysis letters*, *68*(3), 215–221.

Ebata Shuji and Hirayama Hiroyuki and Uchiyama Takako (1994). Process for production of alpha–hydroxycarboxylic acid amide. EP0433611 B1.

Amanda Simson and Robert Farrauto and Marco Castaldi (2011). Steam reforming of ethanol/gasoline mixtures : Deactivation, regeneration and stable performance. *Applied Catalysis B : Environmental*, *106*(3–4), 295–303.

Aimee W. Smith and Ian T. Jackson and Jamileh Yousefi (1999). The use of screw fixation of methyl methacrylate to reconstruct large craniofacial contour defects. *European Journal of Plastic Surgery*, *22*(1), 17–21.

James J. Spivey and Makarand R. Gogate and Joseph R. Zoeller and Richard D. Colberg (1997). Novel catalysts for the environmentally friendly synthesis of methyl methacrylate. *Industrial & Engineering Chemistry Research*, *36*(11), 4600–4608.

Alexander G Stepanov (2002). *Carbonylation–Heterogeneous*. John Wiley & Sons, Inc.

Daniel E Strain (1935). Process for depolymerizing alpha substituted acrylic acid esters. US2030901A.

Bernard Stuyven and Jens Emmerich and Pierre Eloy and Jan Van Humbeeck and Christine E.A. Kirschhock and Pierre A. Jacobs and Johan A. Martens and Eric Breynaert (2014). Molybdenum–vanadium–antimony mixed oxide catalyst for isobutane partial oxidation synthesized using magneto hydrodynamic forces. *Applied Catalysis A : General*, *474*(1), 18–25.

Hirokazu Sugiyama and Ulrich Fischer and Elena Antonijuan and Volker H. Hoffmann and Masahiko Hirao and Konrad Hungerbuhler (2009). How do different process options and evaluation settings affect economic and environmental assessments ? a case study on methyl methacrylate (mma) production processes. *Process Safety and Environmental Protection*, *87*(6), 361–370.

Manzoor Sultan and Sebastien Paul and Maxime Fournier and Daan Vanhove (2004). Evaluation and design of heteropolycompound catalysts for the selective oxidation of isobutane into methacrylic acid. *Applied Catalysis A : General*, *259*(2), 141–152.

M. Sultan and S. Paul and D. Vanhove (1999). Kinetic effects of chemical modifications of PMo_{12} catalysts for the selective oxidation of isobutane. *Studies in Surface Science and Catalysis*, *122*(1), 283–290.

Feifei Sun and Yunfeng Geng and Shunhe Zhong (2002). Selective oxidation of isobutane to methacrylic acid over supported v–mo–p based composite oxide catalysts. *Journal of Natural Gas Chemistry*, *11*(3), 120–126.

Junming Sun and Changjun Liu and Yong Wang and Kevin Martin and Padmesh Venkitasubramanian (2015a). Processes for making methacrylic acid. US 20150218077 A1.

Junming Sun and Changjun Liu and Yong Wang and Kevin Martin and Padmesh Venkitasubramanian (2015b). Use of byproduct acetic acid from oxidative methods of making acrylic acid and/or methacrylic acid. US 20150210607 A1.

Miao Sun and Jizhe Zhang and Piotr Putaj and Valerie Caps and Frederic Lefebvre and Jeremie Pelletier and Jean–Marie Basset (2014). Catalytic oxidation of light alkanes (C_1–C_4) by heteropoly compounds. *Chemical Reviews*, *114*(2), 981–1019.

V. L. Sushkevich and V. V. Ordomsky and I. I. Ivanova (2016). Isoprene synthesis from formaldehyde and isobutene over keggin–type heteropolyacids supported on silica. *Catalysis Science & Technology*, *6*, 6354–6364.

K. Suzuki and T. Yamaguchi (2013). Supported composite particle material, production process of same and process for producing compounds using supported composite particle material as catalyst for chemical synthesis. US8450235.

Jianren Tai and Robert J Davis (2007). Synthesis of methacrylic acid by aldol condensation of propionic acid with formaldehyde over acid–base bifunctional catalysts. *Catalysis today*, *123*(1), 42–49.

Nobuhiro Tamura and Yohei Fukuoka and Setsuo Yamamatsu and Yoshio Suzuki and Ryoichi Mitsui and Tadayuki Ibuki (1979). Process for preparing carboxylic acid amides. GB2008430.

Takeichi Tatsumi and Hiroshi Yoshihara and Gaisuke Uesaka (1970). Method for depolymerizing thermoplastic resins by liquid heat transfer media. US3886202A.

Hiroyuki Tokushige and Akira Kosaki and Tadamoto Sakai (1973). Method for continuously thermally decomposing synthetic macro–molecule materials. US3959357A.

Miyatake Toshiaki and Shibata Junji and Shiraishi Eiichi (2013). Method for producing catalyst for preparation of methacrylic acid and method for preparing methacrylic acid. US8586499.

Takashi Ushikubo (2003). Activation of propane and butanes over niobium- and tantalum-based oxide catalysts. *Catalysis Today*, *78*(1), 79–84.

Dominique Vanhove (1996). Catalyst testing at a lab scale in mild oxidation : Can you control the reaction temperature ? *Applied Catalysis A : General*, *138*(2), 215–234.

Patrick William Vaughan and Donald James Highgate (1992). Depolymerisation. US5663420A.

Jacques C. Vedrine and Ioana Fechete (2016). Heterogeneous partial oxidation catalysis on metal oxides. *Comptes Rendus Chimie*, *19*(10), 1203–1225.

P. Visuvamithiran and K. Shanthi and M. Palanichamy and V. Murugesan (2013). Direct synthesis of mn-ti-sba-15 catalyst for the oxidation of ethylbenzene. *Catalysis Science & Technology*, *3*(9), 2340–2348.

Francis J Waller (1983). Palladium sulfonate catalyst systems for carbonylation of olefins. US4414409.

Baohe Wang and Hui Li and Jing Zhu and Wenjuan Sun and Shuang Chen (2013). Preparation and characterization of mono–/multi–metallic hydrophobic catalysts for the oxidative esterification of methacrolein to methyl methacrylate. *Journal of Molecular Catalysis A : Chemical*, *379*, 322–326.

Guowei Wang and Chunyi Li and Honghong Shan (2016). Catalytic dehydrogenation of isobutane over a Ga_2O_3/ZnO interface : reaction routes and mechanism. *Catalysis Science & Technology*, *6*(9), 3128–3136.

Xitao Wang and Mei Li and Fen Wang and Shunhe Zhong and Shi Jiang and Sihe Wang (2012). Effect of bi promoter on the performances of selective oxidation of isobutane to methacrolein over movo/$AlPO_4$ catalysts. *Journal of Natural Gas Chemistry*, *21*(2), 165–169.

Otto Watzenberger and Gerhard Emig and David T. Lynch (1990). Oxydehydrogenation of isobutyric acid with heteropolyacid catalysts : Experimental observations of deactivation. *Journal of Catalysis*, *124*(1), 247–258.

W.Dormer and R.Gomes and M.E. Meek (1998). Methyl methacrylate : Concise international chemical assessment document 4.

Zhao Wei and Cheng Wei–Guo and Li Zeng–Xi and Wang Lei and Zhang Xiang Ping and Zhang Suo–Jiang (2006). Oxidative esterification of methacrolein to methyl methacylate over supported palladium catalyst. *Chinese Chemical Letters*, *17*(6), 739–742.

Piotr T Wierzchowski and Leon W Zatorski (1991). Aldol condensation in gaseous phase by zeolite catalysts. *Catalysis letters*, *9*(5–6), 411–414.

Robert Wilczynski and Jamie Jerrick Juliette (2011). Methacrylic acid and derivates. Rohm and Haas Company.

Laura Wood (2001). Methyl methacrylate market report.

Shujie Wu and Qiubin Kan and Wenli Ding and Fanpeng Shang and Heng Liu and Jingqi Guan (2012). Partial oxidation of isobutane to methacrolein over $Te_{1.5+0.5x}PMo_{12-x}V_xO_n$ heteropolycompounds with tellurium as counter cations. *Reaction Kinetics, Mechanisms and Catalysis*, *106*(1), 157–164.

Guo Xiaojun and Huang Chongpin and Li Yingxia (2008). Effect of cesium content on the structure and catalytic performances of heteropoly compounds in one-step synthesis of methylmethacrylate from methacrolein. *Korean Journal of Chemical Engineering*, *25*(4), 697–702.

Jinhai Xie and Qinglin Zhang and Karl T. Chuang (2001). Role of steam in partial oxidation of propylene over a pd/sdb catalyst. *Applied Catalysis A : General*, *220*(1–2), 215– 221.

Setsuo Yamamatsu and Tatsuo Yamaguchi (1990). Process for producing methacrylic acid and methacrolein. EP0425666A1.

Setsuo Yamamatsu and Tatsuo Yamaguchi (1993). Process for the preparation of methacrylic acid and methacrolein. US5191116A.

Zheng Yanxia and Zhang Heng and Wang Lei and Zhang Suojiang and Wang Shaojun (2016). Transition metal–doped heteropoly catalysts for the selective oxidation of methacrolein to methacrylic acid. *Frontiers of Chemical Science and Engineering*, *10*(1), 139–146.

Diao Yanyan and He Hongyan and Yang Pu and Wang Lei and Zhang Suojiang (2015). Optimizing the structure of supported pd catalyst for direct oxidative esterification of methacrolein with methanol. *Chemical Engineering Science*, *135*, 128–136.

Yasukazu Yoshida and Yuji Mikami and Motomu Oh–Kita (2002). Process for producing a carboxylic acid ester by reacting an aldehyde and an alcohol using a palladium type catalyst. US6348619.

Guo Yu and Li Huabo and Kameyama Hideo (2011a). Steam reforming of kerosene over a metal–monolithic alumina–supported ru catalyst : Effect of preparation conditions and electrical-heating test. *Chemical engineering science*, *66*(23), 6287–6296.

Jian Yu and Changbin Yao and Xi Zeng and Shuang Geng and Li Dong and Yin Wang and Shiqiu Gao and Guangwen Xu (2011b). Biomass pyrolysis in a micro fluidized bed reactor characterization and kinetics. *Chemical Engineering Journal*, *168*(2), 839–847.

Li Yuchao and Wang Lei and Yan Ruiyi and Han Junxing and Zhang Suojiang (2016). Promoting effects of mgo$(NH_4)_2SO_4$ or MoO_3 modification in oxidative esterification of methacrolein over au/$Ce_{0.6}$Zr0.4O_2–based catalysts. *Catalyst Science & Technology*, *6*, 5453–5463.

Heng Zhang and Ruiyi Yan and Li Yang and Yanyan Diao and Lei Wang and Suojiang Zhang (2013). Investigation of Cu– and Fe–doped $CsH_3PMo_{11}VO_{40}$ heteropoly compounds for the selective oxidation of methacrolein to methacrylic acid. *Industrial & Engineering Chemistry Research*, *52*(12), 4484–4490.

Zhongshen Zhang and Yang Li and Junhui Wang and Hongling Yang and Na Li and Chunyan Ma and Zhengping Hao (2016). Insights into the carbon catalyzed direct dehydrogenation of isobutane by employing modified OMCs. *Catalysis Science & Technology*, *6*, 4863–4871.

Lilong Zhou and Lei Wang and Yunli Cao and Yanyan Diao and Ruiyi Yan and Suojiang Zhang (2017a). The states and effects of copper in keggin–type heteropolyoxometalate catalysts on oxidation of methacrolein to methacrylic acid. *Molecular Catalysis*, *438*, 47–54.

Lilong Zhou and Lei Wang and Yanyan Diao and Ruiyi Yan and Suojiang Zhang (2017b). Cesium salts supported heteropoly acid for oxidation of methacrolein to methacrylic acid. *Molecular Catalysis*, *438*, 153–161.

Lilong Zhou and Lei Wang and Suojiang Zhang and Ruiyi Yan and Yanyan Diao (2015). Effect of vanadyl species in keggin–type heteropoly catalysts in selective oxidation of methacrolein to methacrylic acid. *Journal of Catalysis*, *329*, 431–440.